Phase Equilibrium Measurements at Low-to-Moderate Pressures for Systems Containing n-Hexane, 1-Hexene and n-Methyl-2-pyrrolidone

Renay Sewpersad

Student number: 206500820

Supervisor: **: Prof. D. Ramjugernath**

Co-Supervisor: **: Dr. P. Naidoo**

This thesis is submitted as partial requirement for the degree of Master of Science in Engineering (MSc. Eng.) in the school of Chemical Engineering at the University of Kwa-Zulu Natal

14 May 2012

Preface

I, Renay Sewpersad, declare that:

(i) The research reported in this thesis, except where otherwise indicated, is my original work.

(ii) This thesis has not been submitted for any degree or examination at any other university.

(iii) This thesis does not contain other persons‟ data, pictures, graphs or other information, unless specifically acknowledged as being sourced from other persons.

(iv) This thesis does not contain other persons‟ writing, unless specifically acknowledged as being sourced from other researchers. Where other written sources have been quoted, then:

a. Their words have been re-written but the general information attributed to them has been referenced;

b. Where their exact words have been used, their writing has been placed inside quotation marks, and referenced.

(v) This thesis does not contain text, graphics or tables copied and pasted from the internet, unless specifically acknowledged, and the source being detailed in the thesis and in the References sections.

_____ _____

Renay Sewpersad Date 14 May 2012

Acknowledgements

I would like to take this opportunity to express my sincere gratitude to the following people and organizations, without whom, the aspiration of reading for my master‟s degree would not have been realized:

- My supervisors, Professor D. Ramjugernath and Dr. P. Naidoo for their steadfast support and guidance throughout my studies.

- Wayne Nelson and Brian Satola for their invaluable assistance with Aspen Plus®.

- The workshop and laboratory staff at the University of Kwa-Zulu Natal, especially Ayanda Khanyile and Lindinkosi Mkize.

- My colleagues in Chemical Engineering, specifically Kuveneshan Moodley, Cassandra Petticrew, Bianca Leite, Mark Williams-Wynn, Samuel Iwarere, Khalid Osman, Bruce Phillip Francois, Thokozani Petersen Ngema, Kaniki Tumba, Sivanna Naicker, Rashmika Pritipal, David Lokhat, Shalendra Subramoney, Travis Pio Benecke and Hitesh Lilwanth.

- Sasol Ltd and the National Research Foundation (NRF) of South Africa.

- Felicia Adalene Bisnath, Uraisha Mangalparsad and Nishana Kannie. At some point in our lives we crossed over from being just friends to sisters. You have etched an indelible mark upon my soul and I am richer for knowing you.

- My inspiring parents, Dannie and Reena Sewpersad, and sister, Chandelle Sewpersad. Your support and unconditional love has throughout my childhood provided me with an impervious sense of self-worth and quiet confidence. Thank you for being the most amazing family a kid could ever ask for.

- Most important of all, I must acknowledge the ultimate Supreme Being, Bhagwan, for every success in my life academically but more importantly for the transcendental family and friends I have been blessed with.

Abstract

The primary focus of this study is the measurement and modeling of binary and ternary VLE data. The measurements of binary and ternary systems were undertaken on a fully automated dynamic VLE apparatus. The glass dynamic VLE still was modified to handle pressures ranging from 0 to 500 kPa, however, the safest maximum pressure to which tests had been conducted was 350 kPa. Thus, this limit was not to be exceeded during the measurement of experimental data.

The systems under investigation included the binary and ternary combinations of the following chemicals: n-hexane, 1-hexene and n-methyl-2-pyrrolidone (NMP) at isothermal conditions. A test system consisting of ethanol + cyclohexane was measured at 40 kPa, as well as the system of 1-hexene + NMP at 363.15 K and n-hexane + NMP at 363.15 K. Published literature data for these test systems were employed to verify the measured data for the test systems complied with thermodynamic consistency. All other data constitutes new data, currently unavailable in literature.

The following isotherms were measured:

1) 1-hexene (1) + NMP (2) at 323.15, 343.15, 353.15 and 363.15 K
2) n-hexane (1) + NMP (2) at 353.15, 363.15, 378.15 and 383.15 K
3) 1-hexene (1) + n-hexane (2) at 343.15, 363.15 and 373.15 K, and
4) 1-hexene (1) +n-hexane (2) + NMP (2) at 363.15 K

All system measurements were carried out on the glass low-to-medium pressure VLE still of Lilwanth (2011), with the exception of the test system ethanol + cyclohexane, which was carried out on the low pressure VLE glass still of Hirawan (2007).

The two VLE stills, utilized to carry out measurements in this work, can operate isobarically and isothermally. The temperature on the stills of Hirawan (2007) and Lilwanth (2011) were controlled to within ±0.425 and ±0.089 K respectively and the accuracy of pressure control is to within ±0.320 and ±0.440 kPa respectively. In addition, for the calibration of the various systems: ethanol + cyclohexane, 1-hexene + NMP, n-hexane + NMP, 1-hexene + n-hexane

and 1-hexene + n-hexane + NMP, the accuracies are: ±0.002, ±0.0034, ±0.0033, ±0.0066 and ±0.0083 of a mole fraction respectively.

The binary interaction parameters obtained from modeling the three binary systems were used to predict the ternary system data. Thereafter, the experimentally measured data for the ternary system was then compared to the model prediction, which was completed on Dortmund Data Bank (DDB, 2011).

The measured binary data was regressed utilizing the combined and the direct methods. For the direct method, the cubic equations of state (CEoS) used to describe the vapour phase included the Peng-Robinson (1976) and Soave-Redlich-Kwong (1972) equations combined with the mixing rule of Wong and Sandler (1992) in conjunction with the Gibbs excess energy models, namely the NRTL (1968) and UNIQUAC (1975) models, to describe the liquid phase non-idealities.

For the combined method, the Gibbs excess energy activity coefficient models mentioned above were employed to represent the liquid phase imperfections and the vapour phase non-idealities were represented by cubic equations of state, as mentioned above, as well as the Hayden and O'Connell (1975) virial equation of state for the calculation of the virial coefficients.

To verify whether the measured data is thermodynamically consistent the point and direct tests were applied. Even though the direct test is a more stringent approach to testing thermodynamic consistency, for the systems 1-hexene + NMP and n-hexane + NMP, the point test was utilized as the primary means by which to quantify the data, as the associative effects of the NMP molecule effect the results obtained. For the system 1-hexene + n-hexane the direct test was used as the primary means to test the consistency of data, as no cross- or self-association is present.

After extensive modeling was carried out, it was found that for the systems 1-hexene + NMP and n-hexane + NMP the model which enabled the best fit of the experimental data are the NRTL activity coefficient model in conjunction with the Hayden and O'Connell virial equation of state (EoS). For the system 1-hexene + n-hexane the overall best fit model is

the Peng-Robinson EoS in conjunction with the Wong-Sandler mixing rule and the NRTL activity coefficient model.

A single set of binary interaction parameters for each of the three binary systems was obtained (via regression on Aspen Plus®) using the NRTL-HOC models. However, since Aspen Plus® cannot predict ternary system behaviour using the binary interaction parameters of the constituent systems, DDB was utilized. Further, DDB did not have available the HOC virial EoS (for enabling predictions), thus, it was decided to use the ideal gas model for representation of the vapour phase in conjunction with the NRTL activity coefficient model. The use of the ideal gas model does not compromise the integrity of the prediction in any way since the ternary system measurements were carried out in the dilute NMP region. Thus, since the main components in the ternary mixture at any one instant were 1-hexene and n-hexane, and these components behave ideally, the ideal gas model is applicable.

After the predicted behaviour for the ternary system was compared to the experimental data for the same system, the maximum percentage error encountered between the two data sets is 5%.

Contents

List of Figures

Chapter 1

Chapter 2

Chapter 3

Chapter 4

Chapter 5

Chapter 6

Chapter 7

Appendix B

Appendix E

Appendix G

Appendix H

List of Tables

Chapter 2

Chapter 6

Chapter 7

Appendix B

Appendix C

Appendix F

Appendix G

Nomenclature

A	Antoine vapour pressure equation constant
A_*	Parameter in the Peng-Robinson (1976) equation of state
A_i^*	Peak area obtained from the gas chromatograph
A_{12}	Parameter in the Van Laar (1910) model
A_{21}	Parameter in the Van Laar (1910) model
A^E	Excess Helmholtz free energy
a	Parameter for the intermolecular attraction force in the Peng-Robinson (1976) and Soave- Redlich- Kwong (1972) equation of state
a_m	Mixture Parameter for the intermolecular attraction force in the Peng-Robinson (1976) and Soave-Redlich- Kwong (1972) equation of state
a_{vdw}	Van der Waals (1873) equation of state intermolecular attraction force parameter
B	Constant in the Antoine vapour pressure equation
B^*	Parameter in the Peng-Robinson (1976) equation of state
B_{ii}	Second Virial coefficient of pure component i [$cm^3.mol^{-1}$]
B_{ij}	Second Virial coefficient for species i and j interaction [$cm^3.mol^{-1}$]
B_{virial}	Second Virial coefficient [$cm^3.mol^{-1}$]
b	Molecular size parameter in the Peng-Robinson (1976) equation of state
b_m	Mixture molecular size parameter in the Peng-Robinson (1976) equation of state
b_{vdw}	Molecular size parameter in the Van der Waals (1873) equation of state
C	Constant in the Antoine equation
c	Numerical constant defined in Equation (3-74)
D	Summation term in the mixing rule of Wong and Sandler (1992)
F	Response factor
f	Fugacity [kPa]
$\overline{f_i}$	Fugacity in solution of component i [kPa]
G	Molar Gibbs energy [J/kmol]
$\overline{G}$	Partial molar Gibbs energy [J/kmol]
G_{ij}	Parameter in the NRTL model of Renon and Prausnitz (1968)

$g_{ij} - g_{ii}$	Parameter representing energy interactions between species in the NRTL model of Renon and Prausnitz (1968)
H	Enthalpy [J/kmol]
$\overline{H}$	Partial molar enthalpy [J/kmol]
$\Delta H_{VAP,i}$	Enthalpy of vaporisation [J/kmol]
k_{ij}	Binary interaction parameter in the Wong-Sandler mixing rule
L'	Parameter in the Twu et al. (1991) alpha correlation
l_i	Parameter in the UNIQUAC model of Abrams and Prausnitz (1975)
l_{ij}	Binary interaction parameter for the mixing rule of Twu and Coon (1996)
M	Represents a general thermodynamic property
M'	Parameter in the Twu et al. (1991) alpha correlation
N'	Parameter in the Twu *et al*. (1991) alpha correlation
n	Number of moles
P	System pressure [kPa]
P_i	Parachor
Q	Summation term in the mixing rule of Wong and Sandler (1992)
q_i	Pure component area parameter in the UNIQUAC model of Abrams and Prausnitz (1975)
q_i'''	Pure component area parameter in the modified UNIQUAC model (Anderson and Prausnitz, 1978)
R	Universal gas constant [$J.mol^{-1}.K^{-1}$]
R_d	Mean radius of gyration [Å]
r_i	Pure component volume parameter in the UNIQUAC model of Abrams and Prausnitz (1975)
S	Molar or specific entropy [$cm^3.mol^{-1}$]
T	System temperature [^OC or K]
$u_{ij} - u_{ii}$	Parameter representing energy interactions between species in the UNIQUAC model of Abrams and Prausnitz (1975)
V	Molar or specific volume [$cm^3.mol^{-1}$]
$\overline{V}$	Partial molar volume [$cm^3.mol^{-1}$]
x	Liquid phase mole fraction or composition
y	Vapour phase mole fraction
Z	Compressibility factor

z	Coordination number in the UNIQUAC model of Abrams and Prausnitz (1975)

Greek Letters

α	Scaling factor in the Peng-Robinson (1976) equation of state
α_{ij}	NRTL model Parameter representing solution non-randomness
δ	Denotes a residual property such as δP
δ_{ij}	An expression constituting the second virial coefficients
ε^*_p	Constant temperature term in the direct test of Van Ness (1995)
ε^*_T	Constant pressure term in the direct test of Van Ness (1995)
Φ	Ratio of fugacity coefficients and Poynting correction factor
Φ^*_i	Segment fraction in the UNIQUAC model of Abrams and Prausnitz (1975)
ϕ	Fugacity coefficient
$\hat{\phi}$	Fugacity coefficient in solution
Γ_i	Temperature dependent constant of integration
γ	Activity coefficient
γ^∞_i	Activity coefficient at infinite dilution
η	Parameter representing solvation and association
κ	Constant in the Peng-Robinson (1976) equation of state
Λ_{ij}	Wilson (1964) model Parameter
$\lambda_{ij} - \lambda_{ii}$	Wilson (1964) model parameter representing molar interactions between species
μ_d	Dipole moment
μ_i	Chemical potential of component i
θ_i	Area fraction in the UNIQUAC model of Abrams and Prausnitz (1975)
σ	Standard deviation
τ_{ij}	Parameter in the NRTL model of Renon and Prausnitz (1968)
ω	Accentric factor

Subscript

1	Represents component 1
2	Represents component 2
AAD	Represents an absolute average deviation in a property
c	Represents a critical property
calc	Represents a calculated value
exp	Represents an experimental value
i	Represents component 1
j	Represents component 2
m	Represents a mixture property
r	Represents reduced property

Superscript

^{o}	Represents standard state
C	Represents a combinatorial property for the UNIQUAC model of Abrams and Prausnitz (1975)
E	Represents an excess property
ig	Represents an ideal gas
l	Represents the liquid phase
R	Represents a residual property
sat	Represents a property at saturation
v	Represents the vapour phase
α	Represents a thermodynamic phase
β	Represents a thermodynamic phase
π	Represents a thermodynamic phase

Chapter 1: Introduction

Higher α-olefins, C atoms ≥ 6 (such as 1-hexene), are produced primarily by the oligomerization of ethylene. However, there are alternative chemical processes which result in the production of paraffin and olefins. One such process is Sasol‟s Fischer-Tropsch process where the product streams are rich in 1-hexene and 1-octene. It is extremely difficult to recover and purify these α-olefins. This is attributed to the large component spectrum in which the product streams are saturated. For instance, the Fischer-Tropsch product streams contain a minimum of 29 components constituting paraffin, aromatics, branched, internal and cyclic olefins and oxygenates. It is precisely due to this saturation of the product stream with close boiling components that difficulty arises in separation and purification, as the relative volatilities of the components are very close to one. Therefore, normal distillation is an uneconomical undertaking (Wentinka *et al*., 2007).

The separation of components similar in volatility is a very difficult feat to accomplish by simple distillation. This task is made even more complex if the system has azeotropic points. In such instances, the addition of specific solvents ensues to assist in better separation. This occurs via the addition of a high boiling solvent to form a low boiling azeotrope with one of the components. There is a great interest in the study of selective solvents as they are integral to extractive distillation processes. The selective solvent functions in such a way that it actually alters the separation factor, to a great degree, of two components very similar in volatility to enable better separation of those two components (Fischer and Gmehling, 1996).

Additionally, in industry there are some gas streams that have high levels of acid impurities. In certain cases removing these impurities using solvents that are regenerated by heating is uneconomical when taking into consideration the value of the treated gas stream. In such instances financially viable alternatives are sought. This presents itself in the use of non-reactive, organic, polar solvents, such as NMP. NMP is widely used industrially, and one of the prime examples of said use is in the Lurgi Purisol process (Henni *et al*., 2004).

The premise of the Lurgi Purisol process is the discriminatory desulphurization of gases resulting from coal or oil gasification. NMP is an integral component to the chemical industry due its specific affinity for unsaturated hydrocarbons, aromatics, as well as sulphur or oxygen containing compounds. The unique physical attributes of NMP which make it a desirable solvent are that it is: chemically and thermally stable, highly soluble in water and other organic solvents, high in polarity and has a low volatility (Fischer and Gmehling, 1996).

The separation and purification of chemicals is most frequently carried out by extractive distillation processes. Therefore, separation process techniques are in constant need of improvement for technological advancement. The design and implementation of distillation processes for successful operation depend entirely upon the performance and results of vapour-liquid equilibrium experiments conducted on a bench-scale in thermodynamic labs around the world (Fischer and Gmehling, 1996).

Even though there are techniques available at one‟s disposable for the prediction of vapour-liquid equilibrium data sets, these predictive tools are just that: predictions. Although these techniques are useful tools in preliminary design and screening, they will still have to be verified. They are used merely as a guideline during experimental measurements to give an indication of the pattern that the vapour and liquid points may follow. Therefore, actual vapour-liquid equilibrium measurements are invaluable to the chemical industry.

According to research, the predictive tools utilized in estimating the behavior of vapour-liquid equilibrium are not always 100 % accurate at conditions of interest for the chemical industry. This is due to the fact that there are many deviations from ideality for the liquid phase of many systems (especially highly non-ideal systems). Differences in the chemical make-up of components, as well as the composition ratio of components in mixtures all contribute to deviations from a predictive point of view (Seker and Somer, 1992).

Although packages such as Aspen Plus® are available in a predictive and modeling capacity, there are certain limitations as to the extent to which this software may be employed. This arises due to the limited phase equilibrium data available for new, relevant systems.

There is a vast array of data available for low and high pressure systems; however, there is a shortage of publications on moderate pressure measurements (100 – 500 kPa). This pressure range is particularly important as many industrial process operations are based at moderate pressures and temperatures (Reddy, 2006).

At present, there is a limitation on the variety and quantity of data available for systems containing NMP. The excellent measurements conducted by Fischer and Gmehling (1996) were executed on a static synthetic apparatus; therefore, only P-x data is reported. Due to this, a thorough examination of the consistency of the thermodynamic data was not conducted. A recent thesis by Hirawan (2007) includes measurements for the 1-hexene + NMP system at temperatures of 313.15, 335.15 and 363.15 K. However, these measurements were carried out at low pressures (below atmosphere). The thermodynamic consistency tests for these data sets proved successful. However, due to the limitation of pressure in measurements, complete isotherms could not be generated. Therefore, yet again, there is a deficiency in thermodynamic data available for this system.

Isothermal measurements for the system 1-hexene + n-hexane were carried out by Moodley (2009) at 328.15, 353.15 and 378.15 K. These measurements were very difficult to execute due to the high relative volatilities of the components involved. As a consequence, consistent thermodynamic data could not be produced. Therefore, for the purposes of this thesis, it is important that great care be taken in an attempt to produce consistent thermodynamic data for the system 1-hexene + n-hexane.

The scope of this research project is to learn and master the measurement and modeling of VLE data for industrially relevant systems at moderate temperatures and pressures.

The project comprises:

- Mastering the use of the fully automated VLE glass recirculating still as commissioned by Lilwanth (2011)

- Measure test systems to verify the equipment is operating smoothly, as well as to become better accustomed to the experimental process of measuring VLE data. The test systems measured are:
    (1) ethanol + cyclohexane at 40 kPa;
    (2) 1-hexene + NMP at 363.15 K and;
    (3) n-hexane + NMP at 363.15 K.

- The systems under investigation are:
    (1) 1-hexene + NMP;
    (2) n-hexane + NMP;
    (3) 1-hexene + n- hexane and;
    (4) 1-hexene + n-hexane + NMP.

1.1 Relevance of Systems Chosen and Theory on the Bonding Interactions

Vapour-liquid equilibrium measurements were undertaken on the following systems:

5) ethanol (1) + cyclohexane (2) at 40 kPa
6) 1-hexene (1) + NMP (2) at 323.15, 343.15, 353.15 and 363.15 K
7) n-hexane (1) + NMP (2) at 353.15, 363.15, 378.15 and 383.15 K
8) 1-hexene (1) + n-hexane (2) at 343.15, 363.15 and 373.15 K
9) 1-hexene (1) +n-hexane (2) + NMP (2) at 363.15 K

The system ethanol (1) + cyclohexane (2) was selected for measurement as a test system for several reasons, the most prominent of which being (Clifford, 2004):

1) There is a vast assortment of literature data available on this system to be utilized as a reference for comparison.
2) This particular system is highly non-ideal (an azeotrope is present), thus it provides good experience as an introduction to complex thermodynamic measurements.

3) Ethanol and cyclohexane do not pose a significant health risk, *i.e.* they are not markedly toxic, and therefore easy, in this regard, with which to work.
4) There is an abundance of these chemicals available in the thermodynamic laboratory as they are inexpensive in comparison to most other chemicals.

In addition, the system 1-hexene (1) + NMP (2) at 363.15 K was measured as a test system. This system was previously measured by Fischer and Gmehling (1996) and Hirawan (2007). n-Hexane (1) + NMP (2) was also measured as a test system at 363.15 K (Fischer and Gmehling, 1996). This was done to better acquaint oneself with the dynamics of the new systems being measured and to subsequently compare the experimental data with the literature to verify the authenticity of measurements conducted.

The new binary and ternary systems were chosen based on Sasol‟s need for data on separation of these components. An extensive search through the literature such as journals and theses *etc.* as well as through data banks such as Dortmund Detherm showed that the aforementioned systems represent new data. The exception of course being ethanol (1) + cyclohexane (2) at 40 kPa, 1-hexene (1) + NMP (2) at 363.15K and n-hexane (1) + NMP (2) at 363.15 K.

A succinct discussion on the properties of some of the components measured is carried out below. This is necessary to become better acquainted with the systems measured and explains the molecular interactions between the components, thus, adding significance to the results achieved.

1.1.1 n-Methyl-2-pyrrolidone

NMP is an example of an aprotic, dipolar substance. The following is an example of the possible structures for cyclic and chain O- - - N and O- - - C associated NMP dimers.

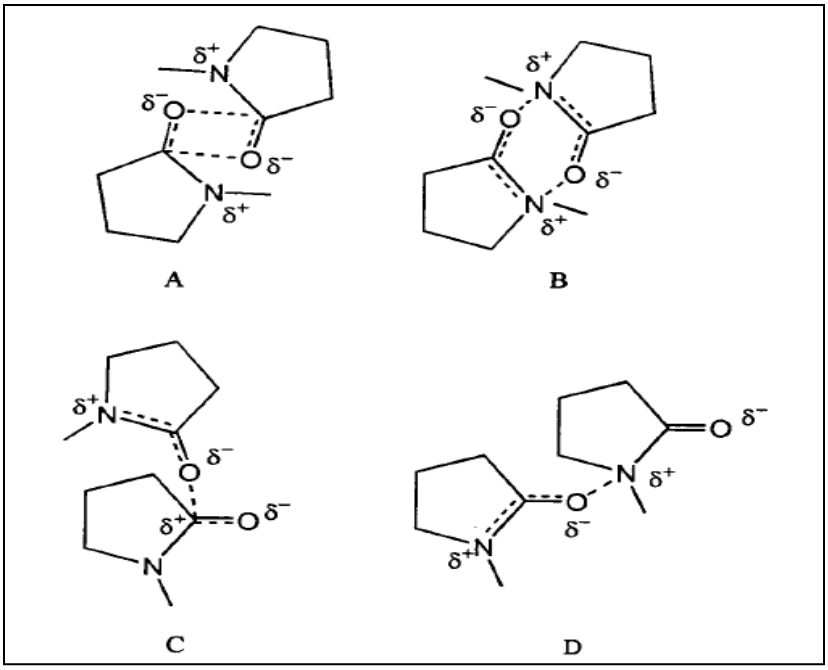

Figure 1-1: Chain and cyclic NMP Structure: O- -C and O- -N associated dimer NMP structures (Dyrkacz, 2001).

Within the NMP molecule there are numerous dipole-dipole oligomers possible, that contribute to association. These various oligomers may be cyclic or chain-like structures. The possibilities that are considered, as evident from the diagrams above, are:

- The oxygen atoms situated on each NMP structure bond with the carbon atom of the corresponding adjacent NMP molecule, resulting in a four centre molecular structure.
- The oxygen of one NMP molecule will bond with the nitrogen molecule on the adjacent NMP molecule.

Between the NMP molecules there are dipolar interactions, as such these interactions compete with the thermal motion of the molecules in solution. Subsequently, the oligomers occupy a smaller volume.

The association effects of NMP are evident when analyzing the thermodynamic excess molar volume of this component. Thermodynamically, the excess molar volume is a measure of the difference between the actual volume of a mixture and the ideal volume it should theoretically

have. Negative or positive deviations from the ideal volume are dependent upon a myriad of factors such as, specific and non-specific electronic interactions between like and unlike molecules and molecular packing, *etc*. (Dyrkacz, 2001). It shall also give an indication of the extent by which a compound shall deviate from Raoult‟s law.

When the species in a mixture vary in their chemical makeup, or when small diluents are utilized, this results in complicated effects on the V_m^E value. Chemicals such as n-hexane and 1-hexene are relatively low carbon number solvents. When these chemicals are mixed with NMP, this has the result of negative V_m^E throughout the composition range, or the V_m^E value changes as the compositions of the species in mixture changes. This observation is as a consequence of the different packing arrangements in the solvent. Another reason for negative V_m^E values is due to association or the formation of complexes **(**Dyrkacz, 2001).

Letcher *et al.* (1998) conducted extensive measurements on the excess molar volumes of NMP in binary combination with an alkanol or hydrocarbon at 298.15 K. One of the systems they measured was 1-hexene (1) + NMP (2). All the V_m^E evaluated for these systems were negative. Even though all excess molar volumes were negative, the region in which the greatest deviation from ideality occurred was between 0.5-0.6 liquid mole fractions of NMP. After conducting extensive research on the NMP molecule in combination with a myriad of components, as well as measurements, Letcher *et al.* (1998) postulate that this deviation in excess molar volumes is an irrefutable indication of association between the highly polar NMP molecule and the polarizable 1-hexene (olefin) as well as a reflection of the complex self-association occurring within the NMP molecule.

A stark observation from the analysis of the experiments and computations of Letcher *et al.* (1998) is that as the measurements for V_m^E graduate from the alkenes to the alkynes the value of this parameter achieves greater negativity. However, it should also be noted that the lower carbon number hydrocarbons in all instances produce greater negative V_m^E than for the hydrocarbons with a higher carbon number of the same family (e.g. C_6H_{12} has more negative V_m^E than C_8H_{16}).

A distinct example of this (Letcher *et al.*, 1998) is for the mixture of NMP + 1-hexene and 1-octene with $V^E_{m,\min}$ at -1.19 $cm^3.mol^{-1}$ at $x_1 = 0.518$ and -0.53 $cm^3.mol^{-1}$ at $x_1 = 0.603$, for those systems respectively. The $V^E_{m,\min}$ for the mixture of NMP + 1-hexyne and 1-octyne is: -1.72 $cm^3.mol^{-1}$ at $x_1 = 0.451$ and -1.12 $cm^3.mol^{-1}$ at $x_1 = 0.487$, respectively. When alkanes and NMP were investigated, negative V^E_m data are also reported, however, these are not as negative as for the alkenes and alkynes.

To minimize the negative volumes arising as a consequence of the associative effects with mixtures containing NMP application of the Flory-Benson-Treszczanowicz (FBT) or the Extended Real Association Solution (ERAS) models is recommended.

An explanation of the FBT model entails taking into consideration the contribution of two factors, the association between the NMP and alkene/ alkane molecules and the self association of the NMP molecule. The Mecke-Kempter continuous association model is utilized by Letcher *et al.* (1998) to evaluate the self-association effects. The interaction effects between the complex NMP molecule and the alkenes and alkynes are dealt with via the use of the Flory theory.

The ERAS theory utilizes the real associated solution model with a free volume contribution via the utilization of the Flory's EoS (Letcher *et al*., 1998). In all instances, where Letcher *et al*. (1998) investigated the effect of the use of the FBT theory and the ERAS models, the calculated V^E_m for both the aforementioned models compared extremely well to the experimentally measured V^E_m. Overall the ERAS model proved to be the most accurate as the data calculated is of the same sign and closest in magnitude to the experimental data.

From the above discussion, the negative V^E_m in the systems of interest occurs, due to (Dyrkacz, 2001):

1) The 1-hexene and n-hexane forming association complexes with the NMP molecule in the binary and ternary solutions.

2) The NMP molecule is self-associating (Letcher *et al.,* 1998).

3) The n-hexane and 1-hexene molecules fit precisely into the empty spaces of the NMP structure, in such a way that even though the volumes of the n-hexane and 1-hexene molecules change with composition, a total increase in solution volume is not affected due to the negligible effect of the non-polar molecules.

4) The fourth, and most unlikely possibility, is that the NMP structure minimizes (in essence shrinks/ becomes more compact) due to its dilution with 1-hexene and n-hexane.

The fourth option is improbable and shall not be considered as the addition of an inert component to associating species shall result in either positive or negative deviations from ideality. In the study where cyclohexane was added to NMP (Dyrkacz, 2001) positive excess volumes are observed. Thus, it is sufficiently acceptable to conclude that the addition of an inert solute to NMP will not result in the formation of a more compact NMP structure causing the negative volumes.

1.1.2. n-Hexane

This compound belongs to the chemical family of alkanes, is non-polar and has the formula, C_6H_{14}. The structure of n-hexane is:

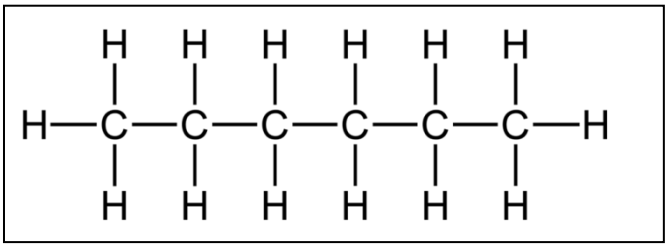

Figure 1-2: n-Hexane structure (Internet source: webbook.nist.gov, 2011).

At room temperature n-hexane is a clear, colourless liquid with a petroleum-like odour. It is a saturated hydrocarbon and therefore unreactive. It is also easily evaporated due to its low boiling point of 342 K. n-Hexane is produced primarily via the refining of crude oil. There is no great deal of electronegativity difference between the carbon and hydrogen atoms of alkanes. Thus, the

molecules have no appreciable polarity. In order for the non-polar n-hexane to dissolve in the polar NMP, heat energy is applied to break up the Van der Waals intermolecular dispersion forces (Internet source: Chemguide, 2011).

1.1.3 1-Hexene

This chemical component is a clear, colourless liquid. It has the chemical formula C_6H_{12} and belongs to the chemical family of alkenes or otherwise known as higher olefins and is also non-polar. The double bond, in the 1-hexene structure, occurs on the primary carbon atom. This is why the 1-hexene is referred to as an alpha-olefin. The location of the double bond has an effect on the 1-hexene molecule as it provides it with a greater reactivity. The chemical structure of 1-hexene is shown:

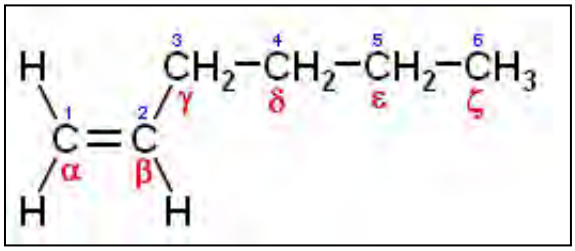

Figure 1-3: 1-Hexene structure (Lappin *et al*., 1989).

There are many approaches to the production of 1-hexene. The most popular are (Lappin *et al*., 1989):

(1) the oligomerization of ethane;
(2) the dehydration of alcohol and;
(3) the thermal cracking of waxes.

The attractive forces between the molecules of alkenes are Van der Waals dispersion forces. As stated above for the case of n-hexane, in order for the non-polar 1-hexene to dissolve in a polar solvent (NMP), heat energy must be applied.

Chapter 2: Thermodynamic Principles of Vapour-Liquid Equilibrium

One possible definition of equilibrium is the state of a system when it is static, where no changes occur with regards to the macroscopic properties over a length of time. The chemical potentials bring about change, thus when equilibrium is established, the chemical potentials of the system are balanced. When dealing with isolated systems (such as the VLE stills employed in subsequent experiments undertaken), there is great contact between the liquid and vapour phases, as such the pressure, temperature and vapour-liquid compositions reach a certain value and thereafter remain constant, even when greater heat is applied to the system. Thus, in such an instance equilibrium would be assumed. In the field of thermodynamics, equilibrium is assumed when the fluctuation in the reading of a property is monitored (example: temperature or pressure) and it oscillates within a tolerable range for approximately 20-50 minutes. This assumption is acceptable, as it does not significantly affect engineering calculations, and also results in satisfactory precision.

Even though one may assume equilibrium when system properties reach a point of stability, the system is still dynamic on a microscopic level. The molecules of the liquid and vapour phase are constantly interchanging. Molecules near the frontier of the surface with a high enough velocity may overcome the surface forces presiding and subsequently pass into the other phase. The average rate at which these molecules cross the interface in both the directions is approximately equivalent, thus it is safe to assume that the net transfer of molecules across the phase boundary is negligible.

The intention of this chapter is to provide insight into the thermodynamic background of VLE, as well as to discuss the procedure of low to medium pressure VLE data modeling and analysis. The technique utilized for determining the fugacity and activity coefficients, together with the regression and correlation of the experimental data is discussed. The two methods employed for the modeling of VLE data are the direct (ϕ-ϕ) and combined (ϕ-γ) methods. Thermodynamic consistency tests are also discussed in the latter portion of this chapter. The thermodynamic relationships exhibited in this chapter were all obtained from Smith *et al.* (2001). Further detailed derivations are available in Appendix A and the original publications which are referenced.

2.1 The Criterion for Phase Equilibrium

For a single-phase, open system case, molecules are able to move in and out of the system easily. Therefore, *nG* will become dependent upon the quantity of moles (*n*) of the chemical components (*i*) present in the system. The Gibbs energy still remains a function of temperature and pressure and the subsequent relation is:

$$nG = g(P,T,n_i) \tag{2.1}$$

$$d(nG) = \left[\frac{\partial(nG)}{\partial P}\right]_{T,n} dP + \left[\frac{\partial(nG)}{\partial T}\right]_{P,n} dT + \sum_i \left[\frac{\partial(nG)}{\partial n_i}\right]_{P,T,n_j} dn_i \tag{2.2}$$

The definition of the chemical potential of a species *i* in the mixture is represented as:

$$\mu_i = \left[\frac{\partial(nG)}{\partial n_i}\right]_{P,T,n_j} \tag{2.3}$$

$$d(nG) = (nV)dP - (nS)dT + \sum_i \mu_i dn_i \tag{2.4}$$

Using the concept of chemical potential, it can be shown that at equilibrium

$$\mu_i^{\alpha} = \mu_i^{\beta} = ... = \mu_N^{\pi} \tag{2.5}$$

where: i = 1, 2, 3, …….., N

The complete derivation for equation (2.5) is provided in Smith *et al*. (2001).

2.2 Fugacity and Fugacity Coefficient

Chemical potential is an important criterion for determining phase equilibrium. However, it is defined in terms of thermodynamic quantities (internal energy and entropy) which are immeasurable. Fugacity is a property which may be related to chemical potential, at constant temperature, by the following equation:

$$\overline{G_i} = \Gamma_i(T) + RT \ln f_i \tag{2.6}$$

$$\overline{G_i} = \left[\frac{\partial(nG)}{\partial(n_i)} \right]_{T,P,n_j} \tag{2.7}$$

Using the concept of fugacity, one can also prove that for a closed system at equilibrium all phases within the system are at constant temperature, thus:

$$f_i^{\alpha} = f_i^{\beta} = ... = f_i^{\pi} \qquad \text{(i =1, 2, …, N)} \tag{2.8}$$

Similarly for species in solutions, the fugacity of a species *i* is:

$$\hat{f}_i^{\alpha} = \hat{f}_i^{\beta} = ... = \hat{f}_i^{\pi} \tag{2.9}$$

Equation (2.9) can be written for two phases, vapour and liquid, in equilibrium in the special case where multiple components are involved:

$$\hat{f}_i^{L} = \hat{f}_i^{V} \qquad \text{(i=1, 2,……, N)} \tag{2.10}$$

The fugacity coefficient is represented by the following equation:

$$\phi_i = \frac{f_i}{P} \tag{2.11}$$

The characterization of fugacity coefficient for a pure species, ϕ_i is extended to include the fugacity coefficient of species *i* in solution, $\widehat{\phi}_i$ (Smith *et al*., 2001). The fugacity of components in solution or a mixture may be expressed for the vapour and liquid phase as follows:

$$\widehat{f}_i^V = \widehat{\phi}_i y_i P \tag{2.12}$$

$$\widehat{f}_i^L = x_i \gamma_i f_i \tag{2.13}$$

γ_i = activity coefficient of species *i* in solution

When a change of state occurs from a saturated liquid to a saturated vapour, with both the vapour and liquid phase at temperature *T* and at vapour pressure P^{sat}, the following equation is obtained:

$$f_i^V = f_i^L = f_i^{sat} \tag{2.14}$$

As a consequence, the corresponding fugacity coefficient is:

$$\phi_i^{sat} = \frac{f_i^{sat}}{P_i^{sat}} \tag{2.15}$$

Subsequently:

$$\phi_i^V = \phi_i^{L}{}_i = \phi_i^{sat} \tag{2.16}$$

For a particular species, *i*, in solution at a constant composition and temperature, the fundamental property relation for Gibbs excess energy, $dG = VdP - SdT$, reduces to:

$$dG_i = V_i\,dP \tag{2.17}$$

Differentiation of the equation for fugacity of a real fluid: $G_i = \Gamma_i(T) + RT\ln f_i$ yields:

$$dG_i = RTd\ln f_i \tag{2.18}$$

Equating (2.17) and (2.18), to eliminate *d*Gi, the following is obtained:

$$d\ln f_i = \frac{V_i}{RT}dP \tag{2.19}$$

Equation (2.19) is isothermally integrated from an initial condition of saturated liquid to a final state of compressed liquid at a certain pressure P, to obtain the equation below:

$$\ln\frac{f_i}{f_i^{sat}} = \frac{1}{RT}\int_{P_i^{sat}}^{P} V_i\,dP \tag{2.20}$$

The liquid-phase molar volume (V_i^L) is weakly dependent upon pressure (P) at temperatures significantly below the critical temperature (T_c). Thus, a fairly accurate approximation in calculations is obtained when V_i^L is assumed constant at the value for saturated liquid. Therefore, considering the effects of pressure negligible, equation (2.20) simplifies to:

$$\ln\frac{f_i}{f_i^{sat}} = \frac{V_i^l\left(P - P_i^{sat}\right)}{RT} \tag{2.21}$$

Substituting equation (2.15) in (2.21) and solving for f_i yields:

$$f_i = \phi_i^{sat}P_i^{sat}\exp\left[\frac{V_i^l\left(P - P_i^{sat}\right)}{RT}\right] \tag{2.22}$$

The exponential term in (2.22) is referred to as the Poynting factor. It allows for the correction of liquid phase fugacity from saturated vapour pressure to the system pressure (Narasigadu, 2006). The Poynting factor approaches unity, differing by only a few parts per thousand, when the variation between the system pressure and the liquids saturation pressure is very small. This arises at low to moderate pressures. In such a scenario the Poynting factor may be omitted, as the error summed in calculations would be negligible. This, however, is not applicable to polar compounds (eg. carboxylic acids) and strongly associating compounds (Prausnitz et al., 1980).

Combining (2.12) and (2.13) and solving for f_i:

$$y_i \Phi_i P = x_i \gamma_i P_i^{sat} \tag{2.23}$$

With:

$$\Phi_i = \frac{\hat{\phi}_i}{\phi_i^{sat}} \tag{2.24}$$

Substituting (2.23) in (2.22) yields:

$$\Phi_i = \frac{\hat{\phi}_i}{\phi_i^{sat}} \exp\left[\frac{-V_i^l\left(P - P_i^{sat}\right)}{RT}\right] \tag{2.25}$$

V_i^l may be evaluated by using the Rackett (1970) equation:

$$V_i = (V_c)_i (Z_c)_i^{[1-(T_r)_i]^{0.285}} \tag{2.26}$$

$T_{r,i}$ is the reduced temperature ($T_{r,i} = \frac{T_i}{T_{c,i}}$)

V_c is the critical molar volume.

T_c is the critical temperature of component i

Z_c is the compressibility factor.

2.3 Equations of State

2.3.1 Virial Equation of State

A multitude of methods are accessible to determine the fugacity coefficient of species in gaseous mixtures. Among the myriad of methods is the virial equation of state (EoS). The theoretical basis of the virial EoS is statistical mechanics and it is also represented by the Taylor series expansion. The virial EoS may be aptly assumed to suitably describe the vapour phase at low to moderate pressures and it may also be utilized to evaluate the fugacity coefficient. The virial equation of state consists of an infinite power series expansion, thus, it is impractical to apply it to realistic exercises. As a consequence, the virial EoS is truncated to varying degrees depending upon pressure and temperature (Narasigadu, 2006). The generalized and pressure explicit representation of the virial EoS, once truncated (after the second term), adequately describes the vapour phase at sub-critical temperatures and pressures up to 15 bar (Perry and Green, 1997).

The equation is as follows:

$$Z = 1 + \frac{BP}{RT} \tag{2.27}$$

Z is the compressibility factor, $\frac{PV}{RT}$

B is the second virial coefficient

The mixture second virial coefficient (B) is a strong function of composition and temperature. Its exact value may be acquired via the application of statistical mechanics. The equation rendering this composition dependence is:

$$B_{mixture} = \sum_i \sum_j y_i y_j B_{ij} \tag{2.28}$$

where: i, j represent species components

y signifies the mole fractions of species in the gas mixture

B_{ij} is the cross virial coefficient

B_{ij} represents a bimolecular interaction between the molecules i and j. Thus,

$B_{ij} = B_{ji}$

For a binary mixture equation (2.28) expands to present:

$$B_{mixture} = y_1^2 B_{11} + 2y_1 y_2 B_{12} + y_2^2 B_{22} \tag{2.29}$$

B_{11} and B_{22} are the mixture pure species virial coefficients. B_{12} is the mixture cross coefficient. Both these virial coefficients are dependent upon temperature only. Since mixture coefficients to pure species and cross coefficients are connected by equations (2.28) and (2.29), these expressions are referred to as *mixing rules.*

Expression (2.29) is modified into the latter equation as a consequence of the assumption that the truncated virial equation of state describes the vapour phase:

$$\Phi_i = \exp\left[\frac{\left(B_{ii} - V_i^l\right)\left(P - P_i^{sat}\right) + P y_j^2 \delta_{ij}}{RT}\right] \tag{2.30}$$

$$\delta_{ji} = 2B_{ji} - B_{jj} - B_{ii} \tag{2.31}$$

The second virial coefficient for mixtures, B_{ij}, and for pure species, B_{ii}, may be evaluated using various experimental methods. A variable volume apparatus may be employed in measuring pressure, temperature and volume (Ramjugernath, 2000). The necessary second virial coefficients are available in compilations such as those by Dymond and Smith (1980) and

Cholinski *et al*. (1986). However, experimental data at a specific temperature and of the required species is often very difficult to obtain. Therefore, in order to obtain an adequate level of accuracy, an appropriate correlation is used to determine the second virial coefficient. The correlations available are: Black (1958), O"Connell and Prausnitz (1967), Nothnagel *et al.* (1973), Tsonopoulos (1974) and Hayden and O"Connell (1975).

The correlation of Hayden and O"Connell (1975) was selected for use in the determination of the second virial coefficients. It provides a simple technique for determining the necessary coefficients for a vast array of compounds, with the input being the components critical properties and molecular parameters.

2.3.2 Hayden and O'Connell Correlation

It has been proven that the various types of intermolecular forces contribute to the second virial coefficient in different and markedly distinct ways. The Hayden and O"Connell (1975) predictive correlation was developed based on the intermolecular interactions that exist between pairs of molecules. This technique is also more accurate in the sense that, for strongly associating substances, it makes excellent predictions of the association and solvation effects of higher densities in a realistic and practical manner, as well as incorporating the chemical theory of dimerization. This is achieved via the utilization of a parameter which is dependent only on the group interaction (Hayden *et al.,* 1975).

The total second virial coefficient is purported to be the sum of several individual contributions:

$$B_{total} = B_{free} + B_{metastable} + B_{bound} + B_{chem} \qquad (2.32)$$

B_{free} is contributions by free pairs of non-polar and non-association molecules

B_{chem} is chemical bonds of molecules

$B_{metastable}$ provides for metastable bound molecular pairs

B_{bound} is the types of interactions between the pairs of molecules as a consequence of potential energy and the distance between the centre of molecules, as well as physically strongly bound pairs of molecules

For further information on the derivation of the model the reader is referred to the publication of Prausnitz *et al*. (1980) and Hayden and O'Connell (1975).

The inputs required to model measured data using this correlation are: critical pressure P_c, critical temperature T_c, Thompson's mean radius of gyration R_d, or the parachor, dipole moment, μ, solvation and association parameters η (Hayden and O'Connell, 1975). These parameters may be obtained from literature resources such as Fredenslund *et al.* (1977), Reid *et al.* (1988), Prausnitz *et al.* (1980) and Dortmund Data Bank (DDB, 2011). Dipole moments may be obtained in two different ways; either via a calculation procedure using the method proposed by Smyth (1955) or one may refer to literature (McClellan, 1974). The mean radius of gyration is evaluated employing a property referred to as the parachor, P'. The parachor parameter is computed utilizing a group contribution method (Reid *et al.,* 1988). The mean radius of gyration and the parachor are related by the following equation developed by Harlacher and Braun (1970):

$$P' = 50 + 7.6R_d + 13.75R_d^2 \tag{2.33}$$

Firstly, P' is evaluated using a group contribution method as stipulated above. Thereafter, this value is substituted in equation (2.33) and the roots of the equation are evaluated. The positive root is the mean radius of gyration.

The relevant association and solvation parameters may be obtained from tables available in Prausnitz *et al*. (1980). In the event that certain parameters are not available in Prausnitz *et al*. (1980), then it is suggested by Fredenslund *et al.* (1977) that the association and solvation parameters for pure halogenated alkanes, sulphides, ethers and hydrocarbons be set equal to zero. Prausnitz *et al*. (1980) has recommended that the values of parameters for chemically similar systems be employed. In the case of interaction between components in a mixture, Hayden and O'Connell (1975) propose that the association and solvation parameters n_{ij} be set to zero except in the event of chemically similar components.

2.3.3 Cubic Equation of State (CEoS)

Cubic equations of state are a more convenient approach capable of accurately describing both the liquid and vapor behaviour. This is due to the fact that the cubic EoS presents a compromise between detailed general applicability and simplicity. The first realistically applicable EoS was presented by J.D. van der Waals in 1873. This EoS took into consideration the attractive forces between molecules as well as the non-zero size of molecules. The van der Waals EoS constitutes two positive constants, *a* and *b*. Depending on the components involved, these constants have different values. Using these constants one may evaluate the pressure (*P*) as a function of volume for diverse values of temperature (*T*).

The van der Waals model is better suited to highly ideal systems; this is due to the fact that the model parameters are not functions of temperature. In addition, the calculation procedure treats the attractive forces between molecules in a very simplified manner.

The first momentous adaptation of the van der Waals EoS was in 1949, the Redlich-Kwong EoS. This enabled improved representation of non-ideal systems. However, one definitive short fall of this method was its poor representation of liquid phase behavior. Over the decades improved techniques for predicting vapour-liquid equilibrium data have been developed. Among the many available the Soave-Redlich-Kwong (SRK) and the Peng-Robinson (PR) equations of state are the most frequently used for non-polar and slightly polar systems. If a suitable mixing rule is employed in conjunction with these equations of state, then systems exhibiting a high level of non-ideality can be accurately described (Anderko, 1990).

2.3.3.1 Popular EoS: Soave-Redlich-Kwong (SRK) and Peng Robinson (PR)

Among the very first modifications made to the Van der Waals (1873) EoS, was that of Redlich-Kwong (1949) followed by Soave (1972). These modifications remain to this day one the most successful equations of state in application. However, even though these are the most frequently used for their accuracy, they too have deficiencies. The Peng and Robinson (1976) EoS postulates that the Redlich-Kwong (1949) and Soave (1972) EoS fail to produce adequate liquid density results for systems under investigation (Narasigadu, 2006). In this regard, the Peng-

Robinson EoS had improved its predictions of liquid density via the inclusion of a more detailed equation representing the volume dependency of the systems being measured. In addition, the Peng-Robinson EoS integrated a binary interaction parameter to more accurately predict data.

In the year 1972, the modifications made by Soave to the original Redlich-Kwong EoS by substituting a temperature dependent function $a(T)$ for $a/T^{0.5}$ lead to the significant improvement of pure substance saturate pressure. This contributed to making the prediction of vapour-liquid equilibria for mixtures a viable option (Mingjian *et al*., 2007).

The original alpha function in the SRK EoS is very sensitive to critical properties. As such a revised alpha function, equation (2.40), was developed to improve accuracy in vapour-liquid equilibria data prediction. In all the comparisons it was found that the new alpha function rendered better results (Mingjian *et al*., 2007). Grabosik and Daubert (1978) revised the alpha constant in the SRK EoS. Mathias and Copeman (1983) developed a new expression for the alpha function, however, with a distinct disadvantage being the 3 constants required for each component (Mingjian *et al*., 2007).

It was found that the alpha expressions proposed by the former researcher‟s bear results with no significant improvement from the expression proposed by Soave, and these later equations representing the alpha function are consequently not considered. In addition, a significant improvement to the expression for the alpha function was later postulated by Twu *et al.* (1995). This new expression renders improved approximations of vapour pressures at low temperatures (Lilwanth, 2011).

Table 2-1: Summary of SRK and PR equation of state.

SRK EoS	**PR EoS**
Defining equation: $P = \frac{RT}{V-b} - \frac{a(T,\omega)}{V(V+b)}$ (2.34)	Defining equation: $P = \frac{RT}{V-b} - \frac{a(T,\omega)}{V(V+b)+b(V-b)}$ (2.46)
$a\ (T,\omega) = a_c \alpha\ (T,\omega)$ (2.35)	$a_i(T,\omega) = a_{c\,i}\alpha_{\ i}(T,\omega)$ (2.47)
$a_c = 0.42747\left(\frac{R^2T_c^2}{P_c}\right)$ (2.36)	$a_{c\,i} = 0.45724\left(\frac{R^2T_{c_i}^2}{P_{c_i}}\right)$ (2.48)
$\alpha(T,\omega) = \left[1+\kappa\left(1-T_r^{0.5}\right)\right]^2$ (2.37)	$a_i\{(T_c)_i;\omega_i\} = \left[1+\kappa_i\left(1-(T_r)_i^{1/2}\right)\right]^2$ (2.49)
$\kappa = 0.480+1.574\omega-0.176\omega^2$ (2.38)	$\kappa_i = 0.37464+1.54226\omega_i-0.26992\omega_i^{\ 2}$ (2.50)
$b = 0.08664\left(\frac{RT_c}{P_c}\right)$ (2.39)	$b_i(T) = b_i(T_c)_i$ (2.51) $b_i = 0.07780\left(\frac{RT_{c_i}}{P_{c_i}}\right)$ (2.52)
Modified alpha function of Mingjian *et al.*,(2007) $\alpha\ (T,\omega) =$ $1+(0.32877+1.1317\omega)\left(T_r^{-0.5}-T_r\right)$ (2.40)	
Cubic equation in terms of compressibility factor: $Z^3-Z^2+Z(A-B-B^2)-AB=0$ (2.41)	Cubic equation in terms of compressibility factor: $Z^3-(1-B)Z^2+(A-3B^2-2B)Z-(AB-B^2-B^3)=0$ (2.53)

$Z = \frac{PV}{RT}$ (2.42)	
$A = \frac{aP}{R^2T^2}$ (2.43)	$A = \frac{a_m(T)P}{R^2T^2}$ (2.54)
$B = \frac{bP}{RT}$ (2.44)	$B = \frac{b_mP}{RT}$ (2.55)
Pure component fugacity coefficient: $\ln\phi = Z - 1 - \ln(Z-B) - \frac{A}{B}\ln\left[\frac{Z+B}{Z}\right]$ (2.45)	Pure component fugacity coefficient: $\ln\phi = (Z-1) - \ln(Z-B) - \frac{A}{2\sqrt{2}B}\ln\left[\frac{Z+(1+\sqrt{2})B}{Z+(1-\sqrt{2})B}\right]$ (2.56)
	Mixing Rules: $a_m = \sum_i\sum_j x_i x_j a_{ij}$ (2.57) $a_{ij} = (1-\delta_{ij})(a_i a_j)^{0.5}$ (2.58) $b_m = \sum_i x_i b_i$ (2.59) Where: δ_{ij}= the binary interaction parameter

where: T absolute temperature b (T) volume corrector

P pressure

R universal gas constant

V molar volume

a (T) attractive force between molecules

In this study, the alpha function of Mingjian *et al*. (2007) has been employed. This is due to the fact that the modified α allows for improved phase equilibria, giving accurate values for mixtures as well as pure components; it is quite simple to use and may be combined with any mixing rules; it is easy to incorporate the new method in programs and software utilizing the original SRK EoS without the need to make cumbersome changes (Mingjian *et al*., 2007).

Table 2-2: Comparison of SRK and PR EoS.

	SRK EoS	PR EoS
Suitable for which components	non-polar or slightly polar substances	Polar, non-polar, associating and non-associating molecules
Drawbacks/disadvantages	• Cannot precisely generate liquid density values (Narasigadu, 2006). • Does not relate the molecular parameters to the model via a suitable binary interaction parameter (Reddy, 2006).	

An in depth discussion of the mixing rules employed in this thermodynamic study shall be discussed. For the full derivation of the mixing rules refer to Appendix A.

2.4 Mixing Rules

Mixing rules are a core necessity in the implementation of equations of state for the representation of vapour-liquid equilibrium data. The mixing rules used in the equations of state will determine the interaction of molecules in the systems under investigation. There are many different types of mixing rules available for use; however, many are empirical in nature. The simplest mixing rule is known as the van der Waals one-fluid-theory classical mixing rule. This mixing rule is exhibited above in expressions (2.57)-(2.59). A more detailed analysis of the types of mixing rules available in thermodynamics is available in Raal and Mülhbauer (1998).

Due to the dilution effect and the problem of invariance (Hernandez-Gaduza *et al.,* 2001) the extension of mixing rules to systems with multiple components has proven problematic. These limitations were identified by two researchers, Michelsen and Kistenmacher (1990) and this type of problem is referred to as Michelsen-Kistenmacher-Syndrome. Fortunately there are mixing rules, which have been developed, that do not succumb to this type of inadequacy (Narasigadu, 2006), the Twu-Coon (1996) and Wong-Sandler (1992) mixing rules.

2.4.1 Wong-Sandler Mixing Rule

The Wong and Sandler (1992) mixing rule is density independent and accurately correlates VLE data. This mixing rule is suitable for application to both complex and simple systems constituting polar and associating components. The Wong and Sandler (1992) mixing rule is particularly successful because the quadratic composition dependence of the second virial coefficient maintaining consistency with statistical mechanics (Raal and Mühlbauer, 1998) is combined with the excess Gibbs free energy models, such as Wilson and NRTL *etc*. This mixing rule has been widely and successfully applied to equations of state and a recent review is available in Orbey and Sandler (1996).

The Wong and Sandler (1992) mixing rule is combined with an activity coefficient model in order to evaluate the excess Helmholtz free energy (A^E). The utilization of the excess Helmholtz free energy (A^E) at infinite pressure in the correct fashion enables computation of the correct low and high densities without becoming dependent upon density. Wong and Sandler (1992) developed expressions for a_m and b_m as follows:

$$\frac{a_m}{RT} = \frac{QD}{(1-D)} \tag{2.60}$$

$$b_m = \frac{Q}{(1-D)} \tag{2.61}$$

where: „m“ denotes mixture properties

„Q“ and „D“ are evaluated as follows:

$$Q = \sum_i \sum_j x_i x_j \left(b - \frac{a}{RT} \right)_{ij} \tag{2.62}$$

$$D = \sum_i x \frac{a_i}{b_i RT} + \frac{A_\infty{}^E}{cRT} \tag{2.63}$$

The fugacity coefficient for the liquid and vapour phases is determined below as follows:

Soave-Redlich-Kwong EoS (Naidoo, 2004):

$$\ln \hat{\phi}_i = -\ln\left[\frac{P(V-b_m)}{RT}\right] + \frac{1}{b_m}\left(\frac{\partial n b_m}{\partial n_i}\right)\left(\frac{PV}{RT}-1\right) + \left(\frac{a_m}{b_m RT}\right)\left[\frac{1}{a_m}\left(\frac{1}{n}\frac{\partial n^2 a_m}{\partial n_i}\right) - \frac{1}{b_m}\frac{\partial n b_m}{\partial n_i}\right]\ln\left[\frac{V}{V+b_m}\right] \tag{2.64}$$

$$c = -\ln(2) \qquad \text{Soave-Redlich-Kwong} \tag{2.65}$$

Peng-Robinson EoS (Naidoo, 2004):

$$\ln \hat{\phi}_i = -\ln\left[\frac{P(V-b_m)}{RT}\right] + \frac{1}{b_m}\left(\frac{\partial n b_m}{\partial n_i}\right)\left(\frac{PV}{RT}-1\right) + \frac{1}{2\sqrt{2}}\left(\frac{a_m}{b_m RT}\right)\left[\frac{1}{a_m}\left(\frac{1}{n}\frac{\partial n^2 a_m}{\partial n_i}\right) - \frac{1}{b_m}\frac{\partial n b_m}{\partial n_i}\right]\ln\left[\frac{V+(1-\sqrt{2})b_m}{V+(1+\sqrt{2})b_m}\right] \tag{2.66}$$

$$c = \frac{1}{\sqrt{2}}\ln\left(\sqrt{2}-1\right) \quad \text{Peng-Robinson} \tag{2.67}$$

The reader is referred to Appendix A for further information on the partial differentials required for evaluation of the fugacity coefficient.

The activity coefficient at infinite dilution is given by:

$$\ln \gamma_i^{\infty} = \frac{1}{RT}\frac{\partial n A_{\infty}^{E}}{dn_i} \tag{2.68}$$

The excess Helmholtz free energy, A^E, is much less pressure dependent than the excess Gibbs free energy, G^E, according to Wong and Sandler (1992). Therefore, greater accuracy in results is obtained at very low and infinite pressures.

An important feature (Marco and Trebble, 1997) is that due to the fact that A^E is weakly dependent upon pressure, its value at infinite pressure is equivalent to that of G^E at very low pressures. In this sense, utilizing low pressure vapour-liquid equilibrium it is possible to predict

VLE data at high pressures. A further suggestion by Raal and Mühlbauer (1998) is that excess Helmholtz free energy and excess Gibbs free energy are interchangeable at constant temperature.

The NRTL activity coefficient model was selected for use in this project to evaluate A^E at infinite pressure, as well as the activity coefficient at infinite dilution. The final representation of this is:

$$\frac{A_{\infty}^{e}}{RT} = \sum_{i} x_i \left(\frac{\sum_{j} x_j \tau_{ji} g_{ji}}{\sum_{k} x_k g_{ki}} \right) \tag{2.69}$$

$$\ln \gamma_i^{\infty} = \frac{\sum_{j} x_j \tau_{ji} g_{ji}}{\sum_{k} x_k g_{ki}} + \sum_{j} \frac{x_j g_{ij}}{\sum_{k} x_k g_{kj}} \left(\tau_{ij} - \frac{\sum_{l} x_l \tau_{lj} g_{lj}}{\sum_{k} x_k g_{ki}} \right) \tag{2.70}$$

The reader is referred to Appendix A for a detailed description of this mixing rule.

2.4.2 Twu-Coon Mixing Rule

This mixing rule employs the hypothesis of a non-random excess Helmholtz free energy for cubic equations of state representing the vapour-liquid equilibrium behavior of non-polar and polar mixtures. It also enables measurements over a wide range of temperatures and pressures. A distinct advantage of this mixing rule over others is that: when the non-random excess Helmholtz free energy is brought to zero, the Twu-Coon (1996) mixing rule simplifies to the van der Waals one-fluid mixing rule. With the conventional Wong-Sandler mixing rule, a singularity problem was encountered at supercritical conditions. However, this is avoided with the Twu-Coon mixing rule (1996). Another advantage of this mixing rule is its applicability to both simple and complex systems; such as those containing hydrocarbons and inorganic gases.

The „*b*“ parameter in the Twu-Coon (1996) mixing rule is described as:

$$b^{*} = \frac{b_{vdw} - a_{vdw}}{\left(\frac{a_{vdw}}{b_{vdw}} + \frac{1}{c} \frac{A_{\infty}^{E}}{RT} \right)} \tag{2.71}$$

The „*a*“ parameter is defined as:

$$a^* = b^*\left(\frac{a_{vdw}}{b_{vdw}} + \frac{1}{c}\frac{A_\infty^E}{RT}\right) \tag{2.72}$$

The a_{vdw} and b_{vdw} parameters as per the van der Waals mixing rule are depicted as:

$$a_{vdw} = \sum_i \sum_j x_i x_j \sqrt{a_i a_j}\left(1 - k_{ij}\right) \tag{2.73}$$

$$b_{vdw} = \sum_i \sum_j x_i x_j \left[\frac{1}{2}\left(b_i + b_j\right)\right]\left(1 - l_{ij}\right) \tag{2.74}$$

The parameters **a^* and b^*** are evaluated as follows:

$$a^* = \frac{aP}{R^2T^2} \tag{2.75}$$

$$b^* = \frac{bP}{RT} \tag{2.76}$$

The fugacity coefficient expressions for the liquid and vapour phases are shown below as:

Peng-Robinson EoS (Naidoo, 2004):

$$\ln\hat{\phi}_i = -\ln\left[\frac{PV}{RT} - b^*\right] + \frac{1}{b}\left(\frac{\partial nb}{\partial n_i}\right)\left(\frac{PV}{RT} - 1\right) - \frac{1}{2\sqrt{2}}\left(\frac{a^*}{b^*}\right)\left[\frac{1}{b}\frac{\partial nb}{\partial n_i} - \left(\frac{1}{na}\frac{\partial n^2 a}{\partial n_i}\right)\right]\ln\left[\frac{V + (1-\sqrt{2})b^*}{V + (1+\sqrt{2})b^*}\right] \tag{2.77}$$

Soave-Redlich-Kwong EoS (Naidoo, 2004):

$$\ln\hat{\phi}_i = -\ln\left[\frac{PV}{RT} - b^*\right] + \frac{1}{b}\left(\frac{\partial nb}{\partial n_i}\right)\left(\frac{PV}{RT} - 1\right) + \left(\frac{a^*}{b^*}\right)\left[\frac{1}{b}\frac{\partial nb}{\partial n_i} - \left(\frac{1}{na}\frac{\partial n^2 a}{\partial n_i}\right)\right]\ln\left[\frac{V + b^*}{V}\right] \tag{2.78}$$

The „Q" and „D" parameters are defined as follows:

$$Q = b_{vdw} - \frac{a_{vdw}}{RT} \tag{2.79}$$

$$D = \frac{a_{vdw}}{b_{vdw}} + \frac{1}{c}\frac{A_{\infty}^{E}}{RT} \tag{2.80}$$

For the full derivation of the Twu-Coon Mixing Rule refer to Appendix A.2.

2.5 Activity Coefficient

Non-idealities within the liquid phase of mixtures are best represented with the introduction of an activity coefficient model. The basis for the definition of the activity coefficient model is to properly detail the standard state fugacity. Therefore, the reference point needs to be specified, *i.e.* the ideal solution. Deviations from ideality are then quantified via the utilization of excess functions. The activity coefficient for a component *i* in solution is given by:

$$\gamma_i = \frac{\hat{f}_i}{x_i f_i^{o}} \tag{2.81}$$

The Gibbs-Duhem equation may be represented in terms of activity as follows:

$$d\left(\frac{nG^{E}}{RT}\right) = \frac{nV^{E}}{RT}dP - \frac{nH^{E}}{RT^{2}}dT + \sum_i \ln\gamma_i dn_i \tag{2.82}$$

For full details on this derivation, refer to Smith *et al*. (2001).

By substituting equation (2.81) in (2.82), the summability relationship may then be simplified to be expressed in terms of the excess properties as follows:

$$\sum_i x_i \, d\ln\gamma_i = \frac{\overline{V}^E}{RT} dP - \frac{\overline{H}^E}{RT^2} dT \tag{2.83}$$

At the physical conditions of constant temperature and pressure, equation (2.83) reduces to:

$$\sum_i x_i \, d\ln\gamma_i = 0 \tag{2.84}$$

2.5.1 Excess Gibbs Energy Activity Coefficient Models

There are a multitude of models available for the description of liquid phase deviations from ideality. Difficulty arises in attempting to analyze the varying systems behaviours, and the greater the difference in components chemical nature as well as molecular size, warrants the application of more complex modeling (Lilwanth, 2011).

The most common liquid activity coefficient models are:

- Van Laar
- NRTL (Non-Random Two Liquid)
- UNIQUAC (Universal Quasi-Chemical Theory)
- Wilson

For this specific study, only the NRTL and UNIQUAC models will be applied as studies performed previously, with regards to the same systems measured in this work, acknowledged these models as the best to represent the liquid phase non-idealities. Moreover, a recent study conducted by Hirawan (2007) and Moodley (2009) discovered that the best model for representing the systems studied in this project is the NRTL model. A distinct advantage of the utilization of these models is that they are capable of characterizing both simple as well as complex systems.

2.5.1.1 The Van-Laar Equation

This model is most often applied to non-polar fluids.

$$\ln \gamma_1 = A_{12}\left(\frac{A_{21}x_2}{A_{12}x_1 + A_{21}x_2} \right)^2 \tag{2.85}$$

$$\ln \gamma_2 = A_{21}\left(\frac{A_{12}x_1}{A_{12}x_1 + A_{21}x_2} \right)^2 \tag{2.86}$$

The Gibbs excess energy model is given by:

$$\frac{G^E}{RT} = \frac{A_{12}A_{21}}{A_{12}x_1 + A_{21}x_2} \tag{2.87}$$

Where: A_{12} and A_{21} are adjustable modeling parameters

A very important point to note is that the constants in the Van Laar equations are empirical in nature. Therefore, a more complex model is required to more aptly describe the complex interactions between molecules in the liquid phase for the systems under discussion in this thesis.

2.5.1.2 The Wilson Model

The premise of the thermodynamics of the molecular behavior of liquids in solution is based on the theory of *local composition.* In liquid solutions, there is a distinct difference between the local and overall mixture composition. This noticeable difference is responsible for the short range order and non-random molecular orientations which result as a consequence of the molecular forces between the molecules and the differences in the actual size of molecules. The concept discussed briefly above was developed by G.M. Wilson in 1964. The activity of components in a binary mixture is represented as follows:

$$\ln \gamma_1 = -\ln\left(x_1 + \Lambda_{12}x_2\right) + x_2\left[\frac{\Lambda_{12}}{x_1 + \Lambda_{12}x_2} - \frac{\Lambda_{21}}{\Lambda_{21}x_1 + x_2}\right] \tag{2.88}$$

$$\ln \gamma_2 = -\ln\left(x_2 + \Lambda_{21}x_1\right) - x_1\left[\frac{\Lambda_{12}}{x_1 + \Lambda_{12}x_2} - \frac{\Lambda_{21}}{\Lambda_{21}x_1 + x_2}\right] \tag{2.89}$$

The Wilson adjustable parameters are related to pure component liquid volumes by:

$$\Lambda_{ij} = \frac{V_i}{V_j}\exp\left[\frac{\lambda_{ij} - \lambda_{ii}}{RT}\right] \tag{2.90}$$

where: V_j and V_i = molar volumes of pure liquids at temperature *T*.

λ_{ij} and λ_{ii} = independent of temperature and composition

The equation applicable to binary systems is:

$$\frac{G^E}{RT} = -x_1 \ln\left(x_1 + \Lambda_{12}x_2\right) - x_2\left(x_1\Lambda_{21} + x_2\right) \tag{2.91}$$

where: Λ_{21} and Λ_{12} are the Wilson adjustable parameters

The Wilson equation has two distinct disadvantages (Narasigadu, 2006):

1) It cannot predict the miscibility of liquids and;

2) It is inappropriate for systems wherein a plot of Ln γ vs. x_i gives a maxima or minima.

2.5.1.3 Non-Random Two Liquid (NRTL) Model

Renon and Prausnitz (1968) introduced the concept of the Non-Random Two Liquid model (NRTL). It is a significant improvement to previously developed local composition models. The

NRTL model is capable of representing both complex and simple systems. It also has a distinct advantage over the Wilson model in that it is able to adequately represent partially miscible liquid systems, as well as completely miscible systems. The activity coefficient and G^E expressions are exhibited below:

$$\ln \gamma_1 = x_2^2 \left[\tau_{21} \left(\frac{G_{21}}{x_1 + x_2 G_{21}} \right)^2 + \frac{\tau_{12} G_{12}}{\left(x_2 + x_1 G_{12} \right)^2} \right] \tag{2.92}$$

$$\ln \gamma_2 = x_1^2 \left[\tau_{12} \left(\frac{G_{12}}{x_2 + x_1 G_{12}} \right)^2 + \frac{\tau_{12} G_{21}}{\left(x_1 + x_2 G_{21} \right)^2} \right] \tag{2.93}$$

$$\frac{G^E}{RT} = \frac{\tau_{21} G_{21}}{x_1 + G_{21} x_2} + \frac{\tau_{12} G_{12}}{x_2 + G_{12} x_1} \tag{2.94}$$

where:

$$G_{12} = \exp\left(-\alpha_{12} \tau_{12} \right) \tag{2.95}$$

$$G_{21} = \exp\left(-\alpha_{12} \tau_{21} \right) \tag{2.96}$$

λ_{ij} is represented as:

$$\lambda_{ji} = \exp\left(a_{ij} + \frac{b_{ij}}{T} + c_{ij} \ln T + d_{ij} T + \frac{e_{ij}}{T^2} \right) \tag{2.97}$$

Further,

$$\tau_{12} = \frac{g_{12} - g_{22}}{RT} \tag{2.98}$$

$$\tau_{21} = \frac{g_{21} - g_{11}}{RT} \tag{2.99}$$

In Aspen® Plus the λ_{ij} parameter used above in equations (2.92) and (2.93), is represented as:

$$\lambda_{ij} = a_{ij} + \frac{b_{ij}}{T} + e_{ij} \ln T + f_{ij} T \tag{2.100}$$

There are three adjustable parameters in the NRTL set of modeling equations. They are: (g_{21}-g_{22}), (g_{12}-g_{11}) and α_{12}. The first two terms account for the interactions between the molecules of species *i* and *j*. The last term, α_{12}, characterizes the non-randomness of the mixture. If α_{12} is set to zero, this implies the mixture is entirely random. Regular values for α_{12} fall in the range of -1 to 0.5. It is recommended by Walas (1985) that for aqueous and non-aqueous mixtures the value for α_{ij} should be 0.4 and 0.3 respectively. This conclusion was reached by Walas (1985) based on the regression of data sets from Dechema. Other sources, such as Raal and Mühlbauer (1998), contest this, and suggest that this alpha value should be determined experimentally from data regression.

2.5.1.4 The UNIQUAC Model (Universal Quasi-Chemical Theory)

This model was developed by Abrams and Prausnitz (1975) as a representation of Gibbs excess energy which extends the quasi-chemical theory of Guggenheim. This model constitutes two parts; a combinatorial and a residual part. The combinatorial part represents the athermal contribution such as the sizes and shapes of molecules and the residual part accounts for the energy of interaction between segments. The UNIQUAC equation contains only two adjustable parameters (per binary system) and may be extended for use in polar and non-polar multi-component systems.

For a binary system:

$$\ln \gamma_1 = \ln \frac{\Phi_1}{x_1} + \frac{z}{2} q_1 n \frac{\vartheta_1}{\Phi_1} + \Phi_2 \left(l_1 - \frac{r_1}{r_2} l_2 \right) - q_1' \ln \vartheta_1' + \vartheta_2' \lambda_{21} + \vartheta_2' q_1' \left(\frac{\lambda_{21}}{\vartheta_1' + \vartheta_2' \lambda_{21}} - \frac{\lambda_{12}}{\vartheta_2' + \vartheta_1' \lambda_{12}} \right) \tag{2.101}$$

$$\ln \gamma_2 = \ln \frac{\Phi_2}{x_2} + \frac{z}{2} q_2 n \frac{\vartheta_2}{\Phi_2} + \Phi_1 \left(l_2 - \frac{r_2}{r_1} l_1 \right) - q_2' \ln \vartheta_2' + \vartheta_1' \lambda_{21} + \vartheta_2' q_2' \left(\frac{\lambda_{12}}{\vartheta_2' + \vartheta_1' \lambda_{12}} - \frac{\lambda_{21}}{\vartheta_1' + \vartheta_2' \lambda_{21}} \right) \tag{2.102}$$

$$\lambda_{ji} = \exp \left[\frac{-\left(u_{ji} - u_{ii} \right)}{RT} \right] \tag{2.103}$$

$$\Phi_i = \frac{x_i r_r}{x_1 r_1 + x_2 r_2} \text{ ; Average segment fraction of component i} \quad (2.104)$$

$$\vartheta_i = \frac{x_i q_i}{x_1 q_1 + x_2 q_2} \quad (2.105)$$

$$\vartheta_i' = \frac{x_i q_i'}{x_1 q_1' + x_2 q_2'} \quad (2.106)$$

$u_{12} - u_{22} - u_{21} - u_{11}$ = adjustable parameters

where: u_{ji} = interaction parameter between components in *i* and *j*.

z = coordination number; $\frac{z}{2} = 5$

q_i = area parameter of component *i*

r_i = size parameter of component *i*.

Z = coordination number and equal to 10

$$G^E = G^E \text{(combinatorial)} + G^E \text{ (residual)} \quad (2.107)$$

where: $$\frac{G^E(combinatorial)}{RT} = \sum_i x_i \ln \frac{\Phi_i}{x_i} + \frac{z}{2} \sum_i q_i x_i \ln \frac{\vartheta_i}{\Phi_i} \quad (2.108)$$

$$\frac{G^E(residual)}{RT} = -\sum_i q_i' x_i \ln \left[\sum_j \vartheta_j' \lambda_{ji} \right] \quad (2.109)$$

„r“ and „q“ are pure component molecular structure constants. In the original derivation $q_i = q_i''$, however, Anderson and Prausnitz (1978) later introduced modifications to the original UNIQUAC equation (q_i'') so that better results are obtained for systems containing lower alcohols and water. According to Walas (1985) the UNIQUAC model is better-qualified to represent systems with a vast array of molecular sizes. In addition, it is also applicable to systems which display huge deviations from Raoult“s Law, including polar and non-polar species.

2.6 Data Regression

A vast array of techniques is at one‟s disposal for the reduction of phase equilibrium data. Each technique, which has been rigorously developed, has its advantages as well as disadvantages. The objective of data regression is to condense the large quantities of experimental thermodynamic data into a simple and useable form for future reference.

This is achieved by using correlative thermodynamic models, such as EoS and liquid phase activity coefficient models, to render thermodynamic interaction parameters specific to each individual system being analyzed. Another beneficial aspect of reduction of data is that the interpolation as well as extrapolation of experimental data is possible, thus enabling the prediction of thermodynamic data in areas which are complex to measure. Among the myriad of techniques at one‟s disposable, the two most feasible are the combined method (γ-ϕ) and the direct method ($\phi-\phi$).

2.6.1 Combined Method (γ-ϕ) Regression

This approach employs a suitable EoS model to describe the vapour phase non-idealities, and an activity coefficient model to describe the non-idealities of the liquid phase. The attainment of the model parameters through regression is accomplished by selecting an applicable algorithm. The technique of least squares, by Marquardt (1963) and Gess et al. (1991) is one such approach. This specific technique of regression is based upon minimizing the deviation between the experimental and predicted values. This difference is called the residual and represented by the symbol δ. Pressure, temperature, vapour and liquid composition, excess Gibbs energy and activity coefficients are selected for minimization. The process of regression of experimental data is executed until the minimum value of the objective function is reached (Van Ness and Abbott, 1982). This objective function is expressed as follows:

$$S = \sum (\delta P)^2 \tag{2.110}$$

The regression of isobaric and isothermal data is represented in the figures below. Where isothermal data is available, values for pressure and vapour composition are determined by bubble point pressure iteration. For the isobaric case, temperature and vapour composition values are computed by bubble point temperature iteration. This is executed for each experimental data point.

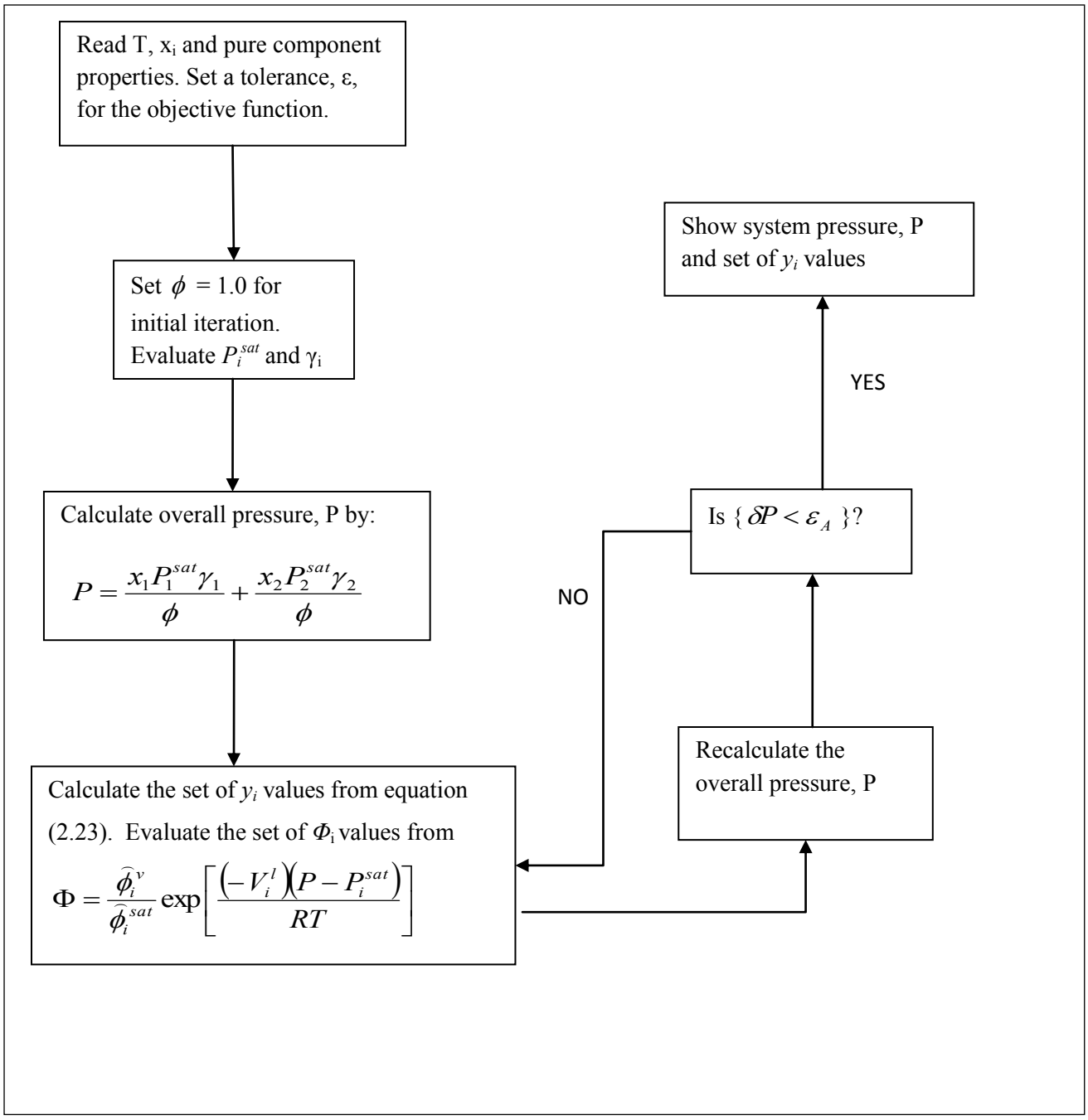

Figure 2-1: Flow diagram for the bubble-point pressure iteration using the combined method (Smith *et al.*, 2005).

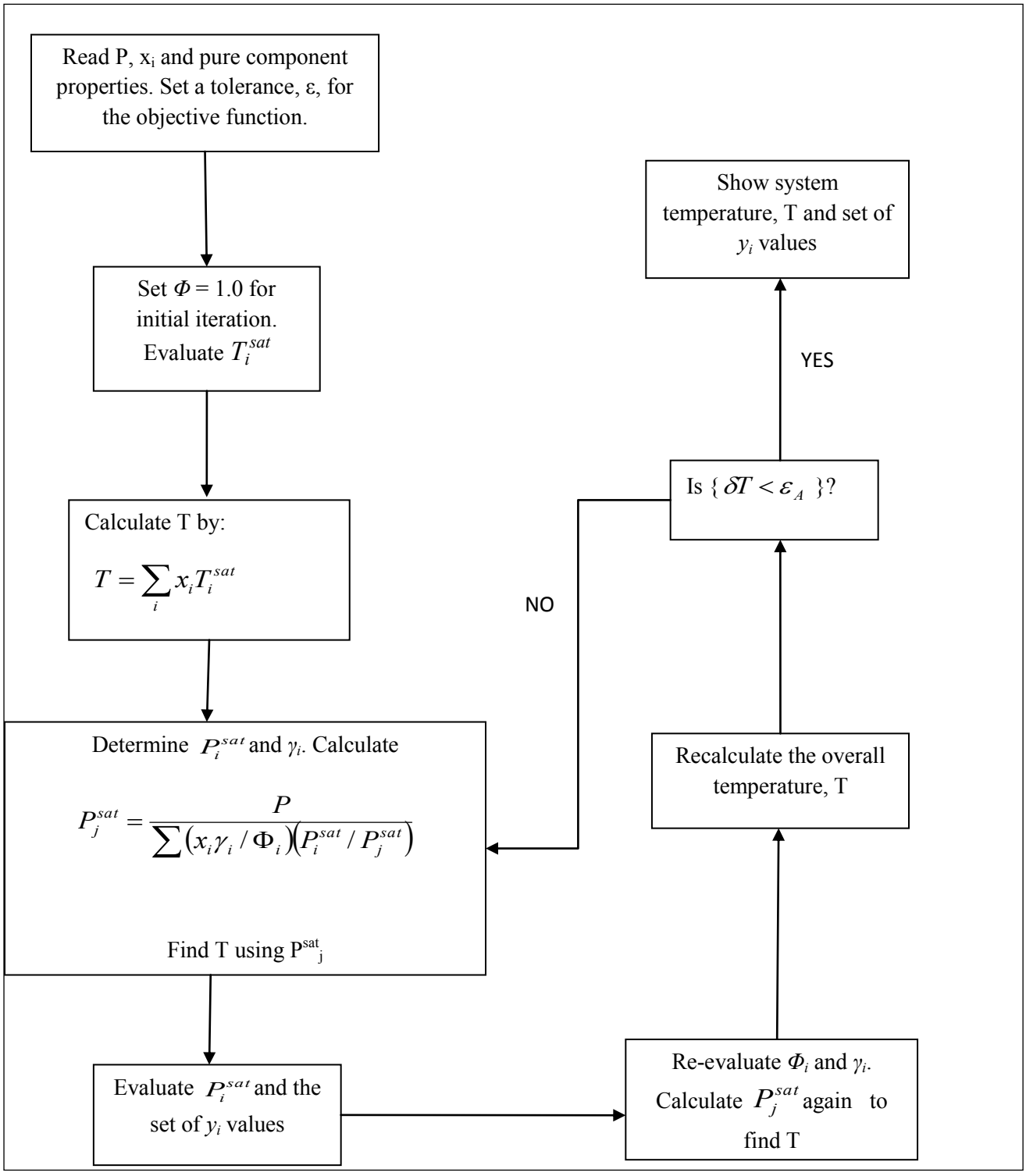

Figure 2-2: Flow diagram for the bubble-point temperature iteration for the combined method (Smith *et al.*, 2005).

2.6.2 Direct Method ($\phi - \phi$)

With this technique, the EoS model represents both the liquid and vapour phase non-idealities. This is accomplished using fugacity coefficients. The equilibrium requirement of equation (2.17) is:

$$x_i \hat{\phi}_i^l = y \hat{\phi}_i^v \tag{2.111}$$

An adequate EoS should be selected so as to justly represent the fugacity coefficients $\hat{\phi}_i^l$ and $\hat{\phi}_i^v$ Thereafter, the best model must be selected to correlate the experimental data. The subsequent two figures illustrate the bubble pressure and the bubble temperature iteration for the direct case.

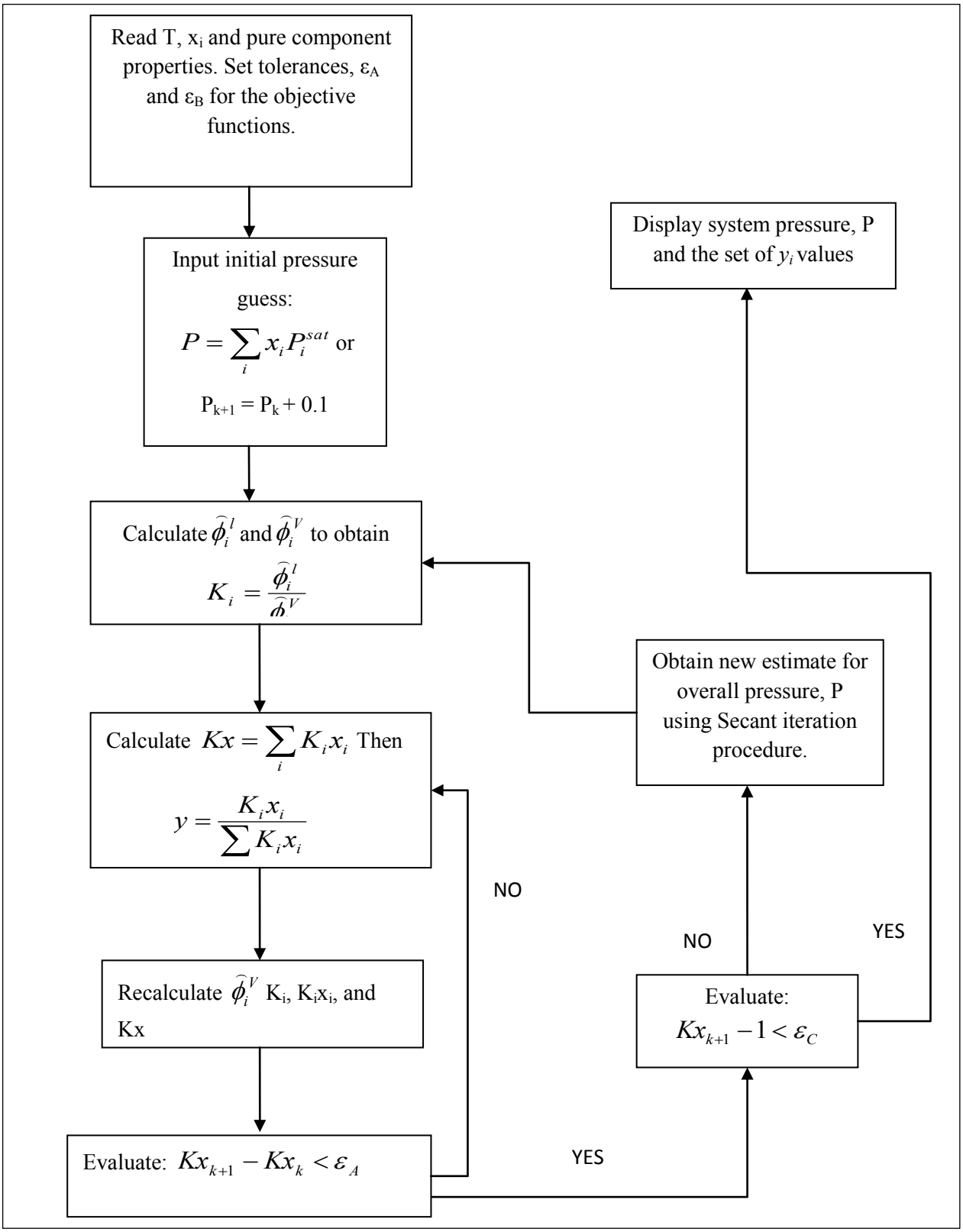

Figure 2-3: Flow diagram for the bubble-point pressure iteration using the direct method (Smith *et al.*, 2005).

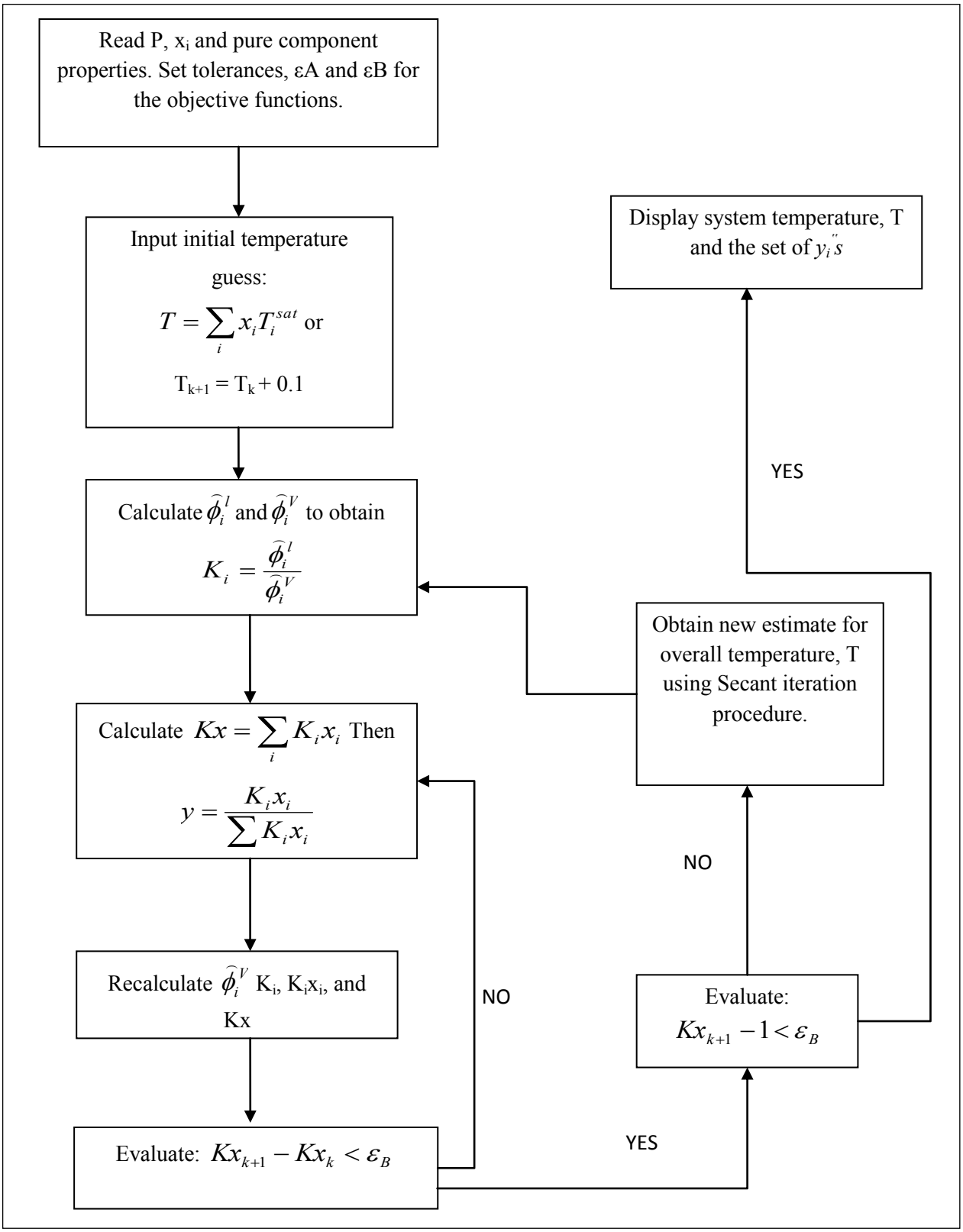

Figure 2-4: Flow diagram for the bubble-point temperature iteration for the direct method (Smith *et al.*, 2005).

2.7 Thermodynamic Consistency Testing

It is important to test the reliability of experimental data via the utilization of a universally accepted method to quantify the integrity of data achieved experimentally. Even though at face value, data may look promising, in actual fact the data could be misleading and of a very poor quality. The four primary consistency tests available are the:

- Slope;
- Area;
- Point and;
- Direct tests.

The point and direct test are the two tests applied to the experimentally measured data in this work, as they are the most stringent and provide the best measure of consistency for thermodynamic data. The Gibbs-Duhem equations were integral in developing the thermodynamic consistency tests. There are four basic quantities which are required in thermodynamic measurements. These are: temperature, pressure and liquid and vapour compositions. However, it is not necessary to specify all of the aforementioned quantities. Any one of these quantities may be determined from the other specified variables employing the Gibbs-Duhem equations. If data satisfies the requirements of the consistency tests, then the measured experimental data may be considered thermodynamically consistent, and it is generally accepted that the data should be of a good quality and reliable. Even though data may satisfy the Gibbs-Duhem equation it is probable that the experimental data is correct, however, there have been instances where data passes the consistency tests and yet is incorrectly assumed to be consistent (Jackson and Wilsak, 1995).

2.7.1 Point Test

The point test utilized for the evaluation of experimental accuracy in this thesis was derived by Van Ness *et al.* (1973). It was introduced as an improvement to the area test. The premise of the point test is the over-specification of variables (*i.e.* temperature, pressure, and liquid and vapour composition). Thus, any one of the aforementioned variables may be evaluated via data regression, and subsequently be compared to the measured experimental data, testing the accuracy. It has been collectively agreed upon by scientists that the vapour composition measurements usually introduce the largest error, thus, it is this variable that is regressed for (Smith *et al*., 2001) to monitor the internal consistency of the system. The thermodynamic point test compares the measured vapour composition (experimental) data to the regressed vapor composition data (calculated). The equation representing this quantitative criterion is:

$$\Delta y_{AAD} = \frac{1}{n}\sum\left[\frac{\left|y_{\exp} - y_{calc}\right|}{y_{\exp}}\right] \qquad (2.112)$$

n is the number of data points obtained experimentally.

When isothermal *P-x-y* data is measured, the regressed y_i values are determined using only the *T-x* data. This is accomplished through the application of Barker‟s method (as per the explanation in § 2.6.1 and § 2.6.2). In this approach, the pressure residual is the objective function. Any errors in the system are transferred to the residual for y_i. Thus, if the y_i data is found to be thermodynamically consistent, this implies the T and x_i data used to regress for the calculated vapour composition are also consistent.

In order for the point test to be considered successful, the following criteria should be met:

- The average absolute deviation ($\left|\Delta y_{AAD}\right|$) of the vapour composition should be less than or equal to a value of 0.01 (Danner and Gess, 1990).

- In some instances, though the ($\left|\Delta y_{AAD}\right|$) may be less than or equivalent to 0.01, the vapour composition residuals ($y_{exp} - y_{calc}$) when plotted against the experimental x_i data

may show a bias present, *i.e.* the points do not scatter randomly about the x-axis. This bias, either positive or negative, would imply there exists severe errors in the system measurements. These errors could be due to any number of reasons such as, the technique employed when measuring the data experimentally, the fugacity coefficient, and activity coefficient or vapour pressure models not fitting the experimental data to a satisfactory extent.

In some instances, certain vapour composition residuals in a data set will possess a value above 0.01, however, the same data set may still be considered consistent if the ($\left|\Delta y_{AAD}\right|$) ≤ 0.01. According to Bradshaw (1985), the experimental data must be suitably represented by an appropriate activity coefficient model and EoS. The thermodynamic model should meet the following specifications:

- the model must be malleable enough such that the accuracy of the calculated binary/adjustable parameters is preserved during the reduction of the experimental data.

- errors stemming from the thermodynamic model implemented should be less than the errors accrued from the experimental technique.

Further, Jackson and Wilsak (1995) recommend the drafting and analysis of three fundamental plots of:

- P-x_i-y_i experimental data against the calculated data using thermodynamic models;

- Pressure residual (P_{exp} - P_{calc}) vs. liquid composition (x_i) and;

- Vapour composition residual ($y_{exp} - y_{calc}$) vs. liquid composition (x_i).

The first two plots give an estimation of how well the modeled data fit the experimental data points. The latter plot will render information on whether a positive/negative bias exists in the y residual for the system under investigation (Jackson and Wilsak (1995).

There are a few important shortcomings, worth noting, of the thermodynamic consistency tests (Jackson and Wilsak, 1995):

- The best thermodynamic model for the system being investigated should be chosen. If the incorrect model is selected, then this may lead to a bias presenting itself in the residual plots mentioned above. An inexperienced learner may hastily and erroneously draw the conclusion that their experimental data is inconsistent. If an appropriate model cannot be located, then these consistency tests should not be implemented.

- In instances where there are sparse sections in the available data (*i.e.* a skip in measurements from a certain liquid composition and pressure to another), certain problems could present themselves, when overly flexible models are utilized. One consequence would be the observation of uncharacteristic fitting of data in the bare regions. This anomalous behavior can only be distinguished on the *P-x-y* plots, as the residual plots would mask this observation.

- Barker‟s method (1953) is employed as the technique for data reduction, with the objective function being the pressure residual. The premise of Barker‟s method is the assumption that no inconsistencies are present in the temperature and liquid composition measured. Thus, even if statistically negligible inconsistencies occur in the temperature and liquid composition measurements in sensitive areas, these small errors are further compounded during data reduction, and lead to biases presenting themselves in residual plots. A more stringent approach to data reduction would be to use the maximum likelihood principle. In this instance T, P, x_i and y_i data is regressed simultaneously.

- In some instances where data fails the point test, the exact reason/s for the failure is difficult to pinpoint. There could be any number of reasons responsible for the discrepancies in a certain region, *i.e.* the data measured could be erroneous or the model selected for data reduction could be inappropriate *etc*. This test alone is insufficient for the correct analysis of data.

- In scenarios where the number of adjustable parameters, derived from regressed data, exceeds the number of experimental data points, the point test cannot be used.

2.7.2 Direct Test

The direct test provides a simplistic, yet effective, approach to determining the consistency of data obtained experimentally. It was developed by Van Ness (1995) and it makes use of the residual $\delta \ln\left(\frac{\gamma_1^*}{\gamma_2^*}\right)$ to determine the extent of deviation from ideality.

The defining equations of this approach are:

$$\varepsilon_p^* = \frac{V^E}{RT}\frac{dP}{dx_1} \tag{2.113}$$

$$\varepsilon_T^* = \frac{-H^E}{RT^2}\frac{dT}{dx_1} \tag{2.114}$$

where: $\varepsilon_p^* = 0$ for isobaric data

$\varepsilon_T^* = 0$ for isothermal data

Therefore, only one value of ε is required for evaluation of the direct test. This value may either be ε_p^* or ε_T^* for the isothermal or the isobaric case respectively.

From the following equations:

$$d\left(\frac{nG^E}{RT}\right) = \frac{nV^E}{RT}dP - \frac{nH^E}{RT^2}dT + \sum_i \ln \gamma_i dn_i \tag{2.115}$$

And,

$$\sum_i x_i d\ln\gamma_i = \frac{\overline{V_i^E}}{RT}dP - \frac{\overline{H_i^E}}{RT^2}dT \tag{2.116}$$

For 1 mole of liquid phase, where: $g = \frac{G^E}{RT}$, the resulting expressions are derived:

$$\frac{dg}{dx_i} = \ln \frac{\gamma_1}{\gamma_2} + \varepsilon^* \tag{2.117}$$

$$x_1 \frac{d \ln \gamma_1}{dx_1} + x_2 \frac{d \ln \gamma_2}{dx_1} - \varepsilon^* = 0 \tag{2.118}$$

The value of ε^* will depend on the data being collected (either isobaric or isothermal).

Since, $$\frac{G^E}{RT} = \sum_i x_i \ln \gamma_i \tag{2.119}$$

for a binary system this reduces to:

$$g = x_i \ln \gamma_i + x_2 \ln \gamma_2 \tag{2.220}$$

Differentiating the previous equation (2.220) with respect to x_i, one obtains:

$$\frac{dg^{\exp}}{dx_1} = x_1 \frac{d \ln \gamma_1^{\exp}}{dx_1} + \ln \gamma_1^{\exp} + x_2 \frac{d \ln \gamma_2^{\exp}}{dx_1} - \ln \gamma_2^{\exp} \tag{2.221}$$

Equation (2.221) may also be represented as:

$$\frac{dg^{\exp}}{dx_1} = \ln \frac{\gamma_1^{\exp}}{\gamma_2^{\exp}} + \varepsilon + x_1 \frac{d \ln \gamma_1^{\exp}}{dx_1} + x_2 \frac{d \ln \gamma_2^{\exp}}{dx_1} - \varepsilon^* \tag{2.222}$$

Subtracting equation (2.221) is from equation (2.222), and simplified to be defined in terms of residuals ($\delta g = g - g^{\exp}$), the following equation is obtained:

$$\frac{d(\delta g)}{dx_1} = \delta \ln \frac{\gamma_1}{\gamma_2} - \left[x_1 \frac{d \ln \gamma_1^{\exp}}{dx_1} + x_2 \frac{d \ln \gamma_2^{\exp}}{dx_1} - \varepsilon^* \right] \tag{2.223}$$

In the event that that an isobaric or an isothermal set of data points is reduced with the objective function $\sum (dg)^2$, then $d(\delta g)/dx_1$ is reduced to zero. Thus:

$$\delta \ln \frac{\gamma_1}{\gamma_2} = x_1 \frac{d \ln \gamma_1^{\exp}}{dx_1} + x_2 \frac{d \ln \gamma_2^{\exp}}{dx_1} - \varepsilon^* \qquad (2.224)$$

According to the Gibbs-Duhem rule of thumb, the expressions on the right hand side are equivalent to zero, when the left hand side of expression (2.224), provides a quantitative measure of the deviations from the Gibbs-Duhem equation. Van Ness (1995) states that the degree to which the values of the residuals fail to scatter about the zero line, gives an indication of the consistency of the thermodynamic experimental data accrued.

Table 2-3: Consistency index for the Van Ness (1995) direct test, displaying the root mean square values (RMS).

Index	RMS	$\delta \ln\left(\frac{\gamma_1}{\gamma_2}\right)$
1	>0	≤0.025
2	>0.025	≤0.050
3	>0.050	≤0.075
4	>0.075	≤0.100
5	>0.1	≤0.125
6	>0.125	≤0.150
7	>0.150	≤0.175
8	>0.175	≤0.200
9	>0.200	≤0.225
10	>0.225	

In addition, Van Ness (1995) also industrialized a numerical guideline indicated in Table 2.3 above. This table contains values which estimate the extent to which experimental data deviates from consistency. It should also be noted that the index 10 implies highly inconsistent data, whereas, a value of 1 indicates excellent data.

Chapter 3: Review of Some Experimental Techniques and Equipment

There are numerous techniques available for measuring phase equilibria. When measuring phase equilibria, the most important variables are those of pressure, liquid and vapour phase compositions, as well as temperature. In order to obtain data with high levels of accuracy, it is imperative that we utilize the correct experimental procedure in the measurement of such data. An important point highlighted by Walas (1985) is that the recording of pressures and temperatures in regions assumed to be at equilibrium must actually be at equilibrium; else the point being analyzed shall render inaccurate data. In addition, when samples from the vapour and liquid sampling ports are being withdrawn for analysis, it is important that this is accomplished with minimal disturbance to equilibrium.

There are a multitude of techniques, as well as equipment, available for the measurement of vapour-liquid equilibrium. Therefore, it is of paramount importance that the correct technique be employed for the purpose for which it is intended. The following two techniques (amongst others) are the most commonly utilized for measuring vapour-liquid equilibrium data, according to Seker and Somer (1992):

a) The static technique; and
b) The dynamic technique

This chapter shall focus upon a few experimental techniques and equipment relevant to the experiments carried out and discussed in this thesis. It is important that equipment be classified in order to be able to ascertain the fluid dynamics of the equilibrium cell being utilized. The classification of the equipment used is based upon the circulation of the vapour phase, liquid phase or both the phases concurrently. When there is circulation of the phases involved, the equipment is classified as dynamic, whereas, if there is no circulation of the phases in the equilibrium cell then the equipment is classified as static.

3.1 Static Technique

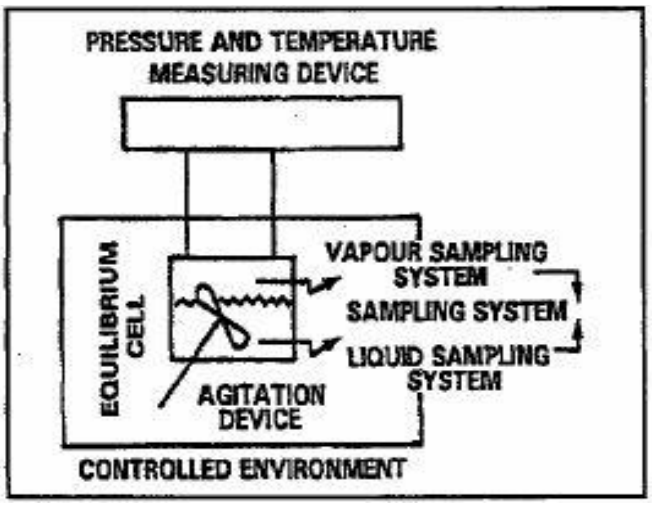

Figure 3-1: A schematic diagram of the static cell (Raal and Mühlbauer, 1994).

As has been previously stipulated, the static technique is categorized by the absence of circulation of the liquid and vapour phases. The operation of the static cell is divided into three categories; the synthetic, analytic or combined sampling method. Briefly, the analytic method entails sampling of both the liquid and vapour phases. However, the synthetic technique does not entail the sampling of the vapour and liquid phases when the system is at equilibrium. The analytic technique is favoured over the synthetic technique as the latter approach is less accurate than the former when dealing with measuring isothermal and isobaric data where large gradients exist. In addition, the synthetic method renders poor results when dealing with greater than two components.

Below is a brief description of the analytic and synthetic methods for the static technique. Too great detail shan't be lavished on this as the dynamic technique was implemented in this study. Thus greater emphasis is placed on the discussion of the dynamic technique for VLE measurements.

3.1.1 Static Analytic Method

The chemical components are added to the equilibrium cell (Figure 3-1). From the equilibrium cell the liquid chemicals are flushed into the equilibrium chamber via the utilization of a compression device (*e.g.* pump). The contents are constantly mixed to encourage greater contact of the phases. Once equilibrium is established, temperature and pressure readings are measured. Thereafter, composition analysis occurs via sampling.

3.1.2 Static Non-Analytic (Synthetic) Method

For this approach to VLE data measurement and analysis a mixture of known composition is charged into the equilibrium cell. Thereafter, the pressure and temperature of the system is adjusted to enable phase separation. The measurement of pressure and temperature data begins as soon as homogeneous phase separation occurs. With this approach to composition analysis the temperature and pressure are manipulated in such a way that concentration gradients are avoided and the mixture forms a single homogeneous phase. Finally, the temperature and pressure are readjusted until a new phase is formed. The pressure, temperature and composition are utilized to describe the phase envelope.

3.1.3 Static Combined Method

It has been observed by Deiters and Scheider (1986) in cases where isothermal and isobaric data produce small gradients in temperature or pressure, this small oscillation induces fluctuations in the phase composition, thus compromising the accuracy of measurements executed. Thus, for phase behaviour in or near the critical region the analytical method is inadequate. Near the critical region the synthetic method is a better option for improved accuracy (as no sampling is required).

For the alternative case, where large gradients in pressure and temperature are observed, the non-analytic method is not applicable as it results in greater error. Thus, the analytic and non-analytic methods were combined in an attempt to improve the accuracy of measurements conducted. For

a more in depth understanding of the equipment capable of carrying out the static combined method reference should be made to the thesis of Ramjugernath (2000).

3.2 Dynamic Technique

For the dynamic approach to vapour-liquid equilibria data measurement, the circulation of both the liquid and vapour phases of the boiling mixture is involved. For this research project emphasis shall be placed on operation of the dynamic still at low to moderate pressures (0 – 500 kPa). The basic understanding of the VLE dynamic still (Raal and Mühlbauer, 1998) is the boiling of a liquid mixture at controlled conditions of pressure and temperature, wherein, there is the separation of the vapour and liquid within the equilibrium chamber. The evaporated vapour phase is condensed within a condenser (the exception of course being scenarios where direct circulation of the vapour phase is occurring) and thereafter returned to the boiling chamber. In the boiling chamber, the liquid and condensed vapour mix again and the cycle continues. The composition of the liquid and vapour phase are continuously changing with time, until such a time that equilibrium has been reached. After a sufficient amount of time has passed to allow for equilibrium to be reached, the steady state pressure and temperature are then recorded. The dynamic method may be utilized to obtain isobaric as well as isothermal data. The dynamic method is divided into two categories (Hala *et al.,* 1967):

- the circulation of the vapour phase only and;
- the circulation of both the vapour and liquid phases.

3.2.1 Recirculation of Vapour Phase Only

The work of Sameshima (1918) was later built on by Othmer (1928) with regards to the recirculating VLE still. In this still the vapour generated from the reboiler is sent to the condenser, after which it is returned to the reboiler. The design of the VLE still of Othmer (1928) is exhibited below. One of the distinct features of this still is that it has sampling points for both phases (liquid and vapour). Many improvements to the still of Othmer (1928) were suggested.

However, due to the many short comings of this equipment further modifications were not pursued (Raal and Mülhbauer, 1998).

Although the design of Othmer (1928) was a huge improvement over the design of Sameshima (1918), it still has many downfalls:

1) The possibility of the saturated vapour condensing on the side of the reboiler wall is a real threat to accuracy. This is a serious faux pas as the composition of the vapour phase is therefore altered.
2) The temperature readings recorded with this apparatus were always off the mark, as the temperature sensor is not in sufficient contact with both phases.
3) When flashing of the vapour occurred, the more volatile component was flashed out. This posed a serious problem.
4) The condensate receiver is too big; as such sufficient agitation could not be accomplished.
5) Insufficient agitation of the reboiler contents posed a serious problem as well.

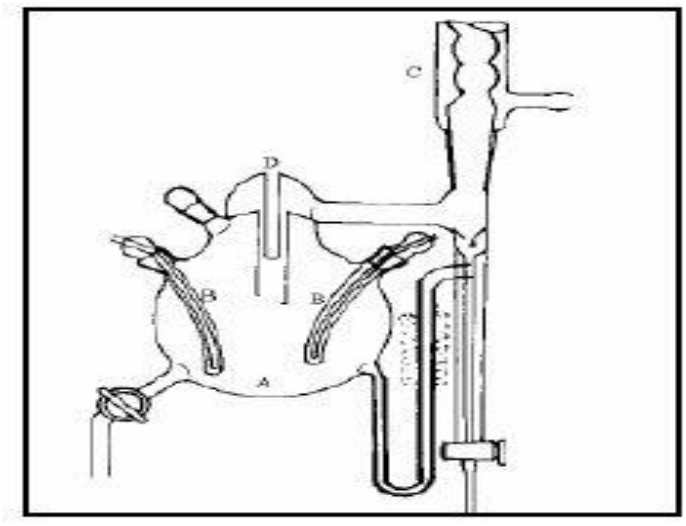

A: Boiling chamber

B: Immersion heater

C: Condenser

D: Thermowell

Figure 3-2: A schematic diagram of the Othmer Still (Malanowski, 1982).

3.2.2 Recirculation of Liquid and Vapour Phases

The earliest work on the design of vapour-liquid equilibrium stills was by Lee (1931). Gillespie (1946) then went on to modify this design to allow it to cater for the circulation of both the liquid and vapour phases. Cottrell (1919) developed the use of a Cottrell pump which enables more efficient circulation, and subsequently more accurate temperature measurements. Even though the design and modification of the VLE still was novel for its time, there were certain weaknesses (Coulson, 1946)), such as:

- The vapour, which was recirculated and sampled as condensate, was not truly in equilibrium with the liquid sample. (The liquid was sampled from the boiling chamber).
- The Cottrell tube does not allow for equilibrium to come about fast enough. This is due to the small contact times and interfacial areas available for mass transfer.
- The absence of insulation around the disengagement vessel allowed for the possibility of partial condensation of the vapour phase.
- The method for the sampling of the liquid and vapour phases as it resulted in a disturbance to the equilibrium position of the system and hence affected the liquid and vapour compositions.

Yerazunis *et al.* (1964) overcame the majority of these setbacks via the modification of the separation chamber. The subsequent modifications made by Yerazunis *et al*. (1964) were made using the fundamentals of Heertjies (1960) and Rose and Williams (1955). Rose and Williams (1955) promoted the utilization of a vapour phase acting as a thermal barrier. Therefore, this would allow the vapour to flow up through the equilibrium chamber.

Heertjies (1960) proposed the passage of the vapour-liquid sample through any suitable packed column after the Cottrell tube. Thus, there would be improved efficiency of mass transfer in the equilibrium chamber. To eliminate the errors in previously designed stills, Raal and Mühlbauer (1998) based this still design on the works of Heertjies (1960) and Yerazunis *et al.* (1964). This was done to bypass the inherent errors of previous designs (Narasigadu, 2006).

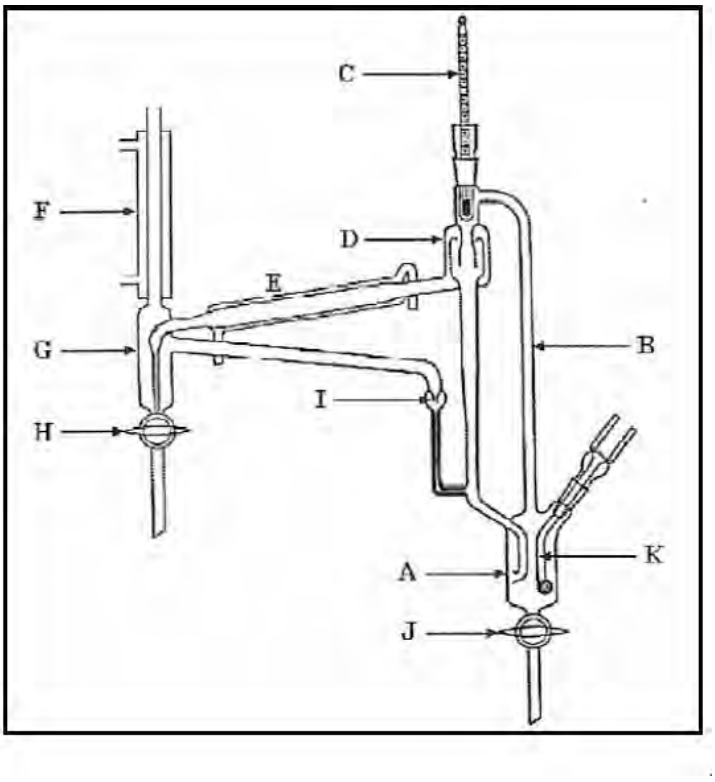

A: Boiling chamber

B: Cottrell tube

C: Thermometer

D: Vapour-liquid separating chamber

E, F: Condensers

G: Condensate receiver

H: Condensate sample cock

I: Droplet counter

J: Liquid sample cock

K: Internal heater

Figure 3-3: The original apparatus of Gillespie (1946).

It is very important to note that all the available experimental techniques and equipment for measuring vapour-liquid equilibria have not been discussed in this chapter. For a greater understanding of the different experimental techniques and equipment available reference should be made to the theses of Narasigadu (2006), Hirawan (2007), Wilson (2008) and Pillay (2010).

3.3 A Simple Example of an Automated Dynamic Apparatus

At the University of Oldenburg, Germany, the undertaking for the automation of dynamic VLE apparatuses commenced as early as 1998/99. The equipments developed at this institution may be utilized to measure binary VLE data (up to atmospheric pressure), vapour pressure data for pure components and activity coefficients at infinite dilution. A schematic representation of the apparatus is exhibited:

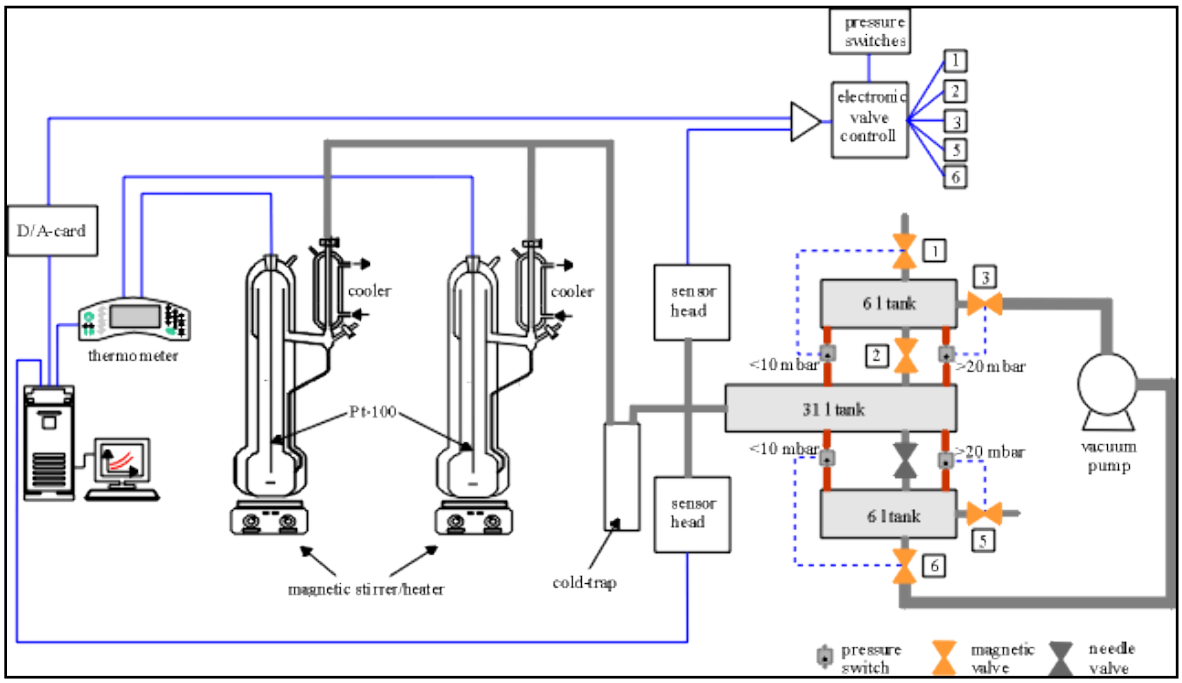

Figure 3-4: Automated dynamic VLE apparatus (Gmehling, 2011).

The temperature range for the operation of this equipment is 253.15 K to 493.15 K, with a pressure range of 3.5 to 131 kPa. The system temperature is measured with a platinum resistance thermometer (Conatex Pt100) and the pressure measurements are accomplished via the utilization of a DRUCK RPT 301 pressure transducer. The computer program which enables automation is the Windows Computer-aided -Ebulliometer-Measuring- System 1.0. In addition, electronic valve control is also employed (Gmehling, 2011).

There are many automated static and dynamic VLE apparatuses which have been developed by institutions around the world. A wealth of information is available on the automation of dynamic and static VLE apparatuses; however, discussing all these advancements is beyond the scope of this work. Therefore, only the simple example mentioned above is discussed here. However, further examples of researchers in the field of fully automated VLE apparatuses are Uusi-kyyny, P (2004) and Tochigi, K *et al*. (2009).

Chapter 4: Equipment Description

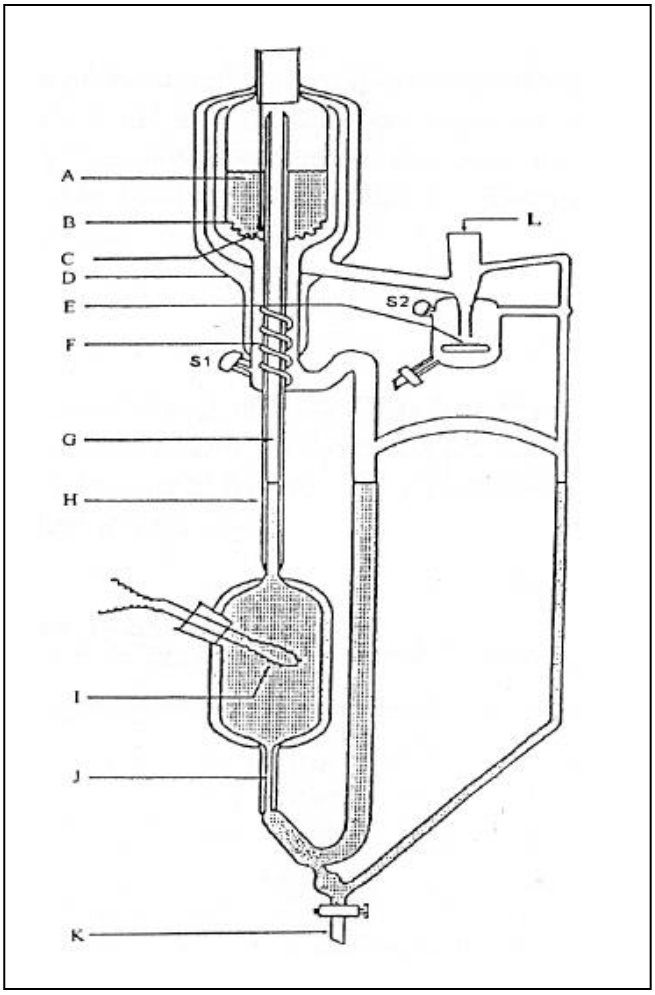

KEY

A: Stainless steel wire mesh packing
B: Drainage holes
C: PT-100 sensor
D: Vacuum jacket
E: Magnetic stirrer
F: Stainless steel mixing spiral
G: Insulated Cottrell pump
H: Vacuum jacket
I: Internal heater
J: Capillary leg
K: Drainage valve
L: Condenser attachment
S1: Liquid sampling septum
S2: Vapour sampling septum

Figure 4-1: Schematic diagram of VLE still (Clifford, 2004).

The intrinsic features of the still designed by Raal and Mühlbauer (1998) are:

- The receiver at the base of the condenser and the boiling chamber both has a magnetic stirrer situated at its base. This allows for the mixture to have a homogenous composition.
- A packed equilibrium chamber - due to the open structure of the packing material, it drastically reduces the problem of pressure fluctuations.
- The equilibrium chamber and the Cottrell tube are thoroughly insulated with a vacuum chamber. Therefore, any possibility of heat loss to the surroundings is eliminated.

- The deliberate Cottrell tube design, which leads into an angularly symmetric equilibrium chamber, produces no favoured radial direction for the development of concentration and temperature gradients of the fluid flowing through.
- Internal and external heaters are connected to the boiling chamber. This allows one to control the amount of heat supplied to the still, as well as the rate of boiling of the mixture.

Any VLE still should satisfy the following criteria (Malanowski, 1982):

- Small samples of the vapour and liquid phases should be removed from the sampling points for analysis, so as not to upset the balance of equilibrium in the VLE still.
- The design, and any subsequent alterations to the VLE still, should maintain a simplistic approach to vapour-liquid equilibrium measurements, which allow for accurate temperature and pressure measurements to be performed.
- It should be easy for steady-state operation to be accomplished once an equilibrium property is altered (for instance temperature or pressure).
- In the vapour phase there should be no liquid droplets being trapped.
- Overheating near or on the temperature sensor should be avoided, and no vapour should be allowed to wholly or partially condense on the temperature sensor.
- The vapour undergoing circulation should be well mixed with the liquid boiling in order to accomplish a consistent composition.
- The flow, as well as the composition of the circulated stream must be maintained constant.
- If there is dead-volume in the VLE still, this could obstruct the compositions from reaching equilibrium. Therefore, the still should not contain any dead-volume.
- When additional material is to be added to the VLE still, it must be done in such a manner so as not to disturb the equilibrium condition.

The recirculating still used in this work to accomplish VLE measurements has transcended the aforementioned difficulties.

The low pressure, dynamic glass still of Joseph *et al*. (2001) contributed excellent measurements toward low pressure VLE data. Thus, the design and development of the current still, used to undertake/perform the measurements in this study, was based on the still of Joseph *et al*., (2001). The modifications to the still employed were undertaken by the Thermodynamics Research Unit of the University of Kwa-Zulu Natal, School of Chemical Engineering.

The modifications made by Lilwanth (2011) dealt with the intent to enable full automation of the standard glass dynamic still operating at low to moderate pressures (0 – 500 kPa), such that pressure and temperature control were fully regulated by a pressure regulator, Labview software and the necessary hardware. The control algorithm, developed by Lilwanth (2011), varies the pressure, via adjustments in computer controlled solenoid valves, to maintain the required isothermal temperature. Therefore, accuracy and speed in the measurement of VLE data is vastly improved.

4. 1. Equipment Description

The still, employed for the measurement of VLE data presented in this thesis, was commissioned by Lilwanth (2011) in order to be able to handle measurements conducted at low to moderate pressures. In the design of this still to handle measurements over a range of pressures, the following equipment was employed:

1) Edwards Speedivac Vacuum pump
2) WIKA TXM 0-5 bar pressure transducer
3) 113L Ballast tank
4) 2 x Pt-100 temperature sensors
5) Water bath with ethylene glycol solution as the cooling medium and a pump
6) 2 x 50 ohms precision resistors
7) 3 solenoid valves and 6 manual valves
8) Power suppliers
9) 2 x Modules N19263 and N19216 (Temperature measurements)
10) DC motor brushes

11) Nitrogen gas cylinder with a regulator
12) ACS Shinko pressure controller

4.2 Operation of Modified VLE Still (Lilwanth, 2011)

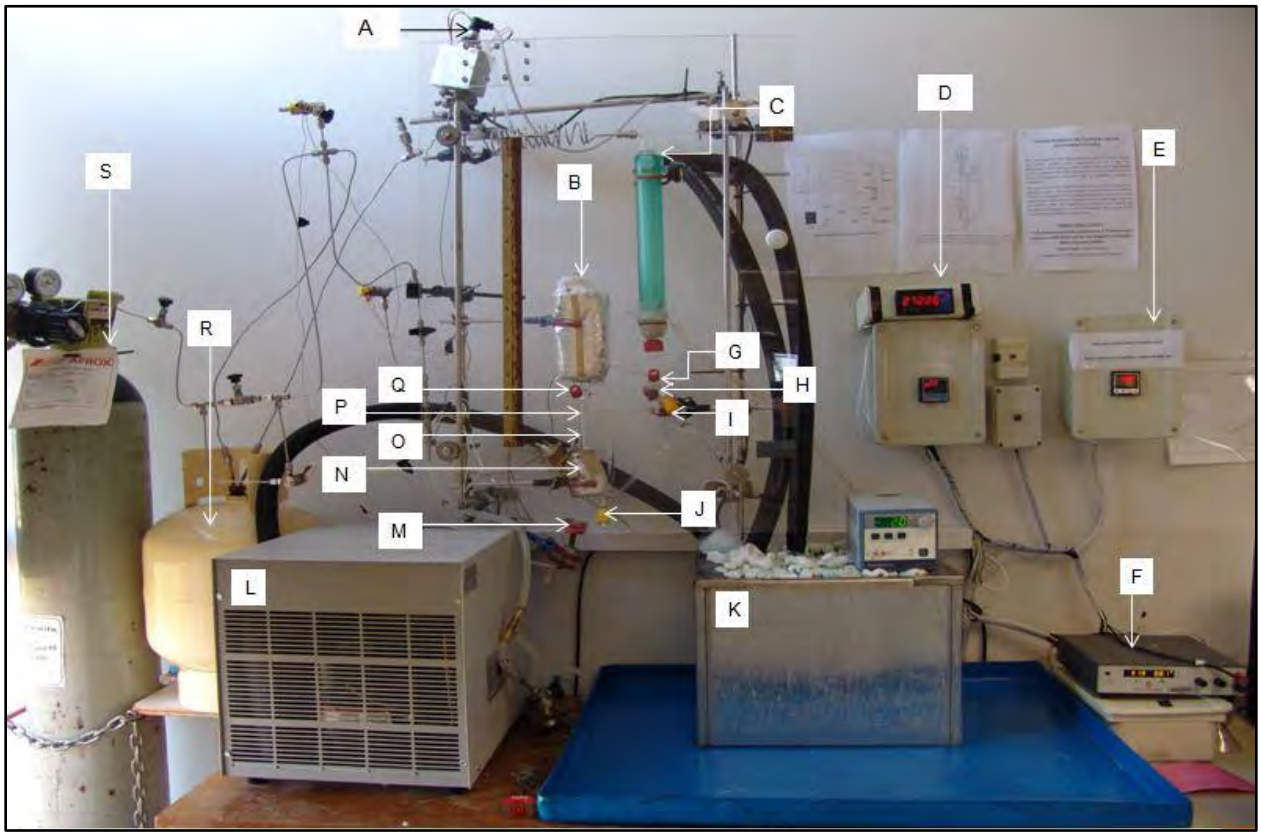

Figure 4-2: Experimental set-up of low-to-medium pressure VLE apparatus.
A: Pressure transducer; **B:** Equilibrium chamber; **C**: Condenser; **D:** Wika pressure transmitter; **E**: ASC controller; **F**: Programmable power supply; **G**: Vapour sampling septum; **H:** Magnetic stirrer; **I:** Drainage valve; **J:** Drainage valve; **K**: Water bath; **L:** Cooling unit; **M:** Magnetic stirrer; **N**: Reboiler; **O:** Vacuum jacket; **P**: Insulated Cottrell pump; **Q:** Liquid sampling septum; **R**: Ballast tank; **S**: Nitrogen tank.

The diagram of the equipment is given in Figure 4-2. The reboiler is charged with a liquid mixture that enables boiling of this mixture by the use of external and internal heaters. The external heater constitutes nichrome wire, which is then wrapped around the boiling chamber. This is done so that heat losses to the surroundings are compensated for. The internal heater,

which is made up of nichrome wire, lines the inside of the boiling chamber. It consists of a heater cartridge. The heat supplied by the internal heater is the parameter which is constantly varied to observe its effect on boiling, as opposed to the external heater which is kept at a constant voltage merely to compensate for natural heat losses to the environment. The internal heater is able to create smooth boiling due to its provision of nucleation sites.

From the boiling chamber, the vapour-liquid mixture then passes through the vacuum insulated Cottrell tube into the equilibrium chamber. The packing within the equilibrium chamber is made up of 3 mm rolled stainless steel wire mesh cylinders. This type of packing creates a larger surface area for improved interaction between the vapour and liquid molecules.

At the tip of the equilibrium chamber is a temperature sensor, the Pt-100. It is placed within the packing of the equilibrium chamber. There are two disengagement points for the liquid and vapour at the base of the equilibrium chamber. The first point, directly below the equilibrium chamber allows the liquid to disengage by gravity into the liquid sampling point, and the other exit point, positioned slightly higher than the liquid one, allows the vapour to flow through it and into the condenser. The vapour initially flows upward and circulates throughout the equilibrium chamber; this therefore, contributes to thermal lagging. After the vapour leaves the equilibrium chamber, it flows up into the condenser, forming condensate, and thereafter collects in the vapour condensate receiver. When the receiver of the vapour condensate overflows, this liquid is returned to the boiling chamber, by way of a standpipe leg, where it then mixes with the overflow liquid from the liquid sampling point.

4.3 Temperature and Pressure Control

The equipment utilized in the measurement of the VLE data presented in this study is a fully automated pressure and temperature regulating advancement, as commissioned by Lilwanth (2011). Pressure readings were acquired with the use of a WIKA model P-10 pressure transmitter. These results are then logged onto a data file on the computer automatically by means of an ACS controller. The resistance readings obtained from the Pt-100 are also transferred to a computer, and the data is captured via the utilization of PC-communication

modules N19263 and N19216. The computer software operates upon the premise of actuating the solenoid valves, V-S1, V-S2, and V-S3 (Figure 3-2), automatically through the ACS controller. This is done so that the pressure set point may be met and maintained accurately. Another effective feature of the software developed by Lilwanth (2011) is that it is also able to calculate the pressure changes necessary to maintain a certain temperature set point during isothermal operation of the still.

4.3.1 Temperature Control

A Pt-100 temperature sensor was employed in determining the temperature of the equilibrium chamber for analysis purposes. The Pt-100 is connected directly to a temperature display. The Pt-100 was calibrated prior to the equipment being used for measurement of novel systems. The temperature of the equilibrium chamber was set by initially inputting the desired temperature set point on the Labview program developed by Lilwanth (2011). With the use of the fully automated Labview automation program the correct pressure (corresponding to the required temperature) is automatically found by the developed program, so long as an appropriate upper and lower limit of pressure is inputted on the software interface. Thus, this guideline is used by the software to determine the correct pressure at which it needs to operate to obtain the desired isotherm. The accuracy of temperature control employing the Labview automation program is to ±0.089 K and the maximum temperature deviation from set point is 1K in measurements.

4.3.2 Pressure Control

The equipment employed in measurement of the pressure is the WIKA model P-10 pressure transducer (0-500 kPa). The pressure transducer is located between the VLE still and the ballast tank (figure 4-2). The function of the ballast tank is to:

- Trap any condensable vapours should the condenser fail;
- Diminish the effects of unforeseen pressure fluctuations.

The pressure was controlled with the Labview automation programme that optimizes the use of a two way solenoid valve connected directly to a vacuum pump and a vent to the atmosphere. The accuracy in pressure is controlled to ± 0.440 kPa and the maximum deviation from set point is 0.2 kPa in measurements.

Executing high pressure measurements on glass VLE equipment is a very dangerous undertaking as a consequence of the high temperatures and pressures involved. Therefore, a well rounded knowledge of the design of the VLE still, its construction as well as the operating experimental procedure is imperative. Among the many important features to adhere to when considering safety, the following were pursued (Ramjugernath, 2000):

1) A transparent plastic sheet was mounted in front of the VLE still. When the still is used over a long period of time, the high pressures could cause an explosion of the VLE glass still. Since the plastic sheet is in place, this would then protect the user‟s eyes and other exposed areas from serious damage.

2) The condenser has a blow-off lid. In the event that the pressure exceeds 3 bar, the glass top of the condenser will pop off.

3) A pressure relief valves is situated at the top of the condenser. When the pressure builds up in the still, the top glass cap of the condenser will pop off. As such the whole VLE still is still safe as well as the user. The pressure relief valve was set for a pressure range for which the glass VLE still had been tested and deemed safely operable at those conditions.

4) Nitrogen gas is being used as the means by which to raise the pressures to approximately 300 kPa during runs. The nitrogen gas creates an environment free of any explosions within the still; if per chance some flammable fluids had to be lying around the still, or had to accidently contaminate the chemicals in the still.
   Nitrogen has an extremely high Henry‟s constant, and is insoluble in the mixtures of study at the temperatures and pressures of concern.

5) Aluminum foil was utilized to wrap heated elements. This enabled better isothermal operation of the equipment as it assisted in insulating the elements.

6) The chemicals in use are not highly toxic; however, the necessary safety precautions were taken at all times. The exhaust fans in the laboratory are on at all times and the exhaust line from the vacuum pump leads to an exhaust fan for safe removal of dangerous fumes.

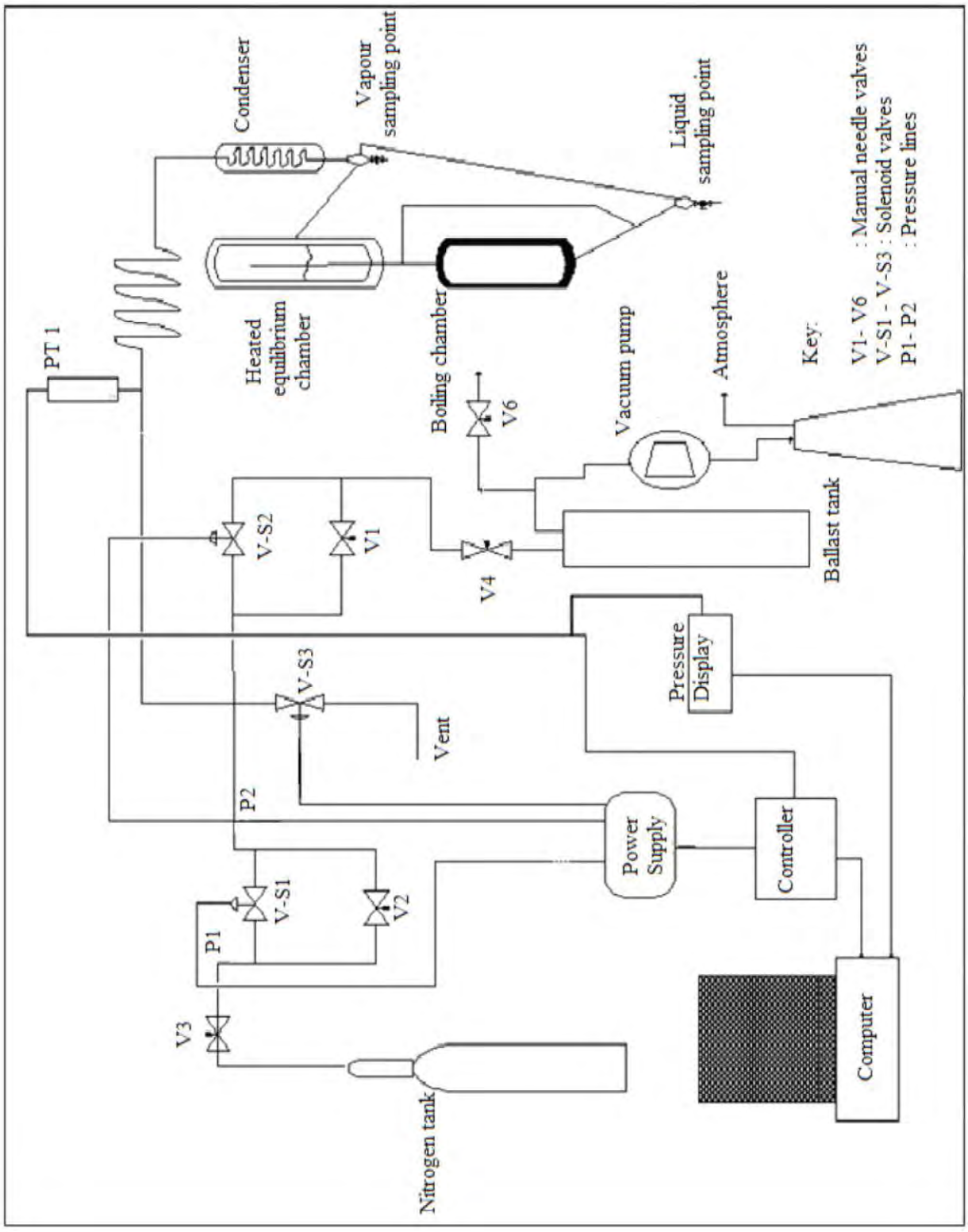

Figure 4-3: Schematic diagram illustrating temperature and pressure control, and the layout of the equipment (Lilwanth, 2011).

Chapter 5: Experimental Procedure

Any and all experimental techniques employed in any thermodynamic work must be reproducible thus improving confidence in the accuracy of measured data. Greater accuracy in measurements is only possible if the equipment utilized for experimentation is calibrated accurately in temperature, pressure and composition, as well as monitored and operated in the correct fashion. The analysis of the vapour and liquid compositions obtained in each experimental run plays a significant role. Therefore, great care should be taken when analyzing samples. This chapter provides succinct and crucial insight into the operation, calibration and preparation of the dynamic VLE still utilized.

5.1 Cleaning the VLE Apparatus

It is imperative that the VLE still is cleaned of all impurities prior to it being calibrated and used for any measurements. The incidence of impurities, even in minute quantities, could significantly alter the VLE data and compromise the integrity of experimental measurements. Due to impurities having such a marked effect on measurements, chemicals of the highest purity are always used and the VLE still must always be properly cleaned before experiments are conducted.

Pure acetone is used to clean the VLE still. The still is operated isobarically, at 40 kPa, while the acetone or any other low-boiling pure chemical, is circulated through the still. This is allowed to continue for approximately 30 minutes, thereafter, the acetone is drained, and the VLE still is refilled with acetone and the process is repeated. This is done 3-4 times.

After draining the still completely from the final cleaning session (with acetone), the pressure is reduced to 40 kPa (or as low as possible) and held at that point for approximately 60 minutes. A little heat is also applied. This is done in order to flash off any residual chemicals that may still be in the still and to dry the VLE apparatus.

5.2 Leak Test

For this specific test, the empty still is brought under vacuum at about 10 kPa and it is observed whether or not the pressure is being maintained on the Labview automation program. Once the desired pressure is reached, the pump and controller are switched off and the system is isolated in this way for several hours.

When dealing with medium to high pressures, soapy water (a surfactant based liquid or S*noop*®) is applied to the seals, fixtures and connecting points on the equipment. If it is observed, during the application of this surfactant, that bubbles appear, then this would indicate the presence of a leak. Once the leak has been detected, depending on the severity of it, Locktite may be applied to the glass joints and vacuum seals on steel pipe joints. In some cases the entire fitting/connecting hose may have to be replaced. Once the leak test has been performed and the equipment deemed leak tight, a cleaning agent, such as acetone or pentane, should be circulated through the still to clean it. The washing of the still should be repeated at least twice.

5.3 Chemical Purity

Before any chemicals are utilized for measurements, it is imperative that the purity is analyzed by gas chromatography, refractive index, as well as the measurement of density and compared against the available literature. This is done to ensure that the purity of the chemical being used has been correctly specified by the supplier. The presence of a substantial quantity of impurities (>1%) in chemicals being used for measurement can severely affect the results obtained. However, if it is found that the chemicals are contaminated substantially (>1%), the degassing of said chemicals is necessary to improve the purity.

5.4 Pressure Calibration

The pressure readings are obtained from a Wika model P-10 pressure transducer. This transducer is capable of reading pressures from 0 up to 500 kPa (absolute). The Wika model P-10 pressure transducer is calibrated using a CP 6000 pressure transmitter that is linked to the still. The set

point pressure is entered on the graphical user interface (GUI), which displays the actual pressure as well as the set point pressure. Once stability within the system has been reached, the pressure from the standard pressure transmitter (actual pressure) is then compared to the display pressure (Wika model P-10 pressure transducer). The pressures being compared should cover a wide range such that the reliability and accuracy of the calibration is accomplished at both very low and very high pressures. The points measured at each setting should be repeated at least three times, progressing from low to high pressure, followed by moving from high to low and again low to high pressure thus yielding three data points per setting. A plot of $P_{display}$ versus P_{actual} will render the calibration equation for pressure fitted to a linear trend line; the scatter of each measured point plotted against the trend line prediction will yield the uncertainty in reproducibility of the measurement.

5.5 Temperature Calibration

The Pt-100 situated within the equilibrium chamber was also calibrated. Temperature calibration requires that the still be operated isobarically at several pressures. This is known as “in situ” calibration, and a very pure component (purity ≥ 99.5%) is circulated through the still. In this case cyclohexane was used. At each pressure, once equilibrium had been established, the resistance was recorded as well as the corresponding temperature set point from the equipment. Antoine‟s equation, or any equation for determining the correct temperature from set pressure readings, was used. Thereafter, a plot of the Pt-100 temperature versus the actual temperature (obtained from Antoine‟s equation) was plotted for the entire operating range. Once the calibration equation was obtained, it was entered in the software program.

5.6 Calibration of the Gas Chromatograph Detector

The equipment used for composition analysis was the Shimadzu (GC-2014) thermal conductivity detector. The GC detector calibration technique developed by Raal (Raal and Mühlbauer, 1998) uses the area ratio method. The GC calibration curves were generated by analysing gravimetrically prepared standard solutions made from pure chemicals. Samples of the mixture required for analysis were prepared in 2 ml vials for analysis. The range of concentration (ratio

of mole fraction range, *e.g.* x_1/x_2 or x_2/x_1) over which analysis is carried out is 0 to 1, in increments of 0.2; however, this composition ratio should not exceed 1.2. The volume of sample injected for analysis should avert overloading of the gas chromatograph as well as flashing. The area ratio technique is the most suitable approach selected for analysis as it is independent of the amount of sample injected into the GC. However, great caution should be taken in avoiding flooding of the GC column. The gravimetric approach to composition analysis is only suitable for the 1-hexene + NMP system. For the systems measured containing n-hexane (*i.e.* n-hexane +NMP, n-hexane+1-hexene and n-hexane+1-hexene+NMP) a volume based method for composition analysis was employed due to immiscibility of the components. This is due to n-hexane having an upper miscibility limit of 328.15 K (Fischer and Gmehling, 1996). Thus at room temperature, two liquid phases are clearly visible and composition analysis using the conventional gravimetric approach is not possible. A 0.5 μl syringe was employed to measure predetermined amounts of sample individually and, thereafter, the moles of each component were determined.

The uncertainty in the composition computed during calibration for the systems 1-hexene+NMP, n-hexane + NMP, 1-hexene+n-hexane, n-hexane+1-hexene+NMP and ethanol + cyclohexane are (mole fraction basis):± 0.0034, ± 0.0033, ± 0.0066, ± 0.0083 and ± 0.002, respectively.

For binary systems the equation representing the area ratio is:

$$\frac{n_1}{n_2} = \left(\frac{A_1}{A_2}\right)\left(\frac{F_1}{F_2}\right) = \frac{x_1}{x_2} \tag{5.1}$$

A_1 and A_2 = peak areas from GC analysis;

n_1 and n_2 = number of moles of component 1 and 2 in the mixture;

x_1 and x_2 = mole fraction of component 1 and 2 in mixture;

F_1/ F_2 = response factor ratio.

The response factor ratio is evaluated from a detailed plot, over the entire composition range, of A_1/A_2 versus x_1/x_2 and A_2/A_1 versus x_2/x_1. The slope from the linear plot of A_1/A_2 versus x_1/x_2 and A_2/A_1 versus x_2/x_1 should render values which are the mathematical inverses of each other.

The response factor ratio for each side evaluated should remain constant as may be observed from the equation from which it is derived. The calibration plot developed is very much dependent upon the system being analyzed, the GC detector as well as the GC settings being used.

5.7 Loading/Filling of the Cell

The VLE still is initially charged with approximately 90 ml of one of the pure components. The component is injected into either one of the vapour and/ or liquid sampling points of the VLE still using a standard 10 ml syringe.

5.8 Plateau Region

During VLE measurements there is a steady relationship that exists between the temperature input and the heat supply to the reboiler (Kniesl *et al.,* 1989). According to Kniesl *et al.* (1989), the vapour and liquid moving through the Cottrell tube is superheated to a small extent as a consequence of the hydrostatic head acting on the fluid as it moves through the tube. As the vapour-liquid mixture is ejected from the Cottrell tube onto the packing in the equilibrium chamber, the superheated portion is relieved. Upon this ejection of the vapour-liquid mixture in the equilibrium chamber, the mixture temperature cools down to its equilibrium temperature. This occurs as a result of the mixtures expansion, as well as the evaporation of a minute quantity of the liquid upon entry into the equilibrium chamber.

Below is a detailed figure exhibiting how the temperature of the vapour-liquid mixture varies as a consequence of the increase in heat input. This diagram clearly illustrates the points outlined by Kniesl *et al*. (1989) that when low heating rates are employed, an increase in the internal heater energy input results in the corresponding increase in vapour-liquid equilibrium temperature. Eventually the temperature profile flattens out; this region is referred to as the “plateau region”. The rise in temperature as the energy input increases implies that the heating rate in that section is insufficient to superheat the liquid and offset the cooling that occurs as a consequence of the expansion of the vapour-liquid mixture in the equilibrium chamber (Kniesl *et al*., 1989). The

plateau region is an indication that the increase in energy input offsets exactly the cooling of the mixture. Therefore, the smooth, flat profile is observed. Further heating results in an increase in temperature again (beyond the "plateau region"), this is due to the superheating being greater than the resultant cooling effects on the vapour-liquid mixture.

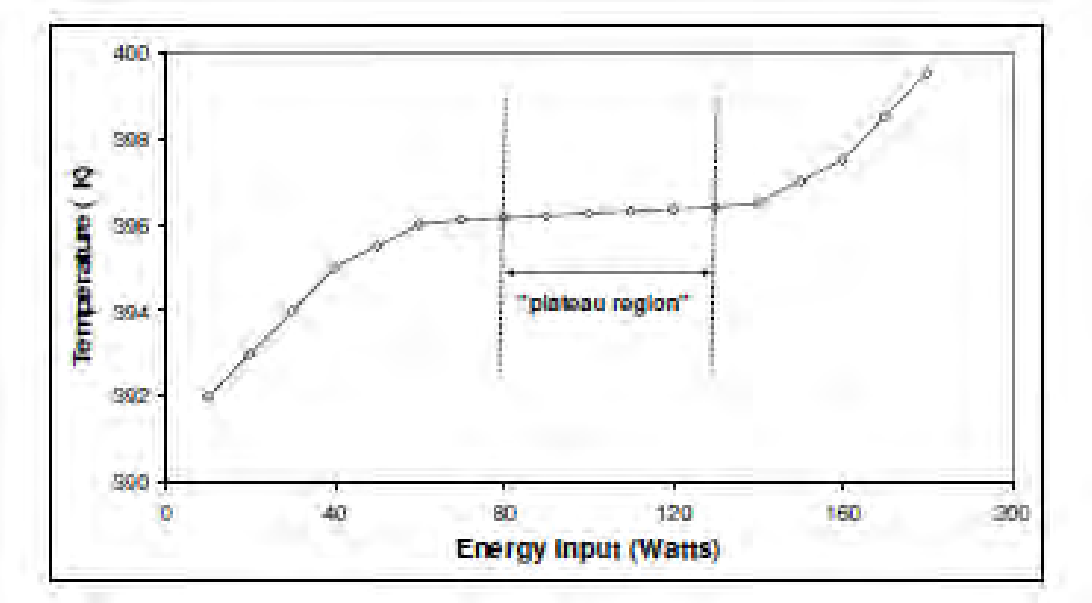

Figure 5-1: Illustration of an ideal plateau region (Pillay, 2010).

It is important to note that depending on the chemistry of the components being measured the region over which the plateau region presides will vary. For low boilers, such as non-polar alkanes, the plateau region is vast and quite distinguishable. However, for high boiling polar compounds, such as amides and alcohols, the plateau region is not as easily distinguishable. For such components the plateau regions are comparatively much smaller and in some instances appear as inflection points. In these cases, the plateau region is analyzed as the region wherein the smallest slope occurs. It is of paramount importance that the true plateau region is located and measurements carried out there, for if this region is incorrectly estimated, incorrect phase equilibrium data will be acquired.

5. 9 Locating Plateau Region

For each liquid and vapour equilibrium point acquired, the plateau region was found a priori. The external heater setting was maintained at 15-20 V for all systems measured. This value need not necessarily be large, as it is merely there to counteract the effects of heat loss to the environment. The internal heater setting is started at a low voltage, such as 15 V, and gradually increased automatically, by the Labview automation program, in increments of 5 V to the final voltage setting specified by the user. This initial voltage was selected as it was the lowest voltage that could be selected at which an even boil-up rate of the mixture, through the Cottrell tube, could be observed.

The time for which equilibrium is allowed at each internal voltage setting is approximately 10 minutes. This allows for complete thermal equilibrium to come about. After each voltage had run for the allotted 10 minutes, the pressure, temperature and internal voltage was recorded automatically by the Labview program, and then only was the internal voltage incremented automatically.

Obtaining the plateau region is the primary objective. Therefore, after each increment, a plot of the measured temperature (K) versus the energy input had to be conducted manually in excel and the slope of the line computed. Once the plateau region was established, the system was operated at those conditions for approximately 50-70 minutes. Equilibration times will vary from system to system. This is as a consequence of the molecular interactions of the different chemicals within each system with each other. Of particular significance is the relative volatility of systems and the circulation rate. Three criteria may be used to ascertain if equilibrium abounds; they are:

- a fast drop rate of the vapour-liquid mixture in the condenser (this should be at least 60 - 90 drops per minute);
- the flow pattern of the vapour-liquid equilibrium mixture up the Cottrell tube (continuous and stable flow of the mixture up this tube is required; slugging, however, is undesired);
- Since the direct method for composition analysis is being employed, this then constitutes another means by which to ascertain if equilibrium presides. If the samples of the binary

or ternary system are analyzed on the GC and the compositions are reproducible, then this would imply phase equilibrium abounds.

5. 10 Isobaric Operation of the Recirculating Still

Start-up Procedure

The water bath and cooling unit are switched on; this enables circulation of the ethylene glycol, thus preventing loss of the vapourised chemicals being measured. The ACS controller, pressure transducer and temperature modules are switched on, as well as the AC/DC power supply to the stirrers to enable mixing of the solution in the still.

5.10.1 Isobaric Operation (P ≤ 100 kPa)

Initially, either one of the two pure components are selected to be charged into the still. For measurements below atmosphere, the boiling chamber should be filled up to approximately 3 centimeters higher than the top of the boiling chamber on the Cottrell pump. In addition the condensate receiver is entirely filled with the solvent. This will enable the chemicals to be forced up the Cottrell tube for easy boiling.

During the operation of the still at below atmospheric conditions the vacuum pump is switched on to maintain the set point pressure. The release valve on the ballast tank to the atmosphere is closed during low pressure measurements. The Labview automation computer program is opened and the pressure set point is entered on the computer via the graphical user interface. The desired initial and final internal voltage must also be entered, as well as the increment in the internal voltage. After the required pressure is entered, the solenoid valves are automatically manipulated to achieve the desired control. The external heater needs to manually be switched on. Once the correct pressure set point has been reached, the internal heater is automatically started at the initial voltage specified for start-up operation. The time for which each internal voltage is maintained may be altered on the actual coding setup of the Labview program. When the final internal voltage setting is reached, the computer will automatically zero the internal voltage.

After this occurs the plateau region is identified by the user. The system is allowed to run at the internal and external heater setting for that plateau region for approximately 50 minutes before a sample of the liquid and vapour phases is removed from the respective sampling ports.

The samples are removed using a GC syringe of 1 µl volume. Once the samples have been analyzed by the GC, and the moles of the components calculated from the peak areas analyzed, the mole ratios of the two components should differ by no more than ±0.02 of a mole fraction.

Once samples of the system are analyzed, a certain volume must be removed (approximately 2 ml) from either the liquid or vapour sampling point in order to measure the proceeding data point. Thereafter, 2 ml or more of the more dilute agent in the still is inserted into either the vapour or liquid sampling point, thus creating a new composition for analysis.

The same procedure is carried out (varying internal heater settings) to establish the equilibrium position. This process is repeated until the midway composition range ($x_1 = 0.5$) is reached. Once this point is reached, the still contents are drained. The still is washed thoroughly with acetone several times and, thereafter, filled with the second pure component. Vapour pressure measurements are carried out for the second component and then the same process as previously discussed is repeated to find the equilibrium compositions and settings for each mixture.

Measuring data covering both ends of the composition range allows for greater accuracy, as it tests the experimental technique since both sides of the equilibrium curves generated should meet smoothly in the middle. If there is discontinuity where the curves should meet, then this implies errors in the experimental method.

5.10.2 Isobaric Operation (100 kPa ≤ P ≤ 350 kPa)

When operating in this pressure range, the vacuum pump is switched off and the nitrogen regulator is opened. Initially, when attempting to reach the set point pressure, the bypass loop may be opened to hasten the process, thus allowing the nitrogen to flow through faster and enabling the new pressure to be reached quickly. The Labview automation program is started-up

and the desired pressure is entered. The same process as stated above for this programs operation is followed. Once the set point pressure is achieved, the computer software will automatically control the solenoid valves connected to the nitrogen tank and the atmosphere to maintain the conditions necessary for operation. The same procedure discussed above is followed to find the plateau region of each composition setting. Finally sampling takes place.

5.11 Isothermal Operation of the Recirculating Still

The program for isothermal operation is opened up. As per isobaric operation, the same start up procedure is followed for the isothermal scenario. The set point temperature, initial and final internal voltage setting, as well as the increment in internal voltage desired are entered on the Labview software interface. The external heater is manually switched on. Once the temperature set point has been reached and maintained constant for a minimum of 5 minutes, then only is the internal voltage incremented by the automation program. The program shall then automatically control the pressure within the still, to achieve the required temperature, via the manipulation of the solenoid valves. If the system is below atmospheric pressure, the vacuum pump should be switched on to maintain the vacuum. The nozzle on the nitrogen tank should be opened at all times during isothermal operation (allowing nitrogen gas to flow through the line freely) to enable a simplistic maneuver from low to higher pressures. Once the plateau region is located (as discussed previously), the samples are withdrawn directly from the still, analyzed and the next composition set is reached by addition of the second, more dilute, component.

5.12 Composition Analysis

Once the contents of the still are operating in the plateau region and it is established that the equilibrium within the still has stabilized (approximately 50-70 minutes), samples of the liquid and vapour are withdrawn. The samples of liquid and vapour are withdrawn from their respective sampling ports. Septa form the interface between the sampling port and the vapour and liquid samples. A 1 µl GC syringe was used to draw the samples. The syringe was supplied by DLD Scientific and was washed with acetone, as well as being washed out several times with the sample, prior to sampling. The septa are also supplied by DLD Scientific and are highly

temperature resistant (0-200˚C). When inappropriate septa (0-100˚C) are used this could lead to the septa exploding while measurements are being carried out, thus wasting a great deal of chemicals, as well as the experimenters time.

The direct technique of analysis is where the liquid/vapour sample is removed from the still and analyzed instantly, as opposed to the indirect technique of placing the samples in glass vials and analyzing the mixture at a later stage. The latter approach has the distinct disadvantage of the samples having to be placed in a chiller until such a time that analysis is possible. In addition, depending on the physical properties of the components in the binary solution (volatility), some species will evaporate. This results in the composition of the sample being altered.

The direct technique was employed for analysis purposes. A minimum of four samples were removed from the liquid and vapour sampling points each and analyzed directly by gas chromatography. This was done to ensure reproducibility in results. It is accepted that for whichever of the species analyzed, a tolerance of ±0.02 of a mole fraction is generally acceptable (Reddy, 2006). This guide allows for uncertainties arising from errors in calibrations and the GC analysis equipment. All deviations in analysis of the compositions remained within a tolerance of 2% for the experiments carried out in this work. There are other manners in which one may undertake composition analysis. They are: refractometry and densitometry. However, the advantage of using the GC above the other techniques is that it is able to detect other peaks, beside those corresponding to the systems of interest. This is important for detecting the presence of impurities, which if available in large amounts (> 1%), could affect the results significantly.

5.13 Shut-Down Procedure

The Labview automation program (be it for isobaric or isothermal operation) is ended by clicking on the „stop button". As a consequence of this the internal heater decreases its heat input to zero. The solenoid valves are no longer manipulated to control the pressure. The variac connected to the external heater is manually switched off. The system is maintained at whatever pressure it is currently sitting on from the previous run, until the still cools down.

If the apparatus was being operated at pressures below atmosphere, then the valve leading from the vacuum pump to the ballast tank should be closed prior to it being shut off. This prevents the oil from the pump being sucked into the ballast tank owing to a pressure gradient developing when the vacuum pump shuts off. Once this has been executed and the still is cool, the valve, releasing pressure accumulated in the ballast tank, may be opened and the apparatus brought to atmospheric pressure.

The valve on the ballast tank is opened, releasing the built-up pressure to the atmosphere. Thereafter, the flow of gas from the nitrogen tank is stopped by closing the appropriate valve. The water bath and cooling unit are switched off, as well as the AC/DC power supply to the stirrers. The contents of the still are then emptied and disposed off in a waste chemical bottle.

Chapter 6: Experimental Results

This chapter showcases the experimental results for the scope of this thesis. Reported herein are the phase equilibrium measurements for this topic, calibrations for the temperature and pressure sensors, as well as the gas chromatograph detector. The uncertainties in temperature, pressure and phase compositions are reported as well as the purity of the chemicals utilized in this work.

6.1 Purity of Chemicals

The most important aspect which must be checked before commencing system measurements is the purity of the chemicals involved. Errors here will merely be compounded and lead to greater inaccuracy in system measurements. The purity of the chemicals in use is quantified by analyzing the refractive indices of the chemicals and then checking this against literature values, as well as analyzing the chemicals on the GC to ascertain the peak areas, and if there are any significant impurities present. The refractive index of chemical components was measured on the high precision ATAGO RX – 7000 α refractometer, with an accuracy of ±0.0001 nD (www.atago.net). The table below summarizes the purity check for chemical components.

Table 6-1: A list of the chemicals used and their respective purities.

Chemical (IUPAC name)	Formula	Supplier	Stated Minimum Purity (mass %)[a]	GC Analysis (Peak area %)	Refractive Index Literature[b]	Refractive Index This work[c]
N-methyl-2-pyrrolidone	C_5H_9NO	Merck	99.5	99.83	1.469	1.469
1-Hexene	C_6H_{12}	DLD Scientific	99.5	99.85	1.385	1.385
n-Hexane	C_6H_{14}	Merck	99.5	99.54	1.372	1.372
Ethanol	C_2H_5OH	Merck	99.5	99.8	1.361	1.361
Cyclo-hexane	C_6H_{12}	Merck	99.5	99.8	1.424	1.424

[a] As stated by supplier

[b] Poling *et al*., 2001; Calibration carried out at 298.15 K

[c] Calibration carried out at 298.15 K

6.2 Equipment Calibration and Accuracy of Measurements

In addition to checking the purity of the chemicals used, another important factor to take into consideration is the accuracy of the measurements undertaken. The accuracy of the temperature and pressure sensors, as well as the accuracy of the composition calibration must be computed. Errors which go undetected in the analysis of accuracy actually compound the errors in experimental work. For a greater understanding of how the accuracies were computed in this work reference should be made to Appendix D.

Table 6.2: Estimated accuracy of measured system variables.

	Apparatus of Hirawan (2007) (Low pressure VLE still)	Apparatus of Lilwanth (2011) (Moderate pressure VLE still)
Temperature/ K	± 0.425	± 0.089
Pressure/ kPa	± 0.320	± 0.440

6.2.1 Pressure, Temperature and GC Detector Calibrations

The pressure transducer used for the low pressure measurements is the WIKA CPH 6000 pressure transducer. For the low pressure VLE apparatus of Hirawan (2007) calibrations for pressure were carried out over the pressure range: 0-100 kPa. These pressure calibrations are presented below in Figure 6.1-6.2.

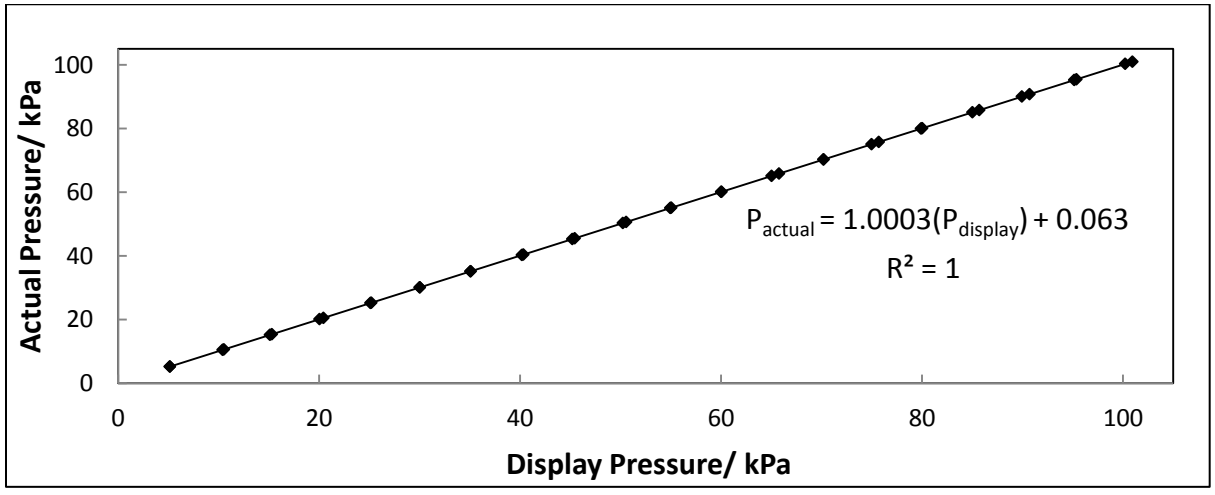

Figure 6-1: Pressure transducer calibration plot for the low pressure VLE apparatus.

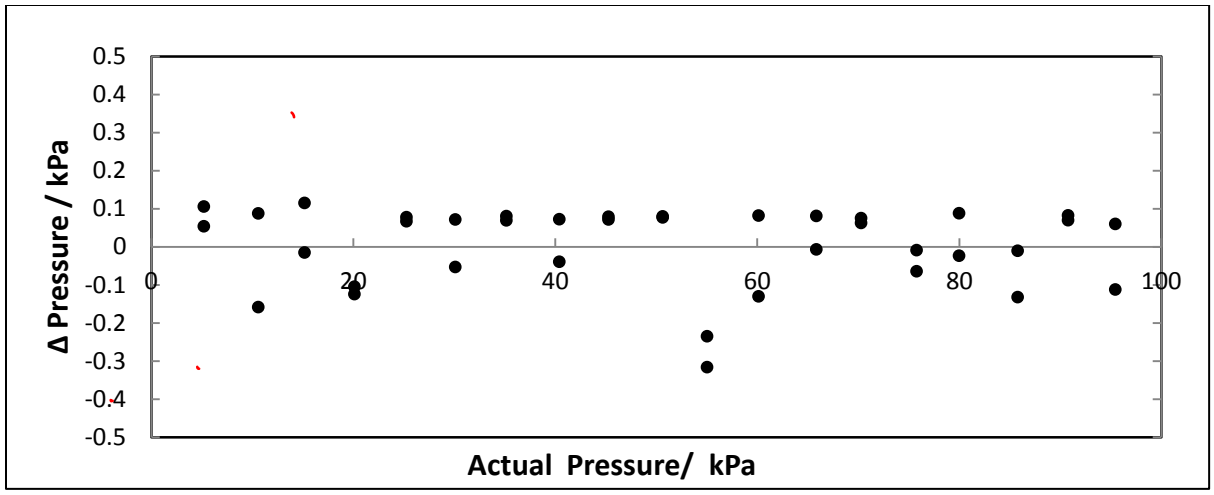

Figure 6-2: Plot of pressure deviation for the low pressure VLE equilibrium still.

The temperature sensor used in the low pressure VLE still of Hirawan (2007) is the Pt 100 1/10 Din and the equipment used for the carrying out the calibration of this sensor is the temperature unit CTH 6500. These temperature calibration plots are presented below in Figure 6.3-6.4.

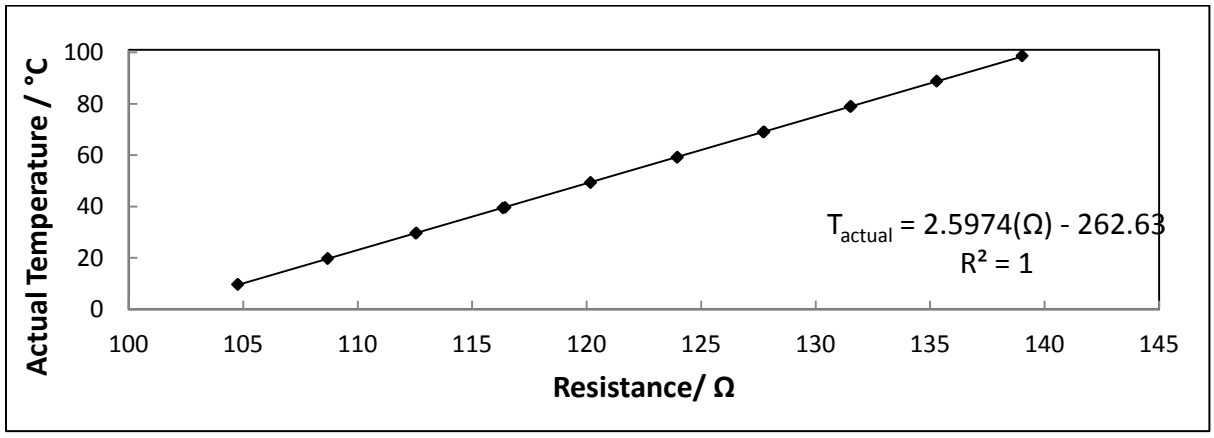

Figure 6-3: Temperature sensor (Pt-100) calibration plot for the low pressure VLE apparatus.

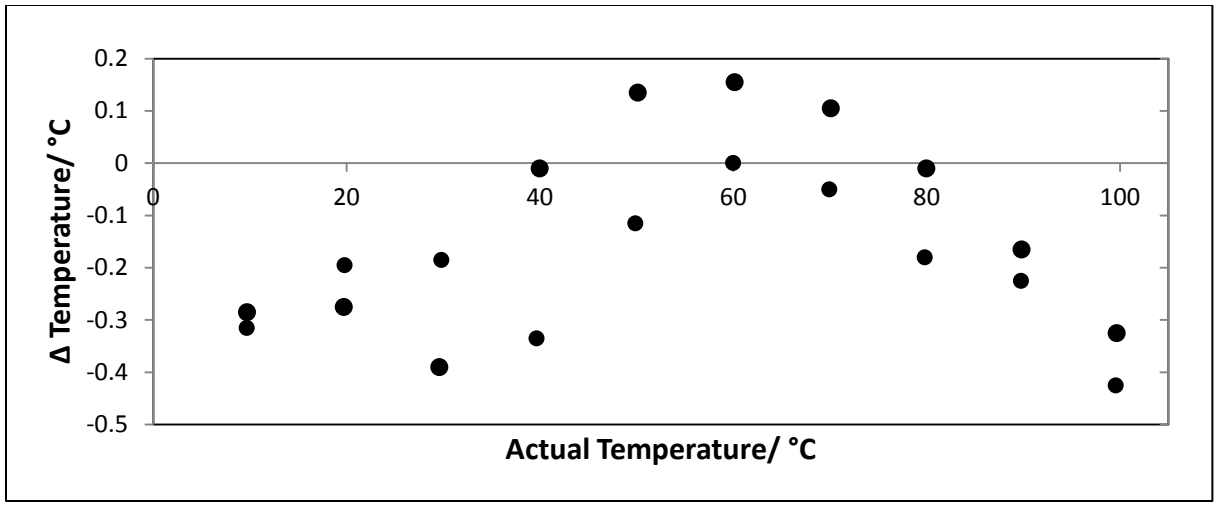

Figure 6-4: Plot of temperature deviation for the Pt-100 in the equilibrium still.

The pressure transducer used for the moderate pressure measurements is the WIKA P-10 pressure transducer. For the low-to-moderate pressure VLE apparatus of Lilwanth (2011) calibrations for pressure were carried out over three different pressure ranges: 0-9 kPa, 9-100 kPa and 100-500 kPa. These pressure calibrations are presented below in Figures 6.5-6.9. The temperature calibration plots are presented in Figures 6.10-6.11.

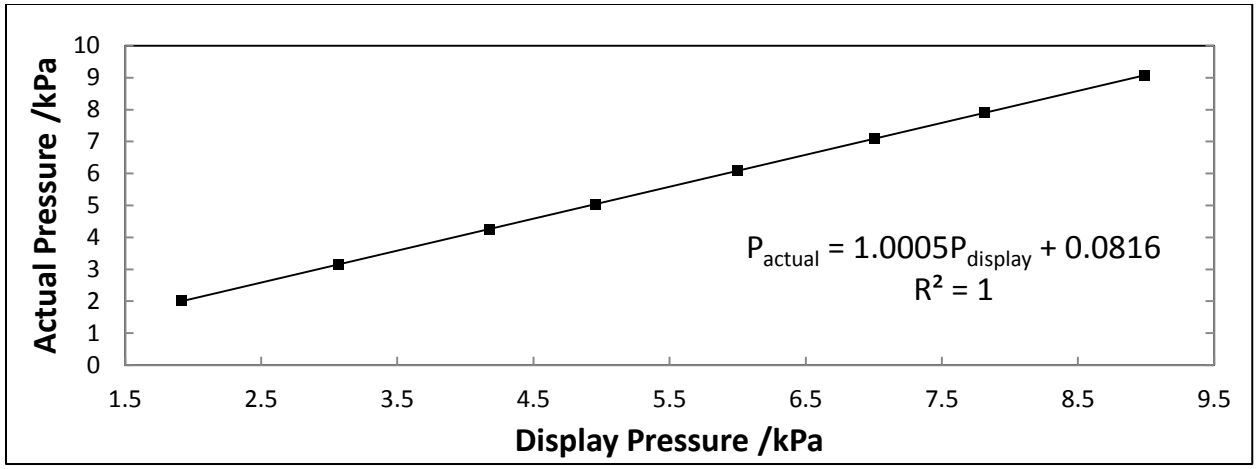

Figure 6-5: Pressure transducer calibration plot for the moderate pressure VLE apparatus (0-9 kPa).

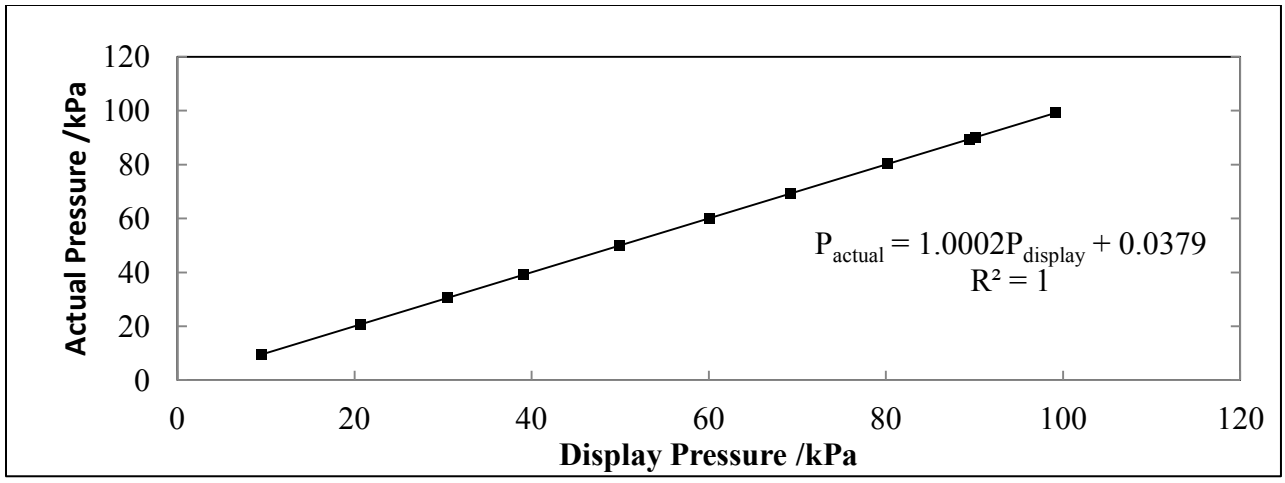

Figure 6-6: Pressure transducer calibration plot for the moderate pressure VLE apparatus (9-100 kPa).

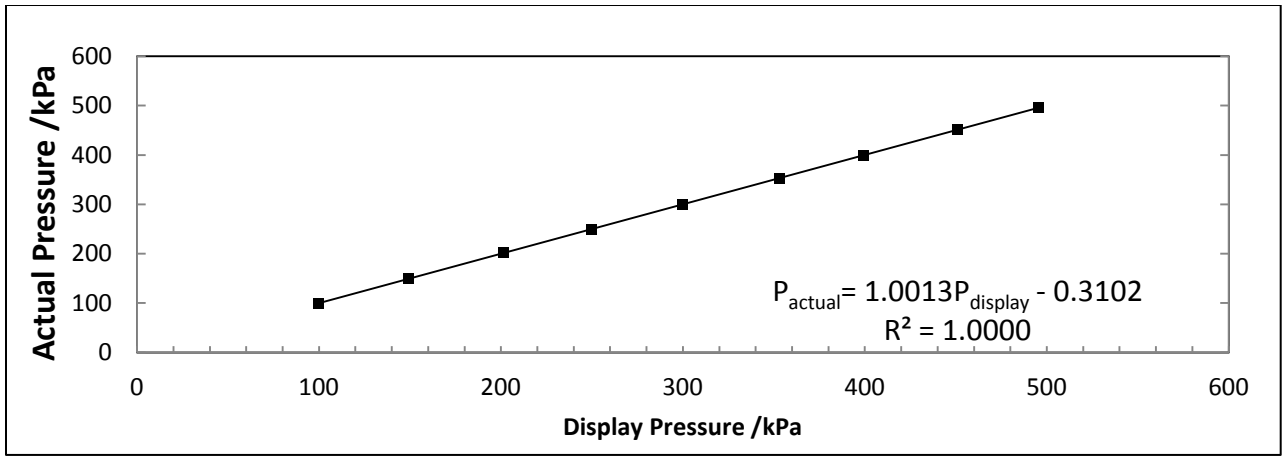

Figure 6-7: Pressure transducer calibration plot for the moderate pressure VLE apparatus (100-500 kPa).

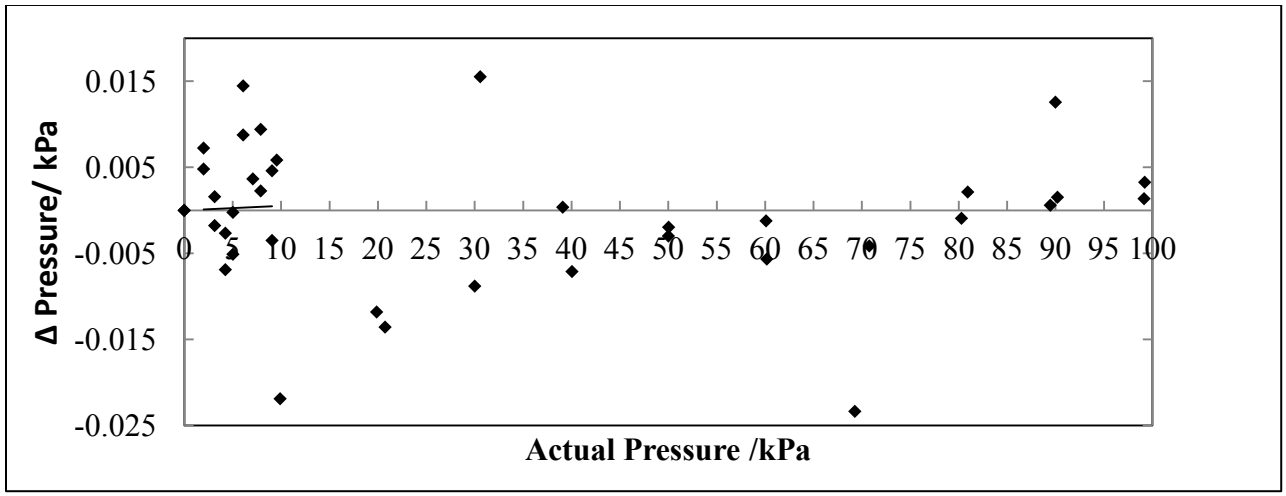

Figure 6-8: Plot of pressure deviation for the moderate pressure VLE apparatus (0-100 kPa).

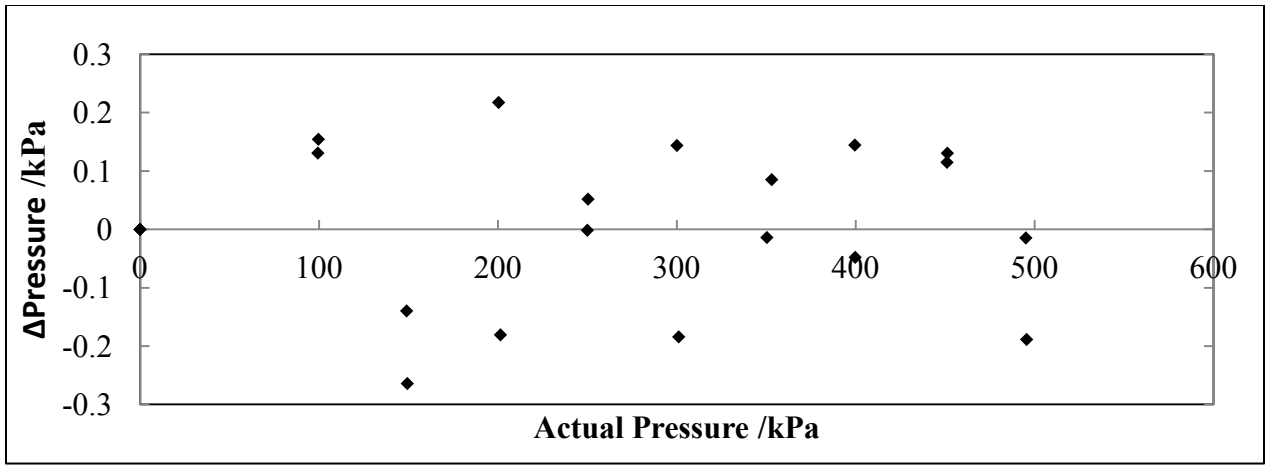

Figure 6-9: Plot of pressure deviation for the moderate pressure VLE apparatus (100-500 kPa).

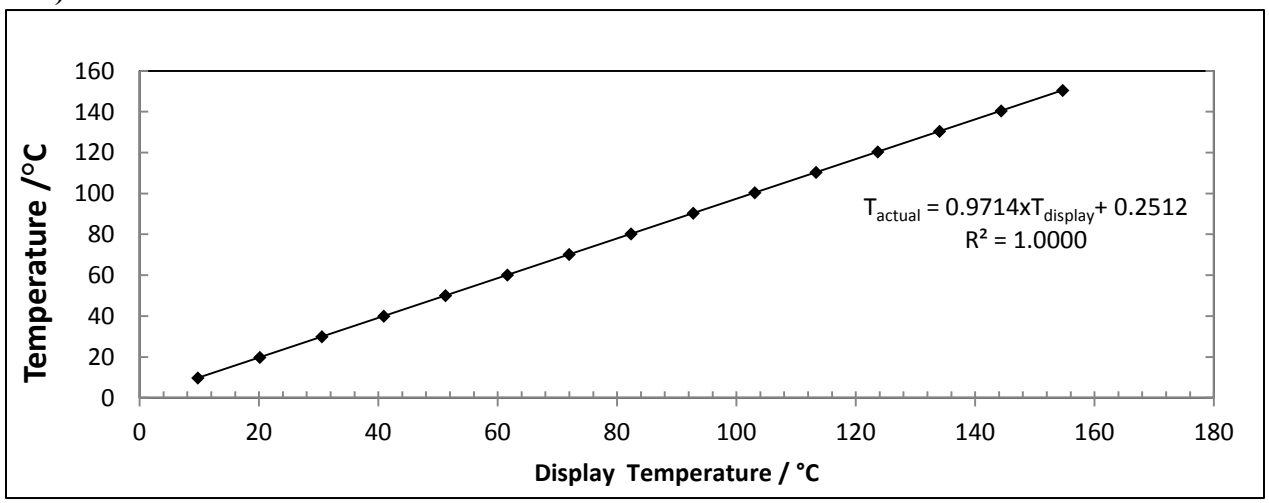

Figure 6-10: Temperature sensor (Pt-100) calibration plot for the moderate pressure VLE apparatus.

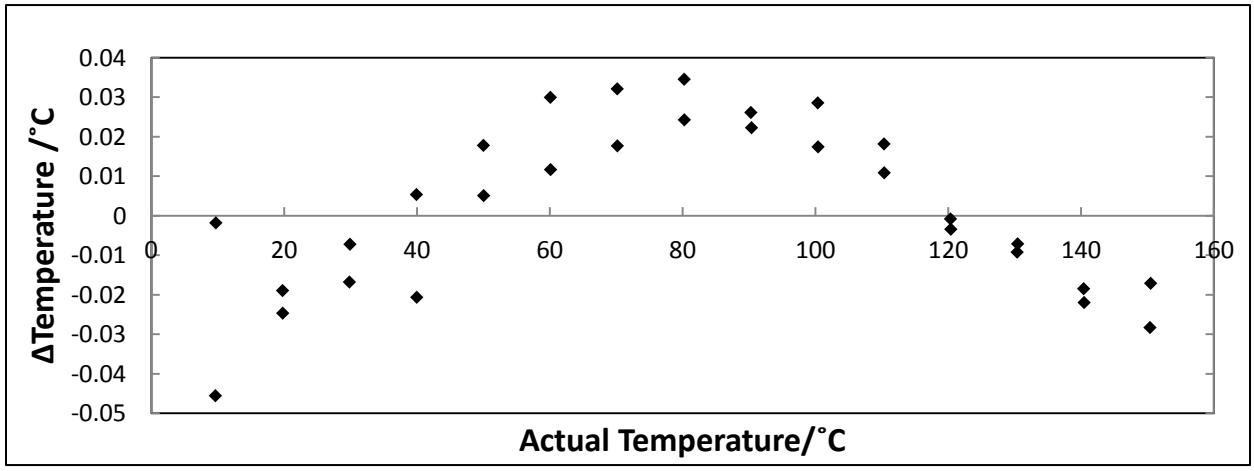

Figure 6-11: Plot of temperature deviation for the Pt-100 in moderate pressure VLE apparatus (100-500 kPa).

6.2.2 GC calibrations and Operating Conditions

Tables 6-3 and 6-4 summarize the GC operating conditions for all systems investigated in this study. These conditions are the optimum settings at which the GC should operate in order to obtain the best separation between the chemicals being used.

Table 6-3: Operating conditions for the gas chromatograph.

Operating Conditions		**Settings Used**	
GC model	GC Shimadzu 2014	GC Shimadzu 2014	GC Shimadzu 2010
System	1-hexene + NMP	n-hexane + NMP	ethanol + cyclohexane
Column	Porapak-Q	Porapak-Q	HP-5 Capillary
Type	Packed	Packed	Capillary
Serial Number	13284	13284	19091J-413
Length/ m	4	4	30
Inner Diameter/ mm	2.20	2.20	0.32
Injector Profile			
Injector temperature/K	513.15	513.15	513.15
Carrier gas	Helium	Helium	Helium
Injection mode	Split less	Split less	Split less
Total flow/ $ml.min^{-1}$	30	30	20
Detector Profile			
Detector type	TCD	TCD	TCD
Detector temperature/K	593.15	593.15	513.15
Make up flow/ $ml.min^{-1}$ (Helium gas)	40	40	40
Oven Profile			
Temperature control mode	Isothermal	Isothermal	Isothermal
Oven Temperature/K	423.15	393.15	423.15
Elution Time/ min			
NMP	8.349	7.740	-
1-hexene	0.788	-	-
n-hexane	-	0.707	-
Ethanol	-	-	1.866
Cyclohexane	-	-	1.566

Table 6-4: Operating conditions for the Shimadzu 2010 gas chromatograph.

Operating Condition	Settings used	
GC model	GC Shimadzu 2014	GC Shimadzu 2014
System	1-hexene + n-hexane	1-hexene + n-hexane + NMP
Column	Ohio Valley – 1	Ohio Valley – 1
Serial Number	112219	112219
Length/ m	30	30
Inner Diameter/ mm	0.53	0.53
Injector Profile		
Injector temperature/ K	473.15	473.15
Carrier gas	Nitrogen	Nitrogen
Injection mode	Split with ramp	Split with ramp
Column pressure/ kPa	12.4	12.4
Column flow/ $ml.min^{-1}$	2.73	2.73
Linear velocity/ $cm.sec^{-1}$	20	20
Total flow/ $ml.min^{-1}$	31.6	31.6
Carrier gas flow rate (FID)/ $ml.min^{-1}$	30	30
Split ratio	10	10
Detector Profile		
Detector type	FID	FID
Detector temperature/K	473.15	473.15
Make up flow/ $ml.min^{-1}$ (H_2: Air)	40:400	40:400
Oven Profile		
Temperature control mode	Ramp	Ramp
Oven Temperature/ K	303.15	303.15 K for 7 minutes then increase at 308.15K/min until 423.15K
Elution Time/ min		
1-hexene	5.132	5.132
n-hexane	5.677	5.677
NMP	-	13.765

The purpose of the GC detector calibration is to determine the gradients of each of the components in their dilute regions. The gradient is referred to as the response factor ratio, F_1/F_2 and F_2/F_1, and is obtained from the plot of A_1/A_2 versus x_1/x_2 and A_2/A_1 versus x_2/x_1 respectively. The slope from the linear plot of A_1/A_2 versus x_1/x_2 and A_2/A_1 versus x_2/x_1 should render values which are the mathematical inverses of each other. The response factor ratio for each side evaluated should remain constant. If the response factor ratios are not mathematical inverses of each other to within 1%, then during calculations for liquid and vapour mole fractions for the two different dilute regions, the response factor evaluated for that specific region must be used, instead of merely applying the inverses of each interchangeably.

Figures 6-12 and 6-16 display the GC calibration plots for the systems ethanol + cyclohexane and 1-hexene + NMP.

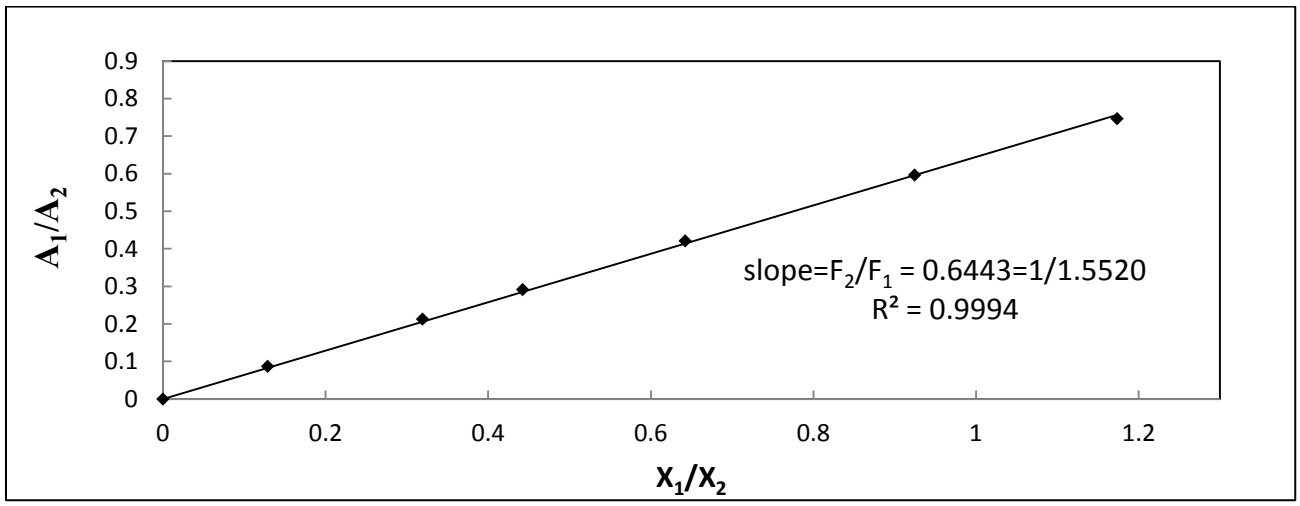

Figure 6-12: GC calibration plot of the System Cyclohexane (1) + Ethanol (2) (Ethanol Dilute Region).

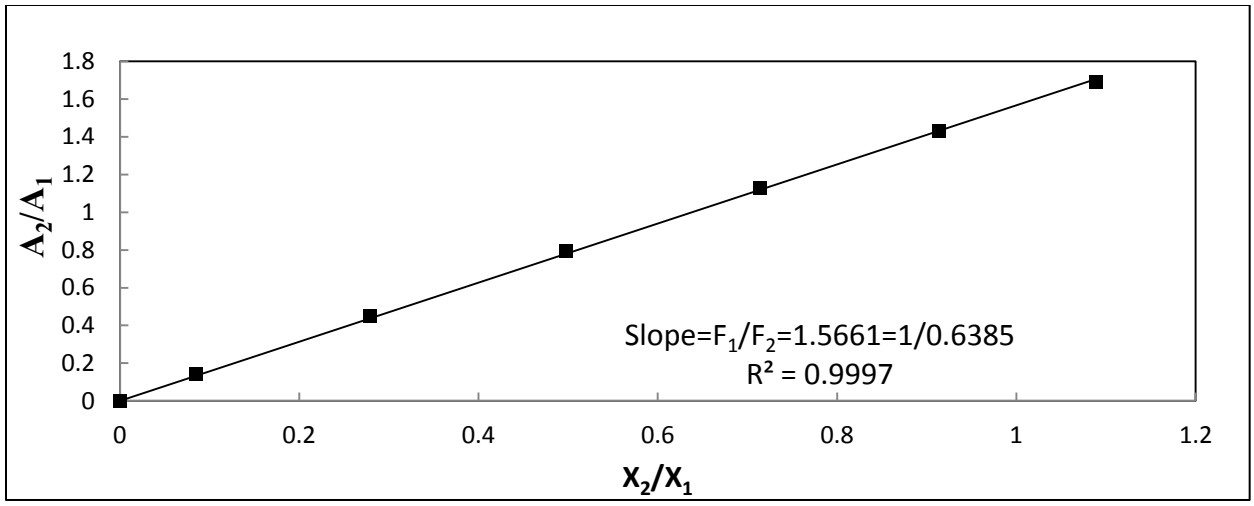

Figure 6-13: GC calibration plot of the System Cyclohexane (1) + Ethanol (2) (Cyclohexane Dilute Region).

From Figures 6-12 and 6-13 one observes that the inverse of the gradients of the graphs are in close proximity of each other with a 0.9002% deviation. For the aforementioned system, the uncertainty in calibration is ±0.002 to a mole.

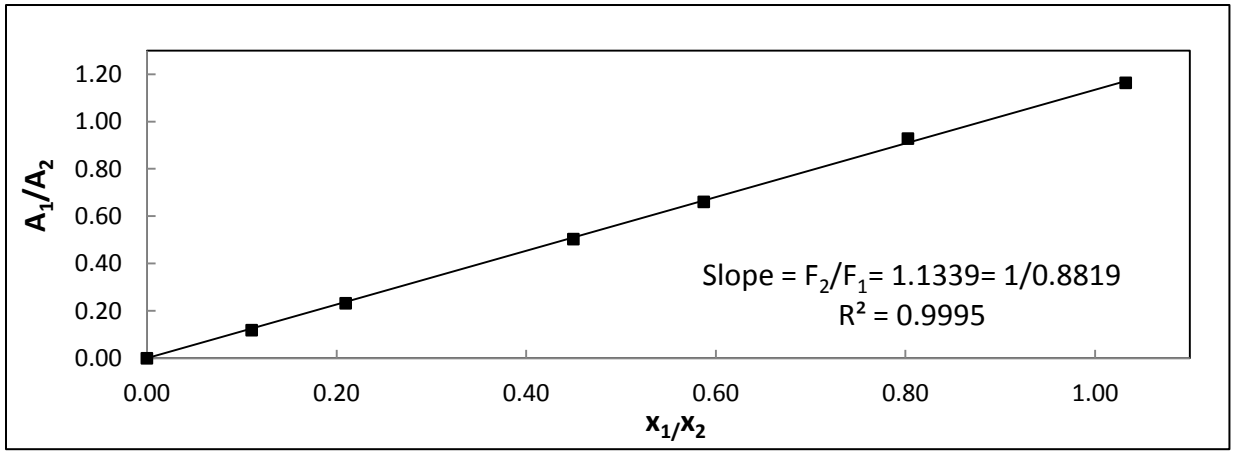

Figure 6.14: GC calibration plot of the System 1-hexene (1) + NMP (2) (1-Hexene Dilute Region).

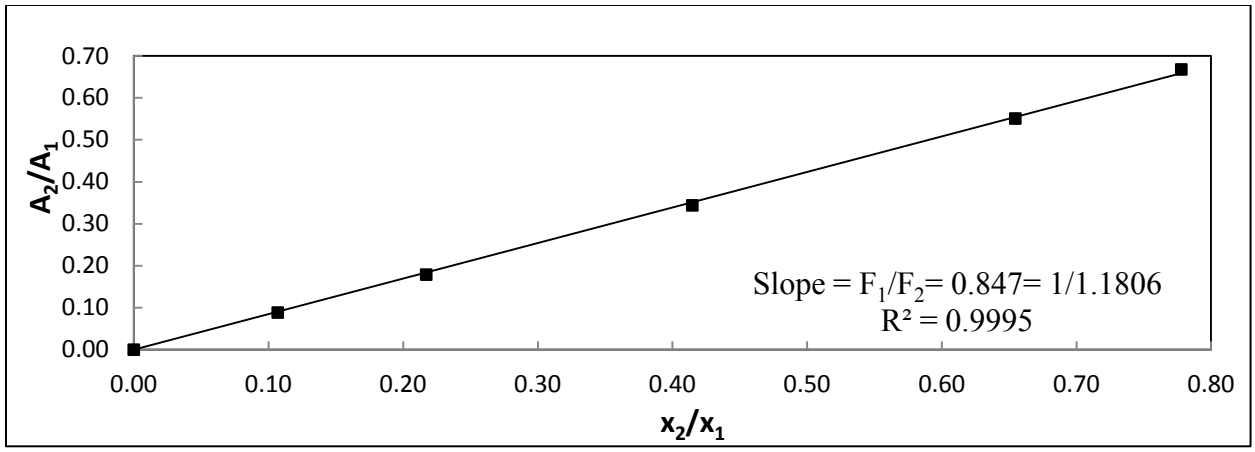

Figure 6.15: GC calibration plot of the System 1-hexene (1) + NMP (2) (NMP Dilute Region).

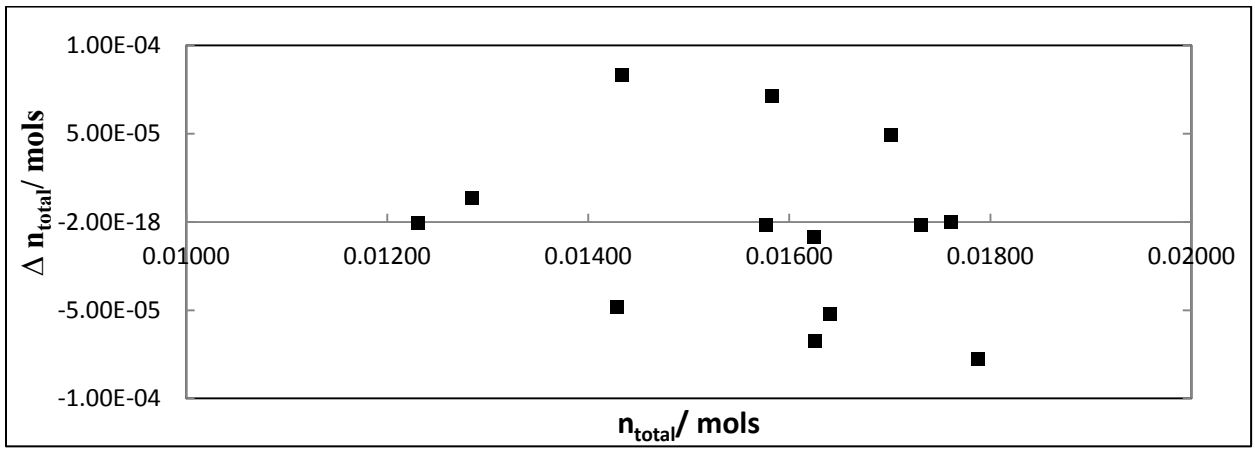

Figure 6-16: Scatter plot for the system 1-hexene (1) + NMP (2) showing the deviation in moles.

For the system 1-hexene + NMP, it is clear that the inverse of the response factor ratio of one dilute region deviates significantly from the slope of the other. This deviation is approximately 4.1185 %. This indicates that when calculations are carried out for the x-y compositions, the separate slope values specific to each dilute region should be used. The accuracy in the calibration for this system is ±0.0034.

The calibration plots shown below pertain to the systems: n-hexane (1) +NMP (2), 1-hexene (1) + n-hexane (2) and 1-hexene (1) + n-hexane (2) + NMP (3). The calibration for each system was carried out using a volume based technique, where a known volume of each component was

directly injected in the GC and the peak area recorded. Thereafter, the number of moles corresponding to the volume injected is computed and a plot of area versus the number of moles is carried out. This method was employed as n-hexane is immiscible at temperatures ≤ 328.15 K. Thus, this volumetric method had to be carried out for all the components again in order to avoid complications when measuring the ternary system.

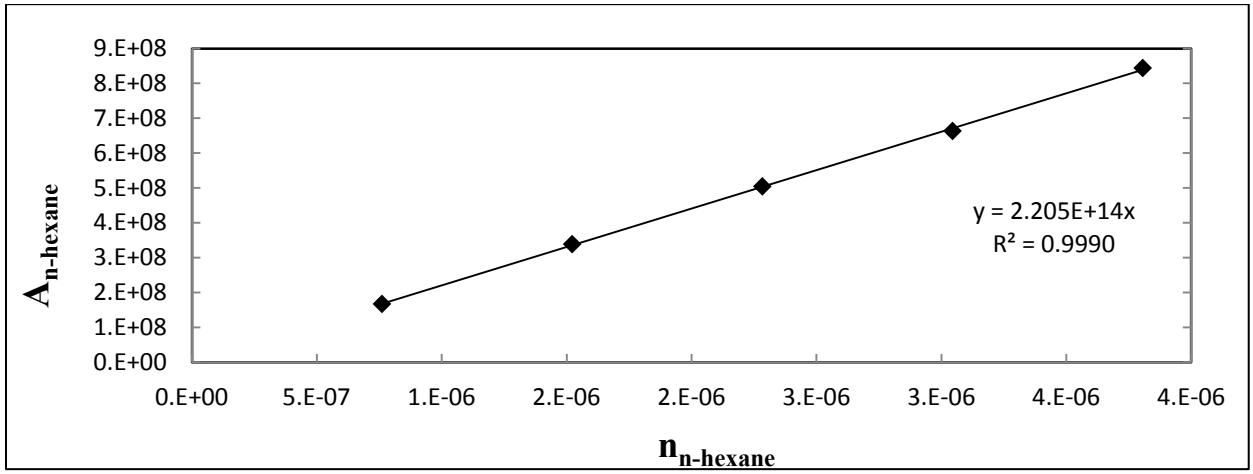

Figure 6-17: GC calibration plot for n-hexane (volumetric method for GC calibration).

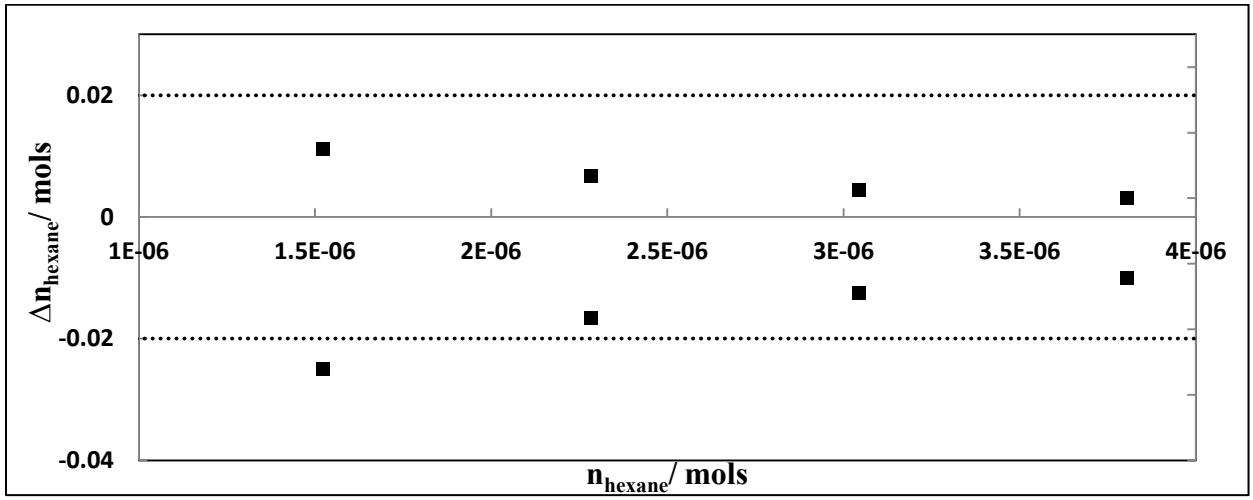

Figure 6-18: Scatter plot for the mole deviation of n-hexane on the Shimadzu 2014 GC.

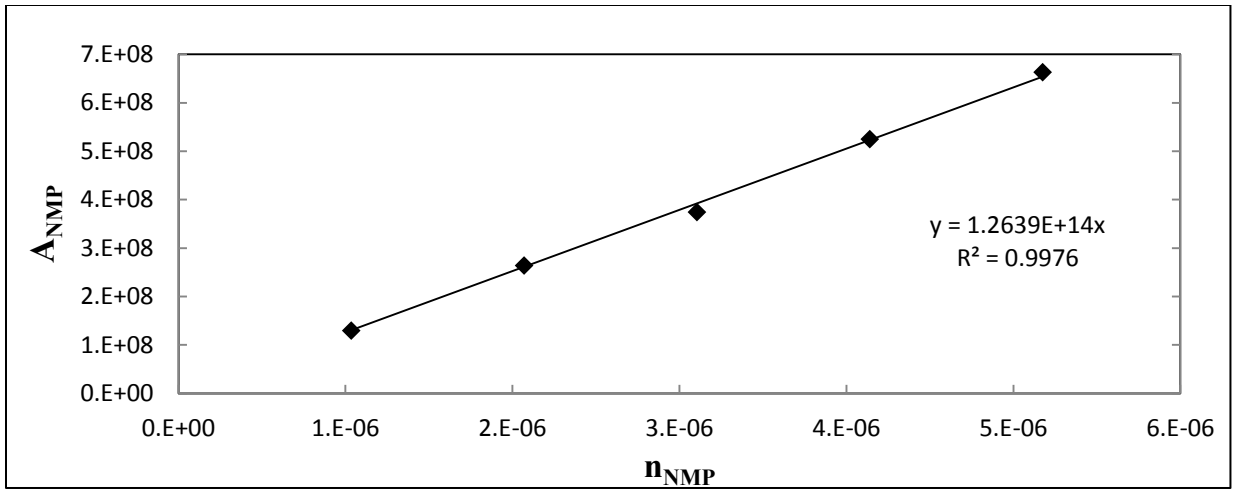

Figure 6-19: GC calibration plot for NMP (volumetric method for GC calibration).

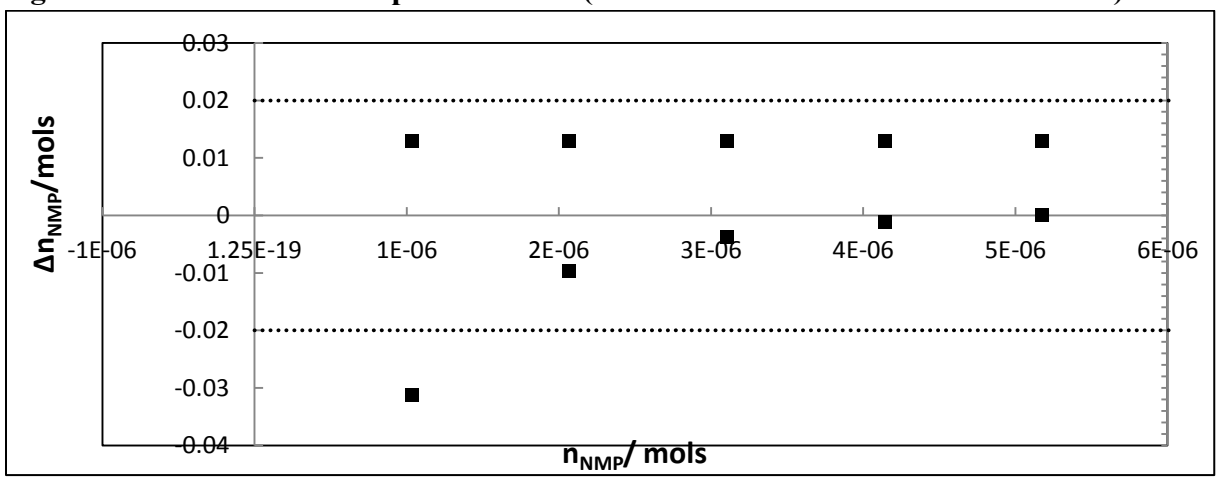

Figure 6-20: Scatter plot for the mole deviation of NMP on the Shimadzu 2014 GC.

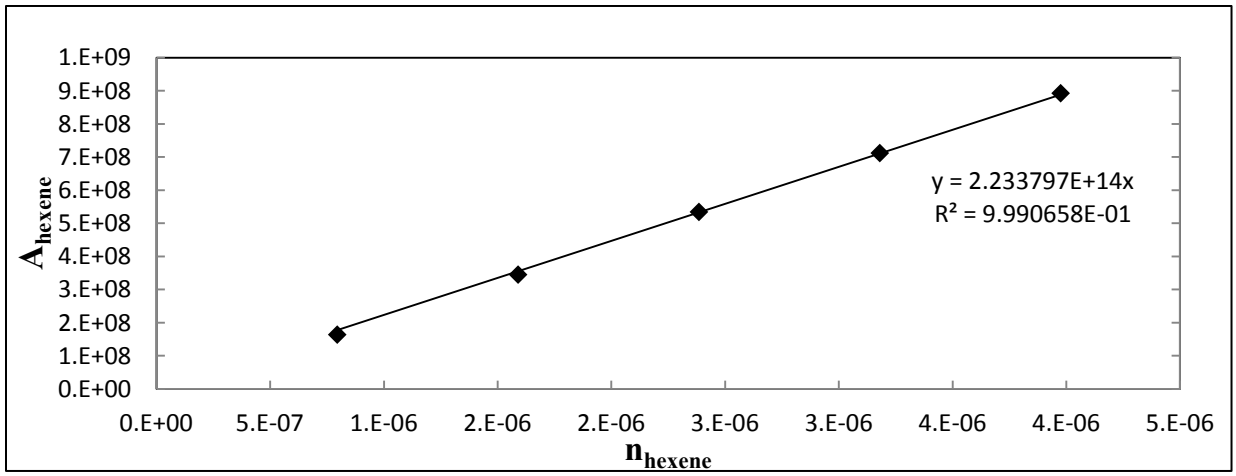

Figure 6-21: GC calibration plot for 1-hexene (volumetric method for GC calibration).

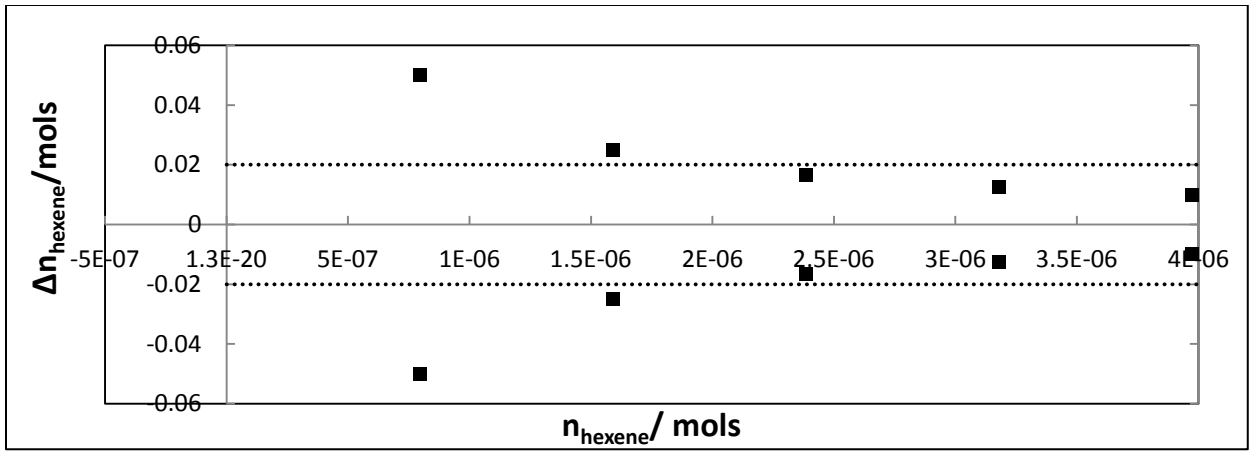

Figure 6-22: Scatter plot for the mole deviation of 1-hexene on the Shimadzu 2014 GC.

6.3 Pure Component Vapour Pressure Measurements

Vapour pressure data were measured for ethanol, 1-hexene, n-hexane and NMP. These measurements are crucial as a preliminary test of the purity of the chemicals being used. The measured data was then compared to literature data, where available, to compare the accuracy. Vapour pressure measurements are useful for verifying that the equipment is functioning properly (for example checking for leaks, calibrations *etc*) as well as becoming better acquainted with the experimental procedure. In order to quantify the accuracy of the measured vapour pressure data, the deviations of the experimental data from literature is computed as follows:

$$\%\ \text{deviation of pressure}\left(\frac{\Delta P}{P}/\%\right) = 100 \times \frac{P^{\exp} - P^{lit}}{P^{\exp}} \tag{6.1}$$

$$\%\ \text{deviation of temperature}\left(\frac{\Delta T}{T}/\%\right) = 100 \times \frac{T^{\exp} - T^{lit}}{T^{\exp}} \tag{6.2}$$

The superscripts “exp” and “lit” refer to experimental and literature data respectively, that were available for the corresponding measurements being carried out. The resultant vapour pressure measurements conducted as well as the percent deviation from literature are presented in tables 6-5 to 6-8. The graphical illustrations of this data are provided in Figures 6-23 to 6-26. The

measured vapour pressure data was regressed employing Aspen Plus® to obtain the constants for the Antoine equation. This is represented in Table 7-1 in Section 7.1, together with the average absolute percentage deviations from available literature values exhibited in Table 7-2.

Table 6-5: Literature and experimental vapour pressure data for 1-hexene.

Pressure (This work)/ kPa	Temperature (This work)/ K	$\frac{\Delta T}{T}$ (% Error)			$\frac{\Delta P}{P}$ (% Error)		
		Lit [A]	Lit [B]	Lit [C]	Lit [A]	Lit [B]	Lit [C]
19.99	293.38	0.075	0.079	0.079	0.02	0.02	0.03
59.98	321.04	0.013	0.013	0.013	0.04	0.18	0.02
100.09	336.21	0.004	0.004	0.004	0.09	0.18	0.08
150.00	349.55	0.009	0.009	0.009	0.001	0.12	0.05
199.98	359.70	0.038	0.038	0.038	0.002	0.32	0.08
224.02	363.70	0.099	0.100	0.100	0.01	0.39	0.07
250.04	367.96	0.084	0.084	0.084	0.02	0.47	0.07

[A] Component Plus (2010)

[B] Dortmund Data Bank (2011)

[C] Poling *et al.* (2001)

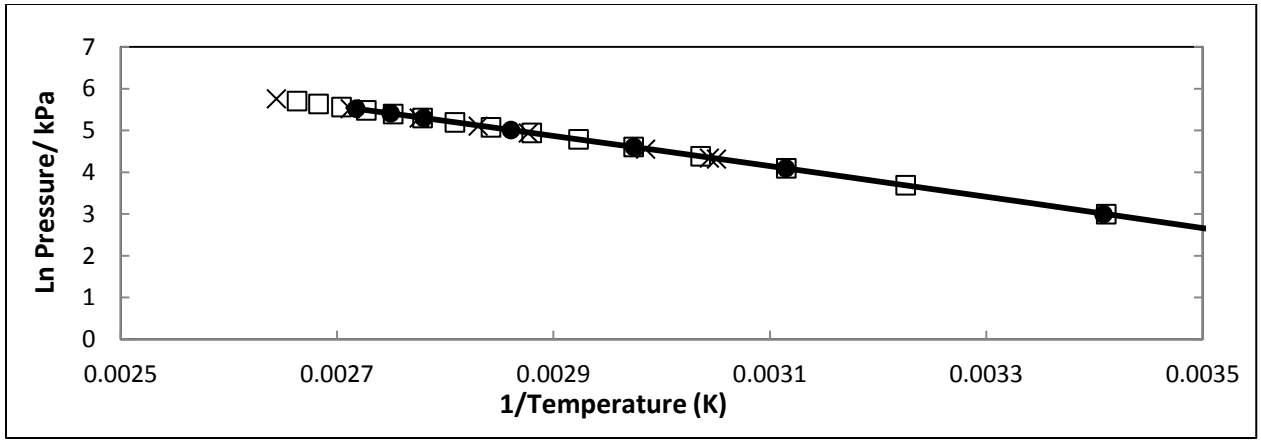

Figure 6-23: Vapour pressure plot for 1-hexene. -■-, This work; -, DDB (2011); -□-, Component Plus (2010); X, Poling *et al.* (2001).

Table 6-6: Literature and experimental vapour pressure data for NMP.

Pressure (Experimental)/ kPa	Temperature (Experimental) / K	$\frac{\Delta T}{T}$ (%) Lit [A]	$\frac{\Delta T}{T}$ (%) Lit [B]	$\frac{\Delta T}{T}$ (%) Lit [C]	$\frac{\Delta P}{P}$ (%) Lit [A]	$\frac{\Delta P}{P}$ (%) Lit [B]	$\frac{\Delta P}{P}$ (%) Lit [C]
1.31	353.20	0.517	0.619	-	0.53	1.32	-
2.18	364.96	0.371	0.496	-	0.69	1.24	-
5.02	382.90	0.051	0.051	-	0.31	1.28	-
10.06	400.70	0.080	0.080	-	0.58	1.19	-

[A] Component Plus (2010)

[B] Dortmund Data Bank (2011)

[C] Poling *et al.* (2001)

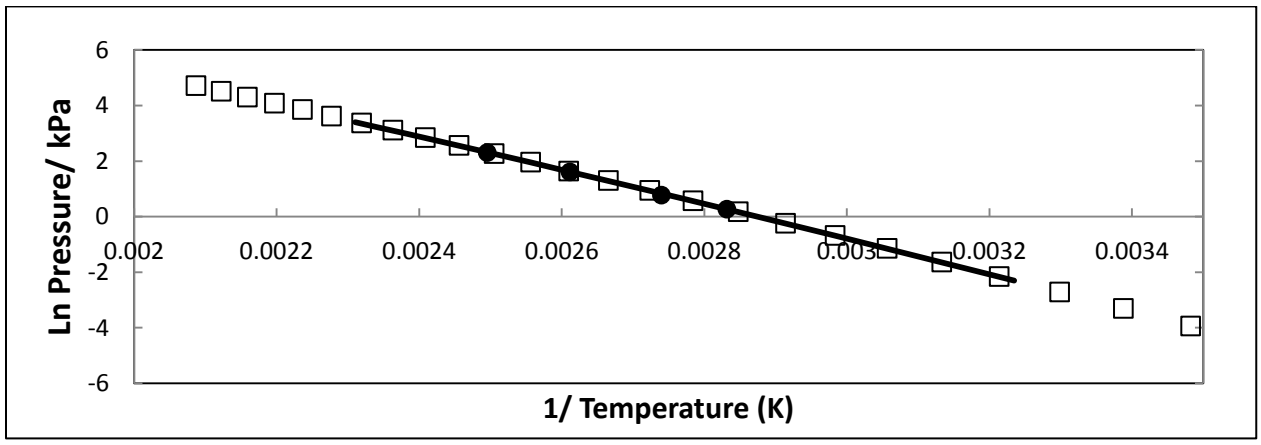

Figure 6-24: Vapour pressure plot for NMP. -●-, This work; ——, Component Plus (2010); □, DDB (2011).

Table 6-7: Literature and experimental vapour pressure data for n-hexane.

Pressure (Experimental)/ kPa	Temperature (Experimental) / K	$\frac{\Delta T}{T}$ (%) Lit [A]	$\frac{\Delta T}{T}$ (%) Lit [B]	$\frac{\Delta T}{T}$ (%) Lit [C]	$\frac{\Delta P}{P}$ (%) Lit [A]	$\frac{\Delta P}{P}$ (%) Lit [B]	$\frac{\Delta P}{P}$ (%) Lit [C]
54.24	323.18	0.010	0.010	0.010	0.03	0.71	0.29
105.58	343.05	0.028	0.028	0.028	0.19	0.38	0.11
187.88	362.75	0.108	0.108	0.108	0.01	0.64	0.55

[A] Component Plus (2010)

[B] Dortmund Data Bank (2011)

[C] Poling *et al.* (2001)

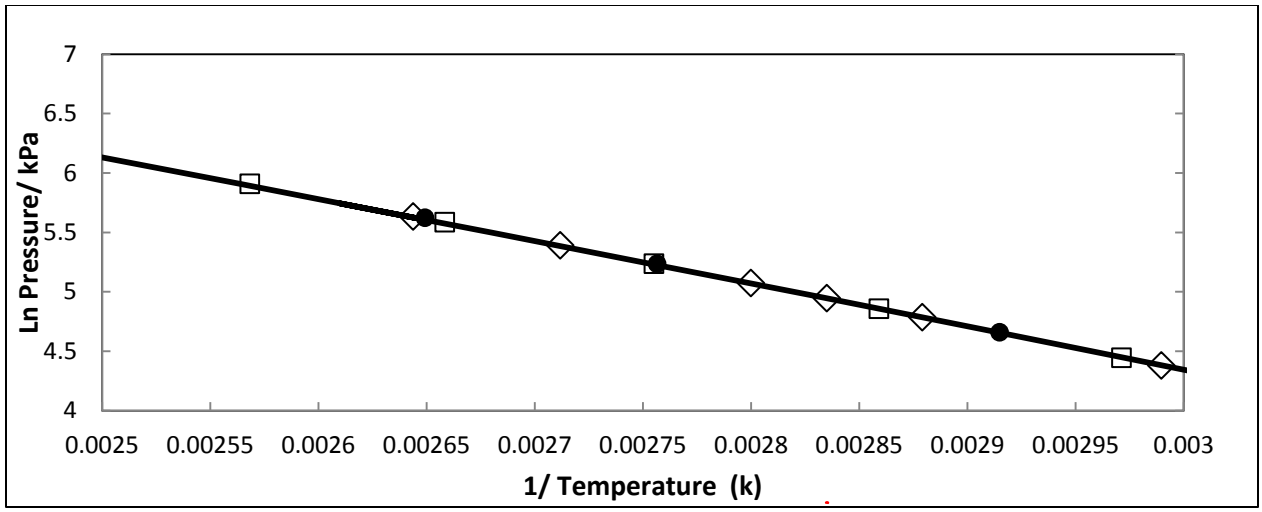

Figure 6-25: Vapour pressure plot for n-hexane. ●, This work; □, DDB (2011); ——, Component Plus (2010); ◊, Poling *et al*. (2001).

Table 6-8: Literature and experimental vapour pressure data for ethanol.

Pressure (Experimental)/ kPa	Temperature (Experimental) / K	$\frac{\Delta T}{T}$ (%)			$\frac{\Delta P}{P}$ (%)		
		Lit [A]	Lit [B]	Lit [C]	Lit [A]	Lit [B]	Lit [C]
25.30	320.11	0.014	0.096	0.046	1.24	1.19	1.19
30.13	323.71	0.137	0.175	0.060	0.49	0.48	0.47
60.27	338.91	0.072	0.102	0.012	0.51	0.51	0.51
80.22	345.65	0.143	0.153	0.010	0.33	0.32	0.32
99.86	351.07	0.024	0.000	0.024	0.09	-0.19	0.31

[A] Component Plus (2010)

[B] Dortmund Data Bank (2011)

[C] Poling *et al.* (2001)

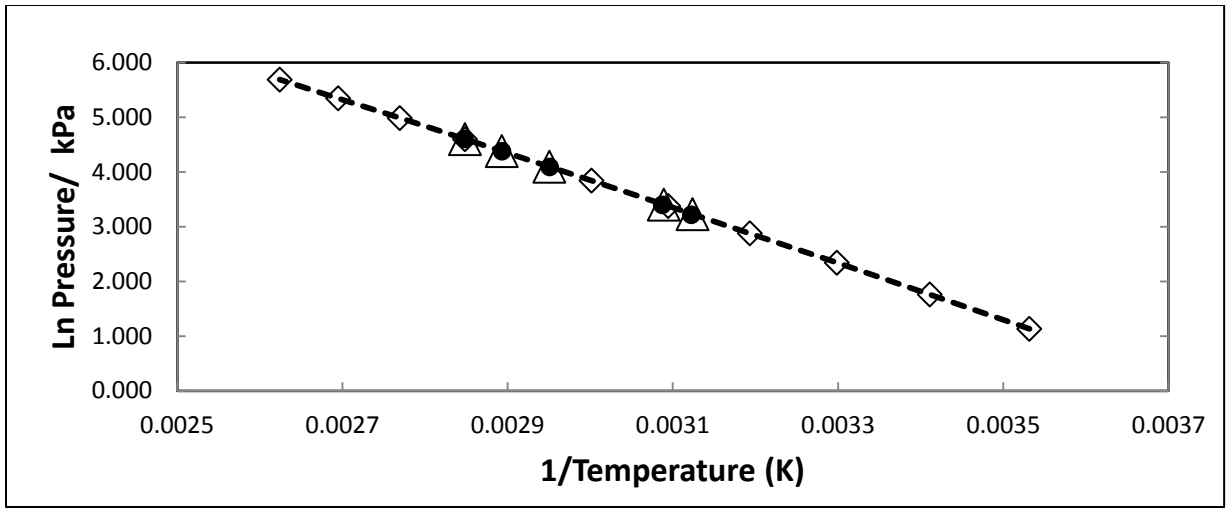

Figure 6-26: Vapour pressure plot for ethanol. Δ, This work; ◊, Component Plus (2010); ▬ ▬ ▬, DDB (2011); ●, Poling *et al*. (2001).

6.4 Binary Vapour-Liquid Equilibria Measurements

6.4.1 Results for the System ethanol (1) + cyclohexane (2)

Measurements for this system were executed at 40 kPa on the low pressure VLE apparatus. This measurement was carried out to familiarize oneself with the experimental procedure as well as the equipment. The low pressure VLE still on which these measurements were executed was not automated. The composition analysis was undertaken on the Shimadzu 2010 GC fitted with a packed Porapak® Q column (settings described in Table 6-2). The experimental T-x-y and x-y plots are compared against the data of Joseph *et al*. (2001) for this isobar. Figures 6-27 and 6-28 show excellent agreement between the experimental data points and the literature data of Joseph *et al*. (2001).

Table 6-9: *T-x-y* data for test system ethanol (1) + cyclohexane (2) at 40 kPa.

T/K	x_1	y_1
325.64	0.0000	0.0000
321.62	0.0052	0.1525
319.72	0.0103	0.2137
318.76	0.0137	0.2348
317.64	0.0219	0.2699
316.60	0.0400	0.3074
316.09	0.0571	0.3172
315.40	0.1054	0.3441
315.04	0.1201	0.4004
314.99	0.5500	0.4024
315.70	0.7254	0.4340
316.65	0.7918	0.4728
317.53	0.8485	0.4953
316.85	0.8135	0.4744
321.36	0.9266	0.6278
323.51	0.9556	0.7164
325.88	0.9758	0.8187
329.72	1.0000	1.0000

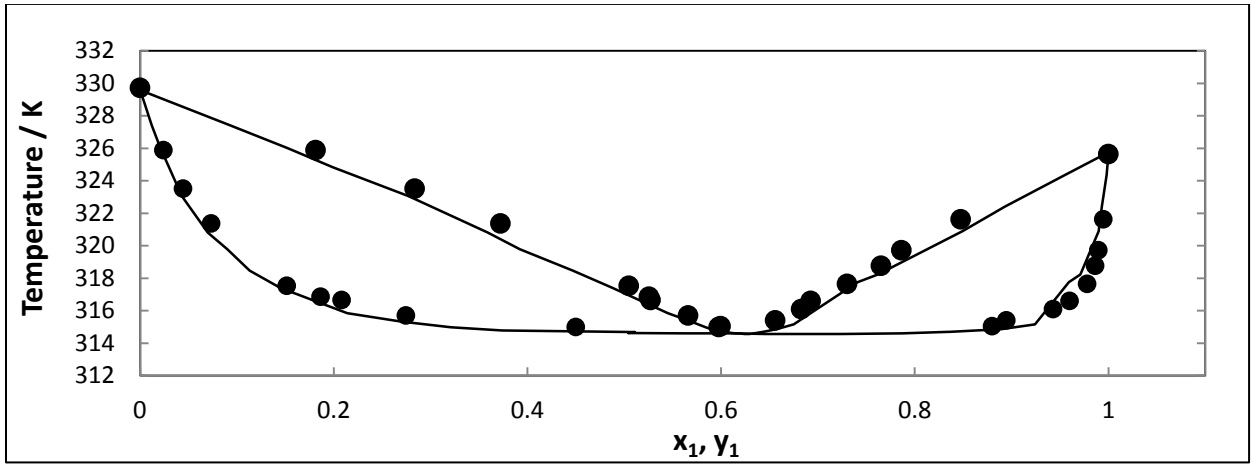

Figure 6-27 *T-x-y* plot for the ethanol (1) + cyclohexane (2) System at 40 kPa. ——, T-x-y (Joseph *et al*., 2001); ●, T-x-y (This work).

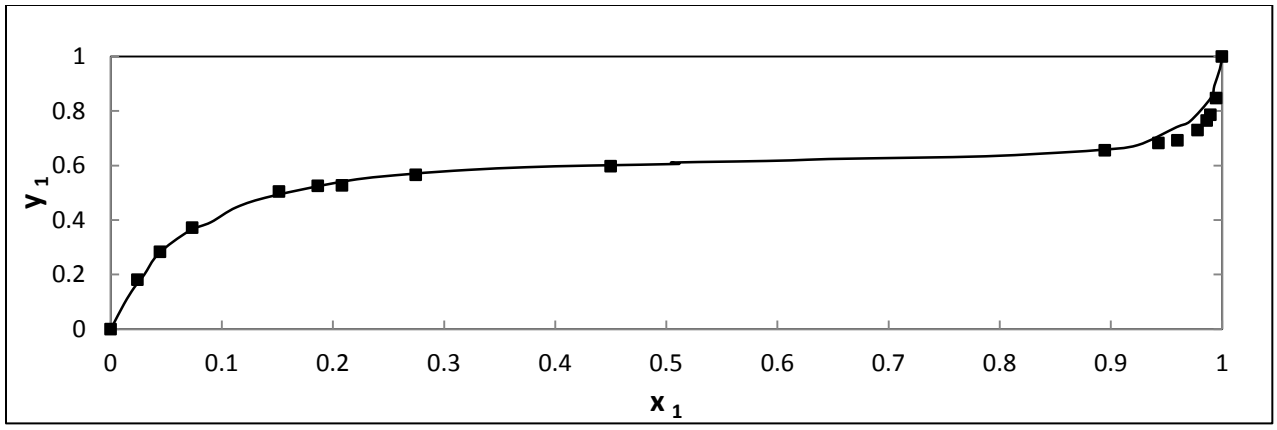

Figure 6-28: *y-x* plot for the Cyclohexane (1) + Ethanol (2) System at 40 kPa. ■, y-x (This work); ——, y-x (Joseph *et al*., 2001).

6.4.2 Results for the System 1-hexene (1) + NMP (2)

This system was measured at 323.15, 343.15, 353.15 and 363.15 K. All data sets are representative of new data. The isotherm 363.15 K has been previously measured by Fischer and Gmehling (1996) and Hirawan (2007). However, Fischer and Gmehling (1996) produced only P-x data due to their use of a static apparatus, and Hirawan (2007) could not generate a full set of isothermal data points at this temperature due to the limitation of the low pressure VLE still that was employed at that time. Thus, the isotherm at 363.15 K reflects new P-y data. The composition analysis for this system was carried out using the Shimadzu 2014 GC with a packed Porapak® Q column, with settings as per Table 6-2 above. The data for this system is shown below in Tables 6-10 and 6-11 and in Figures 6-29 to 6-30.

An important point to note for this system is that due to the associative properties of NMP, the activity coefficients for this component do not approach unity as the mixture becomes concentrated in NMP. The same observation is made for the system n-hexane + NMP. This phenomenon is explained in detail in the discussion section of this thesis.

Table 6-10: *P*-*x*-y data for the system 1-hexene (1) + NMP (2).

Pressure/ kPa	x_1	y_1	γ_1	γ_2	Pressure/ kPa	x_1	y_1	γ_1	γ_2
	T/ K	323.15				T/ K	343.15		
63.55	0.9823	0.9999	1.0109	3.5717	121.44	0.9845	1.0000	0.9939	6.2354
61.30	0.9525	0.9995	1.0065	2.9567	115.72	0.9298	0.9996	1.0048	5.0324
58.29	0.8448	0.9988	1.0801	2.3278	111.47	0.8572	0.9978	1.0498	2.4926
57.50	0.8237	0.9986	1.0929	2.1782	109.42	0.8186	0.9969	1.0791	2.0589
56.81	0.7389	0.9984	1.2038	1.8068	105.76	0.6954	0.9966	1.2292	1.3765
53.63	0.5416	0.9978	1.5521	1.3567	102.50	0.5953	0.9964	1.3931	1.0763
52.59	0.4951	0.9976	1.6656	1.2547	97.52	0.4827	0.9962	1.6378	1.0447
48.35	0.3122	0.9969	2.4325	1.0367	91.69	0.3782	0.9969	1.9714	0.7459
46.30	0.2744	0.9964	2.6512	0.9818	88.54	0.3334	0.9947	2.1580	0.8378
44.47	0.2435	0.9953	2.8691	1.0606	78.61	0.2202	0.9938	2.9100	0.7478
40.29	0.1976	0.9941	3.2070	1.1377	70.38	0.1753	0.9923	3.2807	0.7889
38.26	0.1704	0.9929	3.5317	1.2613	52.96	0.1125	0.9863	3.8509	0.9985
27.99	0.0966	0.9916	4.5779	1.0176	29.89	0.0515	0.9758	4.7433	0.9503
13.32	0.0566	0.9900	4.839	0.7624	18.94	0.0285	0.7804	4.8713	0.7034

Table 6-11: *P-x-y* data for the system 1-hexene (1) + NMP (2).

Pressure/ kPa	x_1	y_1	γ_1	γ_2	Pressure/ kPa	x_1	y_1	γ_1	γ_2
	T/K	353.15				T/K	363.15		
157.43	0.9116	0.9982	1.0094	-	218.00	1.0000	1.0000	1.0045	4.5861
147.59	0.8159	0.9978	1.0333	2.9454	212.16	0.9449	0.9980	1.0042	2.3301
141.41	0.7098	0.9977	1.0858	2.2021	210.07	0.9235	0.9996	1.0196	1.6905
137.46	0.6377	0.9974	1.1986	1.7535	208.83	0.9160	0.9990	1.0218	1.6589
134.68	0.5846	0.9961	1.2983	1.4692	201.73	0.8543	0.9984	1.0601	1.2191
132.05	0.5473	0.9926	1.3872	1.2671	197.99	0.8119	0.9969	1.0946	1.2109
129.09	0.4582	0.9968	1.4491	1.4943	191.81	0.7584	0.9928	1.1328	0.9521
115.03	0.3050	0.9949	1.7014	1.0580	188.27	0.7090	0.9941	1.1924	1.0037
100.96	0.2229	0.9945	2.2849	0.8899	161.62	0.4052	0.9900	1.7996	0.9212
83.33	0.1563	0.9909	2.7584	0.8082	134.24	0.2533	0.9832	2.4973	0.8852
50.93	0.0760	0.9813	3.2576	0.6412	116.07	0.1751	0.9765	2.6198	0.7316
1.02	0.0001	0.0075	4.1042	0.7566	51.57	0.0001	0.0000	3.0135	0.7834
					2.06	0.0087	0.0810	2.8522	0.6519
					2.02	0.0001	0.0000	2.8021	0.7316

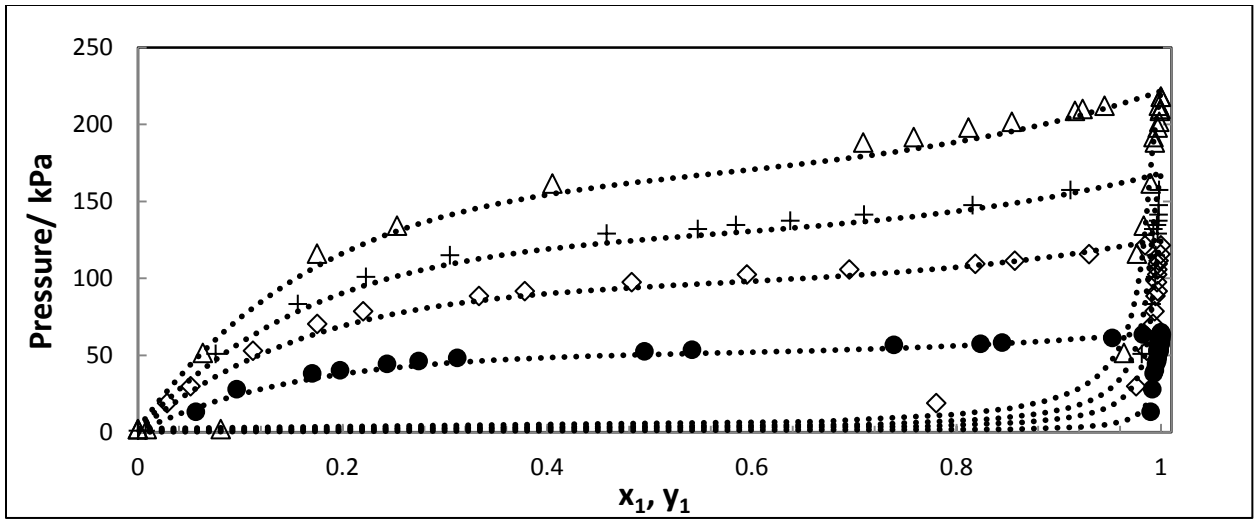

Figure 6-29: *P-x-y* plot for the 1-hexene (1) + NMP (2) System; ●, 323.15 K; ◊, 343.15 K; +, 353.15 K; Δ, 363.15 K; ····, fitted trend line.

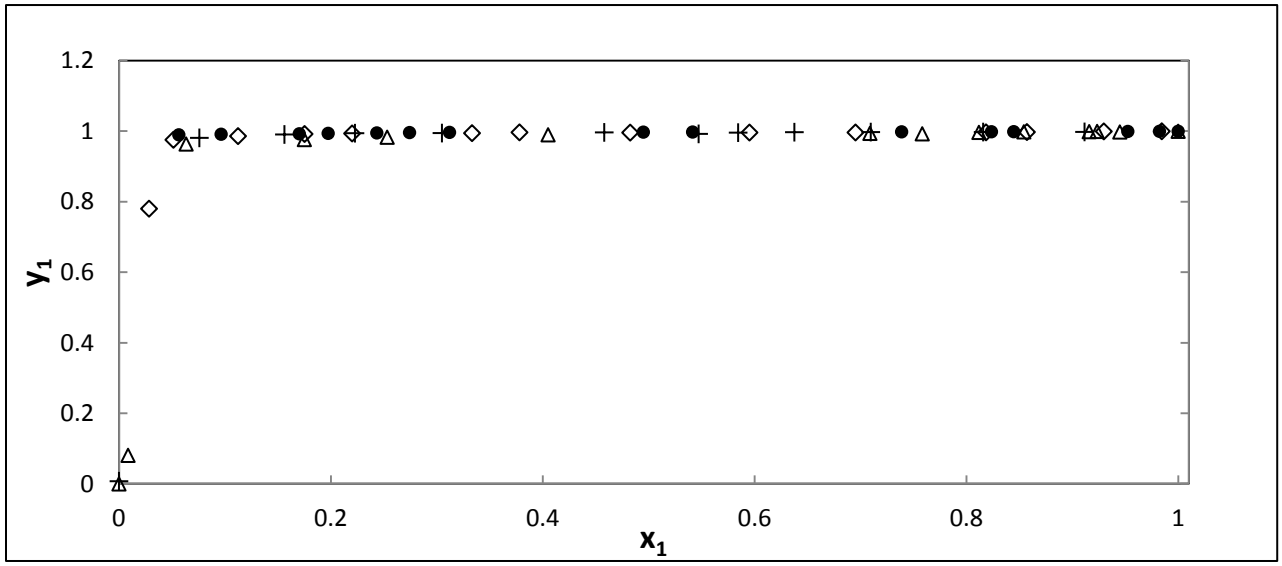

Figure 6-30: *y-x* plot for the 1-hexene (1) + NMP (2) System; ●, 323.15 K; ◊, 343.15 K; +, 353.15 K; Δ, 363.15 K.

6.4.3 Results for System n-hexane (1) + NMP (2)

This system was investigated at 353.15, 363.15, 378.15 and 383.15 K. All data sets are representative of new data. The isotherm 363.15 K has been previously measured by Fischer and Gmehling (1996). However, Fischer and Gmehling (1996) produced only P-x_i data due to their use of a static apparatus. Thus, the isotherm at 363.15 K reflects new P-y_i data. The composition analysis for this system was carried out using the Shimadzu 2014 GC with a packed Porapak® Q column, with settings as per Table 6-2. The data for this system is shown below in Tables 6-12 and 6-13 and is graphically represented in Figures 6-31 and 6-32.

Table 6-12: *P-x-y* data for the system n-hexane (1) + NMP (2) at 353.15 and 363.15 K.

Pressure/ kPa	x_1	y_1	γ_1	γ_2	Pressure/ kPa	x_1	y_1	γ_1	γ_2
		T/ K	353.15				T/ K	363.15	
133.88	0.8873	0.9923	1.0578	6.3569	179.38	0.9090	0.9933	1.0352	5.8012
130.48	0.7955	0.9919	1.1513	3.6113	177.43	0.8978	0.9932	1.0373	5.4874
129.88	0.7364	0.9914	1.2376	2.9519	173.00	0.7248	0.9923	1.2540	2.4965
128.57	0.7330	0.9906	1.2306	3.1473	166.74	0.6190	0.9902	1.4159	1.7677
127.30	0.6337	0.9905	1.4100	2.3028	165.43	0.5116	0.9896	1.6997	1.4566
126.18	0.5469	0.9900	1.6194	1.9405	163.72	0.4576	0.9882	1.8792	1.4775
124.41	0.4226	0.9895	2.0673	1.5715	161.41	0.3898	0.9860	2.1723	1.5323
119.47	0.3054	0.9896	2.7533	1.2513	156.98	0.3409	0.9855	2.4190	1.4333
116.81	0.2700	0.9894	3.0479	1.1954	144.99	0.2463	0.9838	3.1020	1.3028
111.35	0.2331	0.9885	3.3696	1.1775	126.98	0.1700	0.9819	3.9563	1.1774
100.46	0.1704	0.9869	4.1734	1.1284	86.51	0.0875	0.9764	5.2965	0.9743
75.31	0.1017	0.9834	5.2829	1.0054	65.12	0.0615	0.9671	5.6669	1.0078
52.178	0.0644	0.9784	5.8107	0.8843	1.96	0.0003	0.0004	0.0147	0.9020

Table 6-13: *P-x-y* data for system n-hexane (1) + NMP (2).

Pressure/ kPa	x_1	y_1	γ_1	γ_2	Pressure/ kPa	x_1	y_1	γ_1	γ_2
	T/K	**378.15**				**T/K**	**383.15**		
265.56	0.9127	0.9962	1.0513	4.4253	297.73	0.8965	0.9943	1.0619	5.7131
261.13	0.8769	0.9936	1.0750	3.8250	289.90	0.8611	0.9929	1.0777	3.4623
245.24	0.7438	0.9895	1.1921	2.5193	280.00	0.8434	0.9928	1.0663	3.1647
241.67	0.6070	0.9874	1.4382	1.6371	276.80	0.8334	0.9923	1.0674	3.1488
239.73	0.5416	0.9866	1.5989	1.4744	275.79	0.7392	0.9915	1.1985	1.9207
231.96	0.46544	0.9853	1.8029	1.3495	273.16	0.6563	0.9912	1.3378	1.6829
230.90	0.4621	0.9834	1.8048	1.5054	270.02	0.5477	0.9908	1.5856	1.3283
213.29	0.2929	0.9813	2.6413	1.2037	268.77	0.5116	0.9907	1.6904	1.2639
180.12	0.1773	0.9766	3.7125	1.1181	266.81	0.4846	0.9902	1.7719	1.1604
131.04	0.0899	0.9686	5.3731	1.0128	252.48	0.3624	0.9846	2.24033	1.0445
80.58	0.0538	0.9491	5.5111	0.9988	239.99	0.2879	0.9789	2.6768	1.2233
4.16	0.0022	5.E-05	0.0004	1.0035	201.06	0.1719	0.9737	3.7874	1.1201
					168.15	0.1293	0.9700	4.2434	1.0345
					133.51	0.0889	0.9669	4.9442	0.8846
					95.19	0.0571	0.9567	5.5057	0.8124

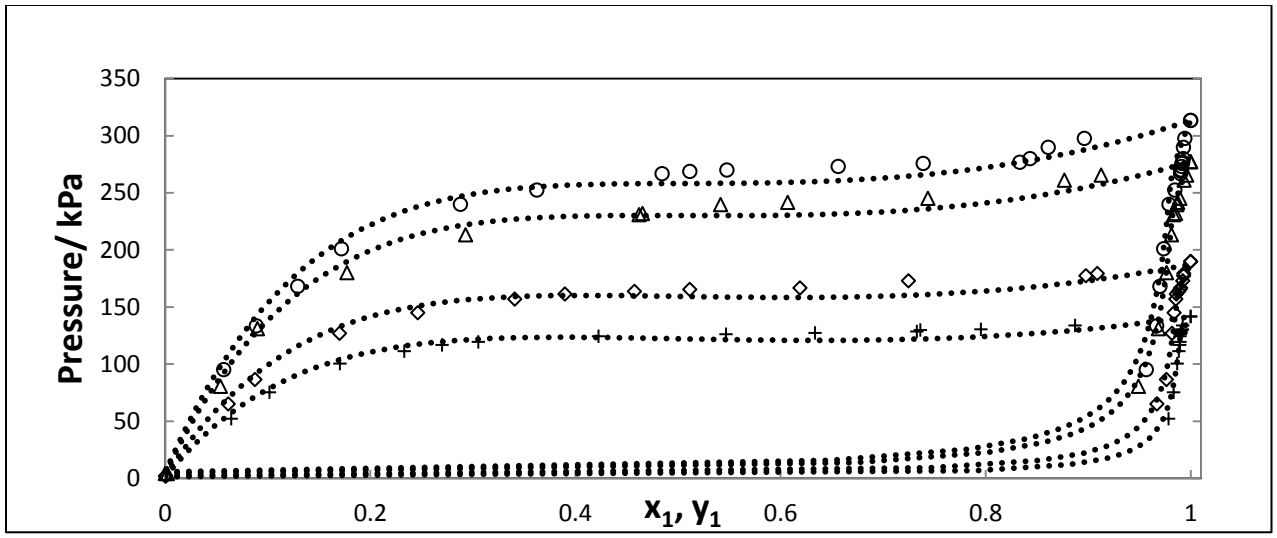

Figure 6-31: *P-x-y* plot of the n-hexane (1) + NMP (2) System. +, 353.15 K; ◊, 363.15 K; Δ, 378.15 K; ○, 383.15 K; ····, fitted trend line.

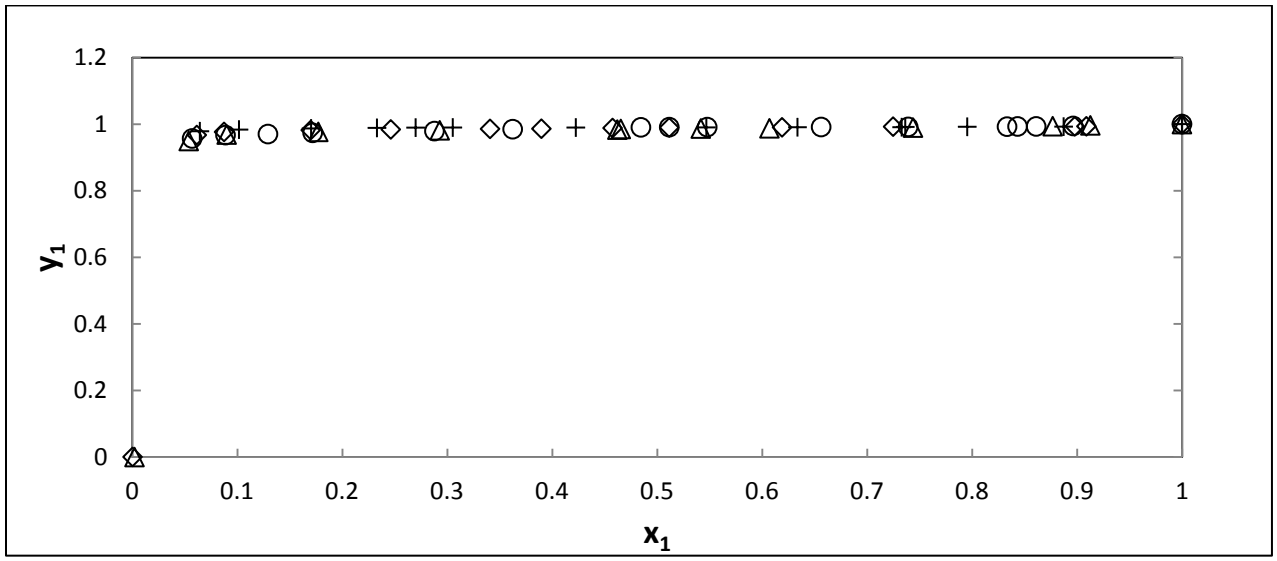

Figure 6-32: *y-x* plot for the n-hexane (1) + NMP (2) System. +, 353.15 K; ◊, 363.15 K; Δ, 378.15 K; ○, 383.15 K.

6.4.4 Results for the System 1-hexene (1) + n-hexane (2)

All data for the system 1-hexene + NMP at the temperatures of 343.15, 363.15 and 373.15 K constitute new data. Achieving separation of these two components was exceptionally difficult; however, it was achieved via the use of an Ohio Valley (OV-1) capillary column on the Shimadzu 2010 GC. The settings for the use of this column to achieve the required separation are presented above in Table 6-3. Tables 6-14 and 6-15 below exhibit the experimental data points, and Figures 6-33 and 6-34 exhibit plots of the data points.

Table 6-14: *P-x-y* data for the system 1-hexene (1) + n-hexane (2).

Pressure / kPa	x_1	y_1	γ_1	γ_2	Pressure / kPa	x_1	y_1	γ_1	γ_2
	T/ K	373.15				T/ K	363.15		
245.01	0.0000	0.0000		0.9999	189.09	0.0000	0.0000		1.0043
245.11	0.0136	0.0148	0.9537	0.9990	189.34	0.0243	0.0250	0.8996	1.0048
246.08	0.0815	0.0851	0.9184	0.9999	189.51	0.0348	0.0354	0.8902	1.0057
248.09	0.1713	0.1882	0.9735	0.9907	189.89	0.0698	0.0725	0.9107	1.0053
252.18	0.3222	0.3542	0.9887	0.9779	190.93	0.1526	0.1578	0.9112	1.0071
256.11	0.4309	0.4649	0.9841	0.9787	193.38	0.2606	0.2849	0.9749	0.9916
261.92	0.5638	0.6014	0.9931	0.9706	193.78	0.2716	0.3037	0.9990	0.9820
264.82	0.6334	0.6775	1.0058	0.9437	197.13	0.4103	0.4374	0.9677	0.9957
270.90	0.7557	0.7873	1.0000	0.9533	198.70	0.4679	0.4953	0.9680	0.9972
272.99	0.7974	0.8234	0.9981	0.9610	201.57	0.5601	0.5966	0.9871	0.9769
276.96	0.8816	0.8982	0.9977	0.9603	204.61	0.6426	0.6948	1.0159	0.9223
280.00	0.9419	0.9558	1.0030	0.8580	210.01	0.7833	0.8191	1.0065	0.9234
281.68	0.9786	0.9786	0.9943	1.1339	214.92	0.9087	0.9243	1.0000	0.9368
282.90	1.0000	1.0000	0.9982		217.52	0.9745	0.9822	1.0020	0.7974
					218.64	1.0000	1.0000	0.9988	

Table 6-15: *P-x-y* data for the system 1-hexene (1) + n-hexane (2).

Pressure/ kPa	x_1	y_1	γ_1	γ_2
		T/ K = 343.15 K		
105.68	0.0000	0.0000		1.0031
105.78	0.0067	0.0079	1.0148	1.0027
106.39	0.0260	0.0260	0.8645	1.0095
107.29	0.0811	0.0874	0.9394	1.0106
108.04	0.1348	0.1558	1.0137	0.9995
110.43	0.2510	0.2859	1.0200	0.9972
113.30	0.4016	0.4362	0.9938	1.0112
113.97	0.4455	0.4797	0.9966	1.0099
116.44	0.5726	0.6082	1.0005	1.0082
118.51	0.6694	0.7048	1.0084	0.9986
120.72	0.8023	0.8214	0.9980	1.0278
122.78	0.9179	0.9243	0.9975	1.0654
123.91	0.9935	0.9957	1.0013	0.7735
124.05	1.0000	1.0000	1.0002	

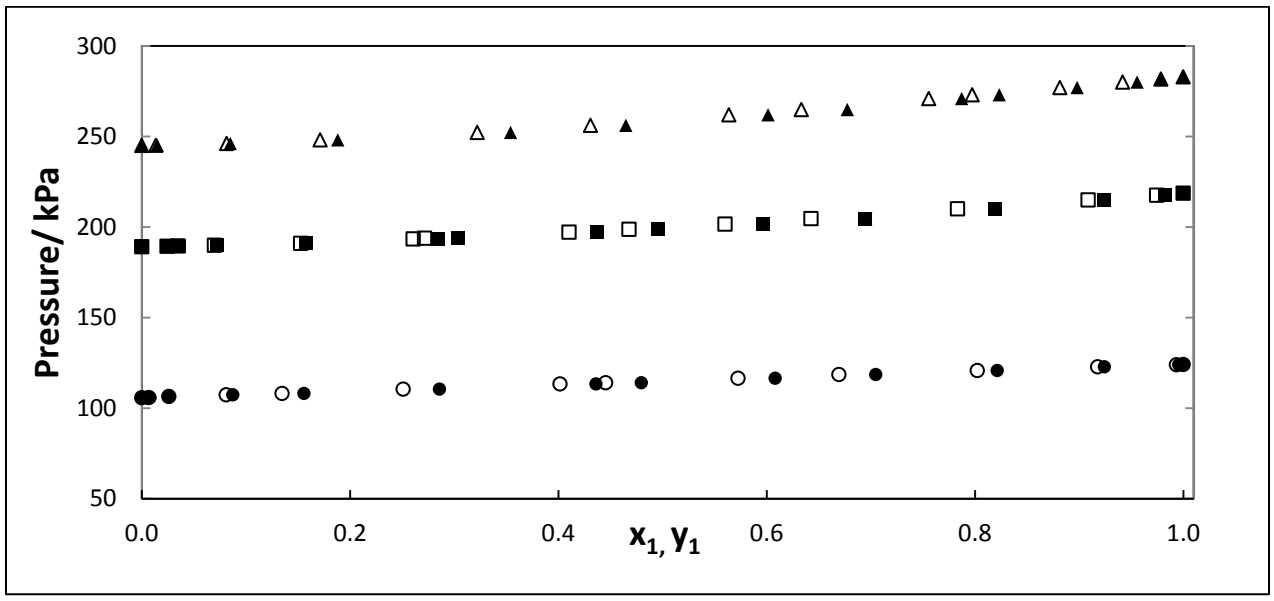

Figure 6-33: *P-x-y* plot for the 1-hexene (1) + n-hexane (2) system. ○, 343.15 K; □, 363.15 K; Δ, 373.15 K.

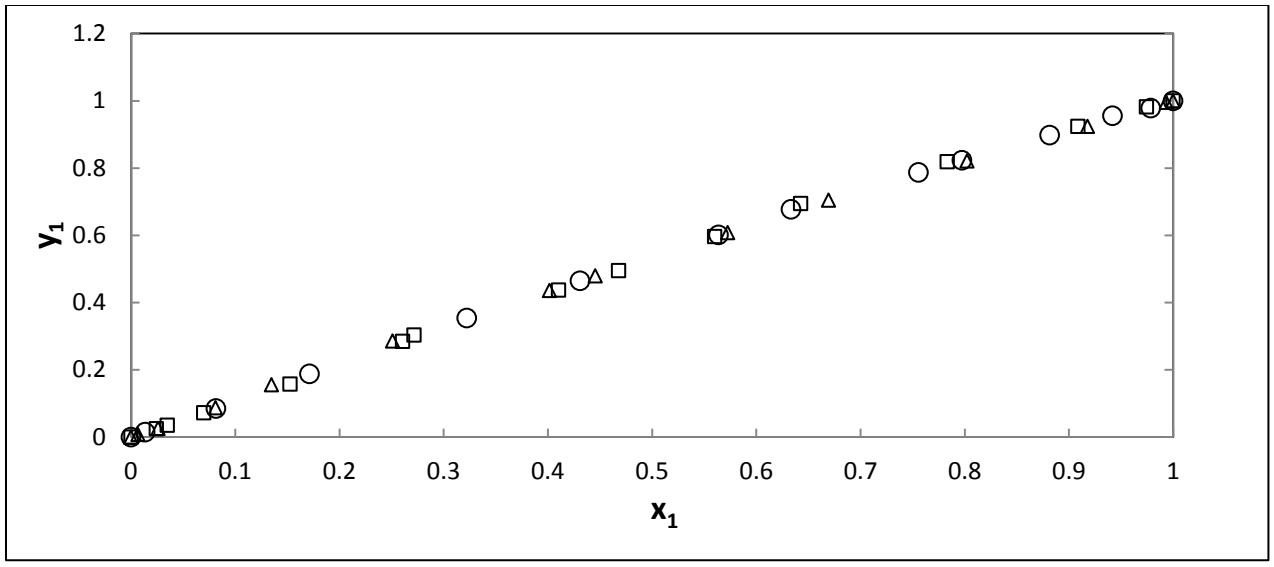

Figure 6-34: *y-x* plot for the 1-hexene (1) + n-hexane (2) system. ○, 343.15 K; □, 363.15 K; Δ, 373.15 K.

6.4.5 Results for the System 1-hexene (1) + n-hexane (2) + NMP (3)

This ternary system was measured at 363.15 K and the OV-1 capillary column was utilized to achieve separation. The Shimadzu 2010 GC was employed for composition analysis and the detector is flame ionization. The following measurements constitute new data.

Table 6-16: *P-x-y* data for the ternary system 1-hexene (1) + n-hexane (2) + NMP (3) at 363 .15 K.

Pressure/kPa	x_1	x_2	x_3	y_1	y_2	y_3
84.94	0.0505	0.0408	0.9087	0.5311	0.3777	0.0912
113.00	0.0799	0.0671	0.8530	0.5323	0.4131	0.0547
148.23	0.0764	0.1869	0.7367	0.3006	0.6703	0.0291
159.35	0.0710	0.2607	0.6683	0.2279	0.7511	0.0209
160.47	0.0191	0.3243	0.6566	0.0599	0.9188	0.0212
161.77	0.1893	0.1807	0.6299	0.5282	0.4550	0.0168
166.56	0.2150	0.2064	0.5786	0.5439	0.4422	0.0139
180.18	0.4481	0.1680	0.3839	0.7586	0.2353	0.0060
187.28	0.3801	0.1909	0.4290	0.7012	0.2911	0.0077

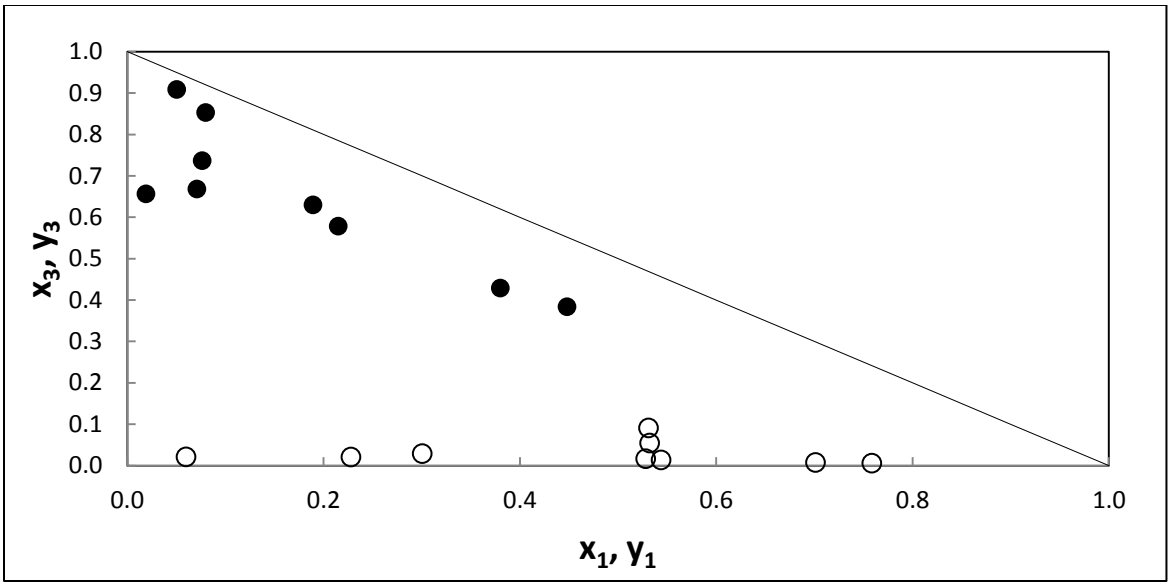

Figure 6-35: *y*-*x* plot of the 1-hexene (1) + n-hexane (2) + NMP (3) system at 363.15 K. ●, liquid composition experimental points (x_i); ○, vapour composition experimental points (y_i).

Chapter 7: Data Analysis and Discussion

The following chapter focuses on the results obtained from experiments conducted and a thorough discussion of the analysis of these results. An in-depth explanation of the theoretical aspects of the data reduction and consistency testing has been conducted in Chapter 3 and, therefore, shall not be repeated.

7.1 Experimental Vapour Pressure Data for Pure Components

Measuring the correct vapour pressure data is extremely important for many reasons. Foremost, it gives an indication as to whether the equipment (temperature and pressure sensors, VLE apparatus *etc.*) are functioning in the correct manner and if the experimental technique is accurate. If the equipment is fully operational, then the vapour pressure measurements will provide a check for the purity of the chemicals being measured.

The vapour pressure data is crucial to the modeling of the binary experimental data. Vapour pressure data were measured and are reported in Section 6 for all components involved in this investigation. Table 7-2 below allows one to observe the average absolute deviations in temperature and pressure between the experimental vapour pressure data and the literature sources. Literature resources utilized for this purpose are Poling *et al*. (2001), DDB (2011) and Component Plus (2010).

The following equation was used to regress for the Antoine parameters using measured vapour pressure data:

$$Ln P_i^{sat}(kPa) = A_i + \frac{B_i}{T/^{\circ}C + C_i} \qquad (7.1)$$

The Antoine parameters, regressed for each component, are represented below in conjunction with the ΔP_{AAD} for each data set.

The average absolute deviation in pressure and vapour composition, as well as the overall average absolute error, is computed as indicated below:

$$AAD\%(\Delta P) = \frac{100}{n}\sum_{i}^{n}\frac{\left|P_i^{\exp} - P_i^{calc}\right|}{P_i^{\exp}} \tag{7.2}$$

$$AAD\%(\Delta y) = \frac{100}{n}\sum_{i}^{n}\frac{\left|y_i^{\exp} - y_i^{calc}\right|}{y_i^{\exp}} \tag{7.3}$$

$$AE\% = \frac{100}{n}\sum_{i}^{n}\left[\left(\frac{\left|P_i^{\exp} - P_i^{calc}\right|}{P_i^{\exp}}\right)^2 + \left(\frac{\left|y_i^{\exp} - y_i^{calc}\right|}{y_i^{\exp}}\right)^2\right] \tag{7.4}$$

Were the superscripts “exp”and “calc” denote experimental and calculated data, respectively.

Table 7-1: Regressed parameters for the Antoine equation (excluding test system: ethanol + cyclohexane).

Parameter	1-hexene	n-hexane	NMP
A	51.98	104.65	68.48
B	-5104	-6995.50	-8467.90
C	0.0005	0.0013	0.0013
ΔP_{AAD}	0.0008	0.0012	0.0034

Table 7-2: Comparison between experimental and literature vapour pressure data.
(Refer to equations 6.1 - 6.2 for explanation of the calculation approach)

	$\Delta T_{average}$/ %			$\Delta P_{average}$/ %		
Component	**Ref 1[a]**	**Ref 2[b]**	**Ref 3[c]**	**Ref 1[a]**	**Ref 2[b]**	**Ref 3[c]**
Ethanol	0.030	0.105	0.078	0.559	0.535	0.532
1-hexene	0.047	0.047	0.145	0.026	0.239	0.058
n-hexane	0.083	0.083	0.078	0.450	0.761	0.046
NMP	_	0.209	0.114	_	1.237	0.526

[a] Poling *et al*., 2001

[b] Dortmund Data Bank, 2011

[c] Component Plus, 2010

- No data available from this literature source to compare with experimentally measured vapour pressure data

As may be observed from Table 7-2, it is evident that the agreement between the literature and experimental data is excellent. The average absolute deviations for pressure and temperature are all well below 1%, the exception of course being for the case of NMP with a high percent deviation for pressure of 1.237 using DDB (2011). Overall, the parameters for evaluating vapour pressure obtained from Poling *et al*. (2001) and Component Plus (2010) showed a better agreement with the experimental data than that presented by the use of the DDB (2011).

7.2 Determination of Experimental Activity Coefficients

In theory, the determination of the activity coefficient from experimental data is determined by either assuming ideal gas behavior for the vapour state (Φ=1) or utilizing a virial equation of state (EoS), or other suitable thermodynamic model, to evaluate the vapour correction term, Φ. When dealing with components which exhibit a high degree of association, the activity coefficients computed are usually of an extremely poor quality. This occurs for systems which do not consider the associative effects of the molecules when computing the activity coefficients. At low pressures, this problem is not significant, however, as the pressure increases the problem of association increases and the resultant activity coefficients become poorer and poorer (Pillay,

2010). Represented below is a plot of the logarithm of the activity coefficients, both experimental and calculated, against the liquid composition of 1-hexene. This plot is for the system 1-hexene + NMP at 323.15 K.

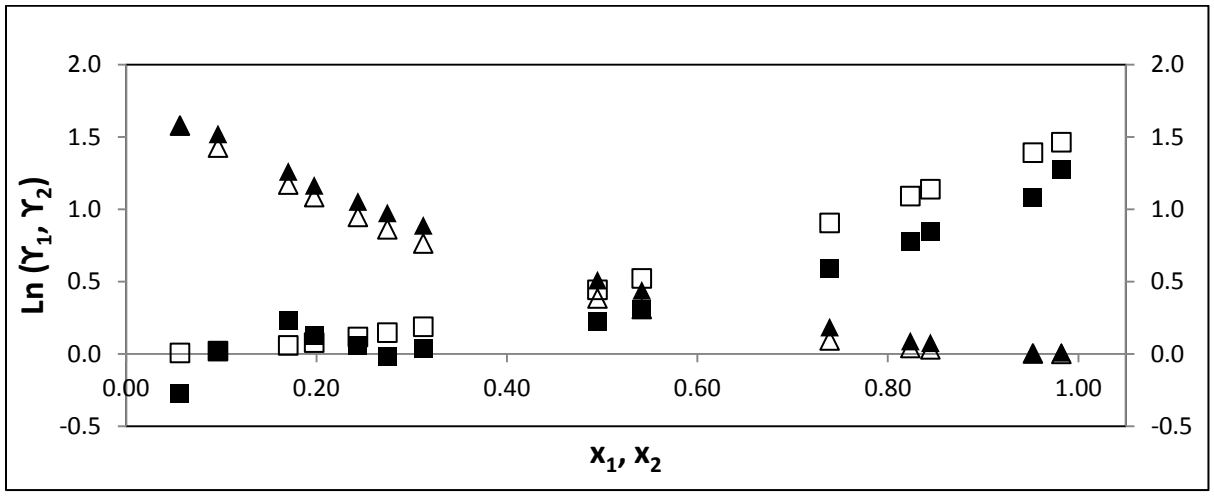

Figure 7-1: Ln (γ1, γ2) vs. x_1 plot for the system 1-hexene (1) + NMP (2) at 323.15 K. Δ, model data for 1-hexene; ▲, experimental data for 1-hexene (this work, calculated using Modified Raoult's Law); □, model data for NMP; ■, experimental data for NMP (this work, calculated using Modified Raoult's Law).

The above plot shows that the experimental data for the component 1-hexene compares very well with the calculated data. However, the plot for NMP shows a deviation between the experimental and calculated model. The deviations exhibited for the NMP molecule are attributed to its self-associative nature (discussed at great length in Chapter 1). As the system becomes more saturated with NMP, the scatter becomes more prevalent, as may be observed in the region of x_1 = 0 to 0.4 mole fraction.

The shape of the plot obtained above for NMP is consistent for all isothermal binary measurements for the systems containing NMP in this work. Thus, one is confident that the self-associative properties of NMP are contributing to this deviation. In addition, since the NMP molecule is associative, the direct test is not utilized as the primary means for assessing consistency, instead the point test of Van Ness *et al*. (1975) is applied.

In addition, referring to the experimentally acquired data tabulated in Section 6, one clearly observes a distinct problem. As the composition of NMP increases and eventually goes to unity (*i.e.* pure component) the value of the activity coefficient for NMP does not approach 1. This issue is once again as a result of the associative nature of NMP. These results clearly show the non-ideal nature of all measurements carried out with NMP in this work.

As discussed in the literature review (Chapter 1), the excess molar volume (V_m^E) can be used as a direct measure of the value of the activity coefficient. Letcher *et al.* (1998) postulate that this deviation is an irrefutable indication of association between the highly polar NMP molecule and the polarizable 1-hexene (olefin) and n-hexane (paraffin) as well as a reflection of the complex self-association occurring within the NMP molecule. These results therefore reflect the association between the NMP molecule and the acidic hydrogen of the 1-hexene and n-hexane (Letcher *et al*., 1998).

Even though the experimental work carried out in this thesis did not extend to measuring V_m^E, the activity coefficients computed prove that there is a negative deviation from Raoult‟s Law. The associations in the systems undertaken in this work are not as severe as for carboxylic acids; however, the self-association of the NMP molecule, as well as the postulated cross association between NMP and 1-hexene or n-hexane (Letcher *et al.,* 1998) cannot be ignored as it has a definitive effect on the activities computed. In addition, there is a consistent shape to the experimental plots of $\mathrm{Ln}\,\gamma$ vs. x, however; these plots do not match the model data. From the experimental measurements (Chapter 6), it is observed that the associative effects of NMP are not as severe for combination with n-hexane as it is for 1-hexene. This is in corroboration with the findings of Letcher *et al.* (1998) and has been discussed in great depth in Chapter 1.

In this experimental work one of the models selected to represent the vapour phase inequalities is the Hayden and O-Connell (HOC) model. Only one associating model was considered to ascertain if this stringent EoS could make a difference to the calculated data for the direct test. The results obtained using the HOC model do prove better than the other EoS such as PR, SRK, PR-WS and SRK-WS. The data generated is marginally better when using HOC as compared to the other models, though it is still poor when analyzing it objectively. The indices for the direct

test computed for the system n-hexane, and 1-hexene + NMP generally lie in the region of 6-10 for all modeled isotherms, the exception being for the system n-hexane + NMP at 353.15 K, with indices in the range of 3-5.

When Fischer and Gmehling (1996) modeled data for the systems 1-hexene, and n-hexane + NMP, the ideal gas equation of state was employed. However, it is important to note that only γ^{∞} were computed. In the extreme dilute regions were 1-hexene and n-hexane are basically pure components, the ideal gas equation may be utilized, as 1-hexene and n-hexane are ideal compounds. For future work, it is suggested that stricter models which consider self-association effects, such as FBT, ERAS and chemical theory be investigated. These models have been discussed at great length in the introduction.

The infinite dilution activity coefficients for any binary/ternary mixture are extremely important to acquire. This value gives industry insight as to the extent of separation between the two components, and whether the selective solvent is functioning in the proper manner. In order to design distillation columns for industrial separation processes, the infinite dilution activity coefficients are crucial. This directly impacts the number of equilibrium trays, reflux ratio, *etc*. It may be observed from the experimental data that the infinite dilution activity coefficients for n-hexane is almost double that for 1-hexene. This indicates that NMP does play a significant role in the separation of the 1-hexene from n-hexane. The very same observation was concluded by Fischer and Gmehling (1996) for 1-hexene+NMP and n-hexane + NMP systems that were measured in the reported article.

Thermodynamically, systems will either show a positive or a negative deviation from ideality. Positive deviations are acknowledged by the Ln γ values being positive, which logically implies the values of γ are above 1 (unity). Conversely negative deviations of Ln γ imply the values of γ are below unity (fractional). Commonly, negative deviations from Raoult‟s Law occur in systems constituting electrolytes or solutions where association and compound formation occur. Due the above mentioned phenomena occurring, the volatility of the system decreases (Carlson and Colburn, 1942). From the results seen in Chapter 6, when analyzing the systems 1-hexene +

NMP and n-hexane + NMP, one notes that as the concentration of NMP increases, the activity coefficients become fractional, implying negative deviations from Raoult‟s Law.

In addition, even at the higher concentrations of 1-hexene or n-hexane, there is a deviation between the experimental activity coefficients for NMP and the calculated one. A possible explanation could be the 1-hexene or n-hexane molecules fit into the spaces between the NMP molecules, thus resulting in smaller volumes, which consequently results in smaller activity coefficients.

The γ values for the system 1-hexene + NMP display a greater deviation from ideality than the system n-hexane + NMP. One possible explanation is that 1-hexene is more polarizable than n-hexane due to the presence of the double bond. Thus, NMP has a greater affinity for cross-association with the 1-hexene molecule (Letcher *et al*., 1998).

7.3 Binary VLE Data Reduction of Experimental Work

The following abbreviations are used in the sections that follow:

HOC = Hayden and O‟Connell
PR = Peng - Robinson
SRK = Soave - Redlich - Kwong
WS = Wong and Sandler
NRTL = Non-random two liquid model
UNIQUAC = Universal Quasi-Chemical theory

The VLE data reduction in this thesis was carried out on Aspen Plus®, a process simulator in widespread use industrially. Aspen Plus® was used in the modeling of VLE data for both the direct and combined technique. The models selected for representing the experimental data were chosen based on a fine balance between the models available on Aspen Plus® and the chemical properties of the components being investigated. The following is a summary of the approaches to VLE data reduction employed in this work.

7.3.1 The Direct Method (Phi-Phi)

This approach to VLE data reduction utilizes an EoS for the representation of both the vapour and liquid phases. The main equation characterizing the description of the fugacity coefficient is:

$$\hat{f}_i^{\,L} = x_i \hat{\phi}_i^{\,L} = \hat{f}_i^{\,V} = y_i^{\,V} \hat{\phi}_i^{\,V} \tag{7.5}$$

The subsequent models were used in the direct method for the regression of the measured VLE data:

NRTL-SRK-WS and NRTL-PR-WS

The above expression has the following sequence: the activity coefficient model is incorporated through the use of a mixing rule in combination with an EoS. The empirical formula is:

$$G^E \textit{ model} - \textit{EoS - Mixing Rule}$$

Therefore, using the above explanation NRTL-SRK-WS denotes the NRTL activity coefficient model incorporated with the Soave-Redlich-Kwong EoS through the use of the Wong-Sandler mixing rule. Similarly, NRTL-PR-WS may be explained by the same explanation as above; however, PR refers to the Peng-Robinson EoS.

7.3.2 The Combined Method (Gamma-Phi)

In this work the NRTL (1968) and UNIQUAC (1975) activity coefficient models were used to account for the liquid phase departure from ideality. Further the Peng-Robinson (1976) and Soave-Redlich-Kwong (1972) EoS were employed in the representation of the vapour phase non-ideality, as well as the Hayden and O'Connell (1975) virial equation of state. The expression giving definition to the combined method is:

$$y_i \Phi_i P = x_i \gamma_i P_i^{sat} \tag{2.23}$$

Where the symbol Φ_i denotes the fugacity coefficient computed by the EoS (SRK/ PR/ HOC), and γ_i symbolizes the activity coefficient calculated using the NRTL or UNIQUAC model and P_i^{sat} is the saturated vapour pressure computed by a suitable correlation for vapour pressures such as the Antoine equation. For the evaluation of the coefficients of the HOC virial EoS (B_{11}, B_{22} B_{12}) reference should be made to Section 2.3.1. In addition, the Φ_i parameter is evaluated as follows:

$$\Phi_i = \frac{\hat{\phi}_i}{\hat{\phi}_i^{sat}} \exp\left[\frac{-V_i^L\left(P - P_i^{sat}\right)}{RT}\right] \tag{2.25}$$

7.3.3 Parameter Optimization and Objective Function

The basis for the regression algorithm is the minimization of error between the experimental and calculated data. The residuals (*i.e.* the difference between the model and experimental data) are defined by Van Ness (1978) as:

$$\delta y_i = y_i^{\exp} - y_i^{calc} \tag{7.6}$$

$$\delta P_i = P_i^{\exp} - P_i^{calc} \tag{7.7}$$

Where: „δ" denotes the residual quantity.

The formally defined residuals are referred to as primary residuals (Van Ness and Abbott, 1982). The data reduction is based on the residuals defined since the minimization algorithm is often written in terms of δy and δP.

For the regression algorithm the objective function employed is Barker"s method. The objective function of Barker (1953) entails the minimization of pressure as follows:

$$Objective\ Function = \sum\left(\delta P_i\right)^2 \tag{7.8}$$

This approach makes use of the P-x_i data entered into Aspen Plus®. In Aspen Plus® there are three steps to the regression procedure. The initialization, middle and end loop. The initialization process is carried out by using the method of Deming; this is an approximate solution method.

For the middle loop, the Britt-Luecke algorithm was employed as opposed to the method of Deming. This was done since Britt-Luecke is a more rigorous approach to the regression algorithm, thus giving more tightly converged parameters. There is another regression method, the weighted least squares approach, however this was not utilized as it does not render satisfactory results (Jeremy, 2010).

Data reduction requires that many models be tried in an attempt to fit the experimental data accurately. This is conducted until a model(s) is found that renders no significant errors, such as showing a negative or positive bias. After the data reduction has been conducted for isothermal data, the adjustable parameters calculated are referred to as true constants. This means that for that specific isotherm, the adjustable parameters computed will apply throughout the concentration range. Unfortunately, the same cannot be said for isobaric data since the temperature is varying constantly with composition, and the adjustable parameters are temperature dependent. If the regression process has been carried out correctly, then T-P-x_i-y_i graphs may be generated at any condition. Discretion should be exercised for cases where extrapolation far outside the pressure and temperature range is occurring.

7.3.4 Parameter Estimation

The NRTL activity coefficient model has three adjustable parameters: τ_{12}, τ_{21} and α_{ij}. As stated previously in the discussion on the NRTL Gibbs excess energy model (Section 2.5.1), regular values for α_{ij} fall in the range of -1 to 0.5. It has been recommended by Walas (1985) that for aqueous and non-aqueous mixtures the value of α_{ij} should be 0.4 and 0.3 respectively. On the other hand some authors, like Raal and Mühlbauer (1998), actually prefer for the VLE data to be regressed. Thus, it is observed that parameter estimation is not a clear cut task. Indeed the estimation of certain parameters using local composition models is a difficult task the world over and different authors have varying opinions.

In conclusion, it was decided, in order to obtain data of a high level of accuracy; the α_{ij} parameter was determined by regression in this work. Two famous researchers, Fischer and Gmehling (1996), have measured two of the systems in this work at different conditions. The

values these researchers obtained for the α_{ij} parameter from the regression of their experimental data are 0.4163 and 0.4567 for the systems; n-hexane + NMP and 1-hexene + NMP respectively.

Thus, additional to the normal modeling conducted where all adjustable parameters are regressed for, a supplementary component is added to this thesis where the α_{ij} parameters are fixed at the values determined by Fischer and Gmehling (1996) to ascertain if the new results obtained from fixing the α_{ij} parameter render better or poorer results than if the alpha parameter is freely regressed for.

The second virial coefficients were calculated as per the equations set out in Section 2.3.1. Liquid molar volumes were evaluated according to the Rackett equation (1970).

7. 3. 5 Thermodynamic Consistency Testing

Testing the consistency of the measured data is the most important aspect of the analysis endeavor, as this will then give an indication as to whether the data is of an acceptable standard and if the model parameters may be used for future work. As per the discussion in Chapter 2, it has been concluded that the area and slope tests shall not be considered as these are not rigorous enough.

Results for the direct test have been computed and tabulated. However, these results are not going to be used as the main means by which to assess the quality of the data (specifically for binary systems containing NMP). Although the systems measured are at low to moderate pressures, the inequalities in the vapour phase are still noteworthy due to the association present as a result of the NMP molecule. The point test for vapour composition and pressure is used as the main means by which to test the thermodynamic consistency of the binary systems measured containing NMP. More specifically, the total absolute error (AE%), which is the sum of the square of the average absolute deviation in pressure (ΔP_{AAD}) and vapour composition (Δy_{AAD}), shall be used as a primary means by which to ascertain which model best fits the experimental data.

The stringent point test of Van Ness (1973) is suitably adequate for the selection of a thermodynamic model as it takes into account both the liquid phase activity coefficient and the vapour phase equation of state. The work path of the point test in the mathematical model is: the P-x_i data entered is regressed to find suitable binary interaction parameters, which are constantly manipulated multiple times to ensure the pressure residual is minimized.

In the process of minimizing the pressure residual, the errors are transferred to the vapour composition (y_i) residual. The model vapour composition values are then computed and compared to the experimentally obtained y_i values. This residual is then used to test the thermodynamic consistency of the system. The average absolute deviation of the vapour composition (Δy_{AAD}) has to be ≤ 0.01 in order for the system to qualify for thermodynamic consistency.

The point test gives intrinsic insight into the models selected to fit the data, as well as the consistency of the data itself. All results obtained from the point test are sensitive to the model employed for the regression operation. Thus, it is important to note that even though a certain data set may fail the point test, this may not necessarily mean that the data is inconsistent, it may actually be related to the use of the incorrect model for the regression analysis or a few data points in the set may need to be removed, instead of the whole data set being dubbed inconsistent.

Similarly, an erroneous data set may actually pass the point consistency test, yet be inconsistent. Even though there does exist the possibility of errors being introduced by the consistency tests, these tests must still be applied as they remain the only means by which one may be able to distinguish the consistency of data, as well as derive other information which would be very difficult to acquire by other means (Jackson and Wilsak, 1995). For the system 1-hexene and n-hexane, there is no association present, as such the direct and point test are both used as means by which to ascertain the consistency of the experimental data.

The methodical approach to data analysis taken in this thesis was to vary the EoS, representing the vapour phase, all the while maintaining the liquid phase activity coefficient model constant.

The EoS utilized are: HOC, PR, SRK and ideal gas models and the activity coefficient model kept constant initially is the NRTL model. It has been deduced that the NRTL-HOC model rendered the best fit to the data in almost all instances, as it consistently delivered the lowest y_i and P residuals. Once the best fit EoS was detected, then only was the activity coefficient model varied to that of UNIQUAC, whilst keeping the EoS fixed as HOC, to ascertain if the results for the residuals improved by varying the activity coefficient model.

The tables in the sections to follow provide insight into the consistency tests performed for all the systems investigated in this work. In some instances the point test passed for all the data points in a specific system at a particular temperature. However, at another temperature the point test may have failed for the same system. Therefore, the tables below illustrate the result of the point test conducted over the entire composition range for the full data set even when the point test has failed, as well as the results of the point test conducted again for the same data set but with certain points strategically removed until the test criterion of $|\Delta y_{i,avg}| \leq 0.01$ is satisfied.

In some instances certain data points were neglected from final analysis as they rendered erroneous results. These points were difficult to spot as problematic at first glance, therefore, only after the modeling was executed was it possible to troubleshoot and remove the complicated point. The full data set is still presented, in an attempt to show how difficult it would be to spot the "problematic" point had consistency tests not been performed. Another point up for consideration is that the "problem" point may actually not be faulty. Perhaps another model, not used in the current analysis, would be able to better represent the system in question.

Points which needed to be excluded from a certain data set are designated by the symbol „*" in the appropriate columns. The absolute average deviations in pressure and vapour composition are indicated at the bottom of each table for both instances where the full set of data is used as well as where certain points have been deliberately neglected in order to satisfy the constraints of the consistency tests. The final binary interaction parameters regressed for are obtained by using the data for which the consistency tests have passed.

7.4 Hydrocarbon (1-hexene or n-hexane) + NMP Systems

The Aspen Plus® PSRK model was employed initially to predict the systems under investigation. There is a deviation between the Aspen Plus® PSRK predictions and the measured data. A possible reason for this deviation is the non-ideal nature of the systems n-hexane + NMP and 1-hexene + NMP. As the liquid composition of n-hexane and 1-hexene in the two separate binary systems steadily increases from 0.5 mole fraction, the greatest deviation between the Aspen PSRK model and the experimental data is observed. The experimental data has a higher pressure than the predicted PSRK model.

Even though there have been a myriad of improvements to the SRK EoS, it still has remnants of inaccuracy when it comes to vapour pressure predictions regarding strongly polar systems. Therefore, the PSRK prediction may be improved by regressing the literature experimental data of Fischer and Gmehling (1996) and thereafter, using the regressed parameters for the PSRK model in the prediction of the VLE behaviour for the system at the temperature required.

One is confident with the results acquired in this work as a consistent shape for the data was obtained throughout this study. In addition, the experimental work compares excellently with the P-x_i data reported by Fischer and Gmehling (1996) at 363.15 K. The plots relevant to the temperatures measured are exhibited below in the designated sections.

The system 1-hexene + NMP was very difficult to measure for many reasons. The difficulty encountered with this system, is that at low pressures, in the range of 25-50 kPa, constant flashing of the mixture would occur as a result of the cold fluid from the condenser mixing with the hot fluid in the boiling chamber. This made it extremely difficult to measure the system of interest in this pressure range for the temperatures chosen. The same problem was encountered for the system n-hexane + NMP. This was anticipated, as 1-hexene and n-hexane are similar in their chemical properties. The problem was overcome by trying to accomplish as many measurements around the region in which the flashing was occurring. Therefore, the credibility of the measurements is not compromised as many data points were measured to generate complete isotherms that could be successfully modeled.

7.4.1 System: n-hexane (1) + NMP (2)

The temperatures selected for analysis were: 353.15, 363.15, 378.15 and 383.15 K. n-Hexane and NMP are immiscible at temperatures ≤ 325.15 K. Thus, it was decided to measure data starting at a temperature of 343.15 K upwards. In addition, an important factor that played a role in deciding these temperatures for measurements was the fact that there is currently no data available for this system at the aforementioned temperatures.

As stated previously, Fischer and Gmehling (1996) have measured data for this system at 363.15 K and the alpha value they obtained from the regression was 0.4163. This value was tested on the experimentally measured work in this thesis, by fixing the alpha value during the regression. For this test, where the alpha value of Fischer and Gmehling (1996) was kept constant, the activity coefficient model was maintained as NRTL throughout, and the EoS models used are HOC, SRK-WS, PR-WS, SRK and PR. The activity coefficient model was not varied, as that would be unnecessary, due to this being a simple comparison.

From the results of modeling with a fixed α_{ij} value (Fischer and Gmehling, 1996), the results obtained for the AE % are very similar to the results extracted through regression for the α_{ij} parameter. From the regression operation for α_{ij} it was discovered that the range in which all values lay is 0-0.55. When the regression was executed on Aspen Plus® no upper or lower bound was placed on α_{ij}. The α_{ij} parameters calculated are very similar to the constant Fischer and Gmehling (1996) determined from their experimental measurements. Thus, due to this similarity it is accepted that the results acquired with respect to the AE % are in such close agreement due to the fact that the α_{ij} parameters are in the same range. Overall, the regression for the α_{ij} parameter produced better results; however, this is on such a marginal scale that the difference in performance is considered practically negligible. It is generally accepted that when values for this parameter remain in the domain of -1 to 0.5 the activity coefficients computed are insensitive to the α_{ij} parameter. The experimental work, carried out for this thesis, is in agreement with this range. For further insight on the tabulated data acquired when modeling with the α_{ij} parameter of Fischer and Gmehling (1996), reference should be made to Appendix F.1, Table F1-F4.

The point-to-point y_1 residual plots for all isotherms show reasonable scatter about the x-axis (Appendix E.2).

7.4.1.1 n-Hexane (1) + NMP (2) at 353.15 K

For n-hexane + NMP at this temperature, all the data points were included in the final regression for binary interaction parameters. The three best fit models, when taking into consideration the AE% and the RMSD values for the direct test, varying the EoS and keeping the activity coefficient model (NRTL) fixed, are the NRTL-HOC, NRTL-SRK-WS and NRTL-PR.

After varying the activity coefficient model to UNIQUAC-HOC, the pressure and y_1 residuals were marginally different to that obtained from NRTL-HOC. NRTL-HOC is favoured, as this model produces a smaller ΔP_{AAD} and Δy_{AAD} than UNIQUAC-HOC with values of 0.0015 and 0.0005 as compared to 0.0027 and 0.0009 respectively. Another factor to consider is that NRTL-HOC achieved an index for RMSD for the direct test of 3 as opposed to 4 for UNIQUAC-HOC. Therefore, overall the NRTL-HOC model is the best fit.

The *P-x-y, x-y*, point and direct test plots are reflected in Figures 7-2 to 7-9.

Only for this isothermal scenario are the plots for the point and direct test exhibited. For all other experimental cases, reference should be made to Appendix E for the point test plots.

Table 7-3: Model analysis and consistency test results for the n-hexane (1) + NMP (2) system at 353.15 K.

Pressure/ kPa	x_1	y_1	NRTL-HOC	NRTL-SRK-WS	NRTL-PR-WS	NRTL-SRK	NRTL-PR	UNIQUAC-HOC
133.88	0.8873	0.9923						
130.48	0.7955	0.9919						
129.88	0.7364	0.9914						
128.57	0.7330	0.9906						
127.30	0.6337	0.9905						
126.18	0.5469	0.9900						
124.41	0.4226	0.9895						
119.47	0.3054	0.9896						
116.81	0.2700	0.9894						
111.35	0.2331	0.9885						
100.46	0.1704	0.9869						
75.31	0.1017	0.9834						
52.18	0.0644	0.9784						
Point test results using select data points								
Data points used			13	13	13	13	13	13
ΔP_{AAD}/ kPa			0.0015	0.0015	0.0013	0.0015	0.0015	0.0027
ΔY_{AAD}			0.0005	0.0006	0.0006	0.0006	0.0006	0.0009
AE (%)			0.00025	0.00026	0.00021	0.00026	0.00026	0.00081
Index Direct Test			3	3	5	4	3	4

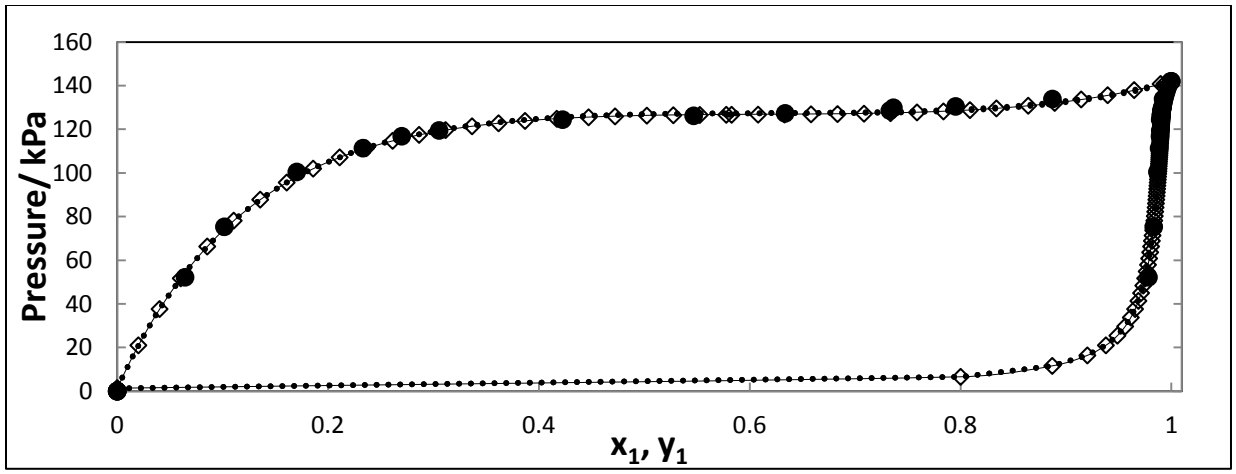

Figure 7-2: *P-x-y* plot for the n-hexane (1) + NMP (2) system at 353.15 K (varying EoS). ●, experimental data; ▬, NRTL-HOC; ◊, NRTL-PR; ····, NRTL-SRK-WS.

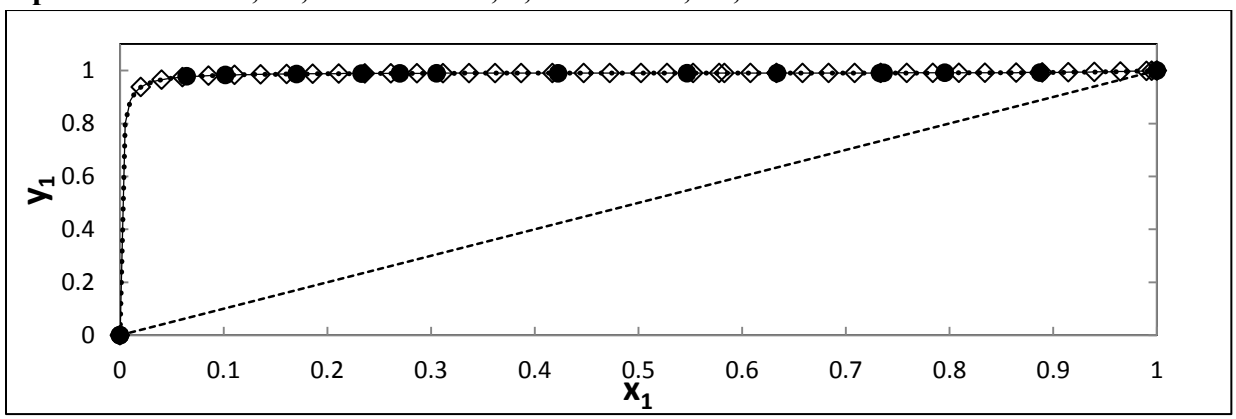

Figure 7-3: *y-x* plot for the n-hexane (1) + NMP (2) system at 353.15 K (varying EoS). ●, experimental data; ▬, NRTL-HOC; ·····, NRTL-SRK-WS; ◊, NRTL-PR.

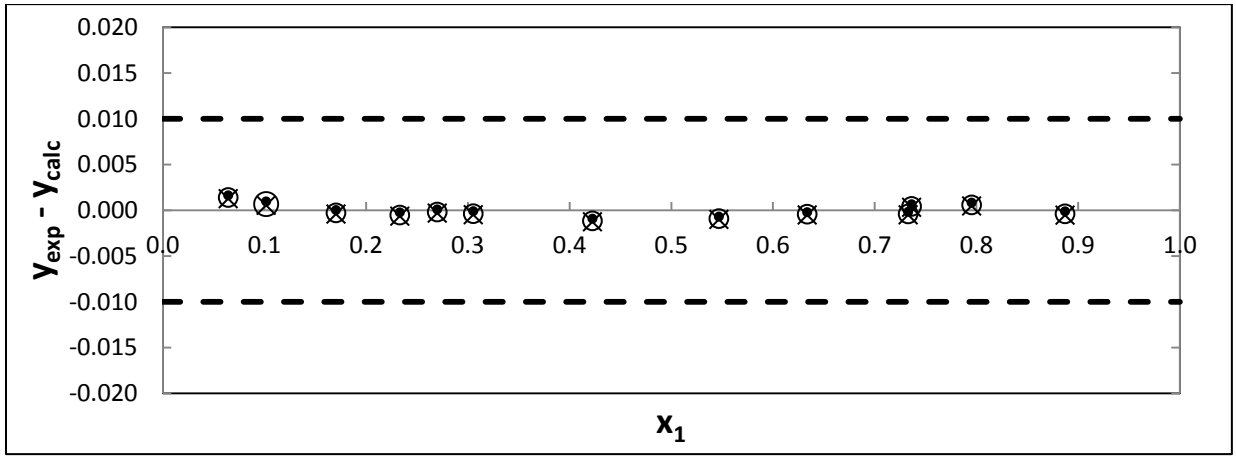

Figure 7-4: Point test (varying EoS): Δy_1 for the n-hexane (1) + NMP (2) system at 353.15 K. ○, NRTL-HOC; •, NRTL-SRK-WS; X, NRTL-PR.

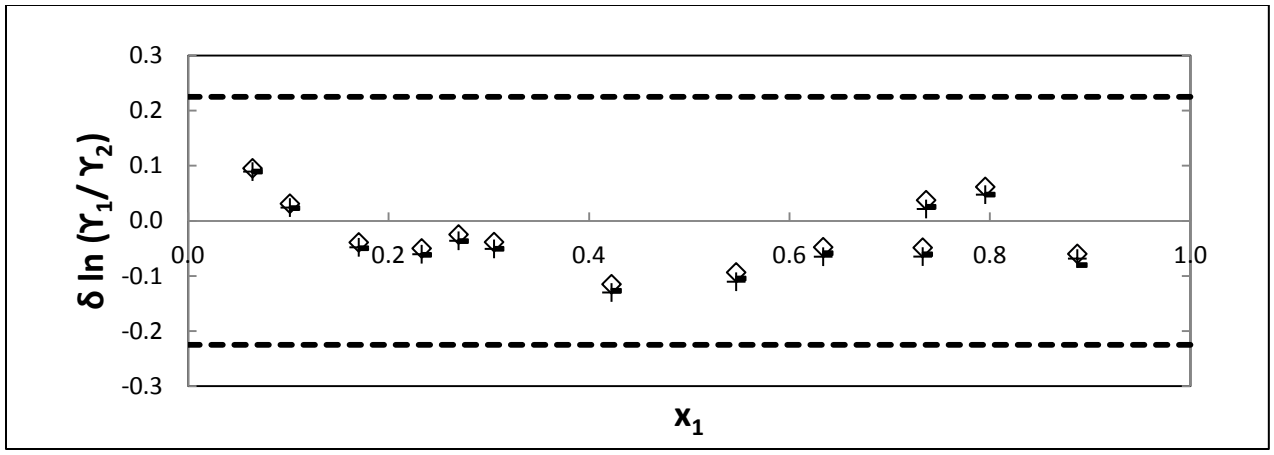

Figure 7-5: Direct test (varying EoS): δ Ln (γ_1/γ_2) for the n-hexane (1) + NMP (2) at 353.15 K . ◊, NRTL-HOC; —, NRTL-PR; +, NRTL-SRK-WS.

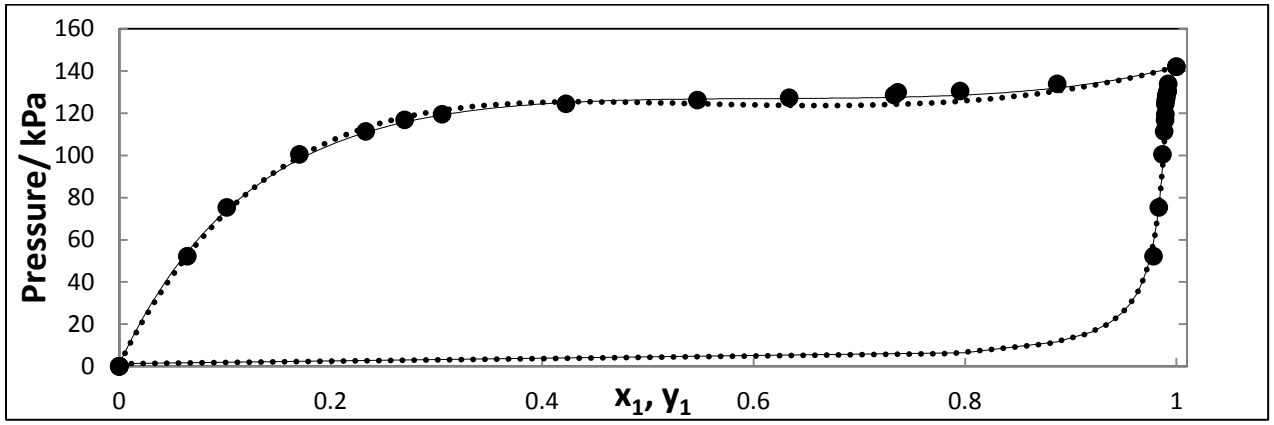

Figure 7-6: *P-x-y* plot for the n-hexane (1) + NMP (2) system at 353.15 K (varying activity coefficient model). ●, experimental data; —, NRTL-HOC; ·····, UNIQUAC-HOC.

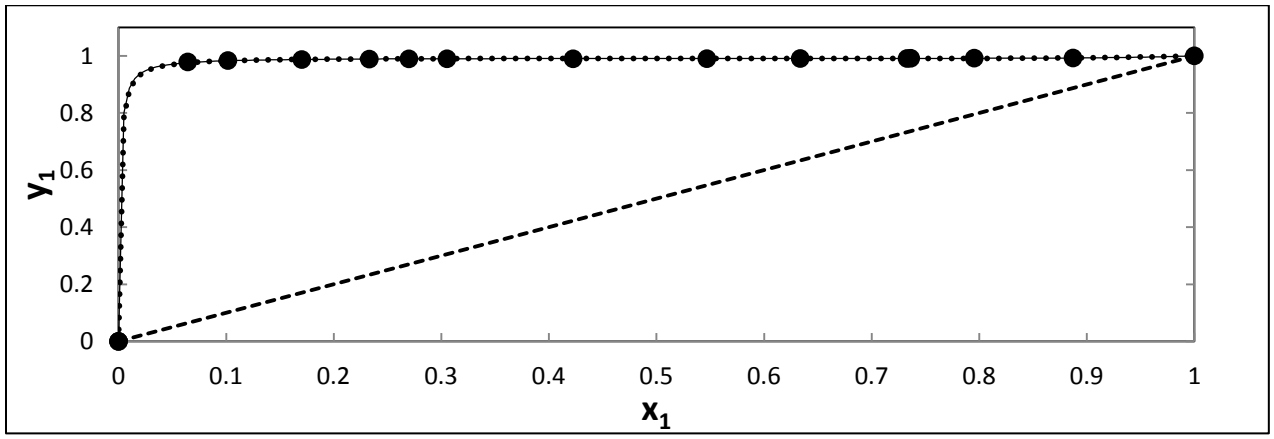

Figure 7-7: *y-x* plot of n-hexane (1) + NMP (2) system at 353.15 K (varying activity coefficient model); ●, experimental data; —, NRTL-HOC; ·····, UNIQUAC-HOC.

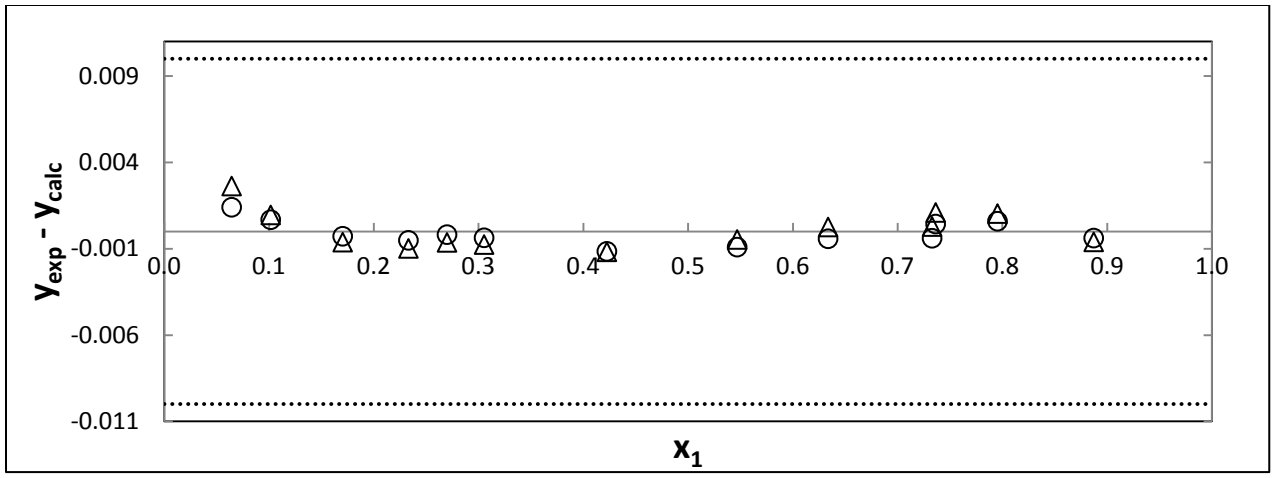

Figure 7-8: Point test (varying activity coefficient model): Δy_1 for the n-hexane (1) + NMP (2) system at 353.15 K. ○, NRTL-HOC; ∆, UNIQUAC-HOC.

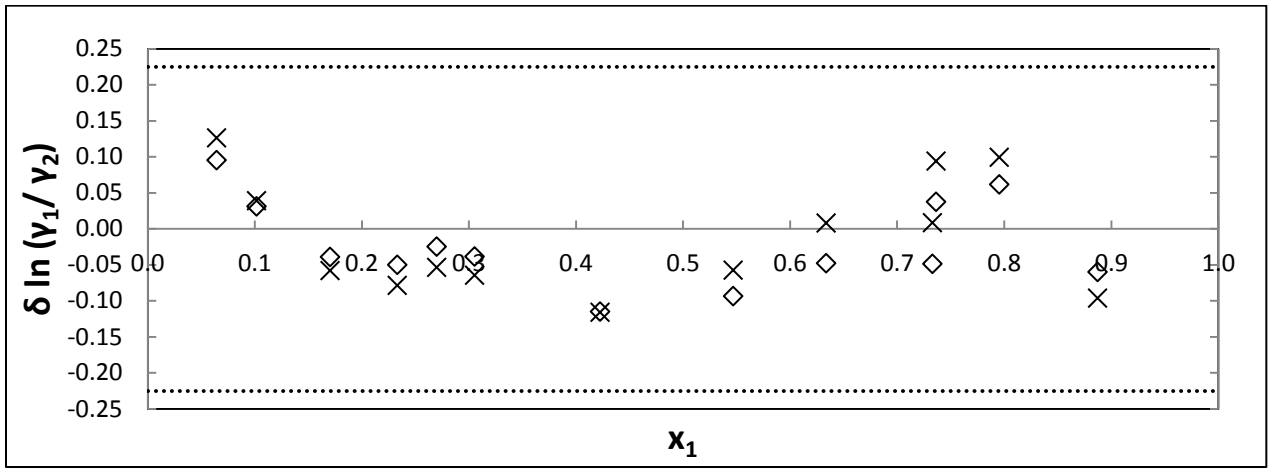

Figure 7-9: Direct test (varying activity coefficient model): δ Ln (γ_1/γ_2) for the n-hexane (1) + NMP (2) system at 353.15 K. ◊, NRTL-HOC; X, UNIQUAC-HOC.

There is a small discrepancy between the Aspen Plus® PSRK model and the measurements conducted at this temperature. As the liquid composition of n-hexane steadily increases from 0.5 mole fraction, the greatest deviation between the Aspen PSRK model and the experimental data is observed.

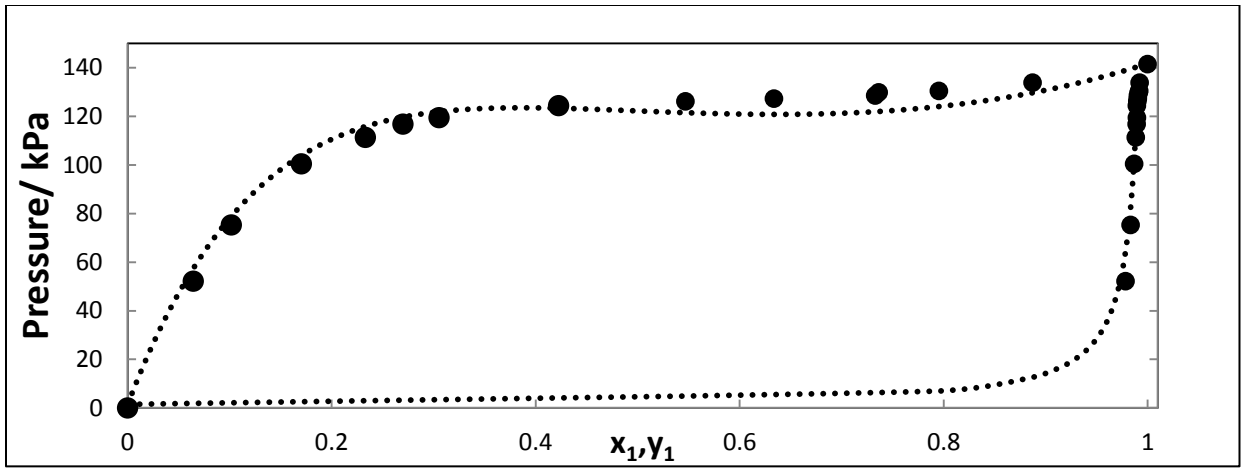

Figure 7-10*: P-x-y* plot for the n-hexane (1) + NMP (2) system at 353.15 K. ●, P-x_1-y_1 (this work); ·····, P-x_1-y_1 (Aspen Plus® PSRK model).

7.4.1.2 n-Hexane (1) + NMP (2) at 363.15 K

At this temperature, the data point corresponding to 1.96 kPa has been ignored for all models so that the various models implemented could pass the point test. When the *y* residual at this point was computed, for all involved models, the greatest deviation between the experimental and calculated y_i was computed. Thus, following logic this point is neglected from data analysis as it is contributing to the greatest error. The region in which this point lies is dilute for n-hexane. In addition, this is a specific region wherein a great deal of error results for the measurements due to it being a region of infinite dilution. As such special equipment is actually required to measure infinite dilution activity coefficients in a section prone to error with the use of regular VLE equipment.

This data point is still showcased in the original data set tabulated below, even though it has been neglected from the final regression process. This is done to exhibit to the reader that when data points are being measured, the trajectory of all the points together appears smooth. However, for points in the dilute regions, in order to verify the authenticity of data informally, in the absence of conducting any modeling) many data points in the dilute regions should be measured.

The three best fit models, varying EoS and keeping the activity coefficient model constant, in descending order are NRTL-HOC, NRTL-PR and NRTL-SRK. After varying the activity coefficient model to UNIQUAC and keeping the EoS constant as HOC, it is observed that the

pressure and vapour composition residuals, as well as the RMSD for the direct test, are very similar for the UNIQUAC and NRTL-HOC case. Overall the NRTL-HOC model produces better results than UNIQUAC-HOC. Thus, in totality, the NRTL-HOC model performed the best.

Table 7-4: Model analysis and consistency test results for the n-hexane (1) + NMP (2) system at 363.15 K.

Pressure/ kPa	x_1	y_1	NRTL-HOC	NRTL-SRK-WS	NRTL-PR-WS	NRTL-SRK	NRTL-PR	UNIQ-HOC
179.38	0.9090	0.9933						
177.43	0.8978	0.9932						
173.00	0.7248	0.9923						
166.74	0.6190	0.9902						
165.43	0.5116	0.9896						
163.72	0.4576	0.9882						
161.41	0.3898	0.9860						
156.98	0.3409	0.9855						
144.99	0.2463	0.9838						
126.98	0.1700	0.9819						
86.51	0.0875	0.9764						
65.12	0.0615	0.9671						
1.96	0.0003	0.0004	*	*	*	*	*	*
Point test results using all data points								
Total data points			13	13	13	13	13	13
ΔP_{AAD} (kPa)			0.0110	0.0112	0.0122	0.0109	0.0109	0.0125
ΔY_{AAD}			11.8929	11.5859	11.2282	11.8543	11.8863	21.5546
Point test results using select data points								
Data points used			12	12	12	12	12	12
ΔP_{AAD} (kPa)			0.0062	0.0062	0.0068	0.0062	0.0062	0.0083
ΔY_{AAD}			0.0039	0.0051	0.0053	0.0047	0.0048	0.0035
Index Direct test			9	10	10	10	10	8
AE (%)			0.0054	0.0064	0.0074	0.0060	0.0061	0.0081

N.B: a '*' in a certain column indicates that that point was excluded from the final regression analysis.

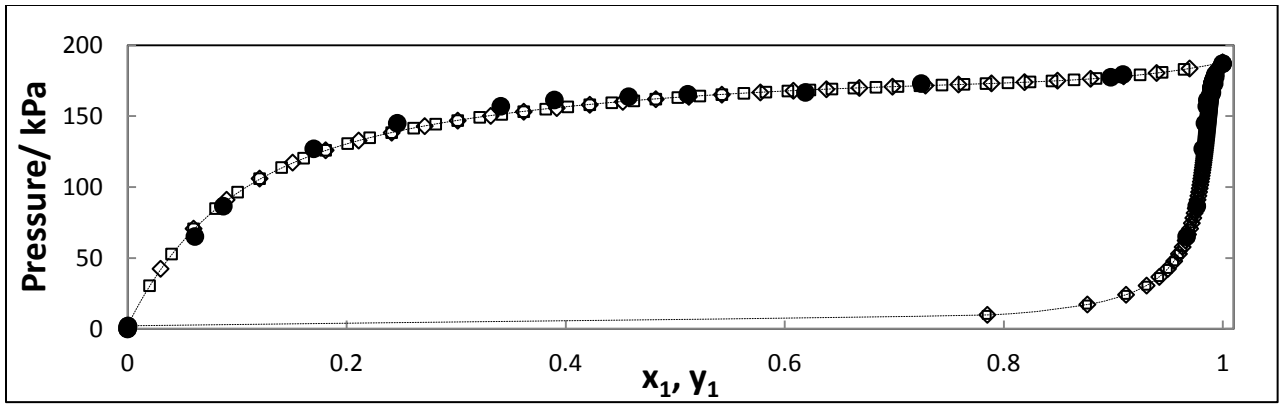

Figure 7-11: *P-x-y* plot for the n-hexane (1) + NMP (2) system at 363.15 K (varying EoS). ●, experimental data; — — —, NRTL-HOC; □, NRTL-PR; ◊, NRTL-SRK.

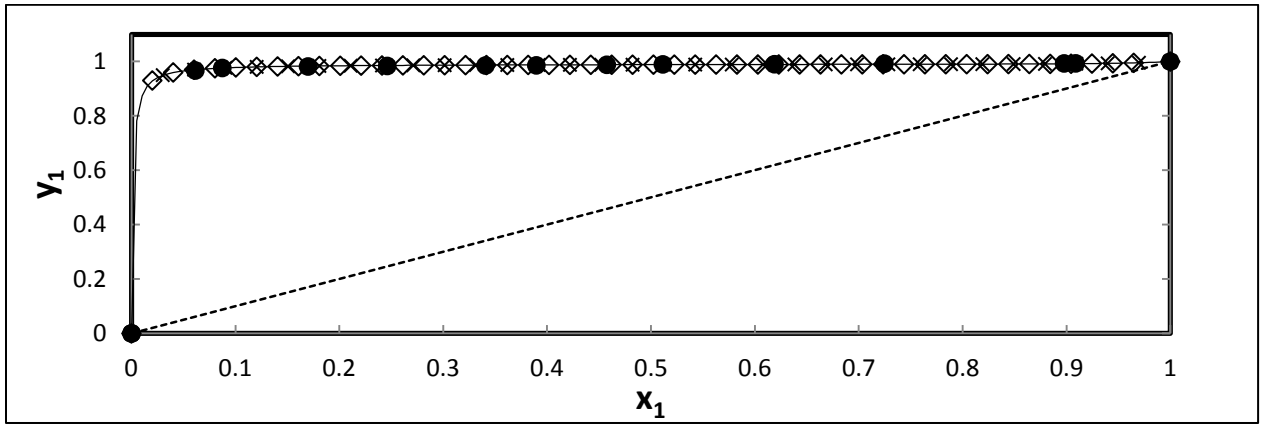

Figure 7-12: *y-x* plot for the n-hexane (1) +NMP (2) system at 363.15 K (varying EoS). ●, experimental data; —, NRTL-HOC; X, NRTL-SRK; ◊, NRTL-PR.

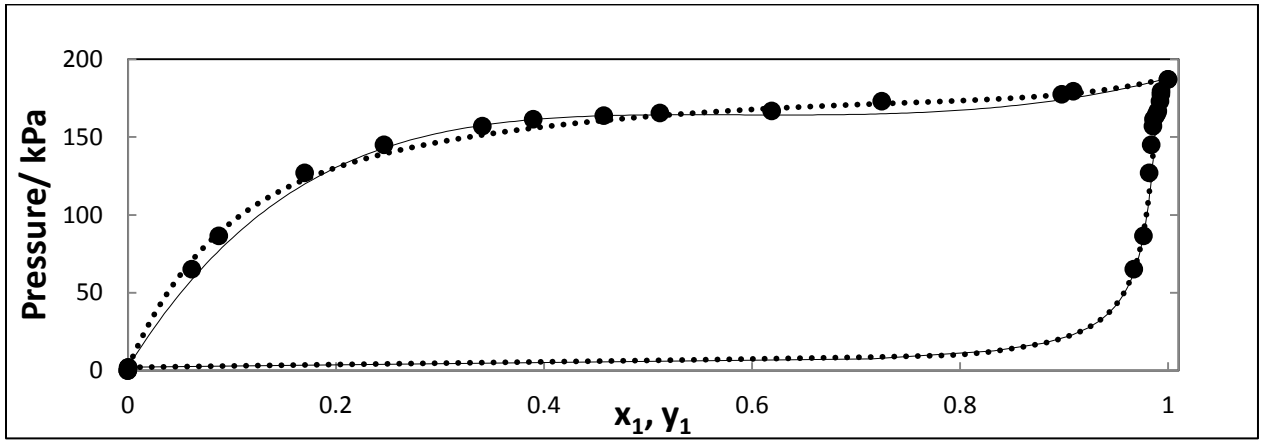

Figure 7-13: *P-x-y* plot for the n-hexane (1) + NMP (2) system at 363.15 K (varying activity coefficient model). ●, experimental data; · · · · ·, NRTL-HOC; —, UNIQUAC-HOC.

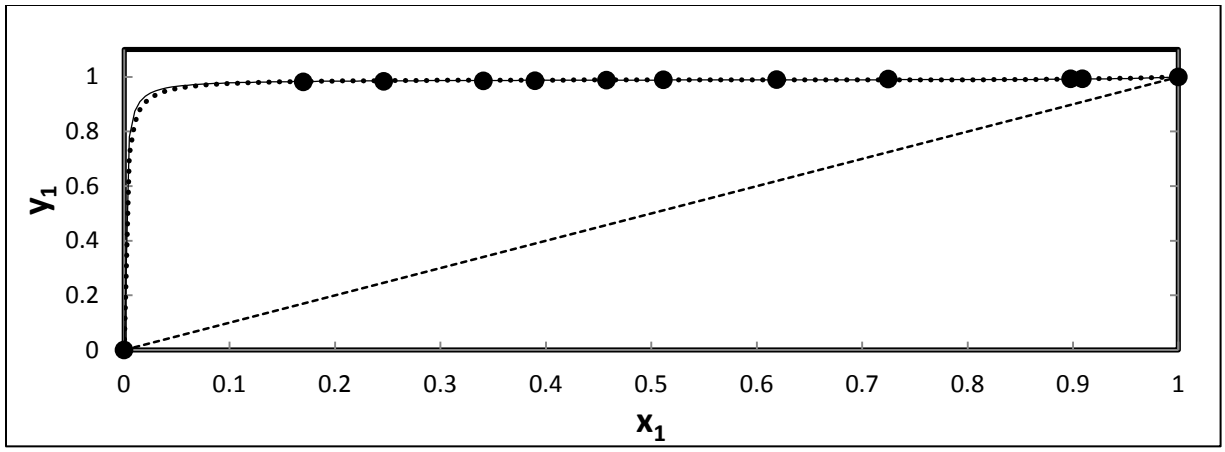

Figure 7-14: *y-x* plot for the n-hexane (1) + NMP (2) system at 363.15 K (varying activity coefficient model). ●, experimental data; ▬, NRTL-HOC; ·····, UNIQUAC-HOC.

The P-x_1 data of Fischer and Gmehling (1996) at 363.15 K and the experimentally measured data on the high pressure VLE still compared very well with each other. However, there is a small deviation between the Aspen Plus® PSRK prediction and the measured data for the test system being investigated. Though, one is confident with the results acquired in this work as it compares very well with the P-x_1 data reported by Fischer and Gmehling (1996).

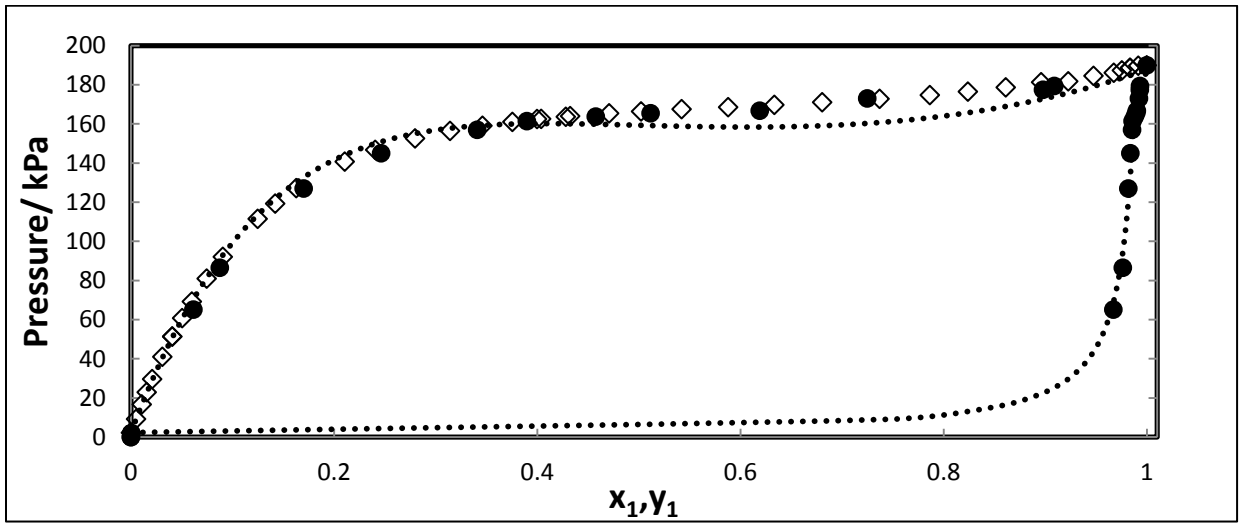

Figure 7-15: *P-x-y* plot for the n-hexane (1) + NMP (2) system at 363.15 K. ◊, P-x (Fischer and Gmehling, 1996); ●, P-x_1-y_1 (this work); ·····, P-x_1-y_1 (Aspen Plus ® PSRK model).

7.4.1.3 n-Hexane (1) + NMP (2) at 378.15 K

The best fit overall model for this system is NRTL-HOC. One data point was neglected from the regression analysis, corresponding to a pressure of 4.16 kPa. Once again this point falls in the dilute region for n-hexane.

Table 7-5: Model analysis and consistency test results for the n-hexane (1) + NMP (2) system at 378.15 K.

Pressure/ kPa	x_1	y_1	NRTL-HOC	NRTL-SRK-WS	NRTL-PR-WS	NRTL-SRK	NRTL-PR	UNIQ-HOC
265.56	0.9127	0.9962						
261.13	0.8769	0.9936						
245.24	0.7438	0.9895						
241.67	0.6070	0.9874						
239.73	0.5416	0.9866						
231.96	0.46544	0.9853						
230.90	0.4621	0.9834						
213.29	0.2929	0.9813						
180.12	0.1773	0.9766						
131.04	0.0899	0.9686						
80.58	0.0538	0.9491			*			
4.16	0.0022	5.E-05	*	*	*	*	*	*
Point test results using all data points								
Total data points			12	12	12	12	12	12
ΔP_{AAD}(kPa)			0.0209	0.0212	0.0213	0.0211	0.0211	0.0254
ΔY_{AAD}			253.9671	250.5181	232.1825	251.2708	253.3821	562.2750
Point test results using select data points								
Data points used			11	11	10	11	11	11
ΔP_{AAD}(kPa)			0.0135	0.0125	0.0102	0.0133	0.0133	0.0162
ΔY_{AAD}			0.0106	0.0121	0.0070	0.0124	0.0124	0.0087
Index direct test			6	10	10	10	10	9
AE (%)			0.0295	0.0303	0.0153	0.0331	0.0331	0.0338

N.B: a '*' in a certain column indicates that that point was excluded from the final regression analysis

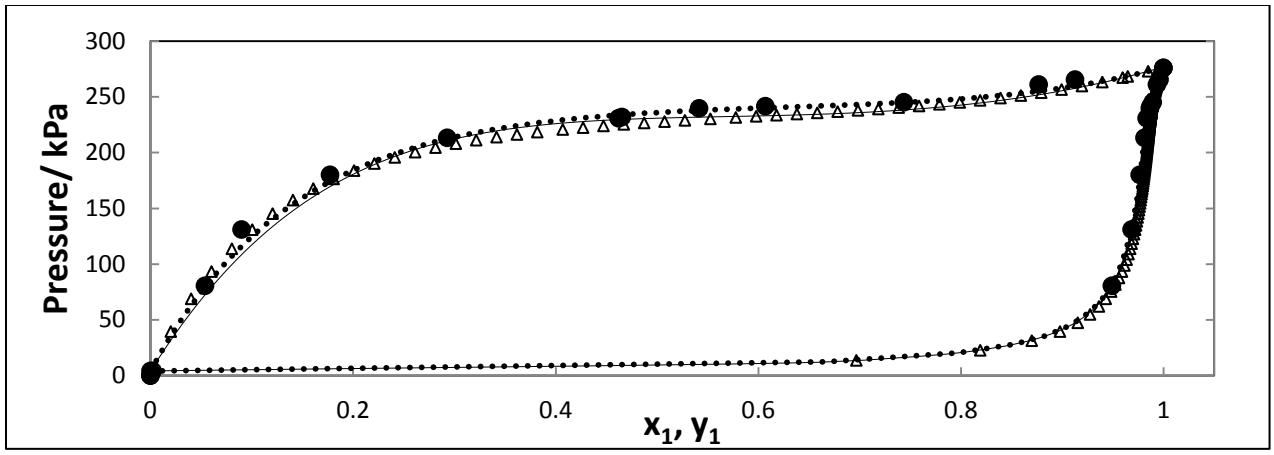

Figure 7-16: *P-x-y* plot for the n-hexane (1) +NMP (2) system at 378.15 K (varying EoS). ●, experimental data; —, NRTL-HOC; ····, NRTL-PR-WS; Δ, NRTL-SRK-WS.

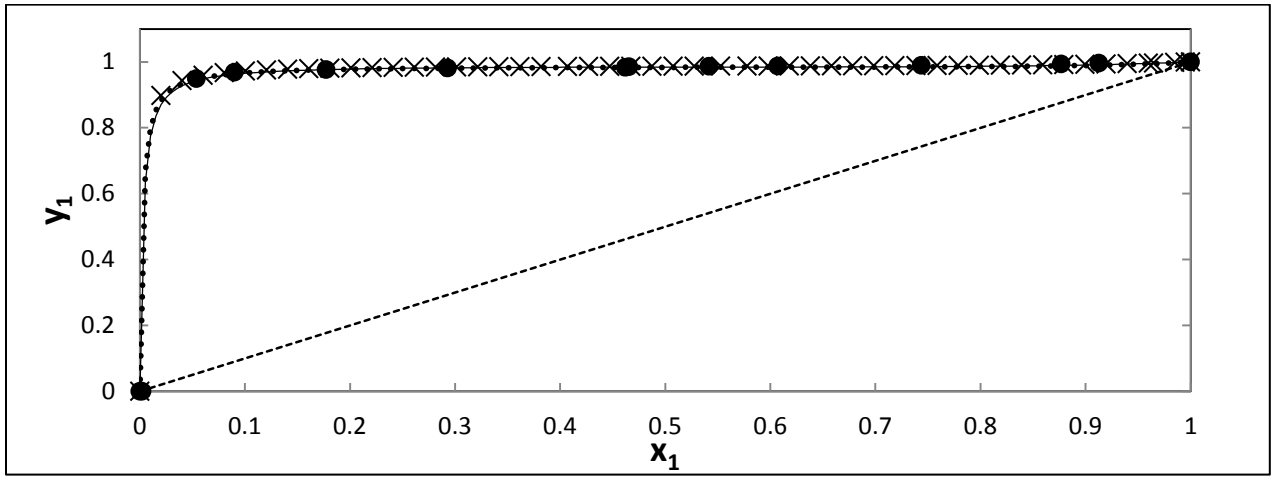

Figure 7-17: *y-x* plot for the n-hexane (1) + NMP (2) system at 378.15 K (varying EoS). ●, experimental data; —, NRTL-HOC; · · · ·, NRTL-PR-WS; X, NRTL-SRK-WS.

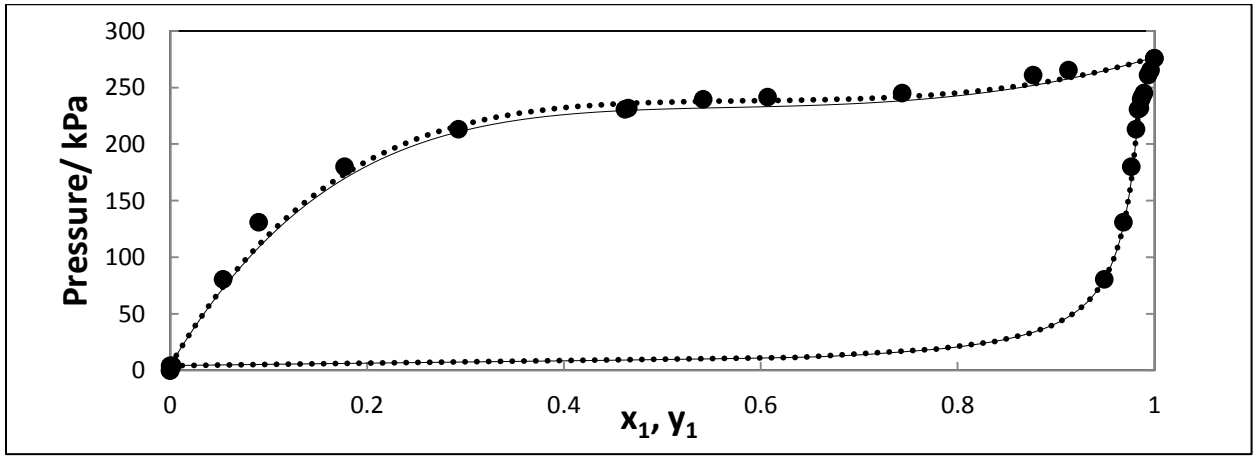

Figure 7-18: *P-x-y* plot for the n-hexane (1) + NMP (2) system at 378.15 K (varying activity coefficient model). ●, experimental data; —, NRTL-HOC; ·····, UNIQUAC-HOC.

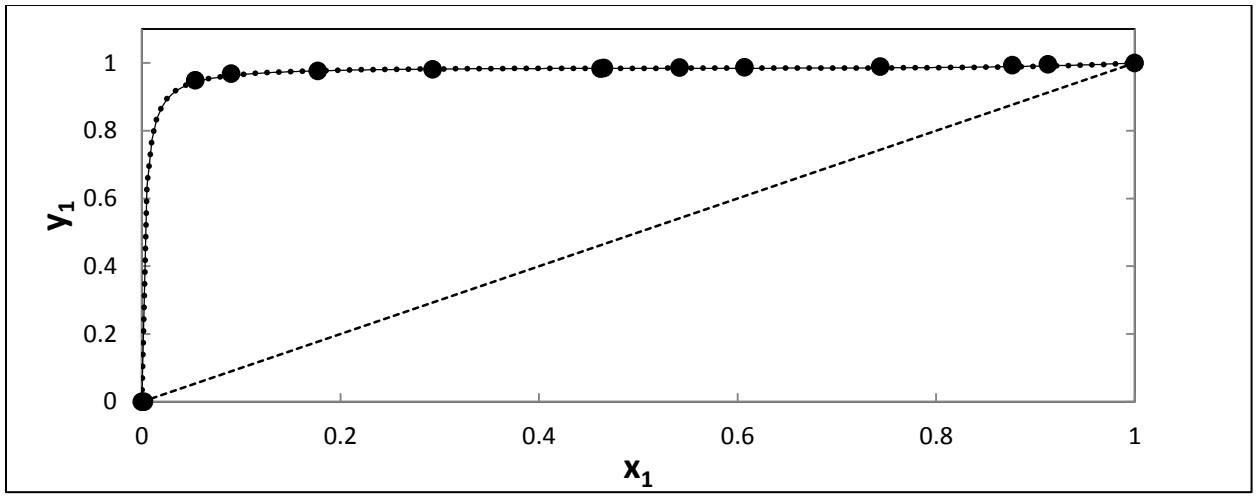

Figure 7-19: *y-x* plot for the n-hexane (1) + NMP (2) system at 378.15 K (varying activity coefficient model). ●, experimental data; ▬, NRTL-HOC; ·····, UNIQUAC-HOC.

As observed in the previous plots of the experimental data against the Aspen Plus® PSRK model, there is good agreement between the different plots. Although the deviation observed where n-hexane steadily increases from 0.5 mole fraction is still evident. This appears to be a trend the PSRK model is generating.

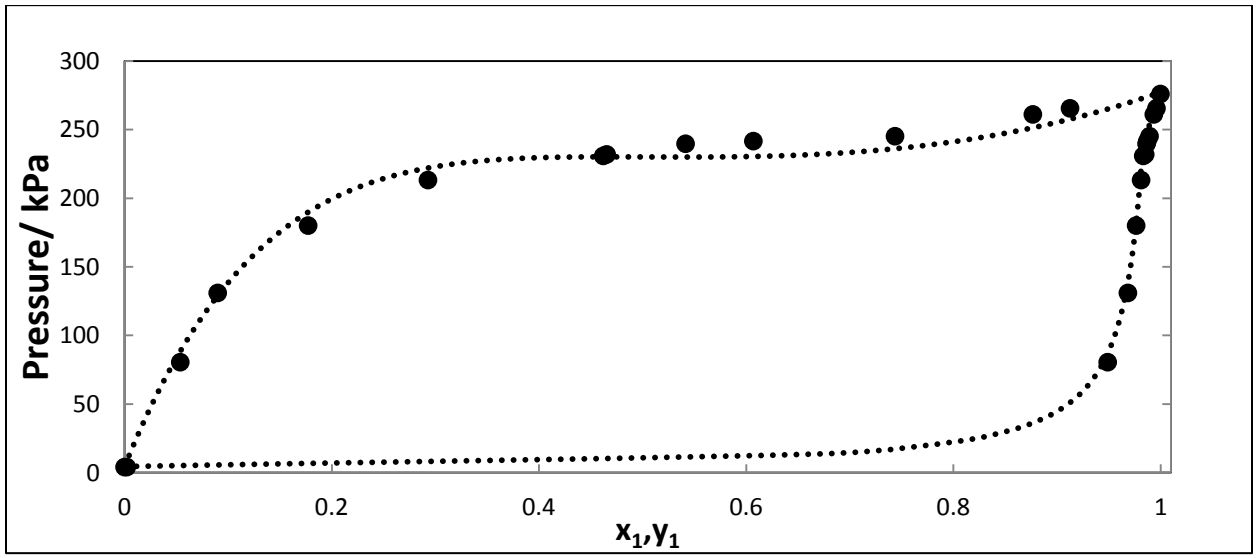

Figure 7-20: *P-x-y* plot for the n-hexane (1) + NMP (2) System at 378.15 K. ●, P-x_1-y_1 (this work); ·····, P-x_1-y_1 (Aspen Plus ® PSRK model).

7.4.1.4 n-Hexane (1) + NMP (2) at 383.15 K

The best fit models for this system are: NRTL-HOC, NRTL-SRK-WS and NRTL-PR-WS, with the overall best fit acquired from the NRTL-HOC model, even when compared to the UNIQUAC-HOC model representation. Both the NRTL-HOC and UNIQUAC-HOC model representations produce results for the direct test with an index of 8, however, when comparing just the AE % of the model fits, the NRTL-HOC model is best overall.

Table 7-6: Model analysis and consistency test results for the n-hexane (1) + NMP (2) system at 383.15 K.

Pressure/ kPa	x_1	y_1	NRTL-HOC	NRTL-SRK-WS	NRTL-PR-WS	NRTL-SRK	NRTL-PR	UNIQUAC-HOC
297.73	0.8965	0.9943						
289.90	0.8611	0.9929						
280.00	0.8434	0.9928						
276.80	0.8334	0.9923						
275.79	0.7392	0.9915						
273.16	0.6563	0.9912						
270.02	0.5477	0.9908						
268.77	0.5116	0.9907						
266.81	0.4846	0.9902						
252.48	0.3624	0.9846						
239.99	0.2879	0.9789						
201.06	0.1719	0.9737						
168.15	0.1293	0.9700						
133.51	0.0889	0.9669						
95.19	0.0571	0.9567						
Point test Results using select data points								
Data points used			15	15	15	15	15	15
ΔP_{AAD}(kPa)			0.0031	0.0040	0.0049	0.1060	0.1061	0.0053
ΔY_{AAD}			0.0021	0.0028	0.0039	0.0045	0.0045	0.0062
Index direct test			8	10	10	10	10	8
AE (%)			0.0014	0.0024	0.0039	1.1256	1.1277	0.0067

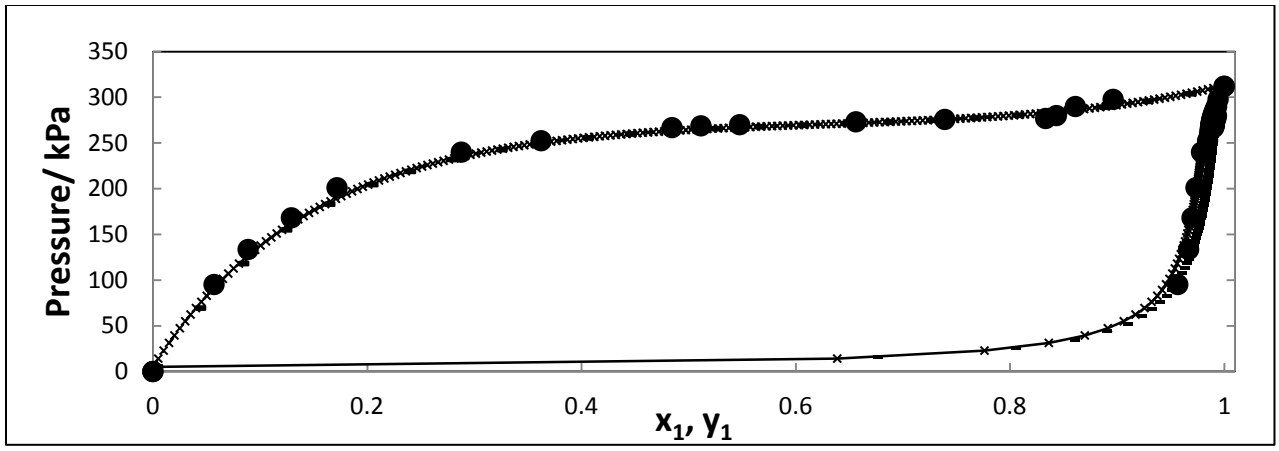

Figure 7-21: *P-x-y* plot for the n-hexane (1) +NMP (2) system at 383.15 K (varying EoS). ●, experimental data; ——, NRTL-HOC; X, NRTL-PR-WS; - - -, NRTL-SRK-WS.

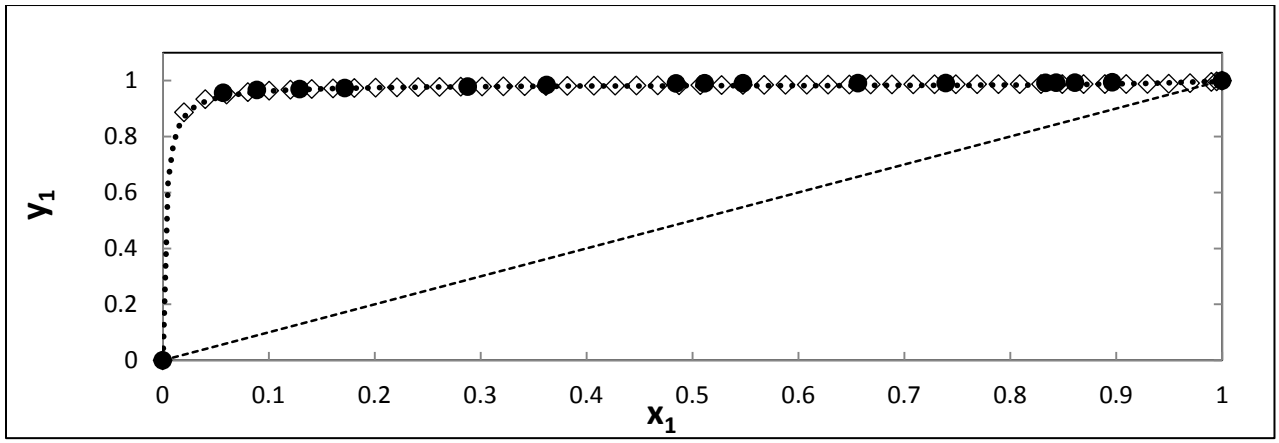

Figure 7-22: *y-x* plot for the n-hexane (1) + NMP (2) system at 383.15 K (varying EoS). ●, experimental data; ——, NRTL-HOC; ·····, NRTL-PR-WS; ◊, NRTL-SRK-WS.

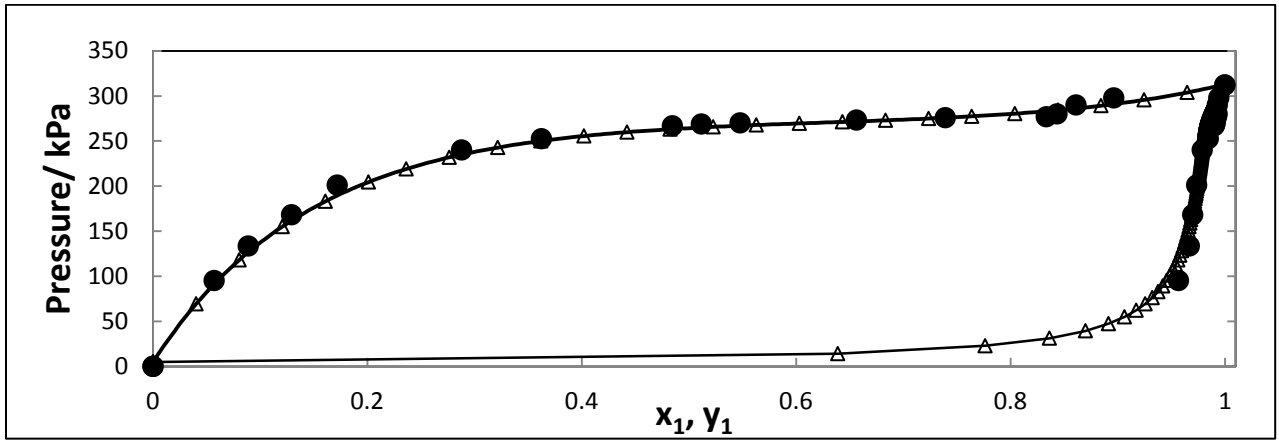

Figure 7-23: *P-x-y* plot for the n-hexane (1) + NMP (2) system at 383.15 K (varying activity coefficient model). ●, experimental data; —, NRTL-HOC; ∆, UNIQUAC-HOC.

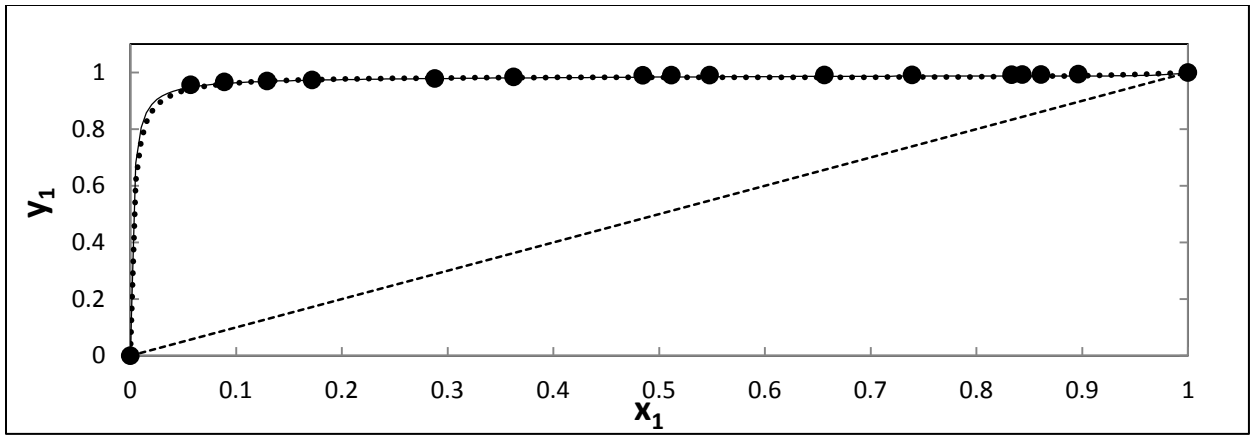

Figure 7-24: *y-x* plot for the n-hexane (1) + NMP (2) system at 383.15 K (varying activity coefficient model). ●, experimental data; ▬, NRTL-HOC; ·····, UNIQUAC-HOC.

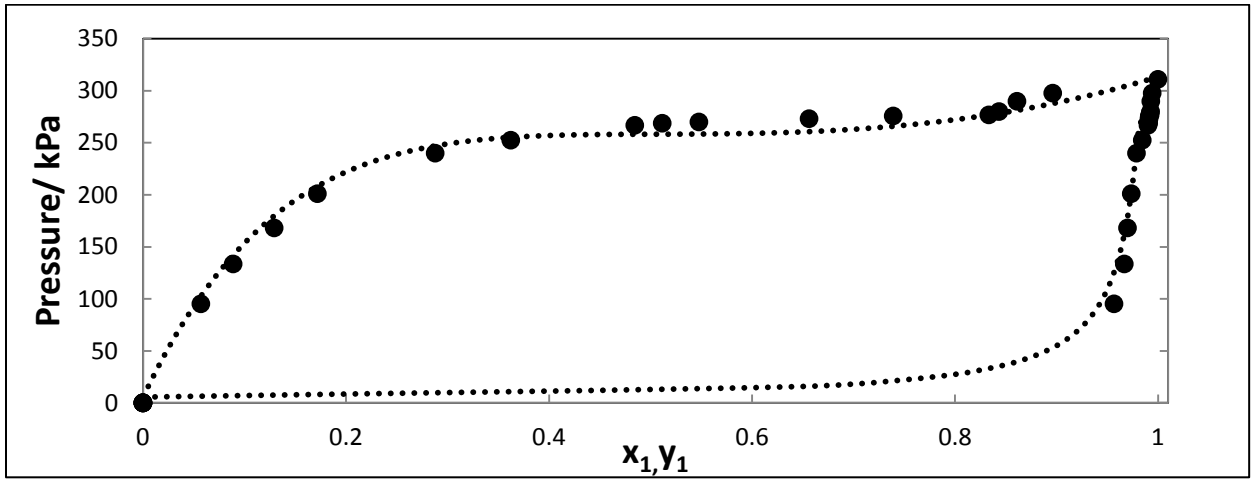

Figure 7-25: *P-x-y* plot for the n-hexane (1) + NMP (2) System at 383.15 K. ●, P-x_1-y_1 (this work); ·····, P-x_1-y_1 (Aspen Plus ® PSRK model).

7.4.2 1-Hexene (1) + NMP (2)

The temperatures chosen for this system to be measured are 323.15, 343.15, 353.15 and 363.15 K. All measured data constitutes new data. Fischer and Gmehling (1996) have measured data for the system 1-hexene + NMP at 363.15 K, however, this data was measured on a static apparatus and only *P*-x_i data were recorded. Therefore, the data measured in this work, at 363.15 K serves as new *P*-y_i data for this system. Hirawan (2007) also measured data for this system at 313.15, 335.15 and 363.15 K. However, further measurements are required due to the fact that complete isotherms could not be generated by Hirawan (2007), as a low pressure VLE glass still was used at that time. Therefore, pressure was a severe limitation in those measurements.

With the use of the newly commissioned still of Lilwanth (2011), complete isotherms are capable of being generated. In addition, the temperatures chosen for measurements have moderately high pressures. As such, not only were the pressure and temperature limits of the newly commissioned still tested, but a greater understanding of the system behavior of 1-hexene + NMP achieved as well as new, and as yet unpublished, *P*-*x*-*y* data for this system at the temperatures stated above.

From the data regression for this system, the α_{ij} values computed all lay in the overall range of 0-0.55, with the majority of the α_{ij} values in the 0-0.3 range. Thus, due to this similarity in the regressed values and the constant value utilized for α_{ij} (Fischer and Gmehling, 1996) it is accepted that the fit of the experimental to the modeled data are in such close agreement due to the fact that the α_{ij} parameters are in the same -1 to 0.5 range.

For the isotherms 323.15, 353.15 and 363.15 K the AE % computed for the data where the α_{ij} parameter was regressed and kept constant, are approximately the same. The regressed data produces a smaller AE%, however, there is such a minute difference between the two case studies that we conclude the results obtained using the two different techniques are equally good.

When the results at 343.15 K were analyzed, the case for the regression of the α_{ij} parameter produced significantly better results that for the fixed α_{ij} case. This observation is discussed in greater depth in the corresponding section.

For further insight on the tabulated data acquired when modeling with the α_{ij} parameter of Fischer and Gmehling (1996), reference should be made to Appendix F.2, Table F5-F7.

The point-to-point y_1 residual plots for all isotherms show reasonable scatter about the x-axis (these plots are available in Appendix E.1.).

7.4.2.1 1-Hexene (1) + NMP (2) at 323.15 K

For the 323.15 K isotherm, all data points were included since the constraints of the point test for all model combinations at this temperature were satisfied. The pressure and vapour composition residuals all satisfy the criterion of a less than 1 % deviation in experimental data from the calculated data. The residuals obtained from varying the EoS models while keeping NRTL model fixed did not render significantly vast differences in the P and y_1 residuals.

All the models, when keeping the activity coefficient model the same (NRTL), produced an index for the direct test of 10. However, a comparison of the AE % for all models revealed that the NRTL-HOC model is best with an AE % of 0.0001. Thereafter, the activity coefficient model was changed to UNIQUAC and the results once again compared.

The P and y_1 composition residuals for the NRTL-HOC model were marginally smaller than the UNIQUAC-HOC model. However, the direct test for the two models showcased the UNIQUAC-HOC model to have an index of 9 as opposed to the NRTL-HOC model which acquired an index of 10. Thus, overall the UNIQUAC-HOC model provides the best fit for the data at 323.15 K.

Table 7-7: Model analysis and consistency test results for the 1-hexene (1) + NMP (2) system at 323.15 K.

Pressure/ kPa	x_1	y_1	NRTL -HOC	NRTL -SRK-WS	NRTL-PR-WS	NRTL-SRK	NRTL-PR	UNIQUAC-HOC
63.55	0.9823	0.9999						
61.30	0.9525	0.9995						
58.29	0.8448	0.9988						
57.50	0.8237	0.9986						
56.81	0.7389	0.9984						
53.63	0.5416	0.9978						
52.59	0.4951	0.9976						
48.35	0.3122	0.9969						
46.30	0.2744	0.9964						
44.47	0.2435	0.9953						
40.29	0.1976	0.9941						
38.26	0.1704	0.9929						
27.99	0.0966	0.9916						
13.32	0.0566	0.9900						
Point test results using select data points								
Points used			14	14	14	14	14	14
ΔP_{AAD}(kPa)			0.0009	0.0052	0.0010	0.0078	0.0073	0.0070
ΔY_{AAD}			0.0005	0.0006	0.0006	0.0012	0.0012	0.0012
AE (%)			0.0001	0.0027	0.0001	0.0062	0.0055	0.0050
Direct Test Index			10	10	10	10	10	9

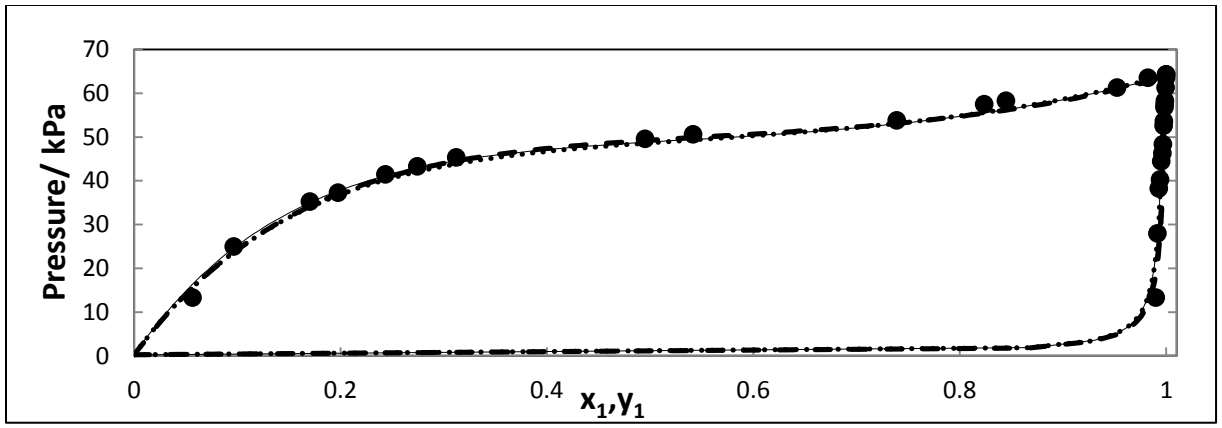

Figure 7-26: *P-x-y* plot for the 1-hexene (1) + NMP (2) system at 323.15 K (varying EoS).●, experimental data; ——, NRTL-HOC; — — —, NRTL-PR-WS; ····, NRTL-SRK-WS.

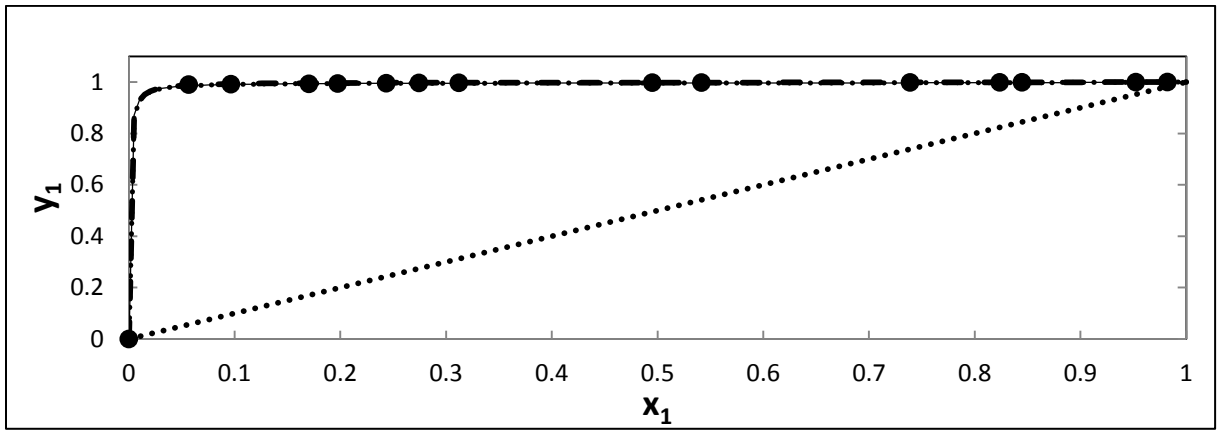

Figure 7-27: *y-x* plot for the 1-hexene (1) + NMP (2) system at 323.15 K (varying EoS). ●, experimental data; —, NRTL-HOC; — — —, NRTL-PR-WS; ····, NRTL-SRK-WS.

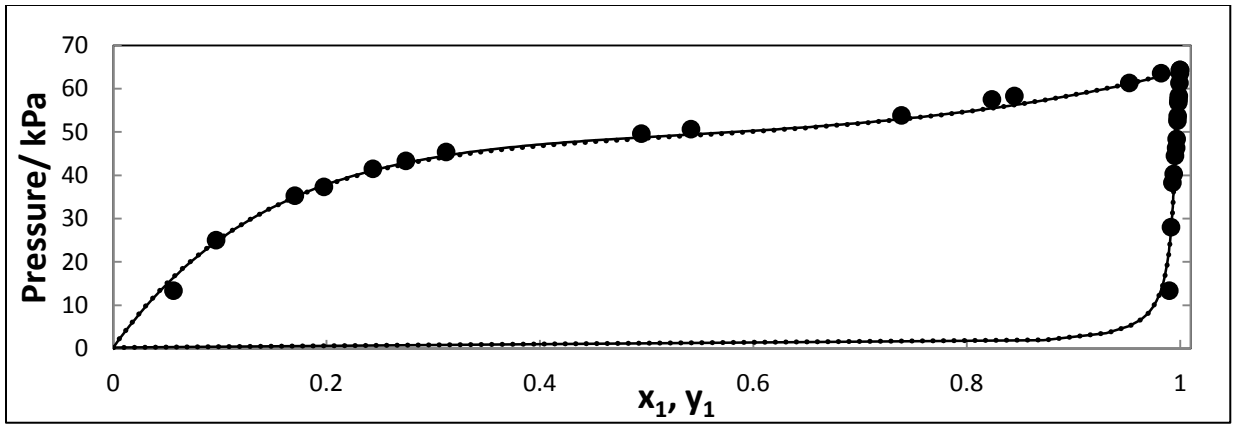

Figure 7-28: *P-x-y* plot for the 1-hexene (1) + NMP (2) system at 323.15 K (varying activity coefficient model). ●, experimental data; —, NRTL-HOC; ·····, UNIQUAC-HOC.

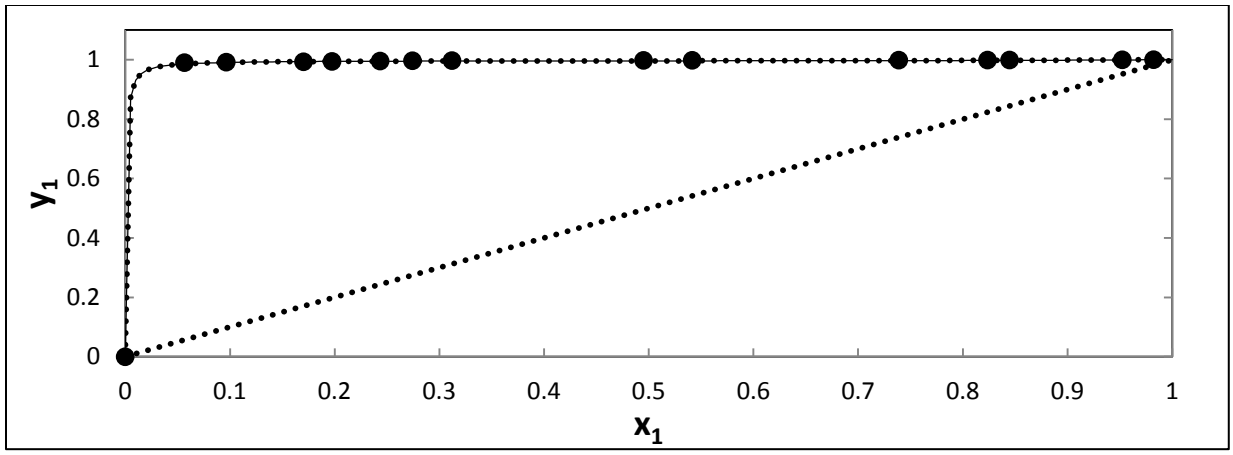

Figure 7-29: *y-x* plot for the 1-hexene (1) + NMP (2) system at 323.15 K (varying EoS). ●, experimental data; ▬, NRTL-HOC; ····, UNIQUAC-HOC.

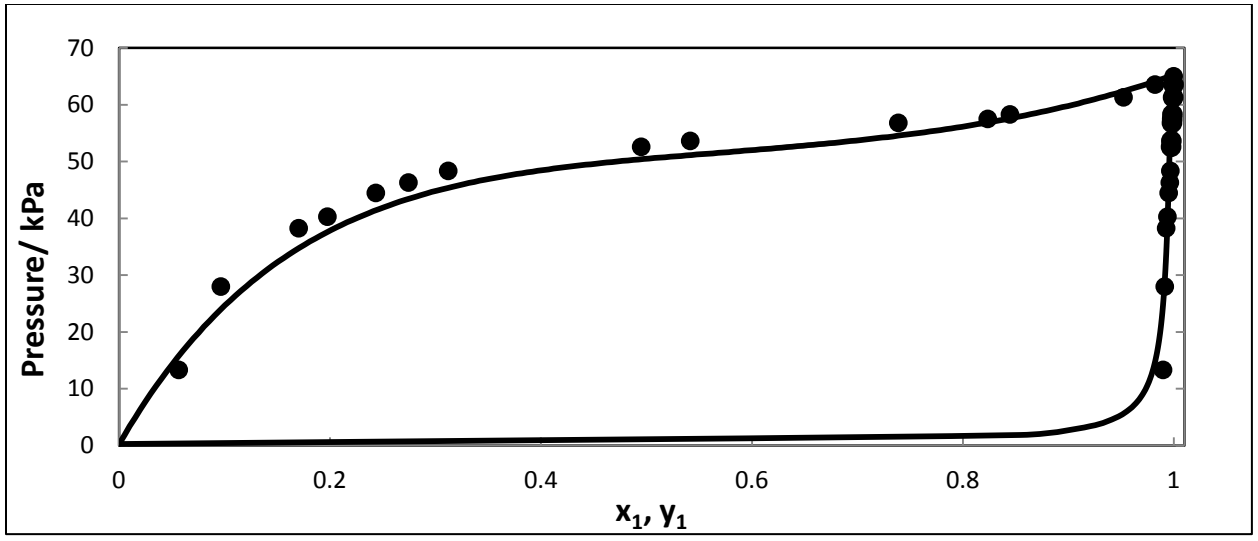

Figure 7-30: *P-x-y* plot for the 1-hexene (1) + NMP (2) system at 323.15 K. ●, P-x_1-y_1 (this work); ——, P-x_1-y_1 (Aspen Plus ® PSRK model).

7.4.2.2 1-Hexene (1) + NMP (2) at 343.15 K

For the 343.15 K isotherm the last data point, *i.e.* 18.94 kPa, is neglected (for all model combinations) in order to enable the criteria of the point test to be met. This data point when modeled showed the greatest deviation from the experimental data point corresponding to it. The best fit model, when varying the EoS models only, is found to be NRLT-HOC with an AE % and direct test index of 0.0298 and 7, respectively. Changing the activity coefficient model to UNIQUAC (with EoS as HOC) one observes an AE % of 0.27044 and a direct test index of 6. However, overall the NRTL-HOC model performs the best.

For this specific isotherm, the regression for the α_{ij} parameter produced a significant improvement in terms of the fit of the experimental data to the calculated data utilizing the various models. When the α_{ij} parameter is fixed to a value of 0.4567 (Fischer and Gmehling, 1996) a greater deal of the experimental data points were neglected in order to pass the point consistency test. This leads one to believe that the limitation placed on this adjustable parameter actually prevents the NRTL activity coefficient model from providing the best possible fit for the given data. A comparison of the results of Table 7-8 to Table 7-9 clearly exhibits, for the NRTL-SRK-WS case, 10 data points are neglected when the α_{ij} of 0.4567 (Fischer and Gmehling, 1996) is used.

Referring to Table 7-9, only for the NRTL-PR-WS model scenario did all points pass the point consistency test, with an AE % of 0.8822. However, for the NRTL-HOC, NRTL-SRK and NRTL-PR additional data points need to be removed in order for the system to pass the point test. When the modeling was carried out on Aspen Plus® too many data points (>10) were necessary for neglect otherwise the point consistency test would not pass. Thus, for these models, the data points were not removed as only two or three points would be left in the data set.

It is clearly exhibited in this case that fixing the αij parameter does not always work. A much more reliable option is to regress the experimental data for all adjustable parameters.

Table 7-8: Model analysis and consistency test results for the 1-hexene (1) + NMP (2) system at 343.15 K.

Pressure/ kPa	x_1	y_1	NRTL-HOC	NRTL-SRK-WS	NRTL-PR-WS	NRTL-SRK	NRTL-PR	UNIQUAC-HOC
121.44	0.9845	1.0000						
115.72	0.9298	0.9996						
111.47	0.8572	0.9978						
109.42	0.8186	0.9969						
105.76	0.6954	0.9966						
102.50	0.5953	0.9964						
97.52	0.4827	0.9962						
91.69	0.3782	0.9969						
88.54	0.3334	0.9947						
78.61	0.2202	0.9938						
70.38	0.1753	0.9923						
52.96	0.1125	0.9863						
29.89	0.0515	0.9758						
18.94	0.0285	0.7804	*	*	*	*	*	*
Point test results using all data points								
Total data points			14	14	14	14	14	14
ΔP_{AAD}/ kPa			0.0166	0.0173	0.0102	0.0180	0.0169	0.0496
ΔY_{AAD}			0.0165	0.0166	0.0175	0.0164	0.0164	0.0229
Point test results using select data points								
Data points used			13	13	13	13	13	13
ΔP_{AAD}/ kPa			0.0172	0.0180	0.0186	0.0191	0.0174	0.0518
ΔY_{AAD}			0.0013	0.0015	0.0013	0.0013	0.0012	0.0046
AE (%)			0.0298	0.0326	0.0348	0.0367	0.0304	0.27044
Index for Direct test			7	10	10	10	10	6

N.B: a '*' in a certain column indicates that that point was excluded from the final regression analysis

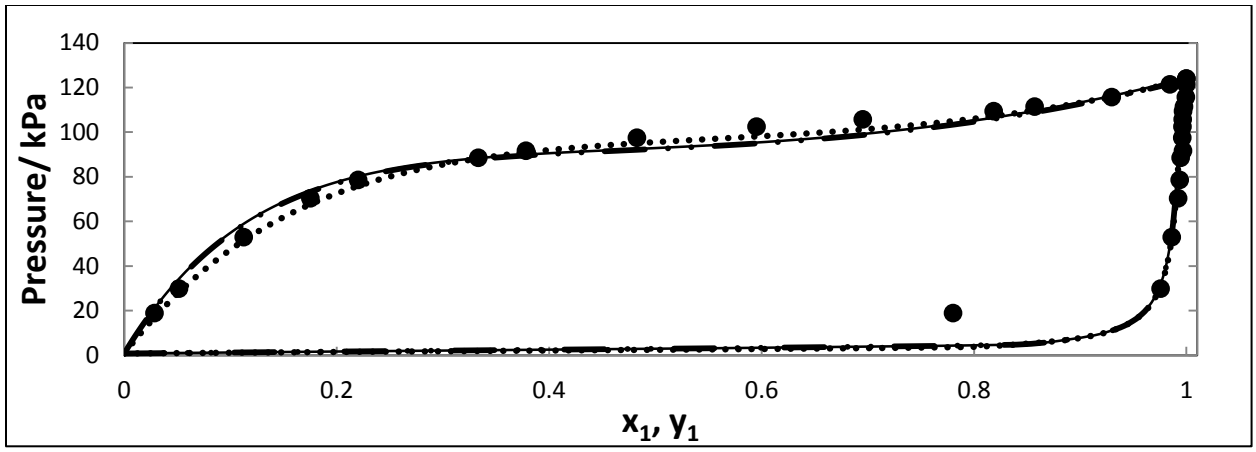

Figure 7-31: *P-x-y* plot for the 1-hexene (1) + NMP (2) system at 343.15 K (varying EoS). ●, experimental data; ▬, NRTL-HOC; ·····, NRTL-PR; —·—·—, NRTL-SRK-WS.

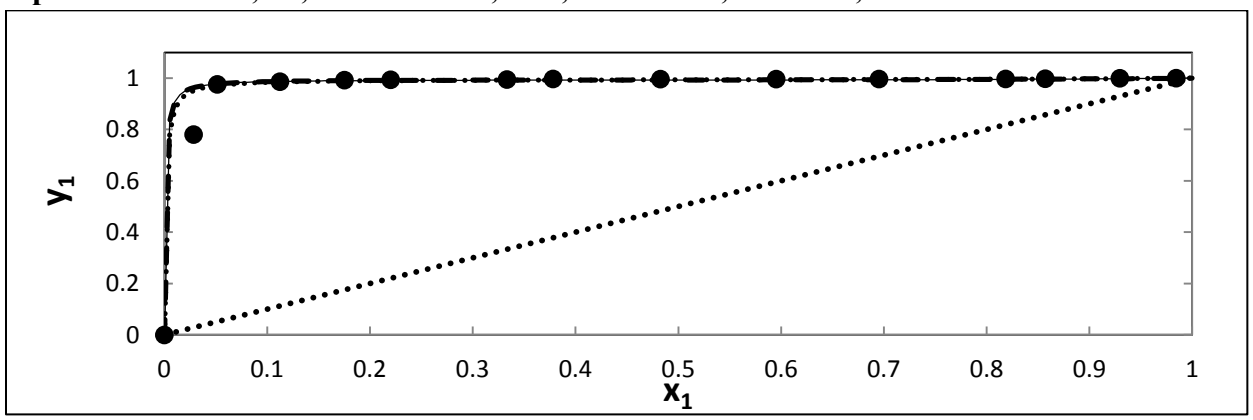

Figure 7-32: *y-x* plot for the 1-hexene (1) + NMP (2) system at 343.15 K (varying EoS).●, experimental data; ▬▬, NRTL-HOC; ·····, NRTL-PR; ▬ ▬ ▬, NRTL-SRK-WS.

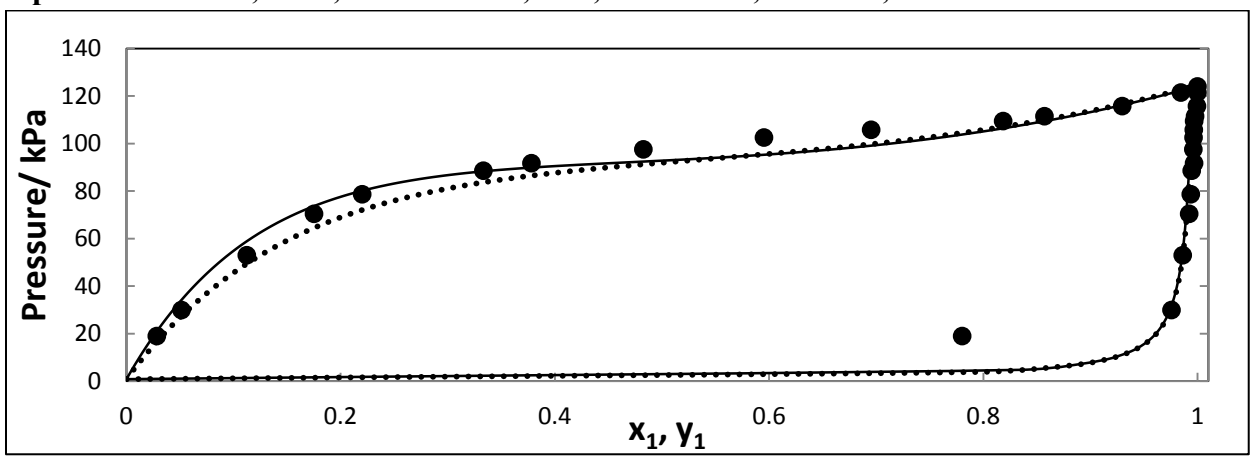

Figure 7-33: *P-x-y* plot for the 1-hexene (1) +NMP (2) system at 343.15 K (varying activity coefficient model). ●, experimental data; ▬, NRTL-HOC; ·····, UNIQUAC-HOC.

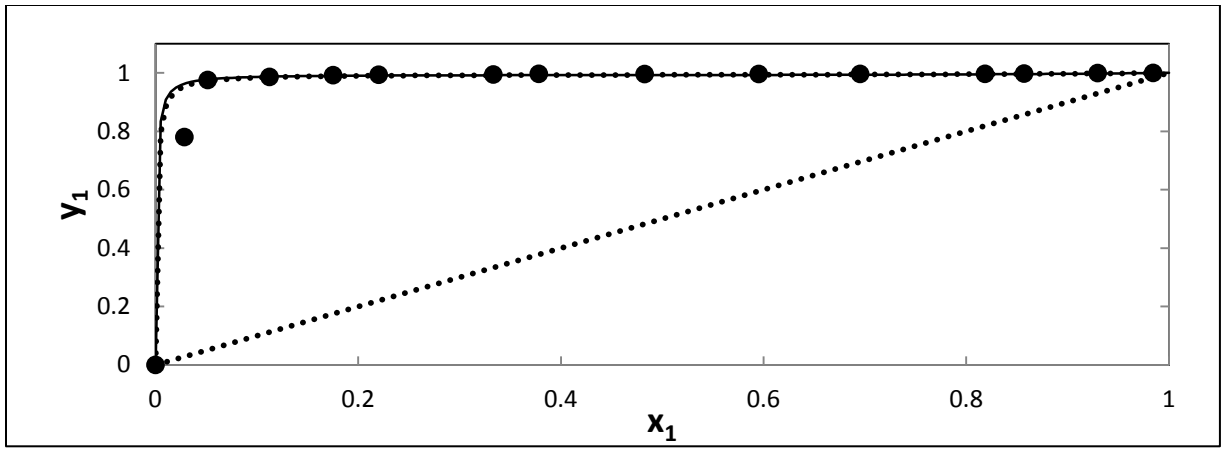

Figure 7-34: *y-x* plot for the 1-hexene (1) +NMP (2) system at 343.15 K (varying activity coefficient model). ●, experimental data; ▬, NRTL-HOC; ·····, UNIQUAC-HOC.

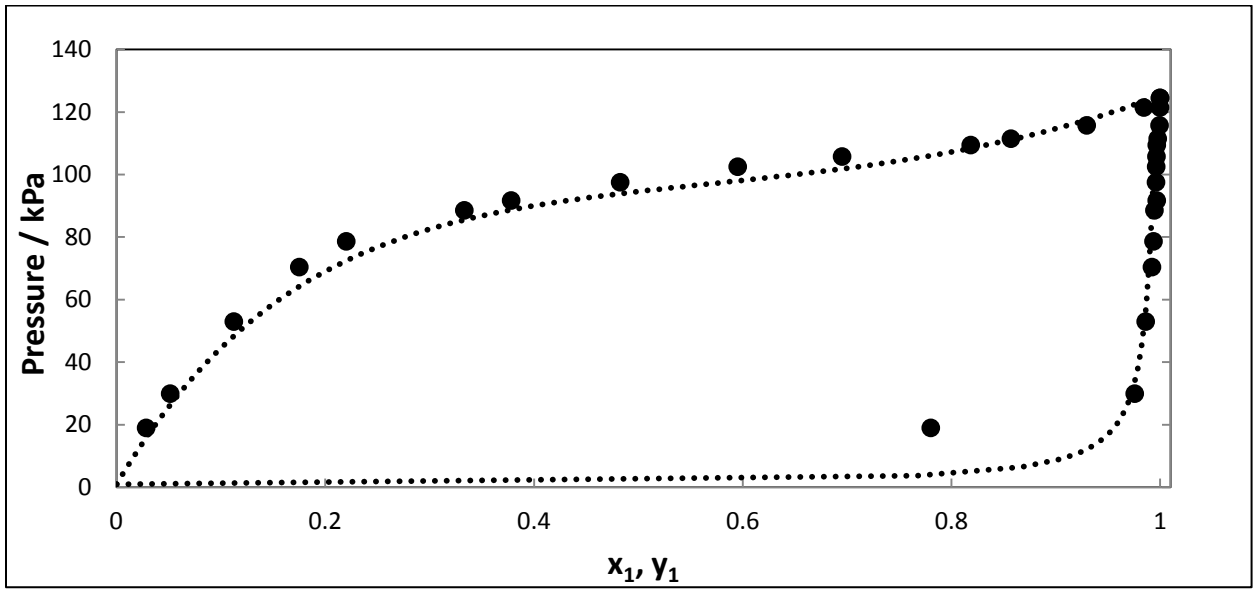

Figure 7-35: *P-x-y* plot for the 1-hexene (1) + NMP (2) system at 343.15 K. ●, P-x_1-y_1 (this work); ·····, P-x_1-y_1 (Aspen Plus ® PSRK model).

Table 7-9: Model analysis and consistency test results for the 1-Hexene (1) + NMP (2) system at 343.15 K using α_{ij} =0.4567 (Fischer and Gmehling, 1996).

Pressure/ kPa	x_1	y_1	NRTL-HOC	NRTL-SRK-WS	NRTL-PR-WS	NRTL-SRK	NRTL-PR
121.44	0.9845	1.0000					
115.72	0.9298	0.9996		*			
111.47	0.8572	0.9978					
109.42	0.8186	0.9969					
105.76	0.6954	0.9966					
102.50	0.5953	0.9964		*			
97.52	0.4827	0.9962		*			
91.69	0.3782	0.9969		*			
88.54	0.3334	0.9947		*			
78.61	0.2202	0.9938		*			
70.38	0.1753	0.9923		*			
52.96	0.1125	0.9863		*			
29.89	0.0515	0.9758		*			
18.94	0.0285	0.7804	*	*		*	
Point test Results using all data points							
Total data points			14	14	14	14	14
ΔP_{AAD} /kPa			3.5605	0.0017	0.0790	65.2292	1.1676
ΔY_{AAD}			0.0209	0.0268	0.0508	0.0212	0.0070
Point test Results using select data points							
Data points used			13	4	14	13	14
ΔP_{AAD} /kPa			4.3586	0.1200	0.0790	69.7362	1.1676
ΔY_{AAD}			0.0029	0.0448	0.0508	0.0027	0.0070
AE(%)			1899.7402	1.6407	0.8822	486227.3	136.3339

N.B: an '*' in a certain column indicates that that point was excluded from the final regression analysis.

7.4.2.3 1-Hexene (1) + NMP (2) at 353.15 K

For the 353.15 K isotherm the last data point (*i.e.*1.02 kPa) is neglected in order to pass the point test for all models. Overall, the NRTL-HOC model provides the best fit to the experimental data.

The results for the direct test with the NRTL-SRK-WS model could not be computed on Aspen Plus®. This is probably due to the fact that the negative excess volumes are quite severe; therefore, proper values of activity cannot be generated using this specific model.

Table 7-10: Model analysis and consistency test results for the 1-hexene (1) + NMP (2) system at 353.15 K.

Pressure/ kPa	x_1	y_1	NRTL -HOC	NRTL-SRK-WS	NRTL-PR-WS	NRTL-SRK	NRTL -PR	UNIQUAC -HOC
157.43	0.9116	0.9982						
147.59	0.8159	0.9978						
141.41	0.7098	0.9977						
137.46	0.6377	0.9974						
134.68	0.5846	0.9961						
132.05	0.5473	0.9926						
129.09	0.4582	0.9968						
115.03	0.3050	0.9949						
100.96	0.2229	0.9945						
83.33	0.1563	0.9909						
50.93	0.0760	0.9813						
1.02	0.0001	0.0075	*	*	*	*	*	*
Point test Results using all data points								
Total data points			13	13	13	13	13	13
ΔP_{AAD}(kPa)			0.0005	0.0072	0.0072	0.0074	0.0074	0.1001
ΔY_{AAD}			0.3301	0.4789	0.4790	0.3599	0.3606	0.6058
Point test Results using select data points								
Data points used			12	12	12	12	12	12
ΔP_{AAD}(kPa)			0.0012	0.0018	0.0021	0.00584	0.0068	0.1003
ΔY_{AAD}			0.0002	0.0013	0.00076	0.0043	0.0039	0.0042
AE (%)			0.0002	0.0005	0.0005	0.0052	0.0061	1.0078
Index for Direct test			10	-	10	10	10	9

N.B: a '*' in a certain column indicates that that point was excluded from the final regression analysis.

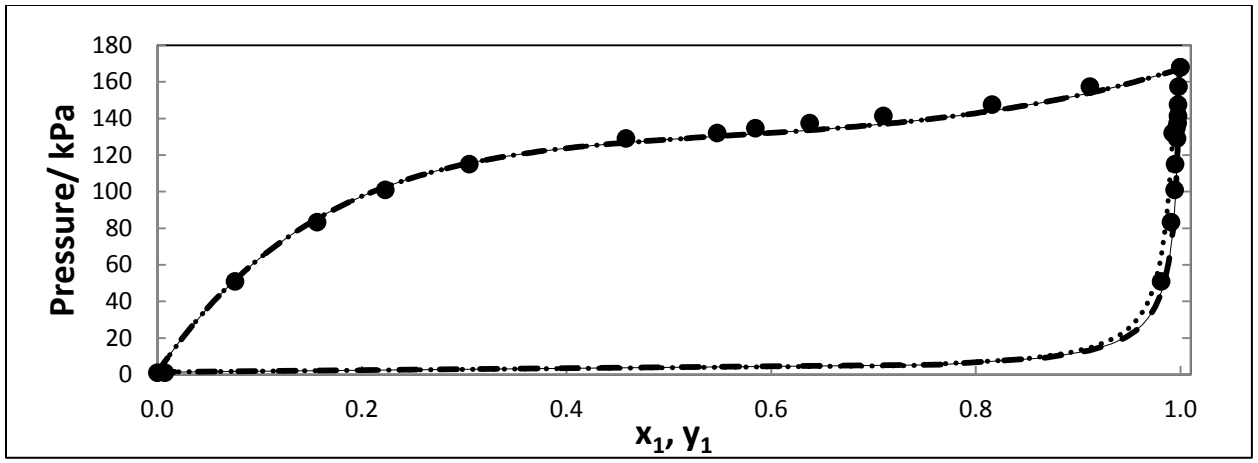

Figure 7-36: *P-x-y* plot for the 1-hexene (1) + NMP (2) system at 353.15 K (varying EoS). ●, experimental data; ——, NRTL-HOC; ·····, NRTL-SRK-WS; — — —, NRTL-PR-WS.

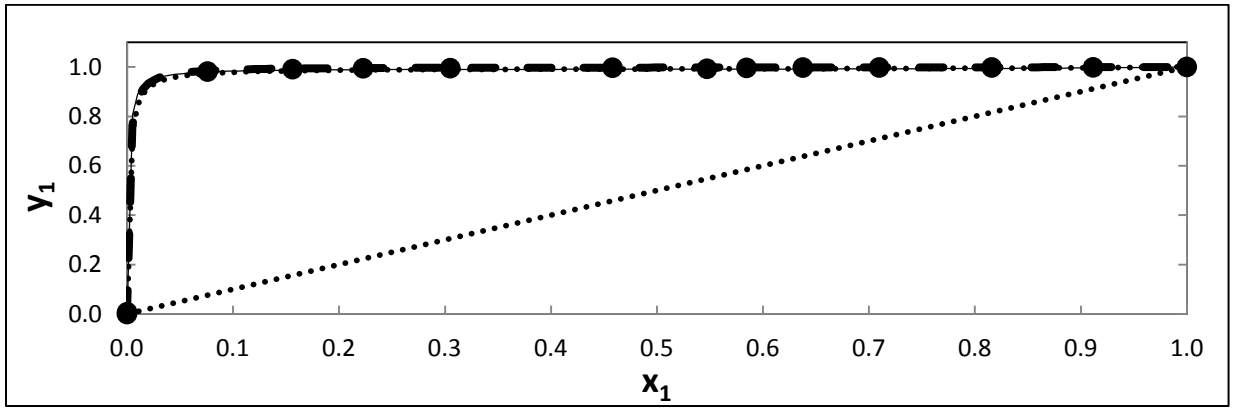

Figure 7-37 *y-x* plot for the 1-hexene (1) + NMP (2) system at 353.15 K (varying EoS). ●, experimental data; —, NRTL-HOC; ·····, NRTL-SRK-WS; — — —, NRTL-PR-WS.

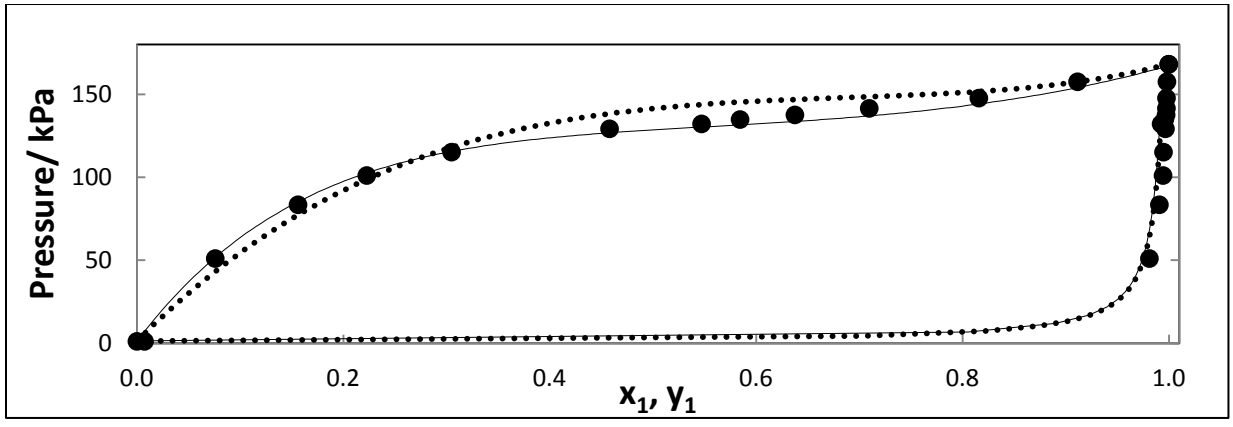

Figure 7-38: *P-x-y* plot for the 1-hexene (1) + NMP (2) system at 353.15 K (varying activity coefficient model). ●, experimental data; —, NRTL-HOC; ·····, UNIQUAC-HOC.

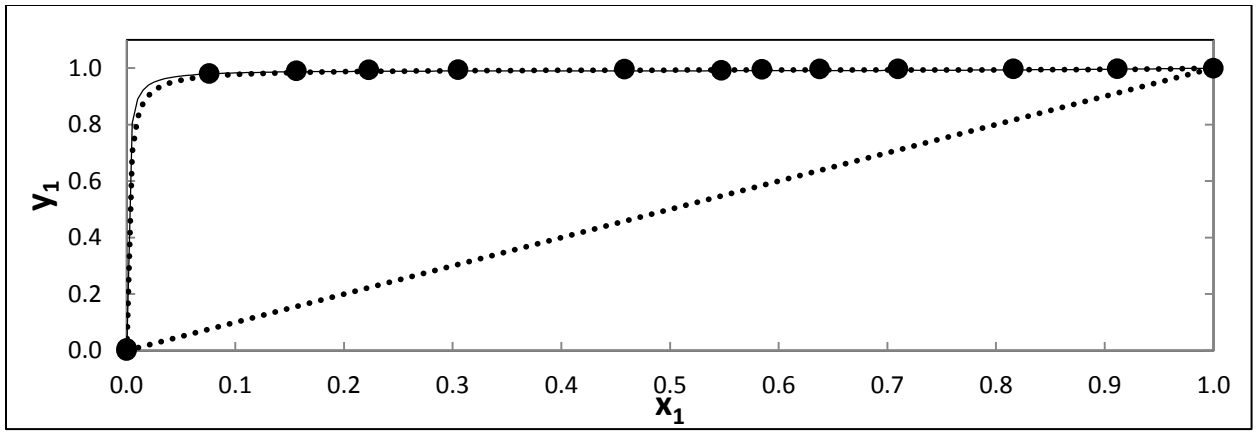

Figure 7-39: *y-x* plot for the 1-hexene (1) + NMP (2) system at 353.15 K (varying activity coefficient model). ●, experimental data; ▬, NRTL-HOC; ·····, UNIQUAC-HOC.

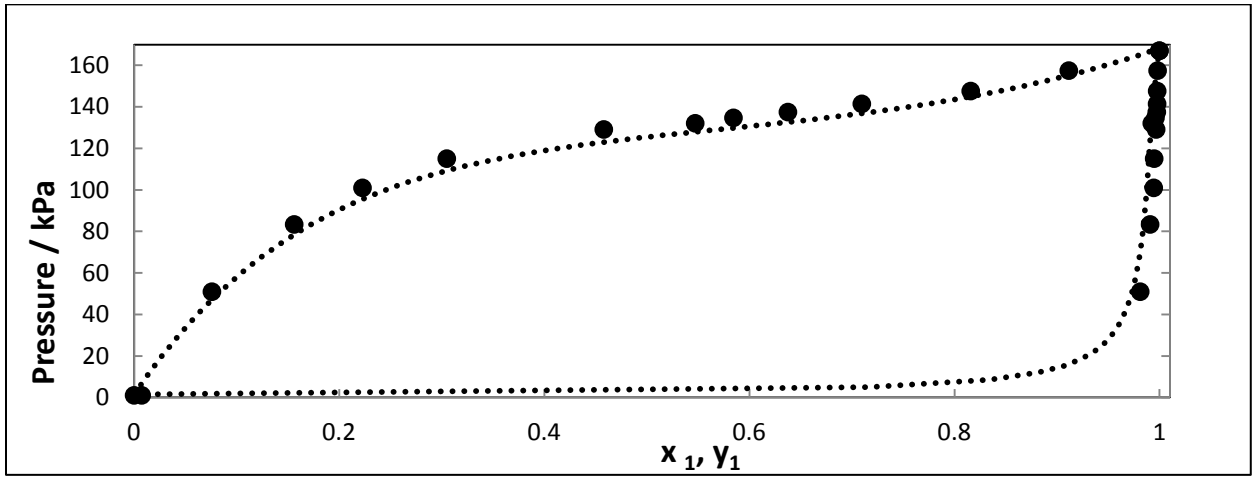

Figure 7-40: *P-x-y* plot for the 1-hexene (1) + NMP (2) system at 353.15 K. ●, P-x_1-y_1 (this work); ·····, P-x_1-y_1 (Aspen Plus ® PSRK model).

7.4.2.4 1-Hexene (1) + NMP (2) at 363.15 K

The NRTL-PR-WS, NRTL-SRK and UNIQUAC-HOC models are neglected for consideration as best fit models as the percent error for ΔP_{AAD} of 2.47, 2.69 and 2.35 %, respectively is significant. The best fit model when varying the EoS is NRTL-HOC. Changing the activity coefficient model, it is obvious the NRTL-HOC model performs better than the UNIQUAC-HOC model.

Table 7-11: Model analysis and consistency test results for the 1-hexene (1) + NMP (2) system at 363.15 K.

Pressure/ kPa	x_1	y_1	NRTL-HOC	NRTL-SRK-WS	NRTL-PR-WS	NRTL-SRK	NRTL-PR	UNIQUAC-HOC
224.00	1.0000	1.0000						
212.16	0.9449	0.9980						
210.07	0.9235	0.9996						
208.83	0.9160	0.9990						
201.73	0.8543	0.9984						
197.99	0.8119	0.9969						
191.81	0.7584	0.9928						
188.27	0.7090	0.9941						
161.62	0.4052	0.9900						
134.24	0.2533	0.9832						
116.07	0.1751	0.9765						
51.57	0.0635	0.9639						
2.06	0.0087	0.0810				*	*	
2.02	0.0001	0.0001	*	*	*	*	*	*
Point test Results using all data points								
Data points used			14	14	14	14	14	14
ΔP_{AAD}/ kPa			0.0200	0.0191	0.0193	0.0213	0.0034	0.0263
ΔY_{AAD}			12.0272	13.5542	0.1634	13.3859	12.4193	45.2239
Point test Results using select data points								
Data points used			13	13	13	12	12	13
ΔP_{AAD}/ kPa			0.0111	0.0169	0.0247	0.0269	0.0075	0.0235
ΔY_{AAD}			0.0062	0.0039	0.0107	0.0036	0.0116	0.0104
Direct test index			9	10	10	10	10	9
AE (%)			0.0162	0.0301	0.0725	0.0737	0.0191	0.0660

N.B: a '*' in a certain column indicates that that point was excluded from the final regression analysis.

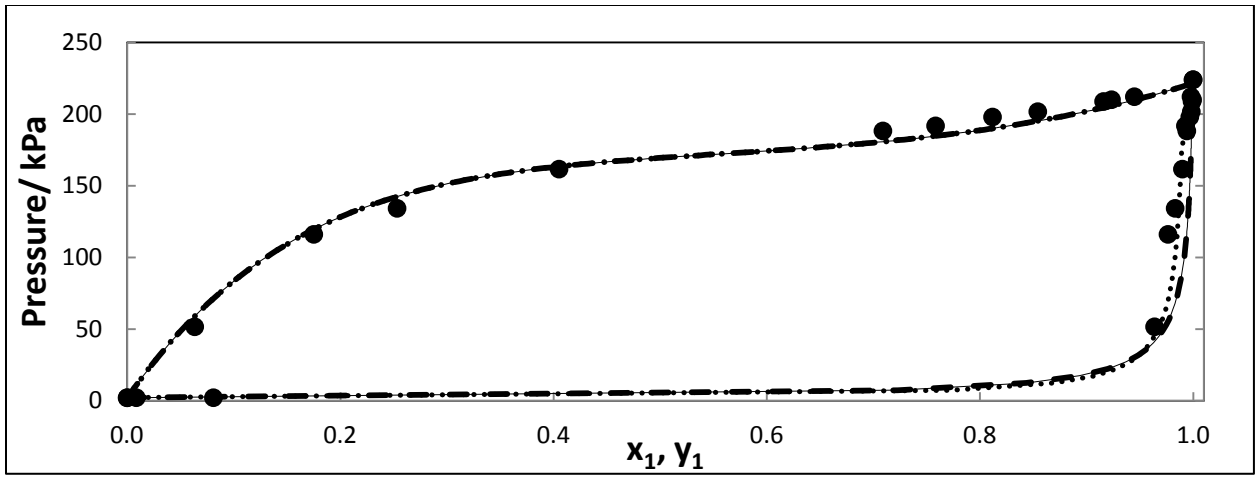

Figure 7-41: *P-x-y* plot for the 1-hexene (1) + NMP (2) system at 363.15 K (varying EoS). ●, experimental data; ——, NRTL-HOC; — — —, NRTL-PR; ••••, NRTL-SRK-WS.

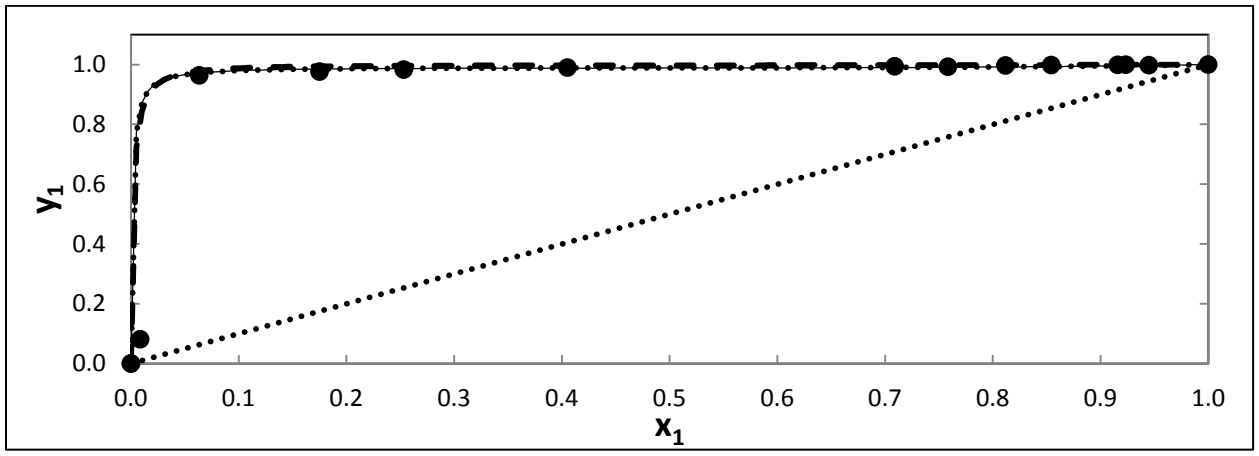

Figure 7-42: *x-y* plot for the 1-hexene (1) + NMP (2) system at 363.15 K (varying EoS).●, experimental data; ——, NRTL-HOC; ·····, NRTL-SRK-WS; — — —, NRTL-PR.

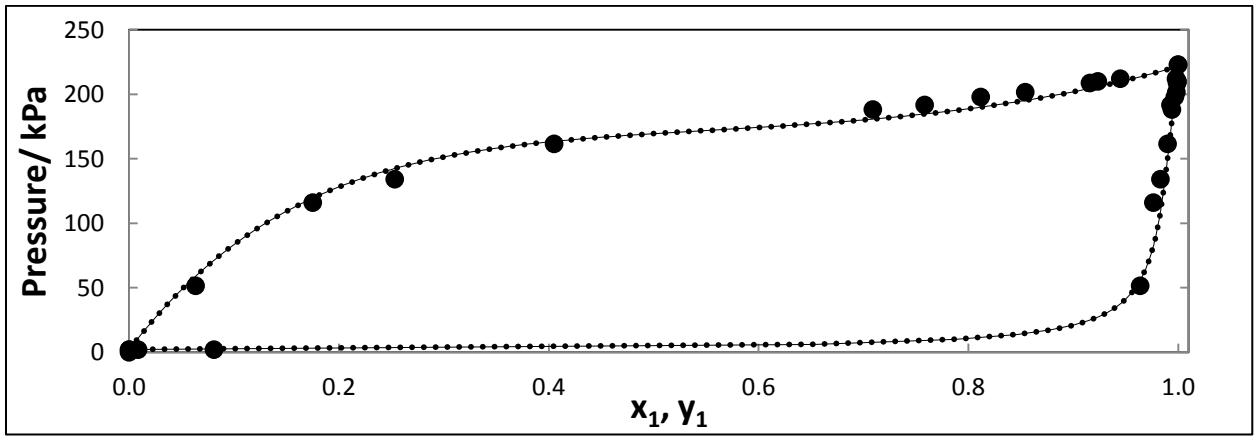

Figure 7-43: *P-x-y* plot for the 1-hexene (1) + NMP (2) system at 363.15 K (varying activity coefficient model). ●, experimental data; ——, NRTL-HOC; ·····, UNIQUAC-HOC.

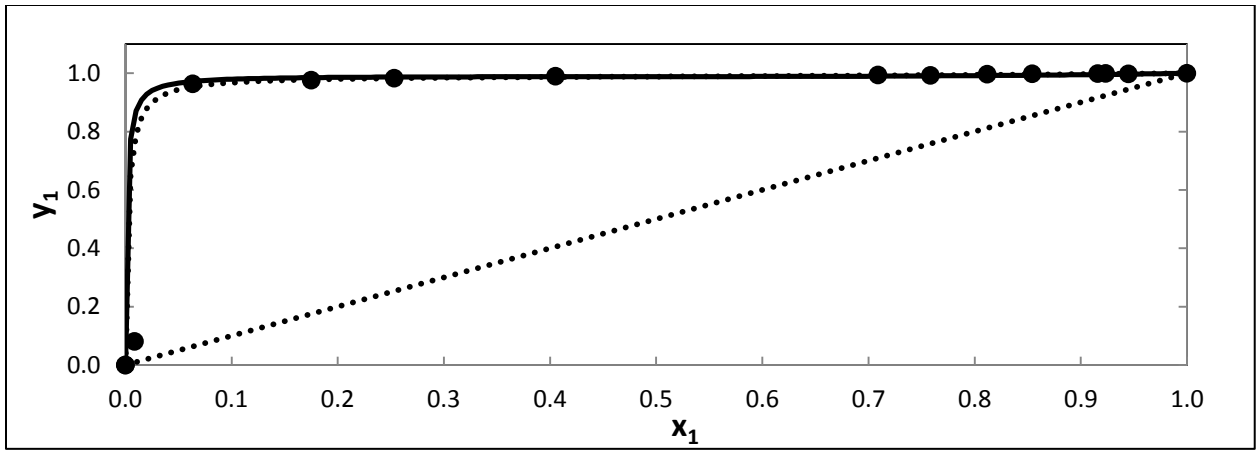

Figure 7-44 *y-x* plot for the 1-hexene (1) + NMP (2) system at 363.15 K (varying activity coefficient model). ●, experimental data; ▬, NRTL-HOC; ·····, UNIQUAC-HOC.

Referring to the plot below, the P-x_1 data of Fischer and Gmehling (1996), the P-x_1-y_1 data of Hirawan (2007), and the measured experimental data on the moderate pressure VLE still compare very well with each other. There is a slight deviation between the Aspen® PSRK model data and the measured data for the system being investigated. The true liquid compositions (x) measured are lower than those predicted by Aspen Plus®. However, it is concluded that the PSRK model is incorrect as the experimental data correlates excellently with that of Fischer and Gmehling (1996) and Hirawan (2007).

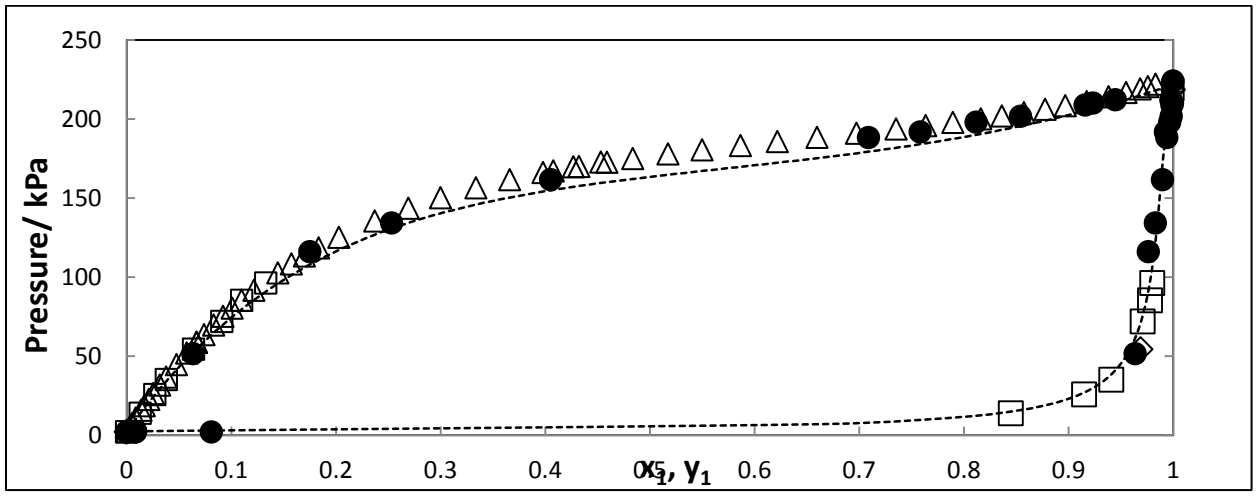

Figure 7-45: *P-x-y* plot for the 1-hexene (1) + NMP (2) System at 363.15 K. ●, P-x_1-y_1 (this work); ·····, P-x_1-y_1 (Aspen Plus ® PSRK model);Δ, P-x (Fischer and Gmehling, 1996); □, P-x_1-y_1 (Hirawan, 2007).

7.4.3 1-Hexene (1) + n-Hexane (2)

Three isotherms were measured for this system at 343.15, 363.15 and 373.15 K. The upper miscibility limit of n-hexane is 328.15 K, thus, all measurements for systems containing this component had to be above 328.15 K. In addition, this system has not been measured at the aforementioned temperatures in literature; therefore, all these measurements constitute new data. The model combinations used to model this system were the NRTL-SRK-WS, NRTL-PR-WS and NRTL-Ideal models.

The NRTL activity coefficient model was retained as the only activity coefficient model, and the EoS models were varied between PR-WS, SRK-WS and the ideal gas model. Analyzing the results from the previous two systems modeled, it is clear that varying the activity coefficient model makes no appreciable difference overall. Thus, the activity coefficient model was not varied for this system.

It is observed that the 1-hexene + n-hexane system exhibits very small positive deviations from ideality, however, due to the minute scale of the deviations, they may be considered negligible. It is postulated that this system is very closely ideal as their activity coefficients approach unity. In addition, this system displays no azeotrope and this is confirmed by the vapour pressure ratios of 1-hexene (1) to n-hexane (2), ($\frac{P_1^{sat}}{P_2^{sat}}$), which, even though are small, is still too large for a system where an azeotrope would exist (Fischer and Gmehling, 1996).

The system 1-hexene + n-hexane has previously been measured by Moodley (2009) at 328.15, 353.15 and 378.15K. It was decided that the system 1-hexene + n-hexane be re-measured at different temperatures in an attempt to obtain more thermodynamically consistent data.

The Aspen Plus® predictions were initially completely different from the experimental data measured in this work for 1-hexene + n-hexane at 343.15, 363.15 and 373.15 K. The PSRK model, in all instances, predicted isotherms which had a much higher pressure than the experimental data for the same vapour and liquid compositions. A possible reason for this

problem is the Antoine constants Aspen is using from its database. Now, there is by no means any implication that the Aspen Plus® version of these parameters in incorrect. The problem with using Antoine parameters from an unknown source is that the temperature range, in which the measurements for those parameters were undertaken, cannot be verified. As such the Antoine parameters in question may not necessarily be able to generate data in good agreement with the user‟s data.

Solutions to the problem would entail either entering one‟s own Antoine parameters in the appropriate sections in the Aspen Plus® interface, or to regress measured experimental vapour pressure data and use the subsequent Antoine parameters when undertaking predictions or modeling data. The latter suggestion was pursued, and referring to the sections that follow, one may observe the results. At 343.15 K, the prediction is in excellent agreement with experimental data, however, for the 363.15 and 373.15 K isotherms, the PSRK model deviated slightly from the experimental data; however, this plot is still significantly better than the original prediction using the Antoine parameters stored in the Aspen Plus® database.

A major problem encountered with this system was attempting to achieve separation of the components on the GC for composition analysis. A flame ionization detector, on the GC, was employed, in conjunction with a capillary column, which is approximately 30 m long. This length enables sufficient time for the components to pass through the column. In addition, the carrier gas was changed from helium to nitrogen. This further slows down the rate at which the components pass through the column and increases the elution time between 1-hexene and n-hexane.

For plots showing the results of the point and direct test for this system, the reader is referred to Appendix E.3.

7.4.3.1 1-Hexene (1) + n-Hexane (2) at 343.15 K

Since this system is highly ideal in nature and there is no existence of cross- or self-association, the direct test may be used as a primary means for selecting the best fit model. For this isotherm, the RMSD for the direct test of the three models involved is very similar (no significant deviation exists; all have an index of 4. Therefore, it falls upon the AE % to decide the most appropriate model. The best fit model is found to be the NRTL-PR-WS.

In addition, all models show an acceptable level of scatter about the x-axis for both the Δy_{AAD} plot as well as the plot of the scatter of the logarithm of the activity coefficients (direct test). The direct test for the tested models exhibited an index of 4 for the systems involved, which indicates data with a high level of consistency.

Table 7-12: Model analysis and consistency test results for the 1-hexene (1) + n-hexane (2) system at 343.15 K.

Pressure/ kPa	x_1	y_1	NRTL-SRK-WS	NRTL-PR-WS	NRTL-Ideal
105.68	0.0000	0.0000			
105.78	0.0067	0.0079			
106.39	0.0260	0.0260	*	*	*
107.29	0.0811	0.0874			
108.04	0.1348	0.1558			
110.43	0.2510	0.2859			
113.97	0.4455	0.4797			
113.30	0.4016	0.4362			
116.44	0.5726	0.6082			
118.51	0.6694	0.7048			
120.72	0.8023	0.8214			
122.78	0.9179	0.9243			
123.91	0.9935	0.9957			
124.06	1.0000	1.0000			
Total data points			14	14	14
ΔP_{AAD} (kPa)			0.0022	0.0022	0.0002
ΔY_{AAD}			0.0175	0.0180	0.0237
Data points used			13	13	13
ΔP_{AAD} (kPa)			0.0018	0.0006	0.0002
ΔY_{AAD}			0.0090	0.0052	0.0116
AE (%)			0.00845	0.0028	0.0135
RMSD δ Ln (γ_1/γ_2)			0.0874	0.0843	0.0857
Index			4	4	4

N.B: a '*' in a certain column indicates that that point was excluded from the final regression analysis.

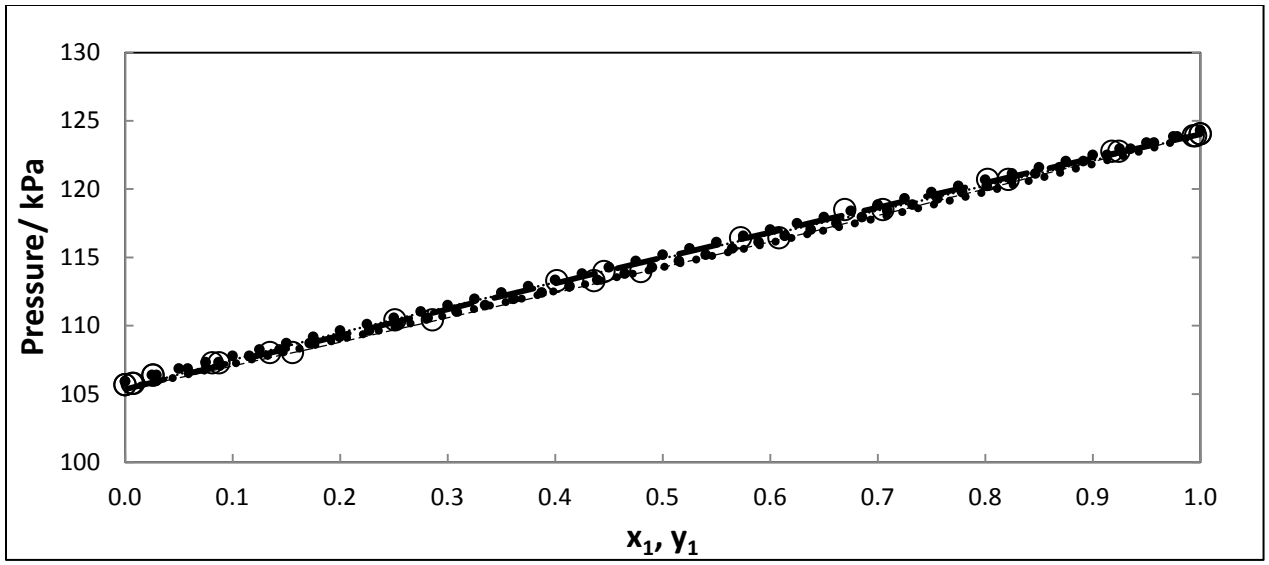

Figure 7-46: *P-x-y* plot for the 1-hexene (1) + n-hexane (2) system at 343.15 K (varying EoS). ○, experimental data; . . . . . , NRTL-PR-WS; — — —, NRTL-SRK-WS; •, NRTL-Ideal.

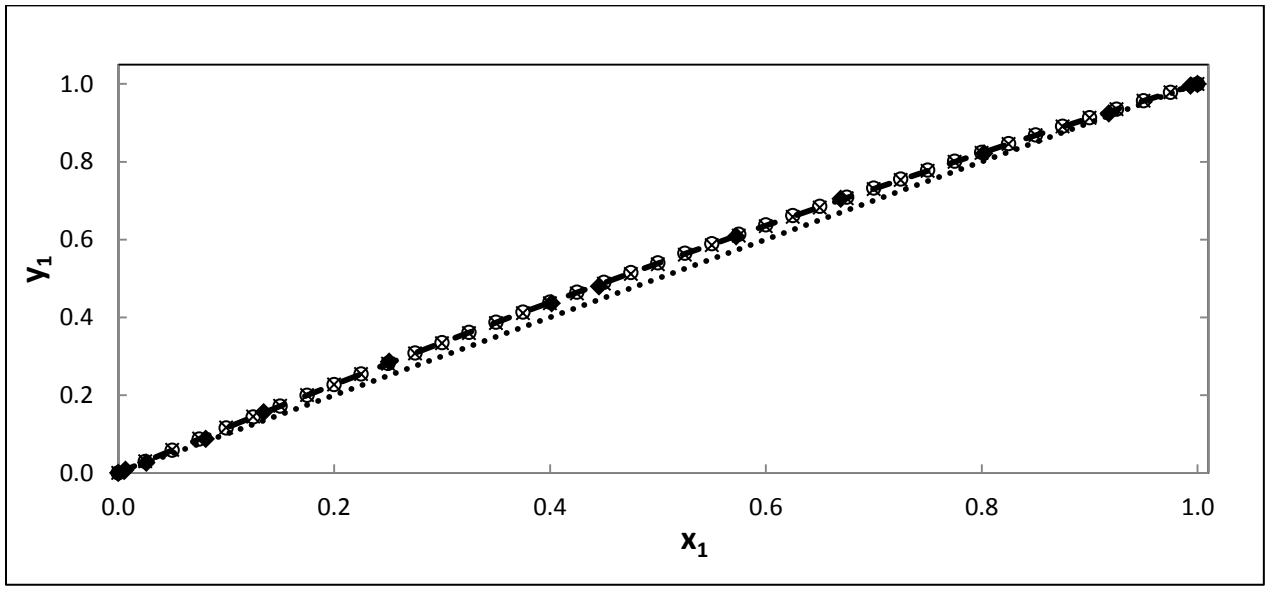

Figure 7-47 *y-x* plot for the 1-hexene (1) + n-hexane (2) system at 343.15 K (varying EoS). ●, experimental data; x, NRTL-PR-WS; — — —, NRTL-SRK-WS; ○, NRTL-Ideal.

As may be observed from the plot below (Figure 7-48), there is excellent agreement between the Aspen Plus® PSRK model data and the measured experimental data.

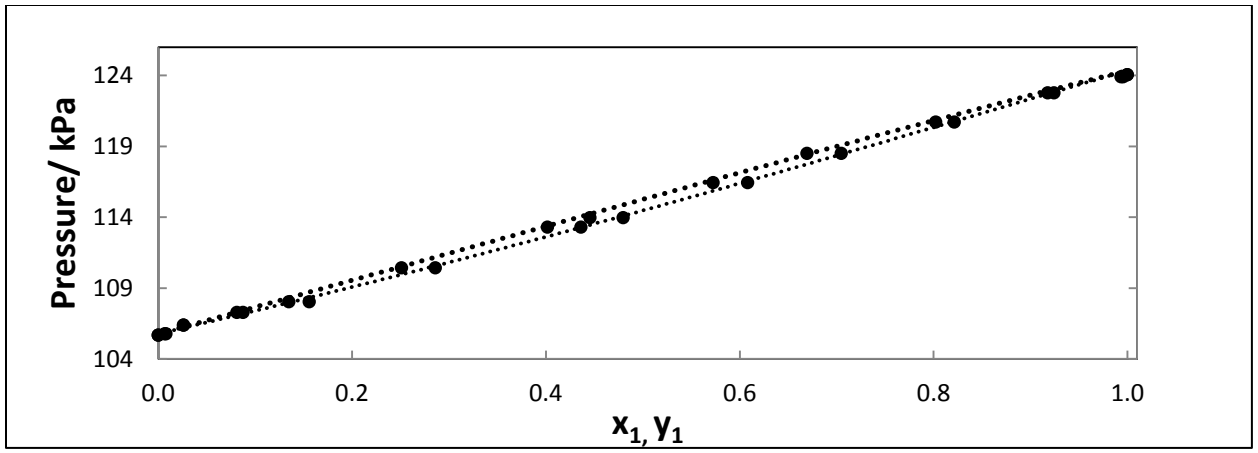

Figure 7-48: P-x-y plot for the 1-hexene (1) + n-hexane (2) system at 343.15 K. ●, P-x_1-y_1 (this work); ·····, P-x_1-y_1 (Aspen Plus ® PSRK model).

7.4.3.2 1-Hexene (1) + n-Hexane (2) at 363.15 K

The best fit model is the NRTL-SRK-WS model. The NRTL-SRK-WS model is, in this instance, superior to the NRTL-PR-WS and NRTL-Ideal gas model but only marginally. The point-to-point test for the vapour residual and $\delta \ln(\gamma_1 / \gamma_2)$ scatter evenly about the x-axis (Appendix E.3).

Table 7-13: Model analysis and consistency test results for the 1-hexene (1) + n-hexane (2) system at 363.15 K.

Pressure/ kPa	x_1	y_1	NRTL-SRK-WS	NRTL-PR-WS	NRTL-Ideal
189.09	0.0000	0.0000			
189.34	0.0243	0.0250			*
189.51	0.0348	0.0354			*
189.89	0.0698	0.0725			
190.93	0.1526	0.1578			*
193.38	0.2606	0.2849			
193.78	0.2716	0.3037			
197.13	0.4103	0.4374			
198.7	0.4679	0.4953			
201.57	0.5601	0.5966			
204.61	0.6426	0.6948			
210.01	0.7833	0.8191			
214.92	0.9087	0.9243			
217.52	0.9745	0.9822			
218.64	1.0000	1.0000			
Total data points			15	15	15
ΔP_{AAD} (kPa)			0.0011	0.0012	0.0005
ΔY_{AAD}			0.0115	0.0112	0.0182
Data points used			15	15	12
ΔP_{AAD} (kPa)			0.0011	0.0012	0.0006
ΔY_{AAD}			0.0115	0.0112	0.0111
AE (%)			0.0133	0.0128	0.0124
RMSD δ Ln (γ_1/γ_2)			0.0573	0.0589	0.0552
Index			3	3	3

N.B: a '*' in a certain column indicates that that point was excluded from the final regression analysis.

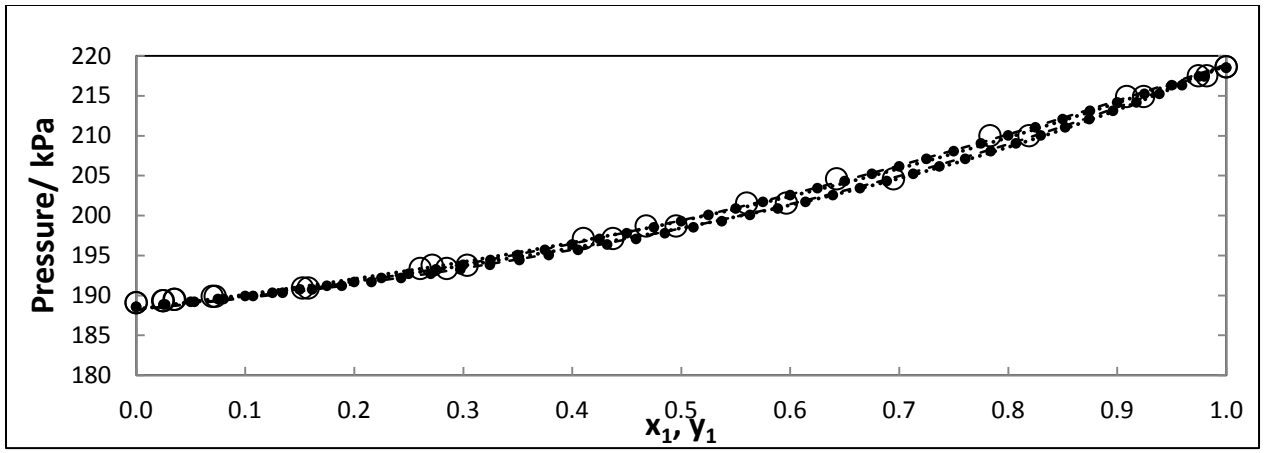

Figure 7-49: *P-x-y* plot for the 1-hexene (1) + n-hexane (2) system at 363.15 K (varying EoS). ○, experimental data; . . . . . , NRTL-PR-WS; — — — , NRTL-SRK-WS; •, NRTL-Ideal.

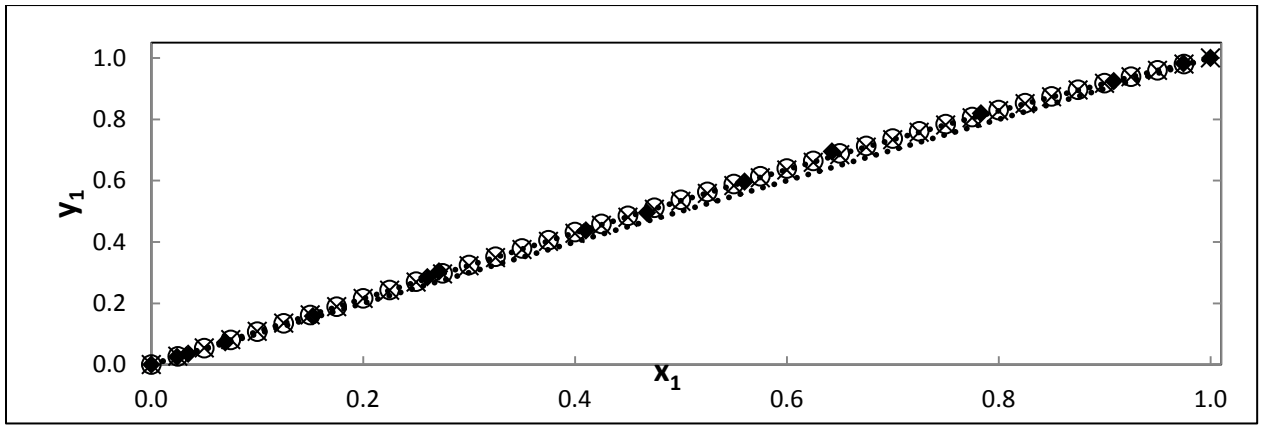

Figure 7-50: *y-x* plot for the 1-hexene (1) + n-hexane (2) system at 363.15 K (varying EoS). •, experimental data; x, NRTL-PR-WS; . . . . . , NRTL-SRK-WS; ○, NRTL-Ideal.

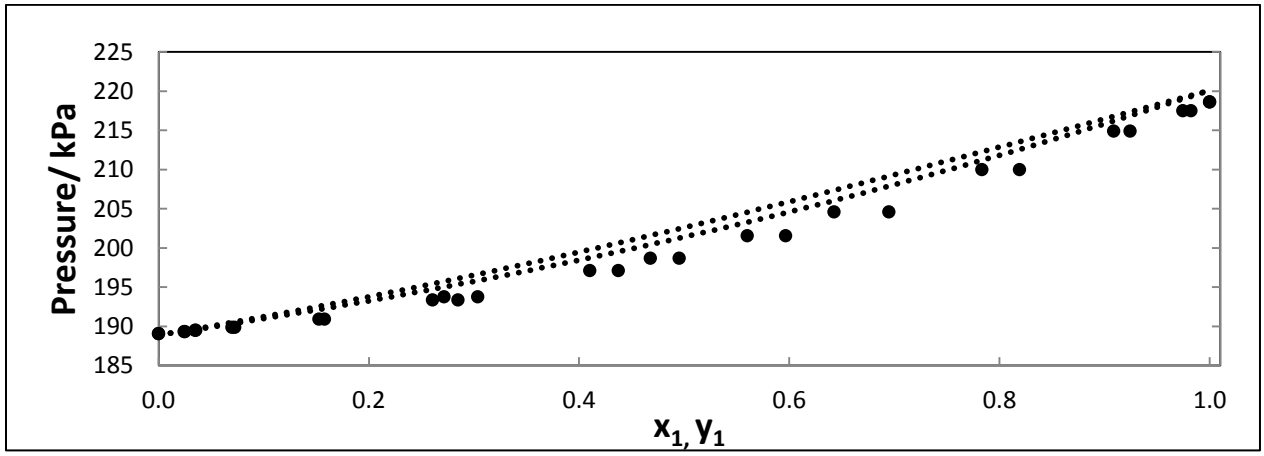

Figure 7-51: *P-x-y* plot for the 1-hexene (1) + n-hexane (2) system at 363.15 K; •, P-x_1-y_1 (this work); ·····, P-x_1-y_1 (Aspen Plus ® PSRK model).

7.4.3.3 1-Hexene (1) + n-Hexane (2) at 373.15 K

At this temperature all the data points are included in the final regression process. The NRTL-Ideal model has the lowest ΔP_{AAD} and the difference in the Δy_{AAD} is very small, thus they all have approximately the same average absolute deviation in vapour composition. The direct test indicates that the NRTL-Ideal model has the lowest errors; however, even in this regard the values for the RMSD for the direct tests are very similar. However, based on the facts, the NRTL-Ideal model is best for this data set.

Table 7-14: Model analysis and consistency test results for the 1-hexene (1) + n-hexane (2) system at 373.15 K

Pressure/ kPa	x_1	y_1	NRTL-SRK-WS	NRTL-PR-WS	NRTL-Ideal
245.01	0.0000	0.0000			
245.11	0.0136	0.0148			
246.08	0.0815	0.0851			
248.09	0.1713	0.1882			
252.18	0.3222	0.3542			
256.11	0.4309	0.4649			
261.92	0.5638	0.6014			
264.82	0.6334	0.6775			
270.9	0.7557	0.7873			
272.99	0.7974	0.8234			
276.96	0.8816	0.8982			
280.00	0.9419	0.9558			
281.68	0.9786	0.9786			
282.90	1.0000	1.0000			
Data points used			14	14	14
ΔP_{AAD} (kPa)			0.0012	0.0010	0.0003
ΔY_{AAD}			0.0090	0.0087	0.0010
AE (%)			0.0082	0.0077	0.0089
RMSD δ Ln (γ_1/γ_2)			0.0666	0.06448	0.0596
Index			3	3	3

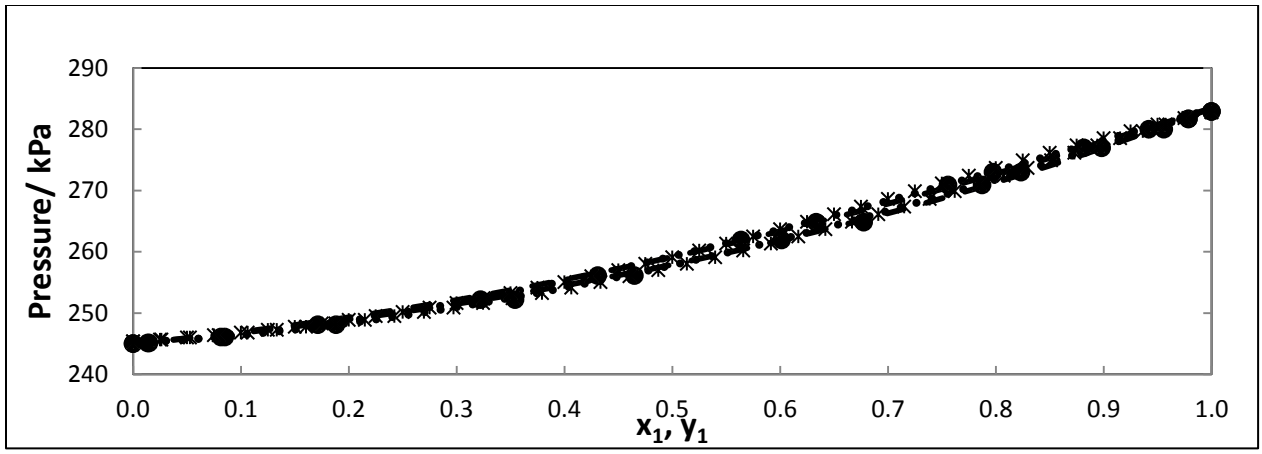

Figure 7-52*: P-x-y* plot for the 1-hexene (1) + n-hexane (2) system at 373.15 K (varying EoS). ●, experimental data; . . . . . , NRTL-PR-WS; — — —, NRTL-SRK-WS; ✕, NRTL-Ideal.

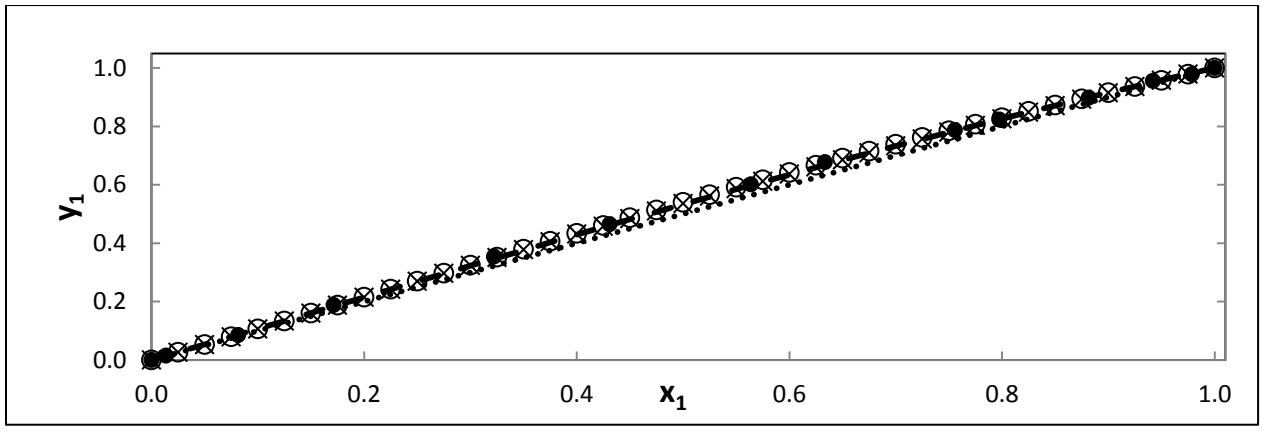

Figure 7-53: *y-x* plot for the 1-hexene (1) + n-hexane (2) system at 373.15 K (varying EoS). ●, experimental data; ✕, NRTL-PR-WS; — — —, NRTL-SRK-WS; ○, NRTL-Ideal.

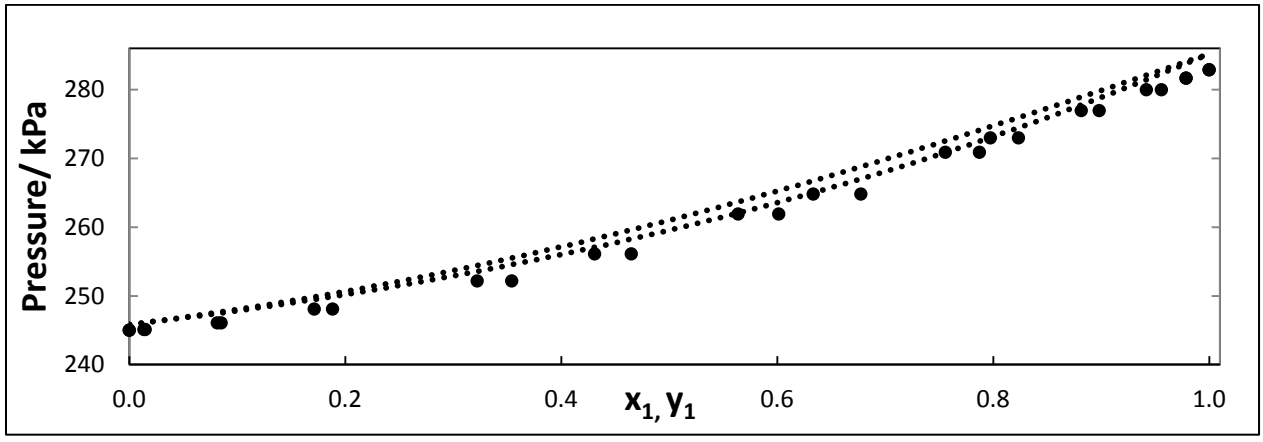

Figure 7-54: *P-x-y* plot for the 1-hexene (1) + n-hexane (2) System at 373.15 K. ●, P-x_1-y_1 (this work); ·····, P-x_1-y_1 (Aspen Plus ® PSRK model).

7.4.4 Ternary System: 1-Hexene (1) + n-Hexane (2) + NMP (3) at 363.15 K

The ternary system was measured at 363.15 K. This isotherm was selected based upon the fact that it is a temperature at which industrial operations are conducted. In addition, there is a wealth of reliable information available on the 1-hexene + NMP and n-hexane + NMP systems at this temperature by Fischer and Gmehling (1996). Thus, confirmation of key measurements for the constituent binaries may be secured by referring to the literature in a comparative capacity.

After the 1-hexene + NMP, n-hexane + NMP and 1-hexene + n-hexane systems had been measured, a common model, which fits all systems best, was employed to predict the resultant ternary system (1-hexene+n-hexane+NMP) using binary interaction parameters obtained from modeling the constituent systems. Since the NRTL-HOC model dominated the systems 1-hexene + NMP and n-hexane + NMP as a best fit model, this model was therefore the model of choice which was used for the 1-hexene + n-hexane system to simultaneously regress all the isothermal data sets of this system to obtain a single set of binary interaction parameters.

The binary interaction parameters were determined using Aspen Plus® software. The intention was to simultaneously regress all isothermal data in each of the three binary systems on Aspen Plus® and thereafter use the single set of binary interaction parameters obtained for each system to predict the ternary system behaviour using a flash calculation on Aspen Plus®. However, the utilization of the binary interaction parameters obtained from the modeling can only be used to predict binary and not ternary systems at different temperatures, using this software package. In addition, Aspen Plus® is only able to predict residue curves and not ternary system behaviour. Therefore, the only other solution was to enlist the use of Dortmund Data Bank (DDB, 2011).

However, when the DDB program was used the NRTL-Ideal model was implemented instead. This resulted as a consequence of the HOC virial EoS not being available for use. The measurements for the ternary system were executed in the NMP dilute region. Thus, the self-associative effects of the NMP molecule will not substantially influence the thermodynamic data obtained. The data predicted was then pitted in a comparative analysis against the experimentally measured data points for the same ternary at the temperature of interest.

Measuring VLE data is time-consuming and necessitates the use of expensive equipment that is sometimes unavailable. Systems of interest, industrially, such as olefins and paraffins are very difficult to separate. Thus, measuring a ternary system with these components is highly difficult. The ability to accurately predict ternary system behaviour would, subsequently, lead to greater convenience.

The results declared below were obtained by simultaneously regressing all isothermal data sets for each system on Aspen Plus®. As stipulated previously, the NRTL-HOC model was selected to model the behavior of the systems required to predict the phase behavior of the ternary system. These results are summarized in the table below:

Table 7-15: Summary of binary interaction parameters obtained from Aspen Plus® using the NRTL-HOC model to simultaneously regress all the isothermal data for each system.

	1-hexene (1) + NMP (2)	n-hexane (1) + NMP (2)	1-hexene (1) + n-hexane (2)
a_{12}	2	0.262	98
a_{21}	-0.384	0.173	-100
b_{12}/ K	-100	139	18146
b_{21}/ K	82	247	-18260
c_{12}	0.057	-0.988	0

Table 7-16: Summary of the ternary prediction for the vapour composition, using the NRTL-IDEAL model on DDB (2011) (predictive option) for the system 1-hexene (1) + n-hexane (2) + NMP (3).

y_1	y_2	y_3	$y_{1,\text{predicted}}$	$y_{2,\text{predicted}}$	$y_{3,\text{predicted}}$	$\Delta y_1\%$	$\Delta y_2\%$	$\Delta y_3\%$	α_{13}	α_{23}
0.7012	0.2911	0.0077	0.6927	0.2997	0.0076	1.216	2.964	1.311	104.84	92.28
0.7586	0.2353	0.0060	0.7511	0.2426	0.0063	0.990	3.080	4.348	103.91	96.02
0.5439	0.4422	0.0139	0.5396	0.4462	0.0142	0.792	0.899	2.385	99.663	90.85
0.5282	0.4550	0.0168	0.5391	0.4433	0.0175	2.057	2.563	4.114	102.56	92.04
0.5323	0.4131	0.0547	0.5471	0.3958	0.0571	2.787	4.177	4.419	97.03	87.60
0.5311	0.3777	0.0912	0.5342	0.3718	0.0939	0.580	1.568	3.010	104.58	94.36
0.3006	0.6703	0.0291	0.3123	0.6582	0.0294	3.897	1.810	1.092	105.54	89.38
0.2279	0.7511	0.0209	0.2350	0.7434	0.0216	3.093	1.029	3.252	107.64	89.07
0.0599	0.9188	0.0212	0.0626	0.9163	0.0210	4.433	0.274	1.108	102.77	84.93

The correlation between the experimental data and the predicted model is good. The maximum percentage deviation between any single experimental point and its corresponding predicted value is 5%. Since the vapour phase composition of NMP in very small (NMP dilute region), and association effects the vapour phase, we may assume that in this dilute region of NMP, the use of the ideal model shall not significantly compromise the results obtained. This system is more concentrated in 1-hexene and n-hexane, consequently the ideal gas model is sufficient to account for the vapour phase of all components and the NRTL model accounts for inequalities in the liquid phase.

7.5 Analysis of Results Produced by the Different Models

Of the myriad activity coefficient models available at the user‟s discretion, the most commonly used are the Wilson (1964), NRTL (1968) and UNIQUAC (1975).

The Wilson equation has many positive features. Some of which are its extension to be used in multi-component systems (in addition to binary systems), as well as the flexibility in its ability to treat highly non-ideal systems, as well as those with G^E plots which exhibit a high degree of asymmetry (Reid *et al*., 1987). However, a stark disadvantage of this model is that the parameters of the Wilson equation are limited in their dependence upon temperature. For scenarios where $\gamma_i < 1$, Walas (1985) states that numerous difficulties are encountered with the use of this model. These entail the result of multiple roots. Negative values of parameters are not allowed for the depiction of the activity coefficients across the composition range. The greatest disadvantage of this model is the inability to represent systems with limited miscibility. Thus, for these reasons the Wilson model was not used in the regression of experimental data.

Only two activity coefficient models were used for representing the liquid phase inequalities. They are the: NRTL and UNIQUAC activity coefficient models. These models were selected on the basis of using renowned literature sources as a reference point as well considering the types of systems to which these models are most applicable.

After dissecting the work of Hirawan (2007) for the system 1-hexene + NMP, the NRTL Gibbs excess energy model showed the best overall performance when compared to the Wilson, van Laar and UNIQUAC models also used in the same work. In addition, from the work of Fischer and Gmehling (1996) the NRTL model was used to fit the equilibrium data measured for the systems: 1-hexene + NMP and n-hexane + NMP. Thus, this was an important factor that contributed to the NRTL model being selected for use in this work.

After the modeling had been conducted, surprisingly the NRTL activity coefficient model outperformed the UNIQUAC model, albeit on a marginal scale. This clearly shows how simpler models can function just as well as the more complex models if the model is well suited to the system under consideration. A conclusion drawn from this work is that since the adjustable parameter, α_{ij} is specific only to the NRTL model, this factor also contributed to achieving a better fit of the experimental data to the calculated data.

Further, it should be noted that the NRTL activity coefficient model is applicable to, and in many instances preferred for the representation of VLE as well as liquid-liquid equilibrium (LLE) data. This model is better suited to the representation of aqueous systems than most other models intended for the same purpose. In addition, it is capable of modeling strongly non-ideal systems accurately, as well as precisely representing polar and non-polar systems equally well.

Even though the UNIQUAC model did not perform better than the NRTL model overall, it must be stated that the NRTL model outperformed the UNIQUAC model on a marginal scale only. Thus, the merits of the latter model should not be overlooked.

One of the reasons it is expected that the UNIQUAC activity coefficient model performed well is that it is capable of representing highly non-ideal, as well as partially miscible and completely miscible systems. It is advocated for use by leading researchers as this model takes into consideration the shape and size of molecules, as well as the intermolecular interaction energies (Malanowski and Anderko, 1992).

Further, since the UNIQUAC model has such a wide range of applicability to a vast array of components such as non-electrolyte mixtures constituting polar and non-polar components, e.g. alcohols, ketones, water, hydrocarbons, nitriles, aldehydes, mixtures of partial miscibility, organic acids and water (Naidoo, 2004), it is usually expected that the UNIQUAC model will render accurate results.

The use of the mixing rule Wong-Sandler in conjunction with the NRTL and UNIQUAC models in all instances rendered better results than if the activity coefficient models were used with the EoS only (combined method). This is anticipated as the Wong-Sandler mixing rule was developed for the representation of complex as well as simple systems which constitute non-polar, polar and associating species.

The EoS that performed the best for the systems: 1-hexene + NMP and n-hexane + NMP is the HOC virial EoS. Taking cognizance of the fact that the NMP molecule is a dipolar, associating compound, the Hayden and O'Connell virial equation of state was considered. The use of HOC EoS to represent VLE data proved exceptionally successful in this work as this correlation enables the prediction of pure component as well as cross second virial coefficients via the application of molecular theories and empirical modifications. This EoS is most suited for systems that operate in the low-to-moderate pressure range. In addition, when the systems under analysis become more complex, the HOC virial EoS is more applicable and significantly more accurate. Another exceptional feature of this model is that for scenarios where very limited or no data is available it affords the most accurate predictions of phase equilibrium data (Hayden and O'Connell, 1975).

A distinct advantage of this model over others is observed when assessing the results of the direct test. The HOC EoS, in all instances, delivered the best results for the direct test due to the fact that it takes the associative nature of NMP into account.

This EoS was tested on 119 mixed non-polar systems and 73 mixed systems involving polar compounds, as well as 39 non-polar and 102 polar and associating compounds (Hayden and

O'Connell, 1975). This is an extensive undertaking, and gives greater confidence in the use of this particular EoS for the representation of the systems containing NMP.

The vapour phase inequalities were also represented by the Peng-Robinson (PR) and Soave-Redlich-Kwong (SRK) EoS. The SRK and PR EoS are very popular industrially, as they require very little start up information, *i.e.* only the accentric parameters and the critical properties are required for the determination of the generalized parameters (Naidoo, 2004).

Further to the integrity of these models is that they represent hydrocarbon systems excellently with respect to the generation of reliable phase equilibrium correlated data (Naidoo, 2004). In addition, from the work of Hirawan (2007) the SRK and PR models were utilized to represent the vapour phase inequalities, thus this was another basis for the use of these models.

Even though the HOC EoS proved most successful for correlation of VLE data, the SRK and PR models performed well above par. They represented the systems accurately in almost every regard, with the exception of course being in terms of the activity coefficients generated. However, this problem was anticipated in advance as it is a well known fact that the SRK and PR models do not take association into account, although these models were used anyway as the degree of self-association that the NMP molecule contributed was not known initially. Thus the critical disadvantage of these models is the poor prediction of liquid densities, as well as poor representation of polar and associating compounds.

The SRK EoS is most applicable for the treatment of non-polar and weakly polar substances and was developed for representation of light hydrocarbons. After the modifications made to the SRK EoS, there were marked improvements in the computation of vapour pressure data for several hydrocarbons, in addition to the improved correlation of VLE data of multi-component systems that constituted non-polar and slightly polar fluids (Naidoo, 2004). However, it gives an inadequate representation of the vapour pressures for strongly polar species (Raal and Mülhbauer, 1998). In addition, this EoS definitely cannot adequately represent, to any satisfactory degree of accuracy, associating components.

With the modified PR EoS a few polar systems are acceptably represented and improvements to the representation of the density function for some liquids have also been noted. On the other hand, the prediction of density for some liquids has proven highly unsatisfactory and unreliable. Another major problem associated with the PR cubic EoS is that results acquired in the critical region are inaccurate. Therefore, the inadequacy of this EoS for representing highly polar, associating fluids (*e.g.* carboxylic acids) and higher hydrocarbons, as well as non-hydrocarbon species, is significant (Reddy, 2006).

For the third system modeled: 1-hexene + n-hexane, the models employed for representation of the vapour phase are the PR, SRK and Ideal Gas. Overall the models used correlated the data to approximately the same level of accuracy. However, if one EoS had to be selected, it would be the PR EoS.

Interestingly, the ideal gas model may only be applied at conditions of low-to-moderate pressures. This criterion is satisfied in this study as all measurements range from 0 to 350 kPa. In addition, another criterion for the application of the ideal gas model is that the system components must be chemically similar (*i.e.* the molecular species are similar in size) and belong to the same chemical family. Once again, this requirement is fulfilled by 1-hexene and n-hexane (Smith et *al.,* 2005).

Since the PR and SRK EoS models are much more complex in nature than the ideal gas model it was expected that these models would perform better than the ideal gas model.

7.6 Thermodynamic Data Reduction

The theory behind the computation of excess thermodynamic properties has been discussed at length in Chapter 2. Thus, to avoid repetition, the theory of excess properties shall not be expanded extensively. Excess properties form an intrinsic aspect in the field of thermodynamics. In order to properly represent a system, the most appropriate G^E models should be utilized. When modeling experimental VLE data, H^E data may also be measured and regressed simultaneously with the experimental data. The temperature dependent H^E data, together with VLE data, are the most important parameters in fitting the binary interaction parameters simultaneously for a

system. H^E data is measured on a flow calorimeter and is related to the computation of activity coefficient as follows:

$$\frac{\partial \ln \gamma_i}{\partial(1/T)} = \frac{\overline{H_i^E}}{R} \tag{7-9}$$

An observation made by Fischer and Gmehling (1996) is the data for $\overline{H}_i^{E,\infty}$ is larger for alkanes over alkenes at lower temperatures than higher temperatures. The same relationship is observed for activity coefficients at infinite dilution. However, an important drawback of operating at lower temperatures is the diminished capacity of NMP at the lower temperatures. Therefore, a careful balance is sought between the operational capacity of NMP and the temperature at which separation is occurring (Fischer and Gmehling, 1996).

An alternative solution to decreasing the temperature is the addition of water to NMP. As reported by Fischer and Gmehling (1996), the effect of the combination of water to NMP has the same effect as operating at low temperatures. However, this solution also has a drawback, as at a certain pressure NMP will have a decreased capacity. Thus, the engineer has an important task of carefully deliberating and reaching a decision that compromises between selectivity and the capacity of the selective solvent, which in this scenario is NMP. The selectivity of the mixture will affect the capital costs, *i.e.* the height of the distillation column, whereas the capacity of the selective solvent affects the operating costs.

It is important to note that once experimental measurements for the molar excess enthalpy, and isothermal VLE data have been conducted for a minimum of three different isotherms for a system, and the experimental activity coefficients calculated, a plot of $\partial(\ln \gamma_i)$ Vs. $\overline{H_i^E}$ is to be undertaken. This graphical representation would then give an indication of the relationship between the activity coefficients of a system and the excess enthalpy. If this is executed, then future isothermal measurements for the same system at different temperatures need not be undertaken, only the excess enthalpy need be measured. From equation (7-9) the activity coefficients of the system may be computed via the use of the graphical relation, when known $\overline{H_i^E}$ data is available. Referring to Chapter 2, it becomes obvious that once the activity coefficients of a system are known, the excess Gibbs energy may be computed as well as the

binary interaction parameters. Once the binary interaction parameters are computed, using a simple matlab or Aspen Plus® program, the P-x-y data of a system may be predicted from measured $\overline{H_i^E}$ data.

Exhibited below are plots of the best fit binary interaction parameters for the different systems at their respective temperatures. For the plots corresponding to the remaining models representing the systems reference should be made to Appendix G.

7.6.1 1-Hexene (1) + NMP (2) System

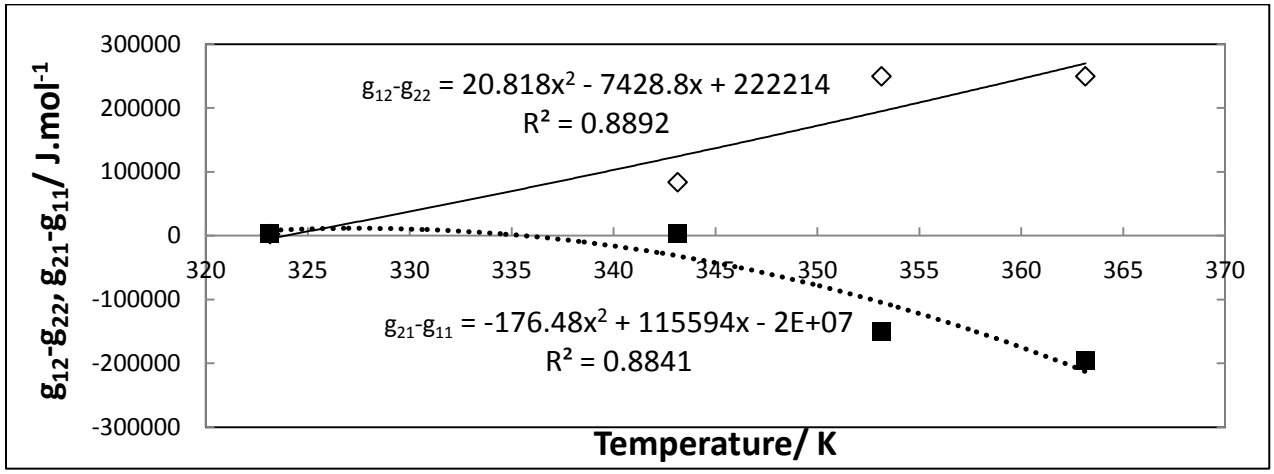

Figure 7-55: Temperature dependence of the NRTL-HOC model parameters for the system 1-hexene (1) + NMP (2). ◊, g_{12}-g_{22}; ■, $g_{21} - g_{11}$; ▬, fit for g_{12}-g_{22}; ·····; fit for $g_{21} - g_{11}$.

7.6.2 n-Hexane (1) + NMP (2) System

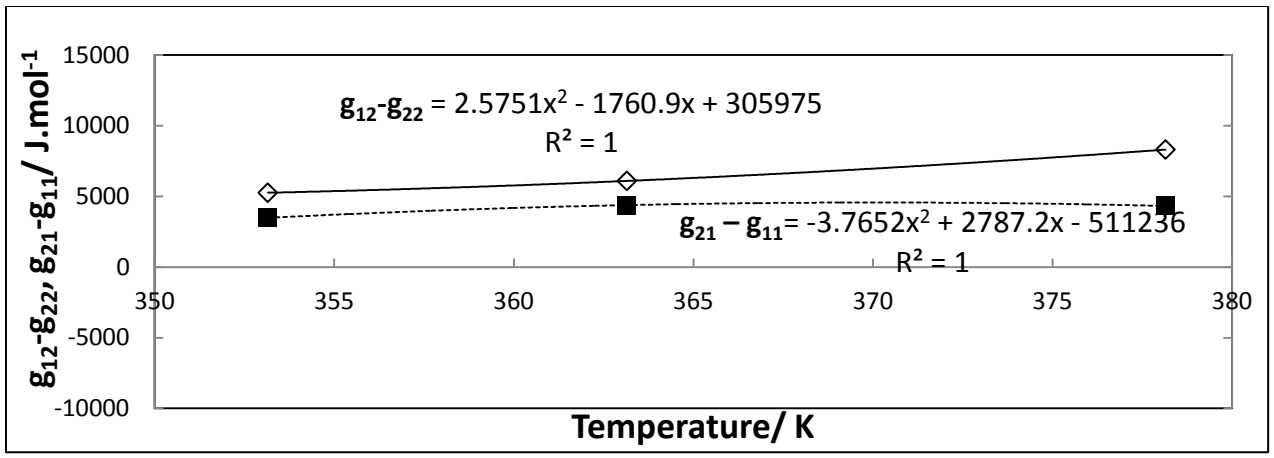

Figure 7-56: Temperature dependence of the NRTL-HOC model parameters for the system n-hexane (1) + NMP (2). ◊, g_{12}-g_{22}; ■, $g_{21} - g_{11}$; ▬, fit for g_{12}-g_{22}; ·····; fit for $g_{21} - g_{11}$.

7.6.3 1-Hexene (1) + n-Hexane (2) system

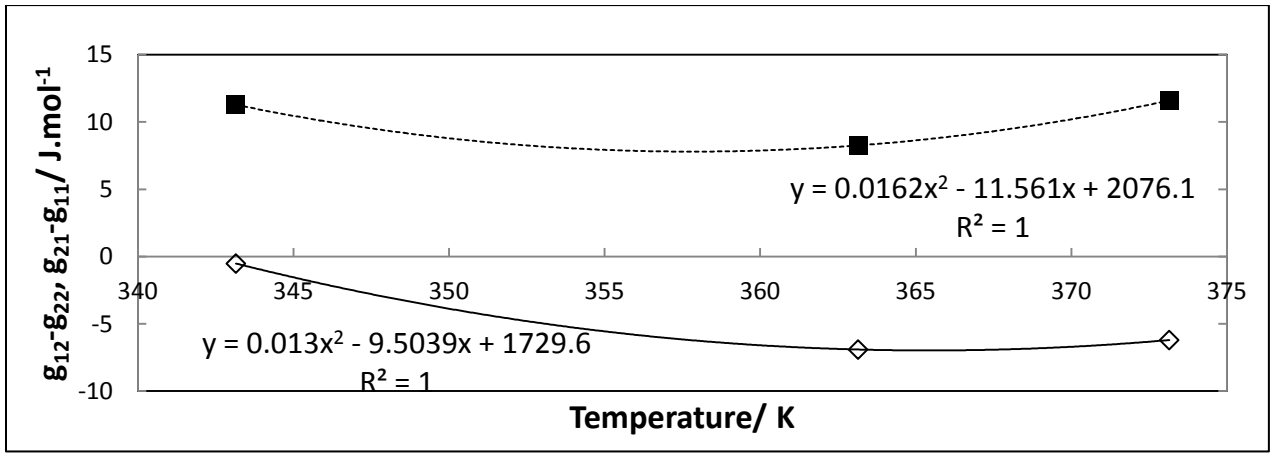

Figure 7-57: Temperature dependence of the NRTL-Ideal model parameters for the system 1-hexene (1) + n-hexane (2). ◊, g_{12}-g_{22}; ■, $g_{21} - g_{11}$; ▬, fit for g_{12}-g_{22}; ·····; fit for $g_{21} - g_{11}$.

7.7 Relative Volatility

Relative volatility assists in determining the viability of separating two components on an industrial scale, *i.e.* the ease with which the more volatile component may be separated from the less volatile. In addition to being used in different types of distillation processes, the relative volatility is also used in separations and absorption processes, which involve contacting liquid and vapour phases over many equilibrium stages.

For a binary mixture, this relative volatility, represented by the symbol α_{ij}, at a certain temperature and pressure is:

$$\alpha = \frac{(y_i / x_i)}{(y_j / x_j)} = \frac{K_i}{K_j} \tag{7-10}$$

From the relative volatilities computed for the ternary system, we observe that as the concentration of NMP in the ternary system increases, so too does the selectivity for separating the alkene from the alkane. We note that the addition of NMP actually increases the separation in the ternary mixture. The relative volatilities of the components 1-hexene and n-hexane in the ternary mixture are altered quite significantly. This implies NMP is a suitable solvent to utilize in extractive distillation. More importantly (from comparing the relative volatilities of the different components, it appears NMP has a greater affinity for n-hexane, thus, 1-hexene shall boil up and exit through the top of the column, whilst NMP and n-hexane shall pass through the bottom of the column.

1-Hexene has a higher boiling point than n-hexane by approximately 3 degrees Celsius. Even though this is a small difference, one would still expect the n-hexane to be the more volatile component and boil up through the column while the 1-hexene passes though the bottoms. However, this is not the case. Instead, as mentioned above, the NMP forms a low boiling azeotrope with the n-hexane and evacuates through the bottom of the column while the 1-hexene passes through the top. This is merely one of the anomalies that prevail.

Referring to Figures 7.58-7.60, the relative volatility plots of the binary systems at 363.15 K is exhibited. It is clearly distinguishable that for the systems 1-hexene + NMP and n-hexane + NMP, the relative volatilities are altered appreciably by the addition of NMP, which is a desired outcome. For the plot of 1-hexene + n-hexane the relative volatilities for this system is basically the same throughout the composition range, indicating the difficulty associated with separating these components. From Figure 7.60 for 1-hexene + n-hexane, it is obvious that an extractive solvent will have to be added to improve the separation. For the full set of relative volatility plots for the systems measured in this work, refer to Appendix H.

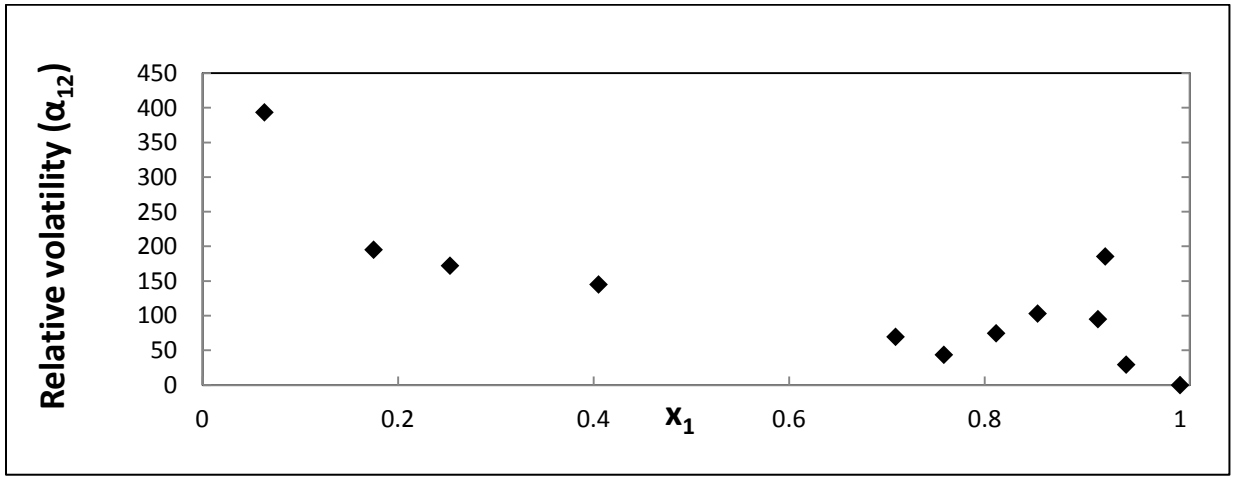

Figure 7-58: Plot of relative volatility for the 1-hexene (1) + NMP (2) system at 363.15 K.

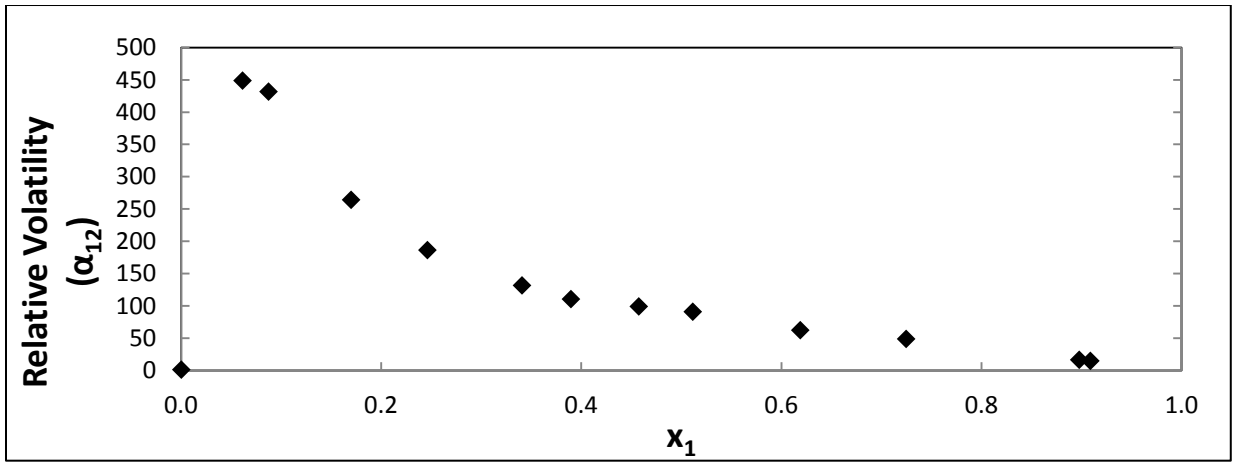

Figure 7-59: Plot of relative volatility for the n-hexane (1) + NMP (2) system at 363.15 K.

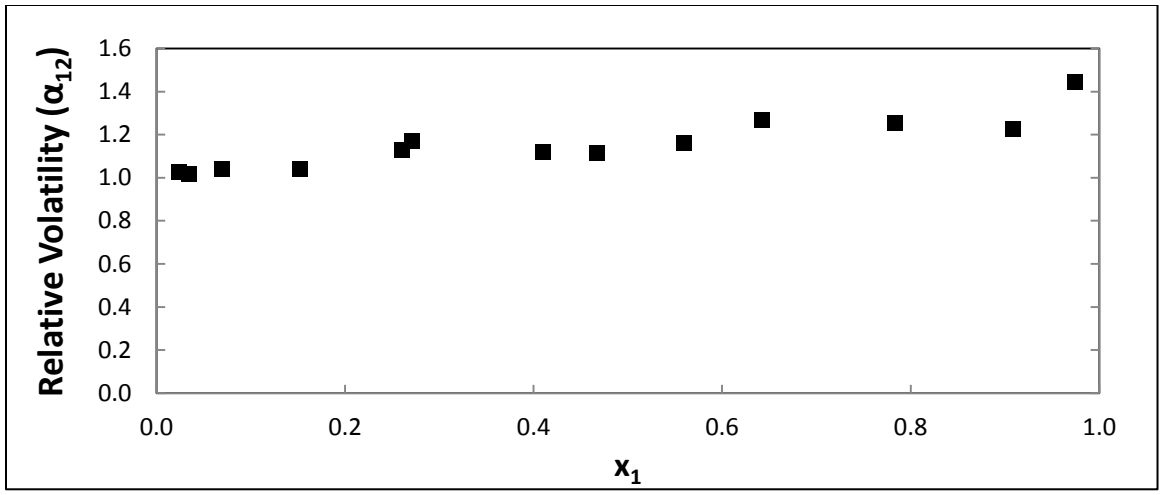

Figure 7-60: Plot of relative volatility for the n-hexane (1) + 1-hexene (2) system at 363.15 K.

7.8 Aspen Plus® as a Modeling Tool

As part of a comparative analysis undertaken in this work, the NRTL non-randomness (α_{ij}) parameter was fixed at 0.4163 and 0.4567 (Fischer and Gmehling, 1996) for the systems n-hexane + NMP and 1-hexene + NMP respectively during the regression for the remaining adjustable parameters (Appendix F). The model results obtained when using a constant α_{ij} value yielded AE % and model fits very similar to the case where the α_{ij} parameter was regressed for. However, for some model combinations at specific conditions severe errors were observed. For the 1-hexene + NMP system at 343.15 K the ΔP_{AAD} values reported for the models are quite significant, even though Δy_{AAD} was well below 0.1 mole fraction.

This occurs as a consequence of fixing the non-randomness parameter, thus the NRTL model does not have sufficient flexibility. This is because Aspen attempts to minimize the error in the vapour residual, so even though the test criterion is met, when an actual plot of P-x-y is made, an inconsistent plot is observed where the model data only fits the experimental data at specific points, however, between the experimental points (where sparse spaces exist), the Aspen model cannot fit a consistent shape.

A distinct drawback of Aspen Plus® is that it is very sensitive to the initial guesses that have to be made for the binary interaction parameters. The initial use of values, not close to the final regressed values, may in some instances lead to Aspen informing the user that an internal error has occurred. The internal error in the Aspen regression procedure results as a consequence of the initial guess being unrealistic. This presents a problem to the user who may be unfamiliar with the program; hence guidance and experience is necessary when working with such design software.

Chapter 8: Conclusions

- Two VLE stills were utilized during the course of this project, the low pressure still of Hirawan (2007) and the low-to-medium pressure still of Lilwanth (2011). The low pressure VLE still is only capable of handling pressures up to 101.325 kPa, whereas, the still of Lilwanth (2011) had a pressure range of 0-500 kPa.

- First, test system measurements were executed for ethanol + cyclohexane at 40 kPa which correlated well with the data of Joseph *et al*. (2001). Thereafter, the systems 1-hexene + NMP and n-hexane + NMP were measured at 363.15 K each. This data compared very well with the literature data of Fischer and Gmehling (1996) and Hirawan (2007).

- The following novel binary and ternary system measurements, additional to the test system measurements, were conducted:

  - 1-hexene + NMP at 323.15, 343.15, 353.15 K
  - n-hexane + NMP at 353.15, 378.15 and 383.15 K
  - 1-hexene + n-hexane at 343.15, 363.15 and 373.15 K; and
  - 1-hexene + n-hexane + NMP at 363.15 K.

- The phase equilibria data measured were modeled using Aspen Plus® (2011) and DDB (2011) and the consistency of the data ascertained using the direct and point tests of Van Ness (1995).

- Due to the strong self association of the NMP molecule (Dyrkacz, 2001), models which account for association need to be considered. Thus, the Hayden and O‟Connell model was selected for use. Initially the associative effects were presumed to be small, thus, only one association model was taken into consideration. However, after analyzing the modeled data, it appeared the self-association of the NMP molecule is more significant

than originally estimated, and models which compensate for the self-association should be implemented, such as FBT or ERAS models.

- The systems measured were modeled using both the direct (Φ- Φ) and combined (ϒ-Φ) methods (Smith *et al*., 2001). The vapour phase fugacity coefficients were computed using the Hayden and O'Connell (1975) virial equation, Peng-Robinson (1976) and Soave-Redlich-Kwong (1972) EoS. Deviations from the liquid phase were accounted for via the utilization of the NRTL (1968) and UNIQUAC (1975) liquid activity coefficient models. The Wong and Sandler mixing rule (1997) was implemented in the direct method.

- Referring to the experimental measurements for the binary systems constituting NMP, we note that as the composition of NMP approaches purity, the γ_{NMP} does not approach unity. This is a direct indication of the associative effects of the NMP molecule. For the 1-hexene + n-hexane system, the activity coefficient values all approach unity as the respective components approach purity in the mixture.

- The use of the NRTL-HOC model combination performed the best with respect to fitting all the experimental data.

- When the consistency tests were performed, it was found that in certain instances specific data points had to be removed from the final regression analysis. This was executed to ensure that the models available could meet the criteria for passing the point test. An observation made is that when certain model combinations are used data points were excluded; however, when a different model is implemented the same point is actually included in the final regression analysis. This clearly indicates the representation of thermodynamic data is greatly dependent upon finding the perfect model applicable to the system, as well as correctly specifying the adjustable parameters required for input. In most instances though, it is preferred to regress for all adjustable parameters.

- There is excellent agreement between the predicted data for the ternary system and the experimentally measured data points, with a maximum deviation of 5% observed. This finding is positive and paves the way for greater ease in ternary and quaternary system measurements. In the future, ternary and quaternary systems need not be measured, as they may be accurately predicted by using the binary interaction parameters of the systems constituting the ternary or quaternary system.

Chapter 9: Recommendations

- NMP is a self-associating, polar compound; as such a greater investigation of the different types of models which can better represent self-associating and associating systems should be examined and applied to the systems in this thesis, such as FBT and ERAS theory models. Due to time constraints, this was not possible for this thesis. However, a comparative analysis would provide in-depth insight into the intricate interactions between 1-hexene/n-hexane/NMP.

- Alternative solvents to NMP should be investigated to examine their effect in the separation of olefins and paraffins. Possible alternatives could be tri-ethylene glycol or di-ethylene glycol.

- Other compounds, originating from the same homologous family as 1-hexene and n-hexane, should be studied in binary and ternary combinations with NMP to ascertain if the same relationships underpinned for the components (1-hexene/ n-hexane/ NMP) in this study extend to other homologous series.

- The method of regression undertaken in this thesis was based upon Barkers method. The major shortfall of this type of regression analysis is that it does not take into account the variation in independent variables, like temperature and liquid phase composition. A better approach would be to utilize the Maximum Likelihood Principle. This regression method minimizes the temperature, pressure, liquid and vapour composition residuals before returning the binary interaction parameters.

- Jackson and Wilsak (1995) recommend that uncertainty in measurements be accounted for via the utilization of statistical methods. This will assist in ensuring the final results delivered by the consistency tests render a greater degree of accuracy. Consistency tests produce results very much dependent upon the type of models being utilized. Therefore, the investigator has to be wary regarding interpretation of these results.

- In order to improve the accuracy of binary interaction parameters obtained from regression programs, additional properties to VLE data should also be included in the regression procedure. This data could range from experimentally measured vapour pressures of the individual components, to excess enthalpies (H_m^E) *etc.*

References

Abbott, M.M., and Van Ness, H.C., (1975), "*Vapour Liquid Equilibrium: Part 3-Data Reduction with Precise Expressions for* G^E," American Institute of Chemical Engineering Journals, Vol.21, Pg.62-71.

Abbott, M.M., (1986), "*Low pressure vapour phase equilibria: Measurement of VLE,*" Fluid Phase Equilibria, Vol.29, Pg.193-207.

Abrams, D.S. and Prausnitz, J.M., 1975, "*Statistical Thermodynamics of Liquid Mixtures: A New Expression for the Excess Gibbs Energy of Partly or Completely Miscible Systems,*" American Institute of Chemical Engineers Journal, Vol. 21, Pg. 116-128.

Anderko, A., 1990, "*Equation-of-State Methods for the Modeling of Phase Equilibria*", Fluid Phase Equilibria, Vol. 61, pp. 145-225.

Anderson, T.F. and Prausnitz, J. M., 1978, "*Application of the UNIQUAC Equation to Calculation of Multicomponent Phase Equilibria. 1: Vapour-Liquid Equilibria; 2: Liquid-Liquid Equilibria"*, Industrial and Engineering Chemistry, Process Design and Development, Vol. 17, pp. 552-567.

Barker, J.A., 1953,"*Determination of Activity Coefficients from Total Pressure Measurements",* .Australian Journal of Chemistry, 6, 207-210.

Berg, C. and McKinnis, A.C., 1948,"*Effect of Temperature on Liquid Phase Activity Coefficients",* Industrial and engineering chemistry, Vol 40.

Carlson, H.C. and Colburn A.P.,1942, "*Vapor-Liquid Equilibria of Non-ideal Solutions. Utilization of Theoretical Methods to Extend Data"*, Industrial and Engineering Chemistry, 34(5), 581-589.

Christiansen, L.J. and Fredenslund, A. 1975, *"Thermodynamic Consistency using Orthogonal Collocation or Computation of Equilibrium Vapor Compositions at High Pressures"* The American Institute of Chemical Engineers Journal, 21(1), 49-57.

Clifford, S.L., 2003,"*Low-Pressure Vapour-Liquid Equilibrium and Molecular Simulation of Carboxylic acids,*" MSc. Eng. Thesis, University of Kwa Zulu Natal, Durban, South Africa.

Component Plus, 2011, Pure Component Database Manager, Component Plus Software Package Version 5.1.2600 Service Pack 3 Build 2600, United States.

Coutsikos, P., Kalospiros, N.K., Tassios, D.P., "*Capabilities and limitations of the Wong-Sandler mixing rule",* Laboratory of Thermodynamics and Transport Phenomena, Department of Chemical Engineering, National Technical University of Athens, 9, Heroon Polyteehniou Str., Zographou Campus15780 Athens Greece, Fluid Phase Equilibria 108 (1995) 59-78.

Dortmund Data Bank, 2010, DDBST Software and Separation Technology GmbH, DDB Software Package Version 2010, Oldenburg.

Dyrkacz, G, 2001, *"The Nature of the Binary Solvent N-Methylpyrrolidone/Carbon Disulphide"* , Argonne National Laboratory, Argonne, Illinois, Energy and Fuels.

Fischer, K. and Gmehling, J., 1996, "*Vapour-liquid equilibria, activity coefficients at infinite dilution and heats of mixing of N-methyl pyrrolidone-2 with C5 orC6 hydrocarbons and for hydrocarbon mixtures*", Fluid Phase Equilibria, Vol.119, Pg.113-130.

Gess, M.A., Danner, R.P., and Nagvekar, M., 1991, *"Thermodynamic Analysis of Vapor-Liquid Equilibria: Recommended Models and a Standard Data Base*", Design Institute for Physical Property Data, American Institute of Chemical Engineers.

Gmehling, J., 2011, "Computer Driven Dynamic Apparatus for the Measurement of Vapour-Liquid Equilibrium Data", University of Oldenburg, Germany, Institute for Applied and Pure Chemistry.

Gnanakumari, P., Rao, M.V.P., Prasad, D.H.L. and Kumar Y. V. L.R., 2003, "*Vapor-Liquid Equilibria and Excess Molar Enthalpies for N-Methyl-2-pyrrolidone with Chloroethanes and Chloroethenes"*, Department of Chemistry, Sri Venkateswara UniversityTirupat517502, India, and Chemical Engineering Division, Indian Institute of Chemical Technology, Hyderabad 500 007, India, J. Chem. Eng. Data, 48, 535-540.

Hala, E.J., Pick, V. F. and Vilim, O., 1967, "V*apour-Liquid Equilibrium*", Second Edition, Pergamon Press, Oxford.

Hansen, R.S. and Miller, F.A., 1954, *"A New Method for Determination of Activities of Binary Solutions of Volatile Liquids"* The Journal of Physical Chemistry, 58(3), 193-196.

Hayden, J.G, and O'Connell, J.P, 1975, "*A Generalised Method for Predicting Second Viral Coefficients*," Industrial and Engineering Chemistry. Process Design and Development, Vol.14, Pg.209-216.

Henni, A, Hromek, J.J, Tontiwachwuthikul,P, and Chakma,A, "*Volumetric Properties and Viscosities for Aqueous N-Methyl-2-pyrrolidone Solutions from 25°C to70 °C"*, J. Chem. Eng. Data 2004, 49, 231-234.

Hirawan, R., 2007, "*Development of a thermodynamic for the purification of 1hexene*" MSc. Eng. Thesis, University of Kwa-Zulu Natal, Durban, South Africa.

Huang, S.H. and Radosz, M., 1990, "*Equation of State for small, large, polydisperse and associating molecules"*, Industrial and Engineering Chemistry Research, 29, 2284.

Iwarere, S.A., 2009, *"Measurement of Phase Equilibria for Oxygenated Hydrocarbon Systems",* MSc. Eng Thesis, University of Kwa-Zulu Natal, Durban, South Africa .

Jackson, P.L. and Wilsak, R.A., 1995, "*Thermodynamic consistency tests based on the Gibbs/Duhem equation applied to isothermal, binary vapour-liquid equilibrium data: data evaluation and model testing*", Fluid Phase Equilibria, 103(2), 155-197.

Joseph, M.A., Ramjugernath, D. and Raal, J.D., 2001, "*Phase Equilibrium Properties for Binary Systems with Diacetyl from a Computer Controlled Vapour-Liquid Equilibrium Still*," Fluid Phase Equilibria, Vol.182, Pg. 157-176.

Lappin, G. R. and Sauer, J. D., 1989, "*Alpha Olefins Applications Handbook*", Organic Chemistry, New York.

Leia, Z., Arlt, W. and Wasserscheid, P., 2007, "*Fluid Selection of entrainers in the 1-hexene/n-hexane system with a limited solubility"*, Phase Equilibria 260, 29–35.

Lilwanth, H., 2011, "*Vapour-Liquid Equilibrium Measurements at Low-to-Moderate Pressures using a Glass Recirculating still",* MSc. Eng. *In progress*, University of Kwa-Zulu Natal, Durban, South Africa.

Letcher, T.M., Domanska, U. and Mwenesongole, E.*, "The excess molar volumes of (N-methyl-2-pyrrolidone + an alkanol or a hydrocarbon) at 298.15 K and the application of the Flory–Benson–Treszczanowicz and the Extended Real Associated Solutiontheories",*Department of Chemistry and Applied Chemistry, University of Natal, SouthAfrica, Fluid Phase Equilibria, 149, 1998, 323–337.

Malanowski, S., 1982, "*Experimental Methods for Vapour-Liquid Equilibria. Part I. Circulation Methods",* Fluid Phase Equilibria, Vol. 8, pp. 197-219.

Malanowski, S. and Anderko, A., 1992, "*Modelling Phase Equilibria: Thermodynamic Background and Practical Tools"*, John Wiley, New York.

Marquardt, D.W, 1963, "*An Algorithm for Least-Squares Estimation of Non-Linear Parameters,*" Journal. Society of Industrial and Applied Mathematics, Vol.11, Pg.431-441 Marsh, K..N., (1989), "*New methods of vapour-liquid-equilibria measurements,*" Fluid Phase Equilibria*,* Vol.52, Pg.169-180.

Mingjian, L., Peisheng, M., Shuqian, X., 2007, "A Modification of α in SRK Equation of State and Vapour-Liquid Equilibria Prediction", Chin. J. Chem. Eng., 15(1) 102-109.

Moodley, P., 2009, "*Vapor Liquid Equilibria Studies for Binary Systems Containing 1-Hexene and n-Hexane*", MSc. Eng. Thesis, University of Kwa-Zulu Natal, Durban, South Africa.

Narasigadu, C., 2006, "*Phase Equilibrium Investigation of the Water and Acetonitrile Solvent with Heavy Hydrocarbons,*" MSc. Eng. Thesis, University of Kwa Zulu Natal, Durban, South Africa.

Naidoo, P., 2004, "*High Pressure Vapour-Liquid Equilibrium Studies*", PhD. Eng. Thesis, University of Kwa-Zulu Natal, Durban, South Africa.

Oliver, N., Fischer, K. and Gmehling, J., 1995, "*Vapour-Liquid Equilibria and Enthalpies of Mixing for the Binary System Water + N-methyl-2-pyrrolidone in the Temperature Range 80-140°C*," Journal of Chemical Engineering Data, American Chemical Society, Vol.41, Pg.1434-1438.

Othmer, D.F., 1928, "*Composition of Vapours from Boiling Binary Solutions. Improved Equilibrium Still"*, Industrial and Engineering Chemistry, Vol. 20, pp. 743-766.

Perry, R.H., Green, D.W., Maloney, J.O., 1997, "*Perry's Chemical Engineers" Handbook"*, 7th Edition, McGraw Hill, New York.

Pillay, J.C., 2009, "*Binary Vapour-Liquid Equilibria for Oxygenated Containing Compounds,*" MSc. Eng. Thesis, University of Kwa-Zulu Natal, Durban, South Africa.

Poling, B.E., Prausnitz, J.M. and O'Connell, J.P., 2001, *"The Properties of Gases and Liquids",* 5th Edition. New York: McGraw-Hill.

Prausnitz, J.M., 1969, "*Molecular Thermodynamics of Fluid Phase Equilibria"*, Prentice-Hall, Englewood Cliffs, New Jersey.

Prausnitz, J.M, Anderson, T.F, Grens, E.A, Eckert, C.A, O'Connell, J.P., 1980, "*Computer Calculations for Multi-component Vapour-Liquid and Liquid-Liquid Equilibria,*" Prentice Hall Englewood Cliffs, NJ.

Raal, J.D and Mühlbauer, A.L., 1998, "*Phase Equilibria: Measurement and Computation,*" Taylor and Francis, Bristol.

Ralf, D., Peper, S. and Fonseca J.M.S., 1972, "*High-pressure fluid-phase equilibria: Experimental methods and systems investigated (2000-2004),*" Fluid Phase Equilibria, Vol. 288, Pg. 1-54.

Ramjugernath, D., 2000, "High Pressure Phase Equilibrium Studies", PhD. Eng. Thesis, University of Kwa-Zulu Natal, Durban, South Africa.

Randic, M., 1974, "On characterisation of molecular branching", Journal of the American Chemical Society; Vol. 97, No. 23, pg 6609-6615.

Reddy, P., 2006, "*Development of a Novel Apparatus for the Measurement of Vapour-Liquid Equilibria at Elevated Temperatures and Moderate Pressures,*" PhD. Eng. Thesis, University of Kwa Zulu Natal, Durban, South Africa.

Redlich, O. and Kister, A.T., 1948, "*Algebraic Representation of Thermodynamic Properties and Classification of Solutions,*" Industrial and Engineering Chemistry, Vol.V40, Pg.345-348.

Redlich, O. and Kwong, J.N.S., 1949, "*On Thermodynamics of SolutionsV: An Equation of State. Fugacities of Gaseous Solutions,*" Chemical Reviews, Vol.44, Pg.233-244.

Reid, C.R, Prausnitz, J.M and Polling, B.E., 1988, "*Properties of Gases and Liquids,*" 4th Edition, McGraw Hill Book Company, Singapore.

Renon, H and Prausnitz, J.M., 1968, "*Local Compositions in Thermodynamics Excess Functions for Liquid Mixtures,*" American Institute of Chemical Engineering Journals, Vol.14, Pg.135-144.

Sameshima, J., 1918, "*On the System Acetone-Ethyl Ether*", Journal of the American Chemical Society, Vol. 40, pp. 1482-1508.

Smith, J.M.,Van Ness, H.C. and Abbott, M.M., 2001, "*Introduction to Chemical Engineering Thermodynamics,*" 6th Edition, McGraw-Hill, New York.

Smith, J.M.,Van Ness, H.C. and Abbott, M.M., 2005, "*Introduction to Chemical Engineering Thermodynamics*" 7th Edition, McGraw-Hill, New York.

Soave, G., 1972, "*Equilibrium Constants from a modified Redlich-Kwong Equation of State,*" Chemical Engineering Science, Vol.27, Pg.1197-1203.

Soo, C.B., 2011, *"Experimental thermodynamic measurements of bio-fuel related associaying compounds and modelling using the PC-SAFT equation of state",* PhD thesis, l"École Nationale Supérieure des Mines de Paris, Paris, France.

Stryjek, R. and Vera, J.H., 1986, "*PRSV: An Improved Peng- Robinson Equation of State for Pure Compounds and Mixtures,*" The Canadian Journal Chemical Engineering, Vol.64, Pg.323-333.

Taylor B.N. and Kuyatt, C.E., 1994, "Guidelines for evaluating and expressing the uncertainty of NIST measurement results", Technical report, National Institute of Standards and Technology, Gaithersburg, MD.

Tochigi, K., Kamihama, N., Matsuda, H., Kurihara, K., Yokoyama, K., 2009, "*Measurement of Vapour-Liquid Equilibria for Binary Systems Containing Tetrahydrofuran Using a Simple and Automatic Apparatus*", Department of Materials and Applied Chemistry, Nihon University, Tokyo, Japan.

Tsonopoulos, C., 1974, "*An Empirical Correlation of the Second Viral Coefficients,*" American Institute of Chemical Engineers Journals*,* Vol.20, Pg.263-272.

Twu, C.H and Coon J.E., 1996, "CEOS/A^E *Mixing Rules Constrained by vdW Mixing Rule and Second Virial Coefficient,*" American Institute of Chemical Engineering Journals*,* Vol.42, Pg.3212-3222.

Uusi-Kyyny, 2004, "*Vapour Liquid Equilibrium Measurements For Process Design*", Doctor of Science in Technology, Helsinki University of Technology

Van Laar, J.J., 1910, "*The Vapour Pressure of binary mixtures,*" Zeitschrift feur Physik Chemie, Vol.72, Pg.723-751 (Cited in Walas, 1985).

Van Ness, H.C., 1995, "*Thermodynamics in the Treatment of Vapor/Liquid Equilibrium (VLE) Data*," Pure and Applied Chemistry*,* Vol.67, Pg.859-872.

Van Ness, H.C., Pedersen, F. and Ramussen, P., 1978, "*Part V. Data Reduction by Maximum Likelihood"*, American Institute of Chemical Engineers Journal, 24, 1055-1063.

Van Ness, H.C. and Abbott, M.M., 1982*, „Classical Thermodynamics of Non-electrolyte Solutions With Applications to Phase Equilibria"*, McGraw-Hill, New York.

Walas, S.M., 1985, "Phase *Equilibrium in Chemical Engineering*" Butterworth, Boston.

Wentinka, A.E.,Kuipers, N.J.M., de Haan A.B., Scholtz, J. and Mulder, H., 2007, "*Olefin isomer separation by reactive extractive distillation: Modelling of vapour–liquid equilibria and conceptual design for 1-hexene purification",* Chemical Engineering and Processing 46, 800–809.

Wilson, G.M., 1964, "*Vapour-Liquid Equilibrium, A New Expression for the Excess Free Energy of Mixing,*" Journal of American Society, Vol.86, Pg.127-130.

Wong, D.S.H and Sandler, S.I., 1992, "*A Theoretically Correct Mixing Rule for Cubic Equation of State vapour-Liquid Equilibrium, A New Expression for the Excess Free Energy of Mixing,*" American Institute of Chemical Engineers Journals*,* Vol.10, Pg.660-665.

Suryanarayana, Y.S., and Van Winkle, M., 1996, *"Solvent Effect on Relative Volatility, n-Hexane-Hexene-1 System"*, University of Texas, Austin, Texas, Vol 11, No.1, Journal Extract.

Internet Sources:

http://www.chemguide.co.uk/organicprops/alkanes/background.html), Accessed 28 July 2011, Time 17:30 PM.

http://www.webbook.nist.gov/cgi/cbook, Accessed 03 January 2012, Time 05:00 AM.

http://www.atago.net, Accessed 15 January 2012, Time 02:30 PM.

Appendix A: Theory

A.1. Wong and Sandler Mixing Rule

The partial derivative of a_m and b_m are:

$$\left(\frac{1}{n}\frac{\partial n^2 a_m}{\partial n_i}\right) = RT\left(D\frac{\partial n b_m}{\partial n_i} + b\frac{\partial nD}{\partial n_i}\right) \tag{A-01}$$

$$\left(\frac{\partial n b_m}{\partial n_i}\right) = \frac{1}{(1-D)}\left(\frac{1}{n}\frac{\partial n^2 Q}{\partial n_i}\right) - \frac{Q}{(1-D)^2}\left(1 - \frac{\partial nD}{\partial n_i}\right) \tag{A-02}$$

The partial derivatives of „Q" and „D" are stated below:

$$\left(\frac{1}{n}\frac{\partial n^2 Q}{\partial n_i}\right) = 2\sum_j x_j\left(b - \frac{a}{RT}\right)_{ij} \tag{A-03}$$

$$\left(\frac{\partial nD}{\partial n_i}\right) = \frac{a_i}{b_i RT} + \frac{\ln \gamma_i^{\infty}}{c} \tag{A-04}$$

The cross-parameter, needed for evaluation of activity is:

$$\left(b - \frac{a}{RT}\right)_{ij} = \frac{\left(b_i - \frac{a_i}{RT}\right) + \left(b_j - \frac{a_j}{RT}\right)}{2}\left(1 - k_{ij}\right) \tag{A-05}$$

Where: k_{ij} = an adjustable parameter

Via the regression of VLE experimental data, k_{ij} may be obtained.

A.2 Twu-Coon Mixing Rule

The partial derivatives of a and *b* are expanded as follows:

$$\frac{1}{b}\left(\frac{\partial nb}{\partial n_i}\right)=\frac{1}{Q}\left[\frac{1}{n}\left(\frac{\partial n^2 Q}{\partial n_i}\right)\right]-\frac{1}{1-D}\left(1-\frac{\partial nD}{\partial n_i}\right) \tag{A-06}$$

$$\frac{1}{na}\left(\frac{1}{n}\frac{\partial n^2 a}{\partial n_i}\right)=\frac{1}{b}\left(\frac{\partial nb}{\partial n_i}\right)+\frac{1}{D}\left(\frac{\partial nD}{\partial n_i}\right) \tag{A-07}$$

Following, the partials of „Q" and „D" are expressed as:

$$\frac{1}{Q}\left[\frac{1}{n}\left(\frac{\partial n^2 Q}{\partial n_i}\right)\right]=\frac{2\sum_j x_j\left(b_{ij}-a_{ij}\right)}{\sum_i\sum_j x_i x_j\left(b_{ij}-a_{ij}\right)} \tag{A-08}$$

$$\left(\frac{\partial nD}{\partial n_i}\right)=\frac{a_{vdw}}{b_{vdw}}\left(\left[\frac{1}{na_{vdw}}\left(\frac{\partial n^2 a_{vdw}}{\partial n_i}\right)\right]-\left[\frac{1}{b_{vdw}}\left(\frac{\partial nb_{vdw}}{\partial n_i}\right)\right]\right)+\frac{\ln\gamma_i^{\infty}}{c} \tag{A-09}$$

Subsequently, the partial derivatives of the previously defined parameters a_{vdw} and b_{vdw} are:

$$\frac{1}{na_{vdw}}\left(\frac{\partial n^2 a_{vdw}}{\partial n_i}\right)=\frac{2}{a_{vdw}}\sum_j x_j a_{ij} \tag{A-10}$$

$$\frac{1}{b_{vdw}}\left(\frac{\partial nb_{vdw}}{\partial n_i}\right)=\frac{2}{b_{vdw}}\sum_j x_j b_{ij}-1 \tag{A-11}$$

In the above equations, the symbols a_{ij} and b_{ij} are referred to as "cross-parameters" and the defining equation representing these cross parameters is:

$$a_{ij} = \sqrt{a_i a_j}\left(1 - k_{ij}\right) \tag{A-12}$$

$$b_{ij} = \frac{1}{2}\left(b_i + b_j\right)\left(1 - l_{ij}\right) \tag{A-13}$$

k_{ij} and l_{ij} are binary interaction parameters. These values may be obtained via the regression of vapour-liquid equilibrium data points obtained experimentally.

A.3: Activity Coefficient Expressions for Binary Systems for the Different Activity Coefficient Models

$$\overline{G}_i^E = RT \ln \gamma_i \tag{A-14}$$

Equation (A-14) may be represented in terms of activity as follows:

$$\ln \gamma_i = \left[\frac{\partial \left(nG^E / RT \right)}{\partial n_i} \right]_{P,T,n_j} \tag{A-15}$$

ln γ_i is a partial property of $\mathbf{G^E/RT}$, as a consequence, the following summability relationship holds true:

$$\frac{G^E}{RT} = \sum_i x_i \ln \gamma_i \tag{A-16}$$

Consequently, the Gibbs-Duhem equation may be represented in terms of activity as follows:

$$d\left(\frac{nG^E}{RT} \right) = \frac{nV^E}{RT} dP - \frac{nH^E}{RT^2} dT + \sum_i \ln \gamma_i dn_i \tag{A-17}$$

Appendix B: Literature Data

B.1. n-Hexane (1) + NMP (2):

The data of Fischer and Gmehling (1996) were measured on a moderate pressure static apparatus. This data is reflected in Table B-1 below.

Table B-1: Vapour-liquid equilibrium for the n-hexane (1) + NMP (2) system at 363.15 K (Fischer and Gmehling, 1996).

x_1	Pressure/ kPa	x_1	Pressure/ kPa	x_1	Pressure/ kPa
0	2.230	0.18354	133.805	0.68048	171.0550
0.00507	9.216	0.21046	140.737	0.73699	172.805
0.01064	16.691	0.24045	146.741	0.78644	174.716
0.01554	22.915	0.27970	152.584	0.82391	176.493
0.02089	29.616	0.31415	156.407	0.86118	178.661
0.03091	41.015	0.34606	159.059	0.89601	181.286
0.04066	51.390	0.37551	161.011	0.92271	183.750
0.04067	51.347	0.39977	162.492	0.94758	186.550
0.05041	60.778	0.40384	162.560	0.96752	189.121
0.05997	69.228	0.42810	163.637	0.97550	190.333
0.07456	80.965	0.43237	163.973	0.98354	191.625
0.09044	92.083	0.47076	165.400	0.98354	191.612
0.10692	102.121	0.50219	166.370	0.99165	192.716
0.12477	111.498	0.54209	167.527	1.00000	192.931
0.1420	119.289	0.58790	168.537		
0.16271	127.188	0.63340	169.722		

B.2. 1-Hexene (1) + NMP (2)

Fischer and Gmehling conducted measurements on this system at 363.15 and 413.15 K. The literature data is reflected below in Tables B-2 and B-3, and exhibited in Figure B-1. Only *P-x* data was measured, as measurements were conducted on a static apparatus.

Table B-2: Vapour-liquid equilibrium for the 1-hexene (1) + NMP (2) system at 363.15 K (Fischer and Gmehling, 1996).

x_1	Pressure/ kPa	x_1	Pressure/ kPa	x_1	Pressure/ kPa
0.00000	2.110	0.14455	102.678	0.62191	185.715
0.00297	5.122	0.15752	108.325	0.65983	188.408
0.00498	7.239	0.16993	113.368	0.69752	190.992
0.00865	10.831	0.18353	118.463	0.73537	193.685
0.01389	15.801	0.20288	125.186	0.76368	195.812
0.01696	18.667	0.23716	135.487	0.78964	197.845
0.02128	22.604	0.26925	143.564	0.81632	200.107
0.02555	26.382	0.30000	150.188	0.83648	201.924
0.03167	31.692	0.33386	156.475	0.85760	203.997
0.03782	36.769	0.36611	161.617	0.87778	206.138
0.04768	44.646	0.39796	166.154	0.89710	208.399
0.05739	51.980	0.40779	167.191	0.91759	211.025
0.06684	58.723	0.42693	169.776	0.93844	214.054
0.06684	58.753	0.43233	169.964	0.95517	216.773
0.07400	63.614	0.45324	172.778	0.96867	219.048
0.08324	69.672	0.45907	172.657	0.97600	220.502
0.09218	75.222	0.48374	174.972	0.98332	222.037
0.10093	80.367	0.51740	177.907	1.00000	224.043
0.10989	85.381	0.55000	180.492		
0.12170	91.674	0.58670	183.211		

Table B-3: Vapour-liquid equilibrium for the 1-hexene (1) + NMP (2) system at 413.15 K (Fischer and Gmehling, 1996).

x_1	Pressure/ kPa	x_1	Pressure/ kPa	x_1	Pressure/ kPa
0.00000	16.895	0.01827	59.153	0.22617	361.764
0.00072	18.374	0.04030	104.923	0.27763	403.754
0.00182	21.012	0.06072	144.197	0.32244	434.031
0.00341	24.704	0.07862	175.834	0.41674	483.358
0.00540	29.522	0.10241	214.161	0.44472	495.366
0.00877	37.177	0.13438	260.176		
0.01217	44.864	0.17713	312.465		

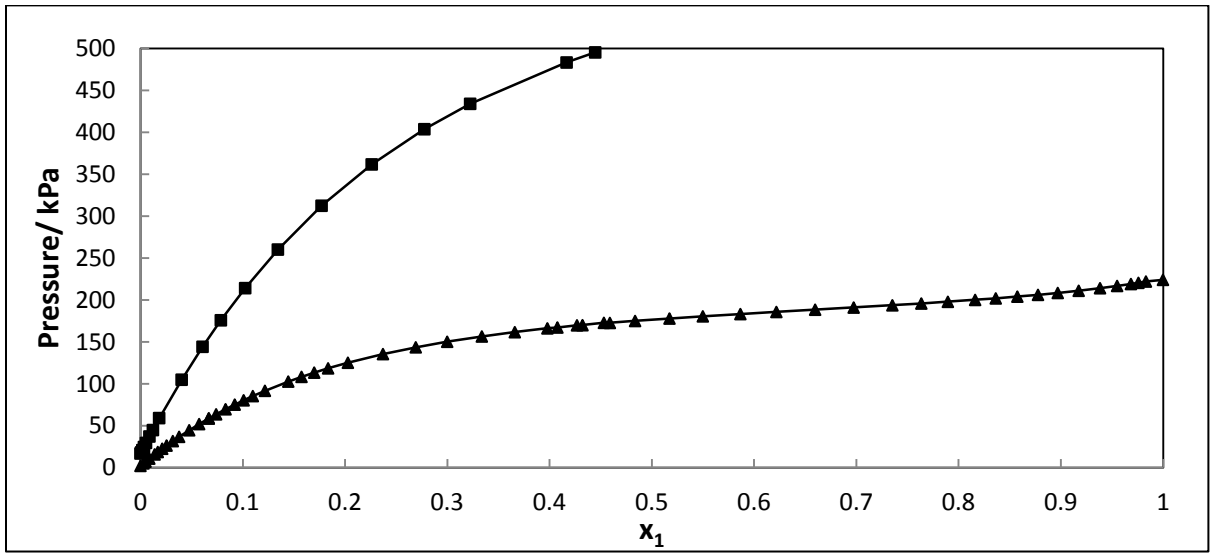

Figure B-1: *P-x* plot for the 1-hexene (1) + NMP (2) system at 413.15 K and 363.15 K. -■-, P-x at 413.15 K (Fischer and Gmehling, 1996); -▲-, P-x at 363.15 K (Fischer and Gmehling, 1996).

Table B-4 to B-6 including Figures B-2 to B-4 reflect the data of Hirawan (2007), measured on a low pressure VLE apparatus for the system 1-hexene + NMP.

Table B-4: Vapour-liquid equilibrium for the 1-hexene (1) + NMP (2) system at 313.15 K (Hirawan, 2007).

Pressure/ mbar	x_1	y_1	Pressure/ mbar	x_1	y_1
1.31	0.000	0.000	407.61	0.666	0.998
303.17	0.212	0.996	420.68	0.811	0.998
332.82	0.295	0.996	434.77	0.948	0.998
375.22	0.468	0.997	450.07	1.000	1.000
390.45	0.543	0.997			

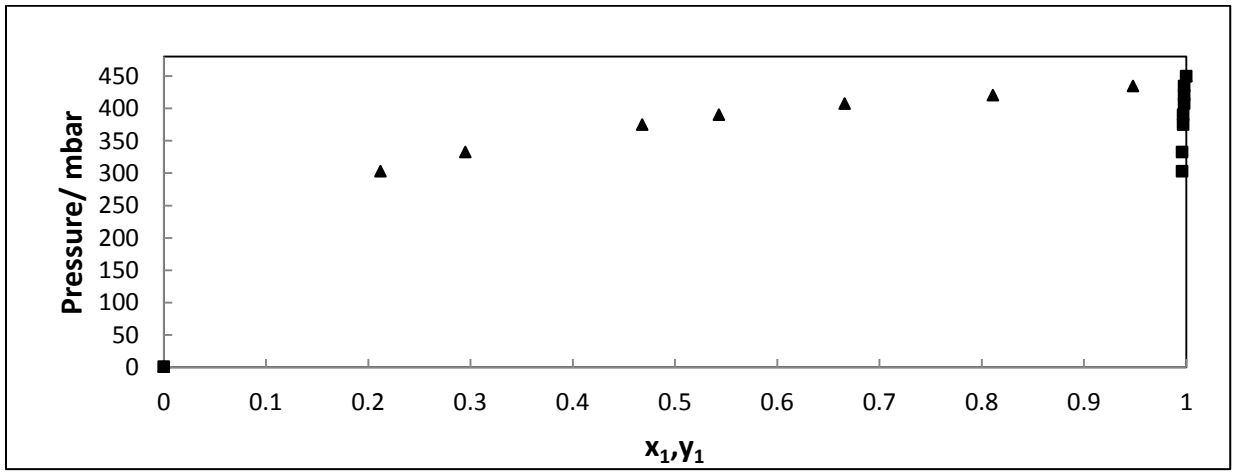

Figure B-2: *P-x-y* plot for the 1-hexene (1) + NMP (2) system at 313.15 K. -▲-, P-x (Hirawan, 2007);-■-, P-y (Hirawan, 2007).

Table B-5: Vapour-liquid equilibrium for the 1-hexene (1) + NMP (2) system at 335.15 K (Hirawan, 2007).

Pressure/ mbar	x_1	y_1	Pressure/ mbar	x_1	y_1
5.10	0.000	0.000	906.521	0.715	0.999
392.12	0.103	0.990	908.845	0.729	0.996
449.18	0.129	0.991	910.265	0.748	0.994
560.26	0.202	0.991	913.584	0.762	0.996
672.35	0.309	0.991	915.760	0.783	0.992
738.42	0.384	0.992	919.581	0.819	0.995
817.48	0.502	0.992	922.432	0.845	0.996
853.53	0.578	0.993	924.585	0.881	0.997
863.54	0.590	0.991	928.592	0.896	0.997
869.55	0.607	0.994	934.608	0.935	0.998
882.56	0.650	0.994	952.616	0.989	0.998
900.58	0.695	0.999	965.628	1.000	1.000

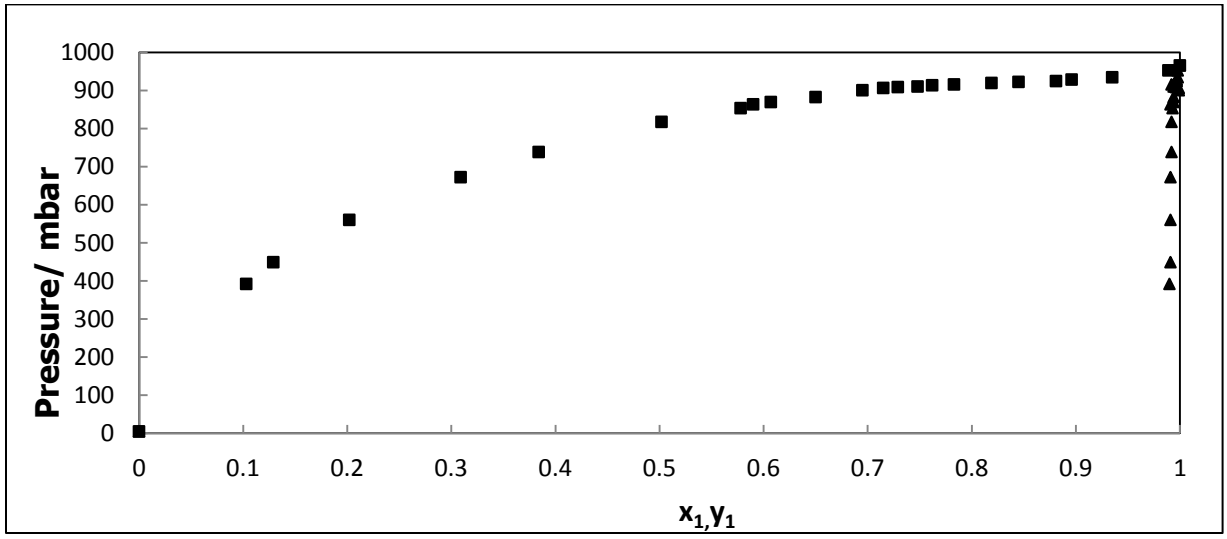

Figure B-3*: P-x-y* plot for the 1-hexene (1) + NMP (2) System at 335.15 K. -■-, P-x (Hirawan, 2007)-▲-, P-y (Hirawan, 2007).

Table B-6: Vapour-liquid equilibrium for the 1-hexene (1) + NMP (2) system at 363.15 K (Hirawan, 2007).

Pressure/ mbar	x_1	y_1
21.78	0.000	0.000
138.89	0.013	0.845
256.99	0.027	0.915
352.01	0.038	0.941
544.09	0.064	0.969
719.41	0.091	0.971
853.00	0.110	0.978
962.63	0.133	0.980
2185.87	1.000	1.000

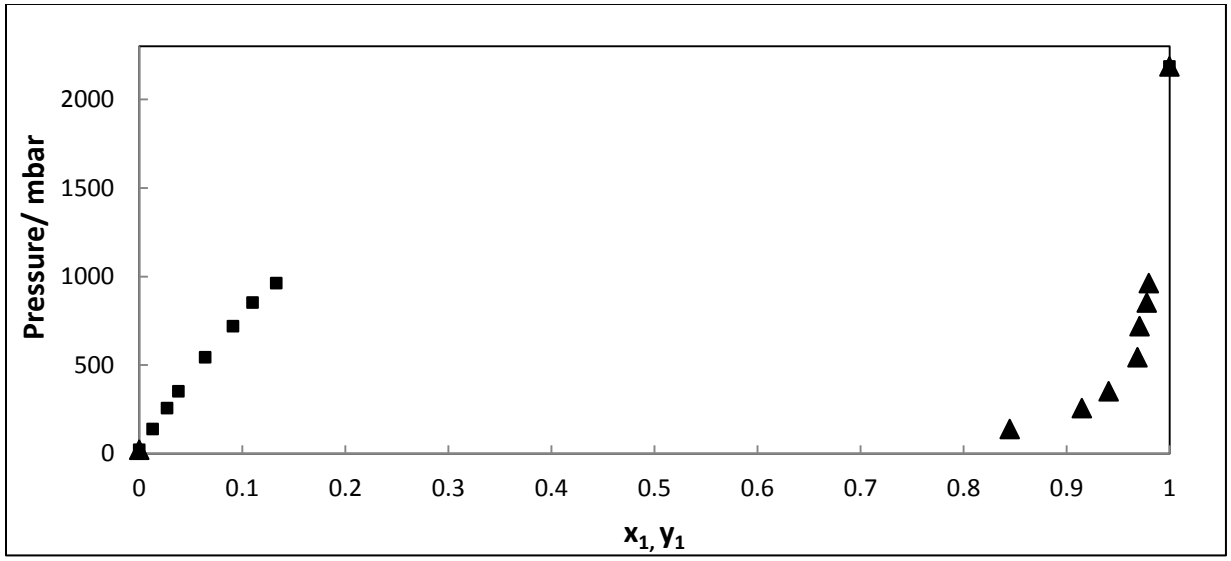

Figure B-4: *P-x-y* plot for the 1-hexene (1) + NMP (2) system at363.15 K. -■-, P-x (Hirawan, 2007)-▲-, P-y (Hirawan, 2007).

B.3. 1-Hexene (1) + n-Hexane (2)

The following data for the system 1-hexene (1) + n-hexane (2) was measured by Moodley (2009) on a stainless - steel high pressure VLE recirculating still. The temperatures at which measurements were carried out were: 328.15, 353.15 and 378.15 K.

Table B-7: Vapour-liquid equilibrium for the 1-hexene (1) + n-hexane (2) system at 328.15 K (Moodley, 2009).

Pressure/ kPa	x_1	y_1
64.46	0.000	0.000
65.06	0.039	0.047
65.36	0.068	0.08
65.96	0.100	0.117
67.16	0.184	0.208
67.91	0.231	0.261
68.26	0.263	0.298
69.36	0.343	0.381
70.26	0.421	0.452
71.46	0.523	0.559
72.26	0.591	0.627
72.86	0.642	0.667
73.96	0.728	0.759
74.56	0.778	0.803
75.96	0.903	0.918
75.06	0.826	0.845
76.66	1.000	1.000

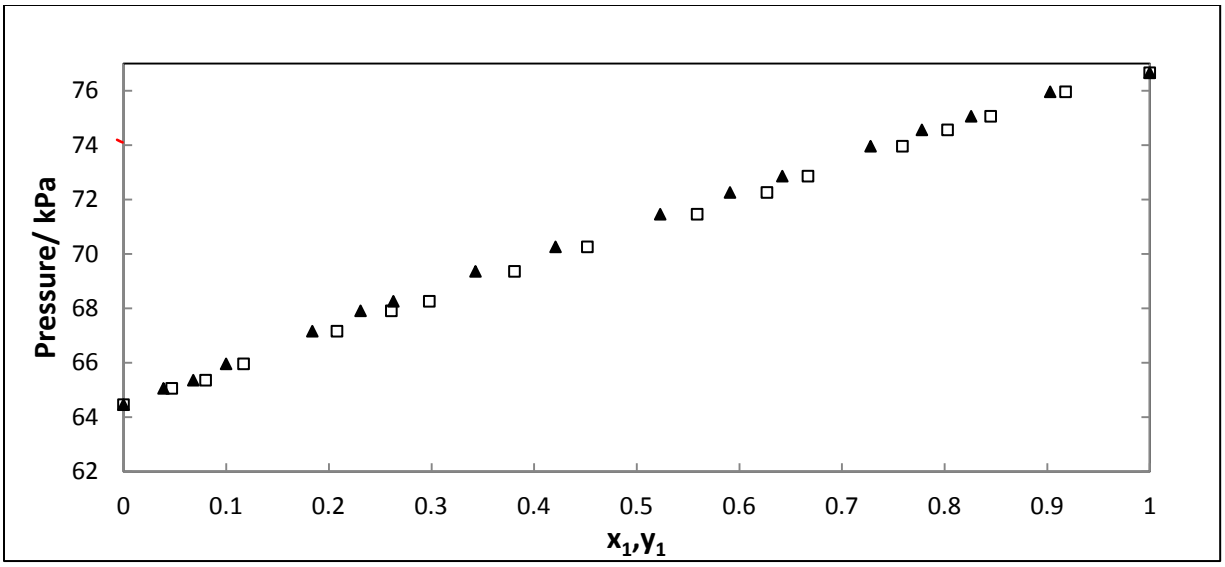

Figure B-5: *P-x-y* plot for the 1-hexene (1) + n-hexane (2) system at328.15 K. -▲-, P-x (Moodley, 2009); -□-, P-y (Moodley, 2009).

Table B-8: Vapour-liquid equilibrium data for the 1-hexene (1) + n-hexane (2) system at 353.15 K (Moodley, 2009).

Pressure/ kPa	x_1	y_1
140.73	0.000	0.000
142.13	0.062	0.070
144.13	0.146	0.156
146.13	0.228	0.246
148.43	0.315	0.334
149.73	0.365	0.381
150.83	0.406	0.426
152.33	0.468	0.493
155.03	0.585	0.613
156.33	0.638	0.663
157.73	0.693	0.718
158.83	0.746	0.76.
162.33	0.896	0.905
164.82	1.000	1.000

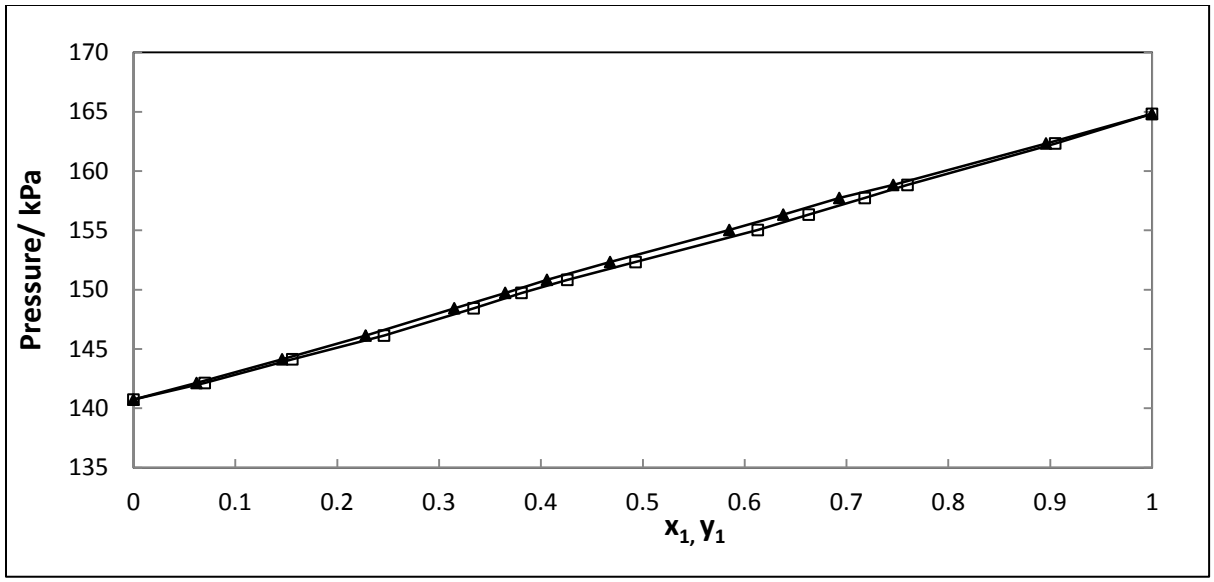

Figure B-6: *P-x-y* plot for the 1-hexene (1) + n-hexane (2) system at 353.15 K. -▲-, P-x (Moodley, 2009); -□-, P-y (Moodley, 2009).

Table B-9: Vapour-liquid equilibrium for the 1-hexene (1) + n-hexane (2) system at 378.15 K (Moodley, 2009).

Pressure/ kPa	x_1	y_1
316.76	1.000	1.000
311.17	0.856	0.861
308.47	0.801	0.809
305.37	0.740	0.746
300.27	0.591	0.603
296.27	0.506	0.513
291.37	0.344	0.359
285.88	0.261	0.274
282.28	0.192	0.205
280.38	0.128	0.139
278.48	0.078	0.085
279.78	0.000	0.000

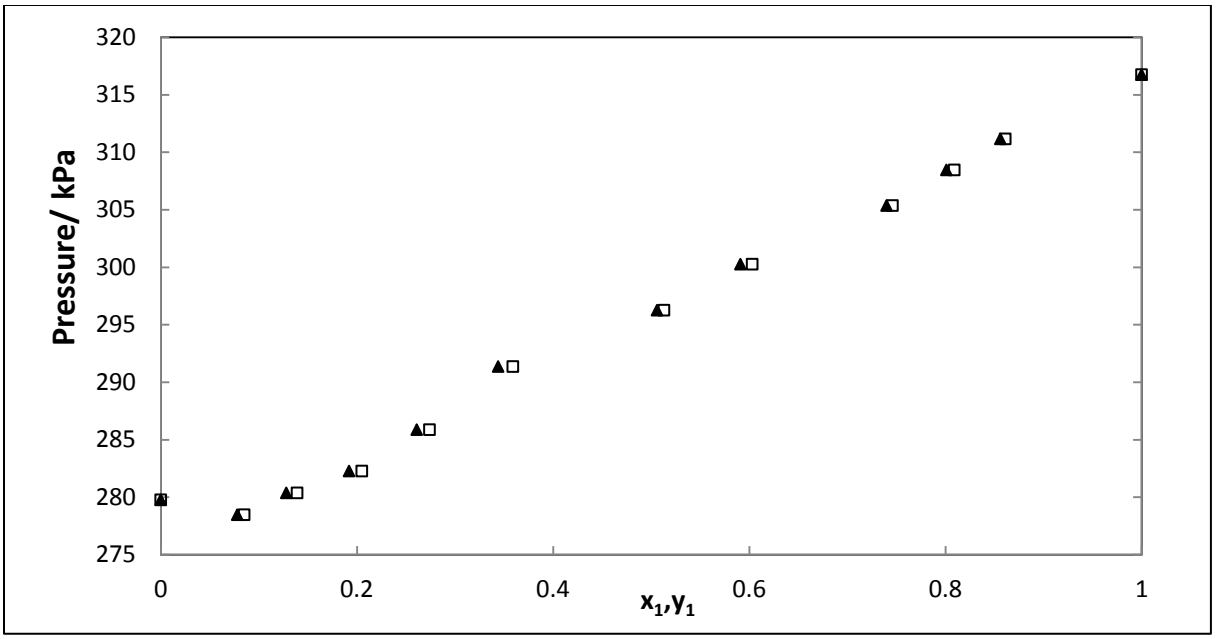

Figure B-7: *P-x-y* plot for the 1-hexene (1) + n-hexane (2) system at 378.15 K. -▲-, P-x (Moodley, 2009); -□-, P-y (Moodley, 2009).

Appendix C: Vapour Pressure Data

The equation used to determine the vapour pressure of the components is the Antoine equation:

$$Ln\,P_i^{sat}(kPa) = A_i + \frac{B_i}{T/^{\circ}C + C_i} \qquad \text{(C-01)}$$

Table C-1: Antoine constants from Poling *et al.* (2001) for vapour pressure.

Component	A	B	C	D	E	P_{min} (bar)	P_{max} (bar)
Ethanol	5.33675	1648.220	230.918	-	-	0	2
	513.92	-8.68587	1.17831	-	-	0	61.32
Cyclohexane	3.93002	1182.774	220.618	-	-	0	2
	3.93002	1182.770	220.618	10.048	-126.96	1.98	40.48
1-hexene	3.98260	1148.620	225.340			0	2
	3.98260	1148.620	225.340	106.260	-3773.6	1.91	26.86
n-hexane	4.00139	1170.875	224.317	-	-	0	2
	507.90	-7.53998	1.83759	-	-	0	30.35

Table C-2: Antoine constants from DDB (2001) for vapour pressure.

Component	A	B	C	T_{min} (˚C)	T_{max} (˚C)
Ethanol	8.20417	1642.89	230.30	-57	80
	7.68117	1332.04	199.2	77	243
Cyclohexane	6.85146	1206.47	223.136	7	81
	7.09926	1380.54	246.526	79	280
1-hexene	6.9641	1207.3	232.154	9	100
	6.81159	1073.08	209.371	62	226
n-hexane	7.011	1246.3	232.99	-95	235
NMP	7.54826	1979.68	222.2	6	206

Table C-3: Antoine vapour pressure constants from Component Plus (2010).

Component	A	B	C	D	E
Ethanol	74.475	-7164.3	-7.327	3.134E-6	2
Cyclohexane	116.51	-7103.3	-15.49	0.016959	1
1-hexene	85.3	-6171.7	-9.702	8.96E-06	2
n-hexane	104.65	-6995.5	-12.702	1.24E-05	2
NMP	67.925	-8438.8	-6.283	3.53E-18	6

Table C-4: Pure component properties from Poling *et al*. (2001).

Component	Mol. Wt/ $g.mol^{-1}$	T_{fp}/ K	T_B/ K	T_C/ K	P_C/ bar	V_C/ $cm^3.mol^{-1}$	$Z_C=\frac{P_cV_C}{RT_c}$	Ω
1-hexene	84.161	133.34	336.63	504.00	31.43	355.10	0.266	0.281
n-hexane	86.177	177.84	341.88	507.60	30.25	368.00	0.264	0.300
Ethanol	46.069	159.05	351.80	513.92	61.48	167.00	0.240	0.649
Cyclohexane	84.161	279.69	353.93	553.50	40.73	308.00	0.273	0.211

Table C-5: Pure component properties from DDB (2011).

Component	Mol. Wt/ $g.mol^{-1}$	T_{fp}/ K	T_B/ K	T_C/ K	P_C/ bar	V_C/ $cm^3.mol^{-1}$	$Z_C=\frac{P_cV_C}{RT_c}$	Ω
1-hexene	84.1613	133.39	336.63	504.03	30.989	354	0.265	0.280
n-hexane	86.1772	177.83	341.88	507.60	29.854	371	0.266	0.301
NMP	99.1326	249.15	477.42	721.8	47.175	310	0.247	0.395

Appendix D: Reporting Uncertainty

Uncertainty is an important aspect that needs to be quantified in order to give an indication of the accuracy of the measurements carried out. It thus provides a range wherein the true measured value resides. According to the NIST standard of computing uncertainty (Taylor B.N. and Kuyatt, C.E., 1994) the standard equation representing uncertainty is:

$$u_c(\vartheta) = \pm\sqrt{\sum_i u_i(\vartheta)^2} \tag{D-01}$$

The symbol „ϑ" refers to the quantity being evaluated for uncertainty. The nature of the quantity „ϑ" is not relevant, as the above equation is standard to the calculation of uncertainty for different quantities across the board. The above equation takes into consideration all the sources of error, ranging from calibration to the measuring instruments being used. For this specific study, the uncertainties are to be computed for pressure, temperature and composition.

D.1. Pressure and Temperature Uncertainty:

The following equation is a standard representation of how to calculate uncertainty for pressure and temperature:

$$u_c(T) = \pm\sqrt{u_{calib}(T)^2 + u_{rep}(T)^2} \tag{D-02}$$

calib = calibration
rep = repeatability

These uncertainties come about due to errors in calibration and from the use of the equipment used to measure the system properties.

The upper and lower limit of uncertainty derived for the temperature function is obtained from the calibration plot, where one may clearly observe the deviation from the set point temperature.

In calculating the uncertainty, we are assuming that the temperature will always fall in the range estimated. Since the uncertainty is calculated based on this approach, it is referred to as Type B (random) uncertainty.

The following equation gives an indication of the rectangular distribution using the random approach:

$$u_{calib}(T) = \frac{b}{\sqrt{3}} \tag{D-03}$$

„b" is the error quantity and is the average of the length between the upper and lower limit of the uncertainty in temperature.

During the sampling of the vapour and liquid, the temperature and pressure at that precise moment is never the same, therefore, uncertainty in the repeatability of measurements must be calculated. The behavior with respect to the repeatability in measurements is known as a Gaussian type of distribution. This is due to the assumption that the measurements are anticipated to fall close to the mean and statistical sciences are utilized to analyse the data set. As such, this is referred to as a systematic uncertainty or *type A* evaluation

This is executed as follows:

$$u_{rep}(T) = \frac{\sigma}{\sqrt{n}} = \sqrt{\frac{1}{n(n-1)}\sum_{i=1}^{n}\left(T_i - \overline{T}\right)^2} \tag{D-04}$$

n is the number of duplicated measurements

D.2. Molar Composition Uncertainty:

Quantifying the uncertainty resulting from molar composition is paramount due to inaccuracies that occur from the GC calibration as well as the averaging of the areas obtained during sampling. The means for computing this uncertainty is parallel to the equation used for determining pressure and temperature uncertainty:

$$u_c(x_i) = \pm\sqrt{u_{calib}(x_i)^2 + u_{rep}(x_i)^2} \tag{D-05}$$

„*i*" represents component *i*.

It must be acknowledged that in quantifying the uncertainty for a specific component (*i.e.* composition), u(θ), the measurement of other quantities, α_i is necessary. As such, the uncertainty in θ can only be accurately represented by measuring the uncertainty arising from the other measurements, α_i. Thus, the root-sum-squared uncertainty is as follows:

$$\theta = f(\alpha_1, \alpha_2, ..., \alpha_n) \tag{D-06}$$

$$u(\theta) = \sqrt{\left[\left(\frac{\partial\theta}{\partial\alpha_1}\right)_{\alpha_i \neq 1} u(\alpha_1)\right]^2 + \left[\left(\frac{\partial\theta}{\partial\alpha_2}\right)_{\alpha_i \neq 2} u(\alpha_2)\right]^2 + \ldots + \left[\left(\frac{\partial\theta}{\partial\alpha_n}\right)_{\alpha_i \neq n} u(\alpha_n)\right]^2} \tag{D-07}$$

During the preparation of standard solutions, certain errors will come about due to the scale (balance) being used to weigh the samples. As such this factor is accounted for and represented by the symbol „*B*" in the following equation:

$$u_{calib}(x_i) = \sqrt{u_B(x_i)^2 + u_{corr}(x_i)^2} \tag{D-08}$$

„x_i" is dependent on the masses of the constituent components making up the system, consequently, the mole fractions may be expressed in terms of masses of the species involved as follows:

$$u_B(x_i) = \sqrt{\left[\left(\frac{\partial x_i}{\partial m_1}\right)_{m2} u(m_1)\right]^2 + \left[\left(\frac{\partial x_i}{\partial m_2}\right)_{m1} u(m_2)\right]^2} \tag{D-09}$$

Using the following basic chemical relationships:

$x_i = \dfrac{n_i}{(n_i + n_j)}$ and $n_i = \dfrac{m_i}{MM_i}$, the above equation may be reduced to:

$$u_B(x_i) = x_1 x_2 \sqrt{\left(\frac{u(m_1)}{m_2}\right)^2 + \left(\frac{u(m_2)}{m_2}\right)^2} \tag{D-10}$$

Appendix E: Results of the Thermodynamic Consistency Tests for All Systems (Regression of Each Isothermal Data Set Individually)

E.1: Thermodynamic Consistency Tests for the System 1-hexene (1) + NMP (2)

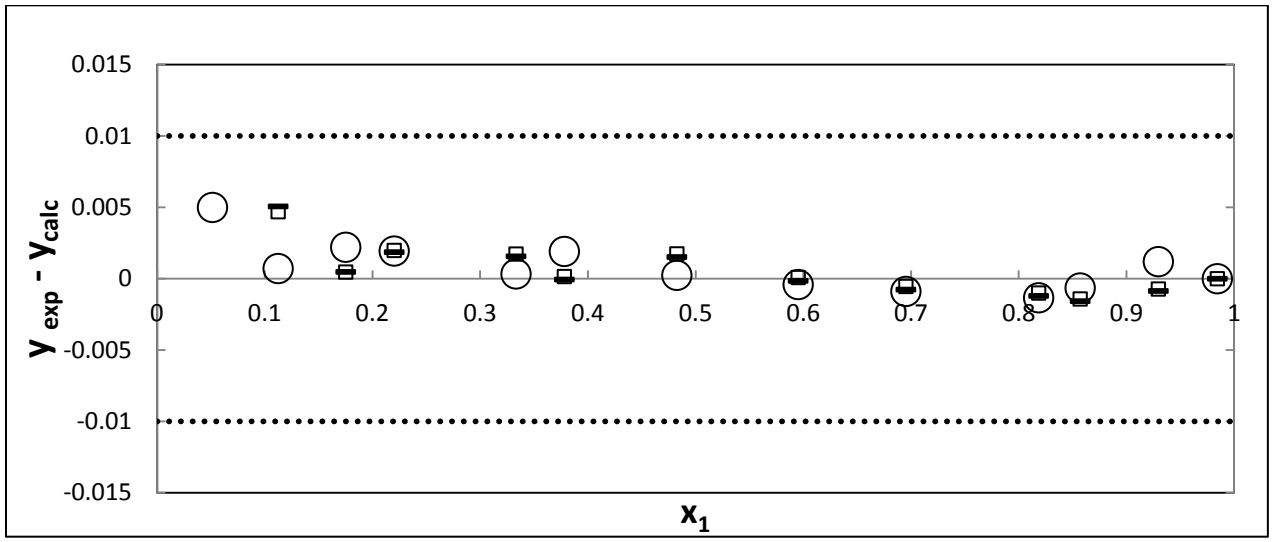

Figure E-1: Point test (varying EoS): Δy_1 for the 1-hexene (1) + NMP (2) system at 343.15 K .○, NRTL-HOC; ▬, NRTL- SRK; □, NRTL-PR.

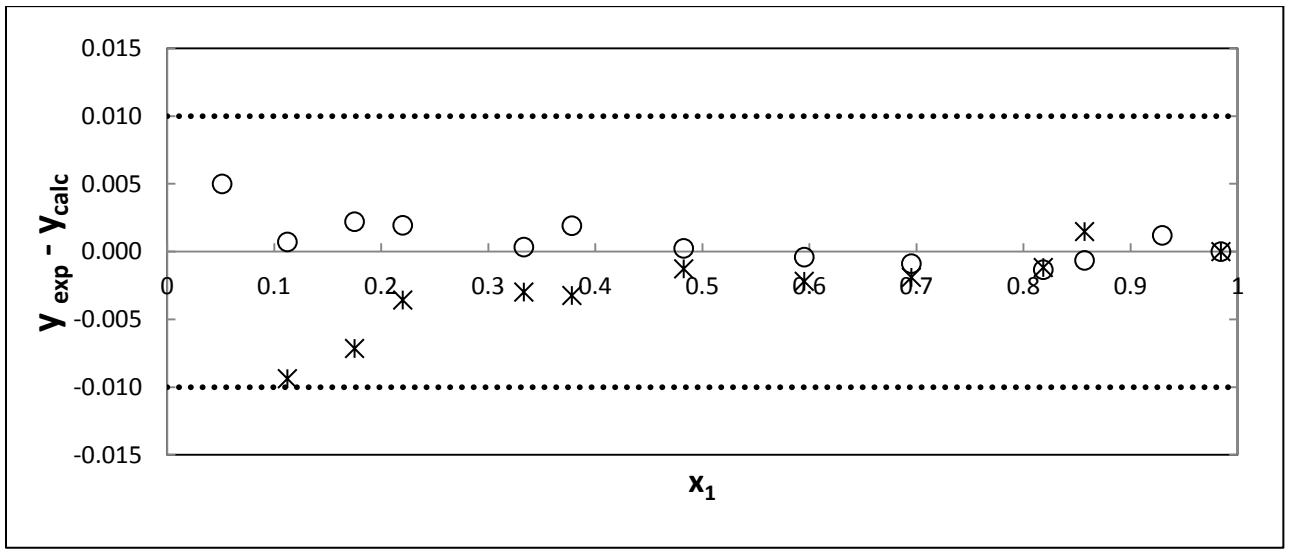

Figure E-2: Point test (varying activity coefficient model): Δy_1 for the 1-hexene (1) + NMP (2) system at 343.15 K. ○, NRTL-HOC; ж, UNIQUAC-HOC.

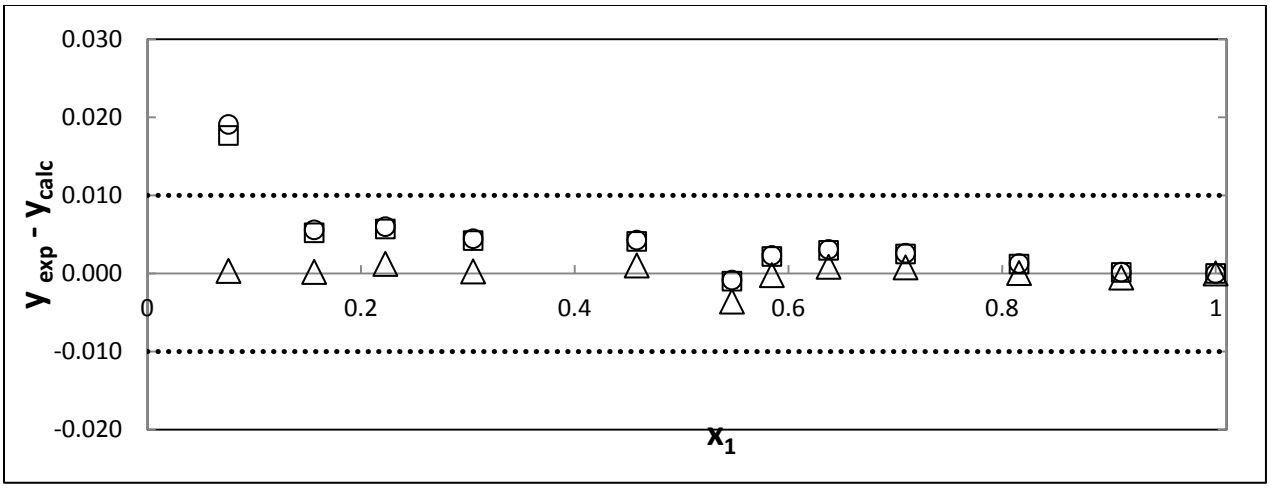

Figure E-3: Point test (varying EoS): Δy_1 for the 1-hexene (1) + NMP (2) system at 353.15 K. ○, NRTL-HOC; Δ, NRTL-PR-WS; □, NRTL-PR.

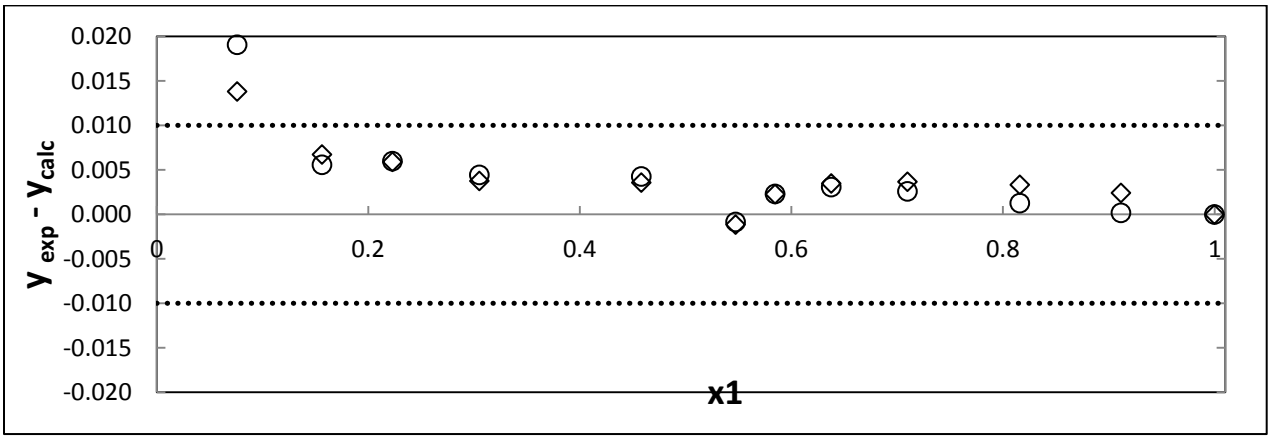

Figure E-4: Point test (varying activity coefficient model): Δy_1 for the 1-hexene (1) + NMP (2) system at 353.15 K. ○, NRTL-HOC; ◊, UNIQUAC-HOC.

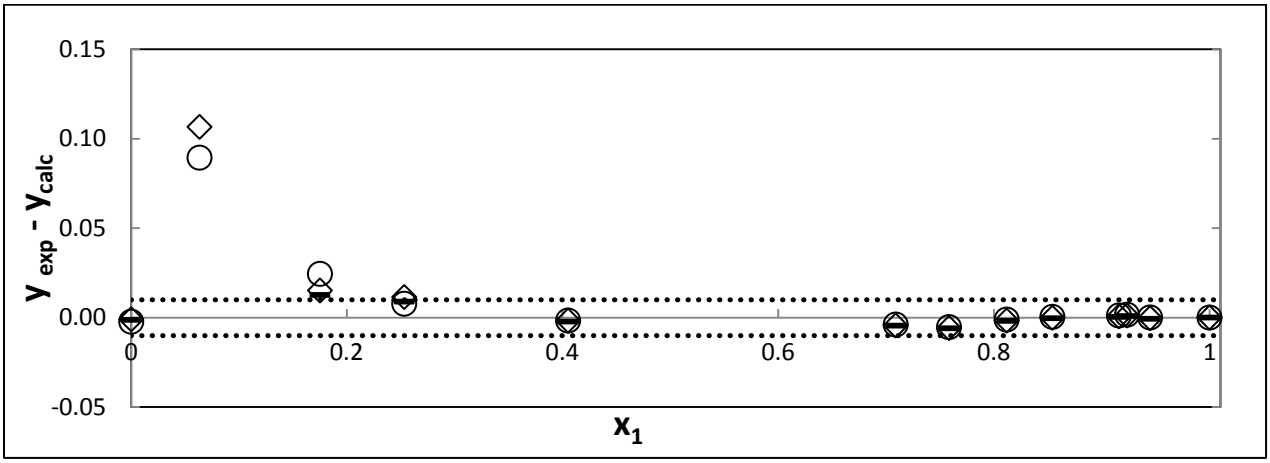

Figure E-5: Point test (varying EoS): Δy_1 for the 1-hexene (1) + NMP (2) system at 363.15 K. ◊, NRTL-HOC; –, NRTL- SRK; ○, NRTL-PR-WS.

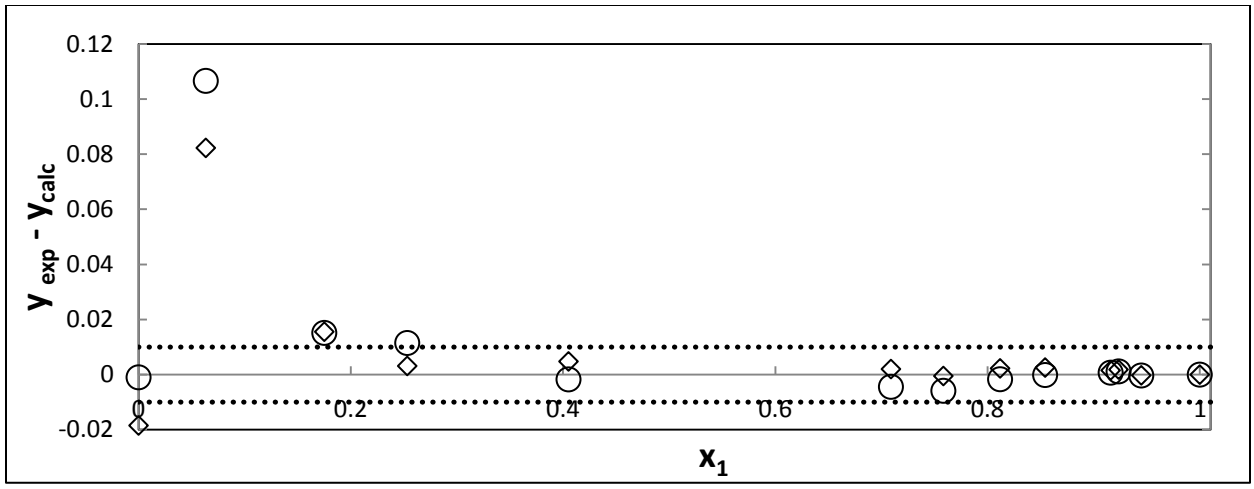

Figure E-6: Point test (varying activity coefficient model): Δy_1 for the 1-hexene (1) + NMP (2) system at 363.15 K. ○, NRTL-HOC; ◊, UNIQUAC-HOC.

E.2: Thermodynamic Consistency Tests for the System n-hexane (1) + NMP (2)

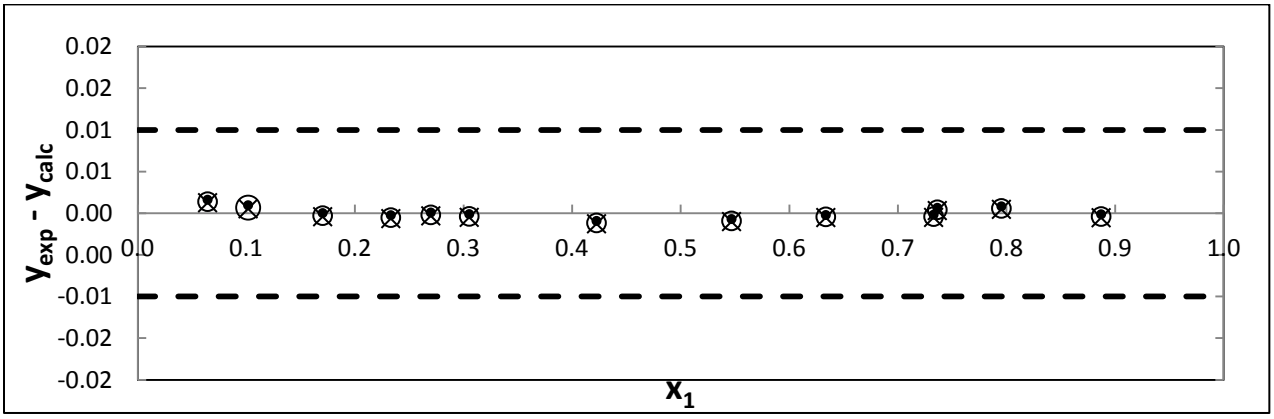

Figure E-7: Point test (varying EoS): Δy_1 for the n-hexane (1) + NMP (2) system at 353.15 K. ○, NRTL-HOC; •, NRTL-SRK-WS; X, NRTL-PR.

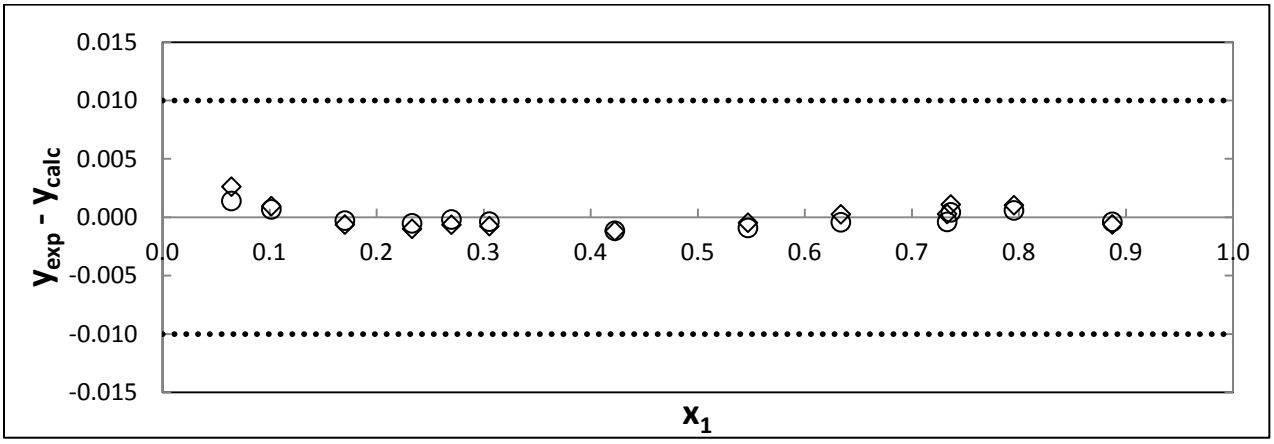

Figure E-8: Point test (varying activity coefficient model): Δy_1 for the n-hexane (1) + NMP (2) system at 353.15 K. ○, NRTL-HOC; ◊, UNIQUAC-HOC.

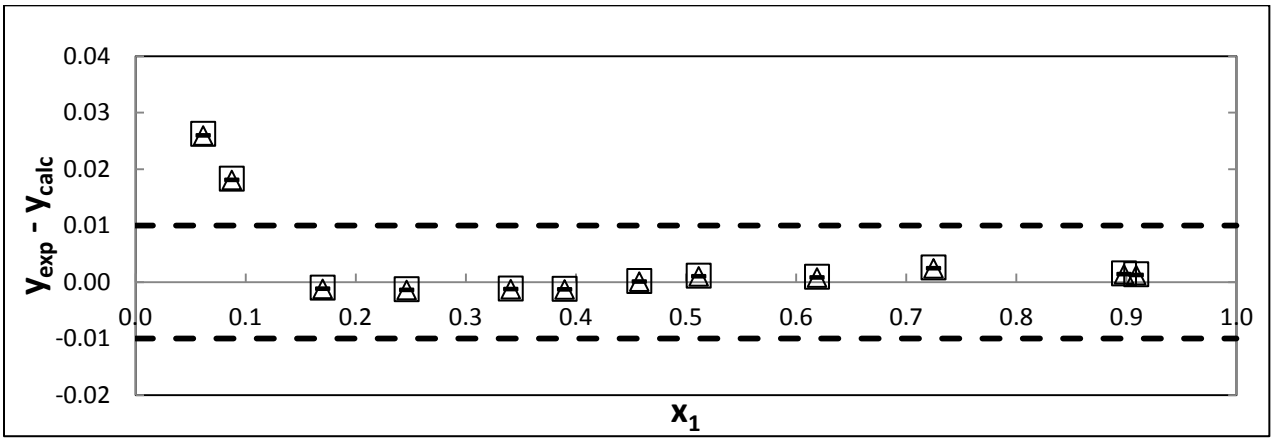

Figure E-9: Point test (varying EoS): Δy_1 for the n-hexane (1) + NMP (2) system at 363.15 K. □, NRTL-HOC; Δ, NRTL- SRK; —, NRTL-PR.

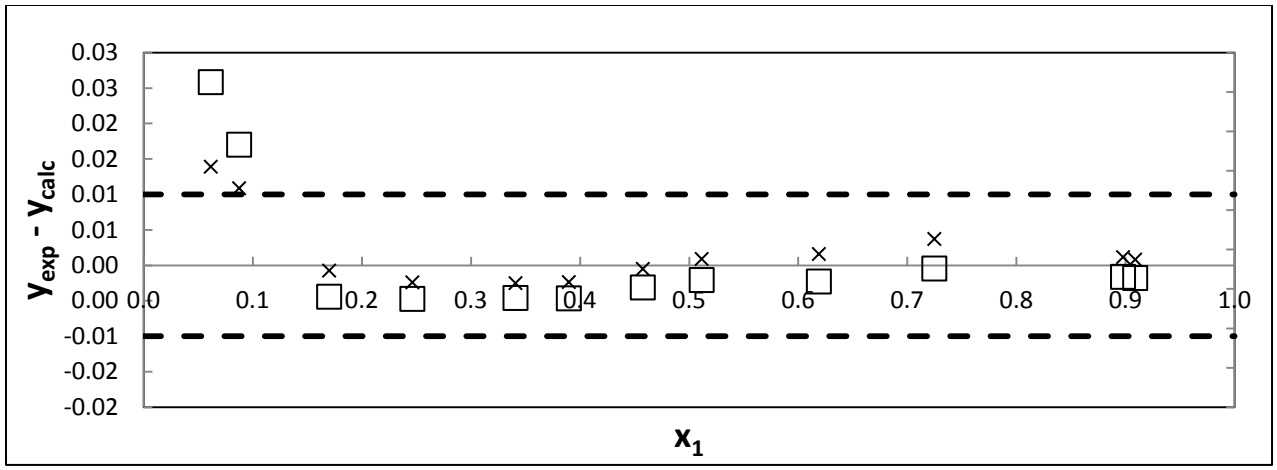

Figure E-10: Point test (varying activity coefficient model): Δy_1 for the n-hexane (1) + NMP (2) system at 363.15 K. □, NRTL-HOC; X, UNIQUAC-HOC.

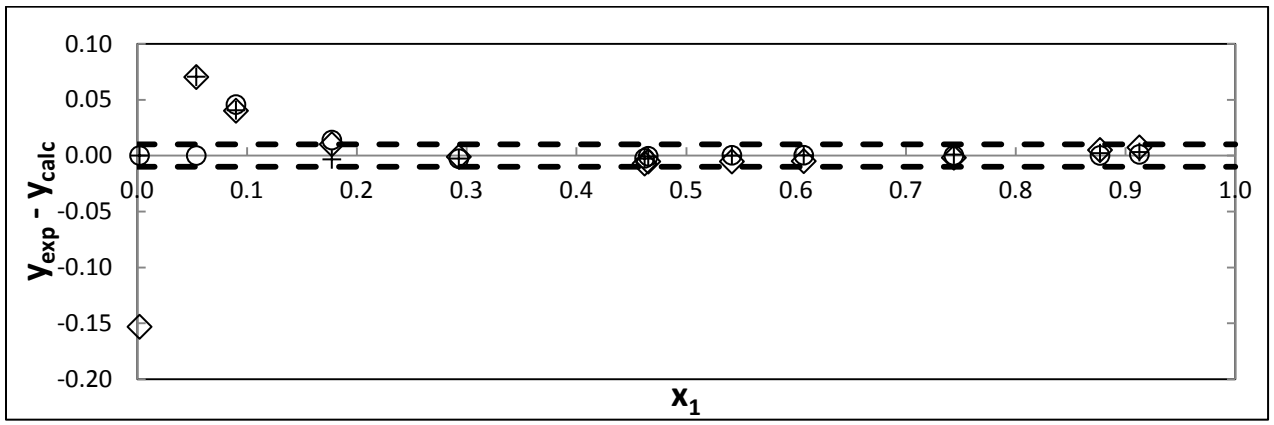

Figure E-11: Point test (varying EoS): Δy_1 for the n-hexane (1) + NMP (2) system at 378.15 K. ◊, NRTL-HOC; ○, NRTL-PR-WS; +, NRTL-SRK-WS.

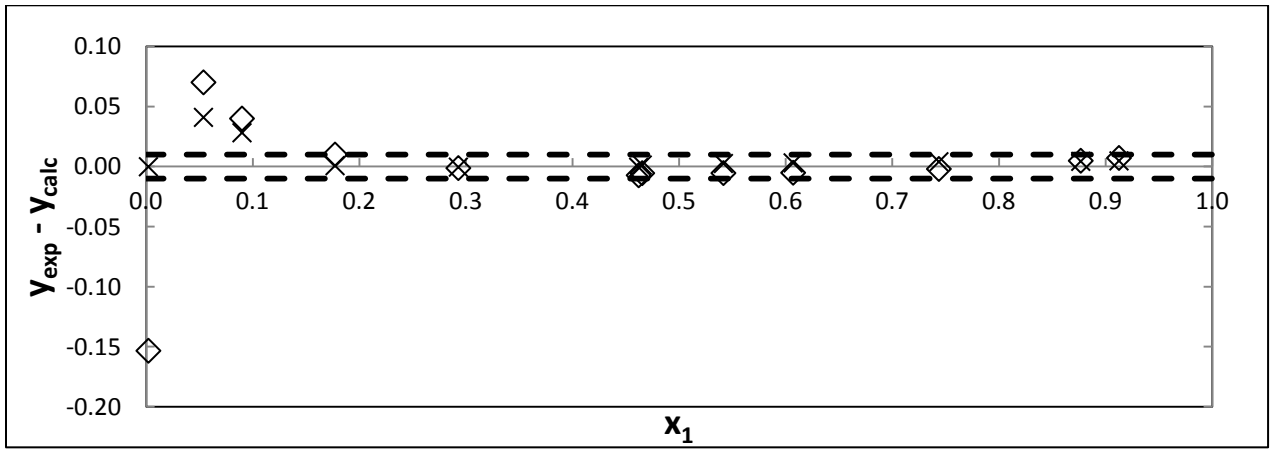

Figure E-12: Point test (varying activity coefficient model): Δy_1 for the n-hexane (1) + NMP (2) system at 378.15 K. ◊, NRTL-HOC; ×, UNIQUAC-HOC.

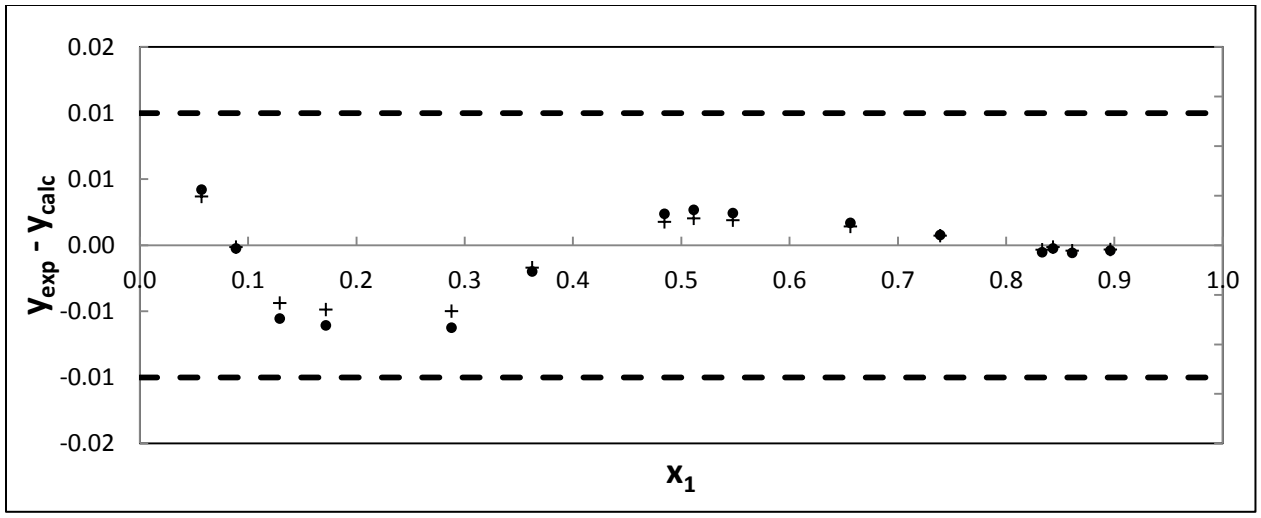

Figure E-13: Point test (varying EoS): Δy_1 for the n-hexane (1) + NMP (2) system at 383.15 K. +, NRTL- SRK-WS; •, NRTL-PR-WS.

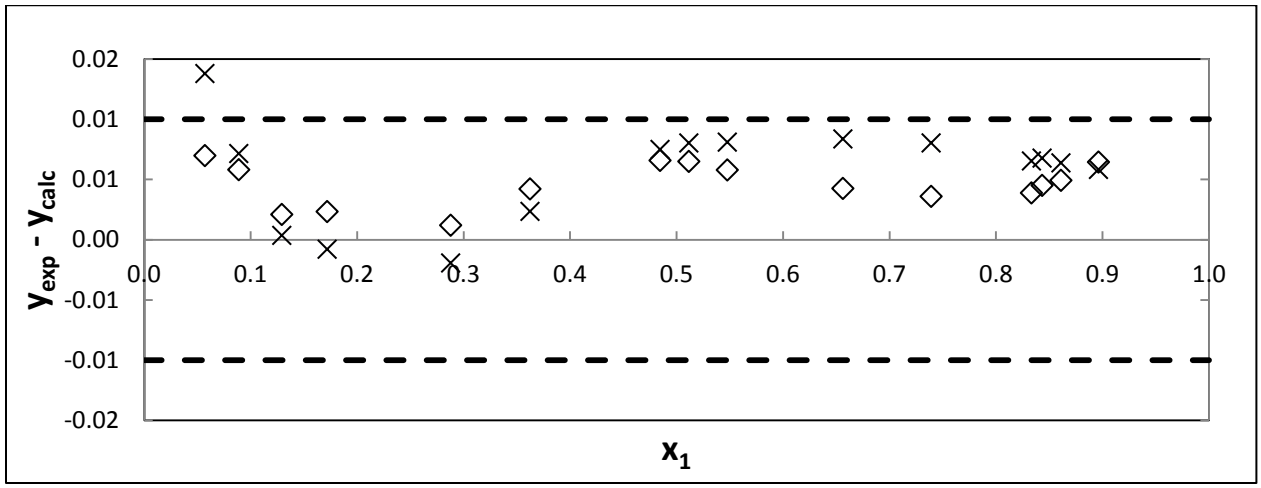

Figure E-14: Point test (varying activity coefficient model): Δy_1 for the n-hexane (1) + NMP (2) system at 383.15 K. ◊, NRTL-HOC; X, UNIQUAC-HOC.

E.3: Thermodynamic Consistency Tests for the System 1-Hexene (1) + n-Hexane (2)

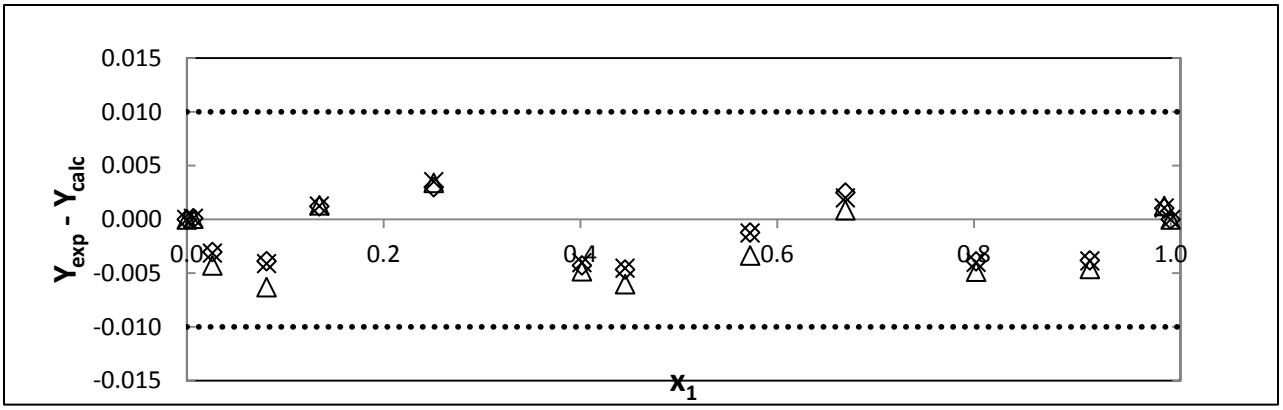

Figure E-15: Point test (varying EoS): Δy_1 for the 1-hexene (1) + n-hexane (2) system at 343.15 K. X NRTL-PR-WS; Δ, NRTL-Ideal; ◊, NRTL-SRK-WS.

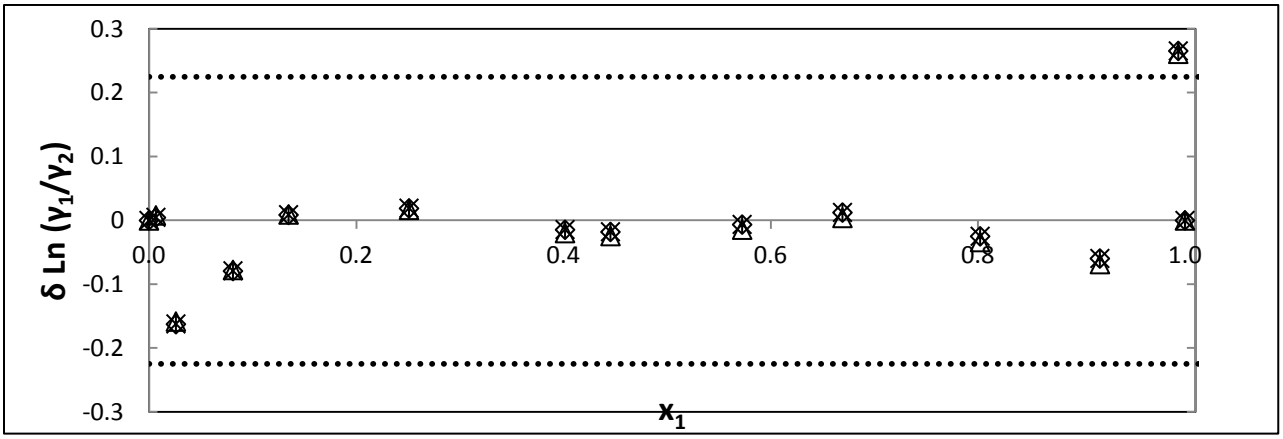

Figure E-16: Direct test (varying EoS): δ Ln (Υ1/Υ2) for the 1-hexene (1) + n-hexane (2) system at 343.15 K. ◊, NRTL-SRK-WS; ✕, NRTL-PR-WS; Δ, NRTL-Ideal.

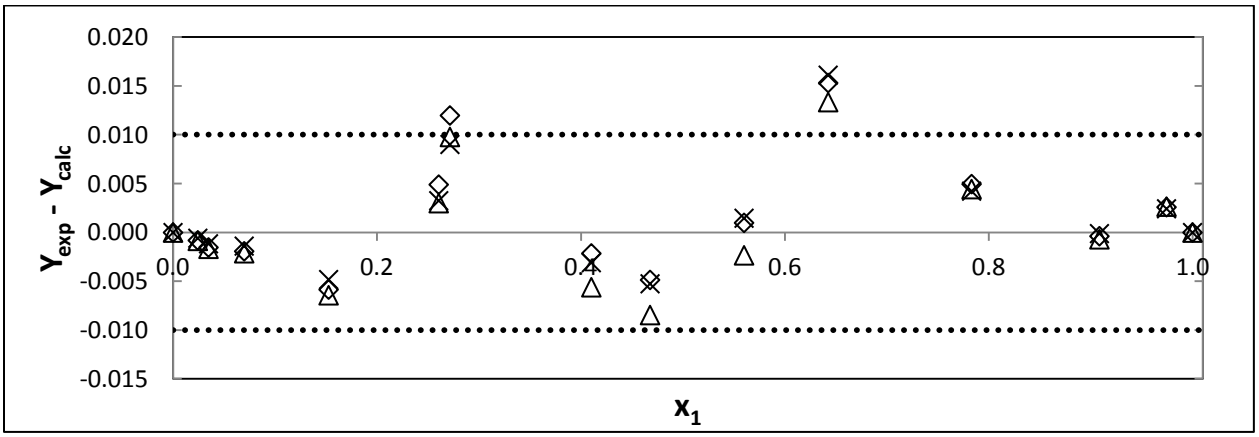

Figure E-17: Point test (varying EoS): Δy_1 for the 1-hexene (1) + n-hexane (2) system at 363.15 K. X NRTL-PR-WS; Δ, NRTL-Ideal; ◊, NRTL-SRK-WS.

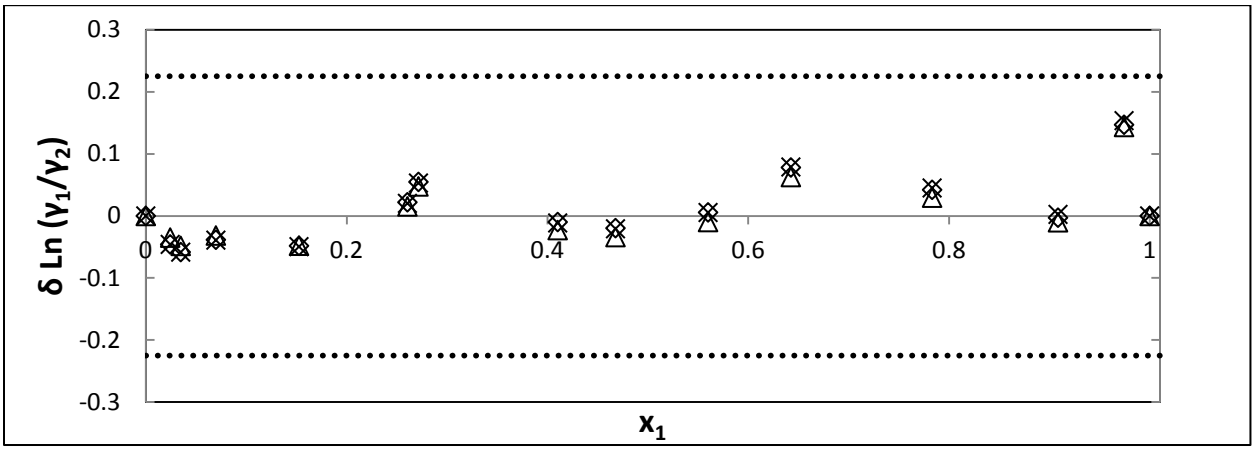

Figure E-18: Direct test (varying EoS): δ Ln (γ1/γ2) for the 1-hexene (1) + n-hexane (2) system at 363.15 K. ◊, NRTL-SRK-WS; ×, NRTL-PR-WS; Δ, NRTL-Ideal.

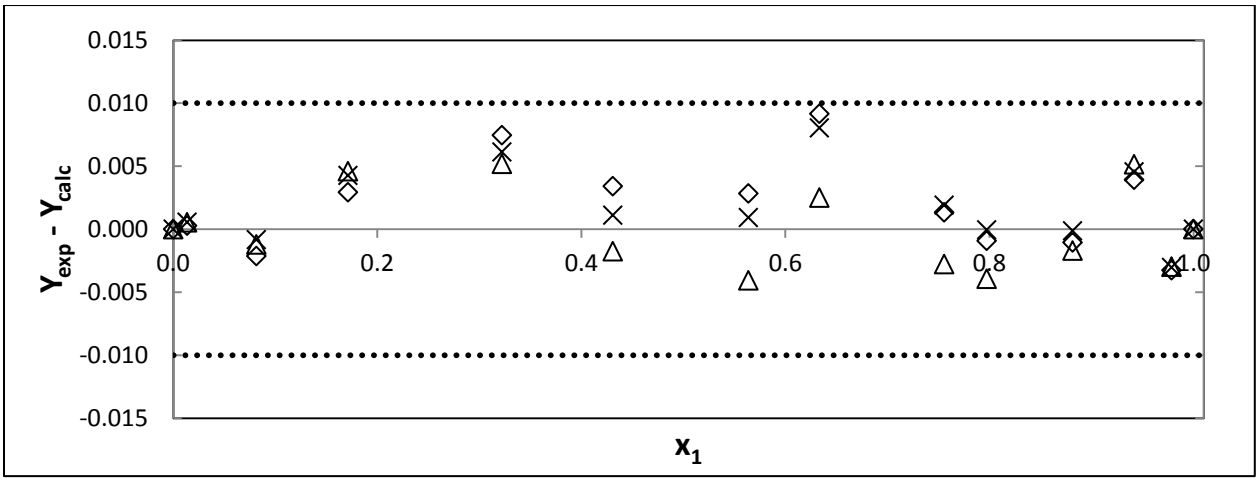

Figure E-19: Point test (varying EoS): Δy_1 for the 1-hexene (1) + n-hexane (2) system at 373.15 K. X NRTL-PR-WS; Δ, NRTL-Ideal; ◊, NRTL-SRK-WS.

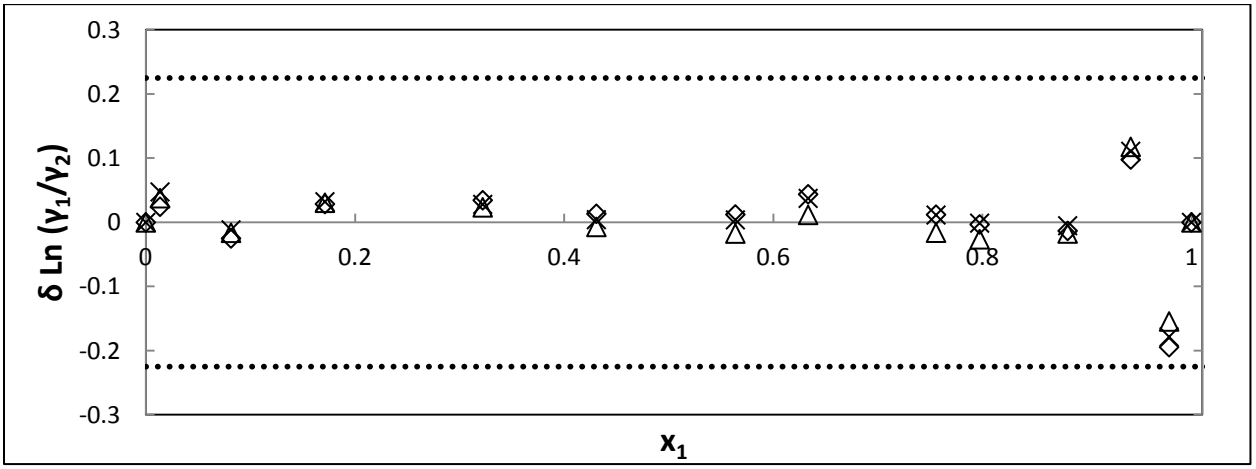

Figure E-20: Direct test (varying EoS): δ Ln (γ1/γ2) for the 1-hexene (1) + n-hexane (2) system at 373.15 K. ◊, NRTL-SRK-WS; X, NRTL-PR-WS; Δ, NRTL-Ideal.

Appendix F: Modeling Systems with Fixed NRTL α_{ij} Parameter (Fischer and Gmehling, 1996)

F.1 System: n-Hexane (1) +NMP (2), α_{ij} = 0.4163 (Fischer and Gmehling, 1996)

Table F-1: Model analysis and consistency test results for the n-hexane (1) + NMP (2) system at 353.15 K.

Pressure/ kPa	x_1	y_1	NRTL-HOC	NRTL-SRK-WS	NRTL-PR-WS	NRTL-SRK	NRTL-PR
133.88	0.8873	0.9923					
130.48	0.7955	0.9919					
129.88	0.7364	0.9914					
128.57	0.7330	0.9906					
127.30	0.6337	0.9905					
126.18	0.5469	0.9900					
124.41	0.4226	0.9895					
119.47	0.3054	0.9896					
116.81	0.2700	0.9894					
111.35	0.2331	0.9885					
100.46	0.1704	0.9869					
75.31	0.1017	0.9834					
52.18	0.0644	0.9784					
Point test results using all data points							
Data points used			13	13	13	13	13
ΔP_{AAD} (kPa)			0.0017	0.0017	0.0024	0.0017	0.0017
ΔY_{AAD}			0.0005	0.0005	0.0006	0.0006	0.0006
AE(%)			0.00031	0.00031	0.00061	0.00033	0.00033

N.B: an '*' in a certain column indicates that that point was excluded from the final regression analysis.

Table F-2: Model analysis and consistency test results for the n-hexane (1) + NMP (2) system at 363.15 K.

Pressure/ kPa	x_1	y_1	NRTL-HOC	NRTL-SRK-WS	NRTL-PR-WS	NRTL-SRK	NRTL-PR
179.38	0.9090	0.9933					
177.43	0.8978	0.9932					
173.00	0.7248	0.9923					
166.74	0.6190	0.9902					
165.43	0.5116	0.9896					
163.72	0.4576	0.9882					
161.41	0.3898	0.9860					
156.98	0.3409	0.9855					
144.99	0.2463	0.9838					
126.98	0.1700	0.9819					
86.51	0.0875	0.9764					
65.12	0.0615	0.9671					
1.956	0.0003	0.0004	*	*	*	*	*
Point test results using all data points							
Total data points			13	13	13	13	13
ΔP_{AAD} (kPa)			0.0123	0.0123	0.0139	0.0025	0.0123
ΔY_{AAD}			22.7063	22.7249	22.0989	22.7071	22.7270
Point test results using select data points							
Data points used			12	12	12	12	12
ΔP_{AAD} (kPa)			0.0068	0.0039	0.0069	0.0067	0.0067
ΔY_{AAD}			0.0033	0.0025	0.0033	0.0032	0.0033
AE(%)			0.0057	0.0022	0.0059	0.0055	0.0056

N.B: an '*' in a certain column indicates that that point was excluded from the final regression analysis

Table F-3: Model analysis and consistency test results for the n-hexane (1) + NMP (2) system at 378.15 K.

Pressure/ kPa	x_1	y_1	NRTL-HOC	NRTL-SRK-WS	NRTL-PR-WS	NRTL-SRK	NRTL-PR
265.56	0.9127	0.9962					
261.13	0.8769	0.9936					
245.24	0.7438	0.9895					
241.67	0.6070	0.9874					
239.73	0.5416	0.9866					
231.96	0.4654	0.9853					
230.90	0.4621	0.9834					
213.29	0.2929	0.9813					
180.12	0.1773	0.9766					
131.04	0.0900	0.9686					
80.58	0.0538	0.9491					
4.16	0.0022	0.0001	*	*	*	*	*
Point test results using all data points							
Total data points			12	12	12	12	12
ΔP_{AAD} (kPa)			0.0060	0.0254	0.0260	0.0257	0.0258
ΔY_{AAD}			595.0918	599.5323	579.6785	594.6648	595.6520
Point test results using select data points							
Data pointsused			11	11	11	11	11
ΔP_{AAD} (kPa)			0.0163	0.0156	0.0140	0.0162	0.0162
ΔY_{AAD}			0.0083	0.0071	0.0071	0.0082	0.0082
AE(%)			0.0335	0.0294	0.0246	0.0330	0.0330

N.B: an '*' in a certain column indicates that that point was excluded from the final regression analysis

Table F-4: Model analysis and consistency test results for the n-hexane (1) + NMP (2) system at 383.15 K.

Pressure/ kPa	x_1	y_1	NRTL-HOC	NRTL-SRK - WS	NRTL-PR-WS	NRTL-SRK	NRTL-PR
297.74	0.8964	0.9943					
289.90	0.8611	0.9930					
280.00	0.8434	0.9928					
276.81	0.8334	0.9923					
275.79	0.7392	0.9915					
273.16	0.6563	0.9912					
270.02	0.5477	0.9908					
268.77	0.5116	0.9907					
266.81	0.4846	0.9902					
252.48	0.3624	0.9846					
239.99	0.2879	0.9789					
201.06	0.1719	0.9737					
168.15	0.1293	0.9700					
133.51	0.0889	0.9669					
95.19	0.0571	0.9567					
Point test results using all data points							
Total data points			15	15	15	15	15
ΔP_{AAD} (kPa)			0.0034	0.0023	0.0044	0.0031	0.0034
ΔY_{AAD}			0.0057	0.0037	0.0023	0.0055	0.0056
Point test results using select data points							
Data points used			15	15	15	15	15
ΔP_{AAD} (kPa)			0.0034	0.0023	0.0044	0.0031	0.0034
ΔY_{AAD}			0.0057	0.0037	0.0023	0.0055	0.0056
AE(%)			0.0044	0.0019	0.0025	0.0039	0.0043

N.B: an '*' in a certain column indicates that that point was excluded from the final regression analysis.

F.2: System1-Hexene (1) +NMP (2), α_{ij} = 0.4567 (Fischer and Gmehling, 1996)

Table F-5: Model analysis and consistency test results for the 1-Hexene (1) + NMP (2) system at 323.15 K.

Pressure/ kPa	x_1	y_1	NRTL-HOC	NRTL-SRK -WS	NRTL-PR-WS	NRTL-SRK	NRTL-PR
63.55	0.9823	0.9999					
61.30	0.9525	0.9995					
58.29	0.8448	0.9988					
57.50	0.8237	0.9986					
56.81	0.7389	0.9984					
53.63	0.5416	0.9978					
52.59	0.4951	0.9976					
48.35	0.3122	0.9969					
46.30	0.2744	0.9964					
44.47	0.2435	0.9953					
40.29	0.1976	0.9941					
38.26	0.1704	0.9929					
27.99	0.0966	0.9916					
13.32	0.0566	0.9900					
Point test results using all data points							
Total data points			14	14	14	14	14
ΔP_{AAD}(kPa)			0.0105	0.0076	0.0128	0.0086	0.0101
ΔY_{AAD}			0.0014	0.0027	0.0040	0.0012	0.0013
Point test results using select data points							
Data points used			14	14	14	14	14
ΔP_{AAD}(kPa)			0.0105	0.0076	0.0128	0.0086	0.0101
ΔY_{AAD}			0.0014	0.0027	0.0040	0.0012	0.0013
AE(%)			0.0112	0.0065	0.0179	0.0075	0.0104

N.B: an '*' in a certain column indicates that that point was excluded from the final regression analysis.

Table F-6: Model analysis and consistency test results for the 1-Hexene (1) + NMP (2) system at 353.15 K.

Pressure/ kPa	x_1	y_1	NRTL-HOC	NRTL-SRK WS	NRTL-PR-WS	NRTL-SRK	NRTL-PR
169.11	1.0000	1.0000					
157.43	0.9116	0.9982					
147.59	0.8160	0.9978					
141.41	0.7098	0.9977					
137.46	0.6377	0.9974					
134.68	0.5846	0.9961					
132.05	0.5473	0.9926					
129.09	0.4582	0.9968					
115.03	0.3050	0.9949					
100.96	0.2229	0.9945					
83.33	0.1563	0.9909					
50.93	0.0760	0.9813					
1.02	0.0001	0.0075	*	*	*	*	*
Point test results using all data points							
Total data points			13	13	13	13	13
ΔP_{AAD} (kPa)			0.0087	0.0120	0.0251	0.0088	0.0084
ΔY_{AAD}			0.6455	0.3122	0.4924	0.6429	0.6488
Point test results using select data points							
Data points used			12	12	12	12	12
ΔP_{AAD} (kPa)			0.0062	0.0059	0.0177	0.0058	0.0059
ΔY_{AAD}			0.0043	0.0040	0.0063	0.0039	0.0041
AE(%)			0.0057	0.0051	0.0353	0.0049	0.0052

N.B: an '*' in a certain column indicates that that point was excluded from the final regression analysis.

Table F-7: Model analysis and consistency test results for the 1-Hexene (1) + NMP (2) system at 363.15 K.

Pressure/ kPa	x_1	y_1	NRTL-HOC	NRTL-SRK -WS	NRTL-PR-WS	NRTL-SRK	NRTL-PR
224.00	1.0000	1.0000					
212.16	0.9449	0.9980					
210.07	0.9235	0.9996					
208.83	0.9160	0.9990					
201.73	0.8543	0.9984					
197.99	0.8119	0.9969					
191.81	0.7584	0.9928					
188.27	0.7090	0.9941					
161.62	0.4052	0.9900					
134.24	0.2533	0.9832					
116.07	0.1751	0.9765		*	*		
51.57	0.0635	0.9639		*	*		
2.06	0.0087	0.0810	*	*	*	*	*
2.02	0.0001	0.0000	*			*	*
Point test results using all data points							
Total data points			14	14	14	14	14
ΔP_{AAD} (kPa)			0.0279	0.0357	0.0357	0.0275	0.0277
ΔY_{AAD}			49.5327	23.7530	23.7187	48.7068	49.7390
Point test results using select data points							
Data points used			12	11	11	12	12
ΔP_{AAD} (kPa)			0.0250	0.0246	0.0278	0.0190	0.0241
ΔY_{AAD}			0.0101	18.8520	25.9225	0.0092	0.0097
AE(%)			0.07270	35539	67197	0.04456	0.06749

N.B: an '*' in a certain column indicates that that point was excluded from the final regression analysis.

Appendix G: Thermodynamic Binary Interaction Parameters and Plots for All Systems

G.1: Tabulated Binary Interaction Parameters for all Measured Systems

Table G-1: Summary of binary interaction parameters for the system 1-hexene + NMP .

	T = 323.15 K	T = 343.15 K	T = 353.15 K	T = 363.15 K
NRTL - HOC				
$g_{12} - g_{22}$ (J.mol^{-1})	2297.84	83518.98	249420.00	249420.00
$g_{21} - g_{11}$ (J.mol^{-1})	2357.13	3078.91	-151010.00	-195386.13
α_{IJ}	0.0340	0.1386	0.0015	0.0034
NRTL-RKS-WS				
$g_{12} - g_{22}$ (J.mol^{-1})	2477.99	81916.87	9309.80	-2773.70
$g_{21} - g_{11}$ (J.mol^{-1})	2033.92	2833.46	-4532.39	5354.80
α_{IJ}	0.0399	0.1402	0.0050	0.0000
k_{ij}	8.6016	-0.9123	5.2050	1.7325
NRTL-PR-WS				
$g_{12} - g_{22}$ (J.mol^{-1})	225250.09	27917.09	221028.03	249420.00
$g_{21} - g_{11}$ (J.mol^{-1})	-215364.33	2813.99	-214534.36	-198858.47
α_{IJ}	0.0003	0.2707	0.0001	0.0031
k_{ij}	9.2224	-0.3826	5.5145	-0.8024
NRTL-RKS				
$g_{12} - g_{22}$ (J.mol^{-1})	-234136.66	81288.82	4798.43	249420.00
$g_{21} - g_{11}$ (J.mol^{-1})	249420.00	2821.41	2411.20	-196998.94
α_{IJ}	0.0005	0.140	0.546	0.0033
NRTL-PR				
$g_{12} - g_{22}$ (J.mol^{-1})	72954.27	82747.60	249420.00	249420.00
$g_{21} - g_{11}$ (J.mol^{-1})	--67779.62	3040.96	4150.60	-195608.48
α_{IJ}	0.0004	0.1394	0.0716	0.0034
UNIC-HOC				
$u_{21}-u_{11}$ (J.mol^{-1})	-1024.53	-13781.50	-2912.36	-259.97
$u_{12}-u_{22}$ (J.mol^{-1})	401.07	1281.05	764.52	-864.66

Table G-2: Summary of binary interaction parameters regressed for the system n-hexane (1) + NMP (2).

	T = 353.15 K	T = 363.15 K	T = 378.15 K	T = 383.15 K
NRTL - HOC				
$g_{12} - g_{22}$ (J.mol^{-1})	5260.09	6096.39	8316.49	8655.12
$g_{21} - g_{11}$ (J.mol^{-1})	3483.70	4385.53	4326.34	4630.73
α_{IJ}	0.3902	0.4984	0.01958	0.5425
NRTL-RKS-WS				
$g_{12} - g_{22}$ (J.mol^{-1})	5323.07	6202.96	6313.02	6830.46
$g_{21} - g_{11}$ (J.mol^{-1})	3458.09	4777.67	4172.33	4203.91
α_{IJ}	0.3928	0.5129	0.4465	0.5276
k_{ij}	-0.3442	0.4652	1.1	1.1
NRTL-PR-WS				
$g_{12} - g_{22}$ (J.mol^{-1})	4010.75	4719.78	4988.40	3415.12
$g_{21} - g_{11}$ (J.mol^{-1})	3113.14	4248.39	5960.71	3455.68
α_{IJ}	0.2858	0.5021	0.0524	0.3433
k_{ij}	-0.6371	-0.0774	0.9118	1.6279
NRTL-RKS				
$g_{12} - g_{22}$ (J.mol^{-1})	5178.24	6089.26	6173.31	8530.92
$g_{21} - g_{11}$ (J.mol^{-1})	3429.59	4427.14	3614.02	4572.84
α_{IJ}	0.3838	0.5021	0.3034	0.5449
NRTL-PR				
$g_{12} - g_{22}$ (J.mol^{-1})	5190.17	6093.13	6191.85	8579.99
$g_{21} - g_{11}$ (J.mol^{-1})	3438.90	4422.18	4218.52	4589.98
α_{IJ}	0.3848	0.50144	0.30779	0.5441
UNIC-HOC				
$u_{21}-u_{11}$ (J.mol^{-1})	-2080.29	-2394.64	-2589.72	-2301.16
$u_{12}-u_{22}$ (J.mol^{-1})	-0.89	251.66	149.47	155.19

Table G-3: Summary of binary interaction parameters regressed for the system 1-hexene (1) + n-hexane (2).

	T = 343.15 K	T = 363.15 K	T = 373.15 K
NRTL-RKS-WS			
$g_{12} - g_{22}$ (J.mol^{-1})	-285.2949	-254.7285	-188
$g_{21} - g_{11}$ (J.mol^{-1})	100.2262	157.7764	33.3878
α_{IJ}	1.00E-06	6.23E-03	7.42E-02
k_{ij}	-0.4035	0.2145	0.0770
NRTL-PR-WS			
$g_{12} - g_{22}$ (J.mol^{-1})	-285.295	-283.5	-6.2056
$g_{21} - g_{11}$ (J.mol^{-1})	88.8607	72.673	11.5982
α_{IJ}	0.0010	0.0014	1
k_{ij}	0.4604	0.3837	0.0461
NRTL-Ideal			
$g_{12} - g_{22}$ (J.mol^{-1})	-0.5181	-2.6850	-6.2056
$g_{21} - g_{11}$ (J.mol^{-1})	11.2800	9.3735	11.5982
α_{IJ}	0.0966	0.0518	1

G.2: Plots of Binary Interaction Parameters for System: 1-Hexene (1) + NMP (2)

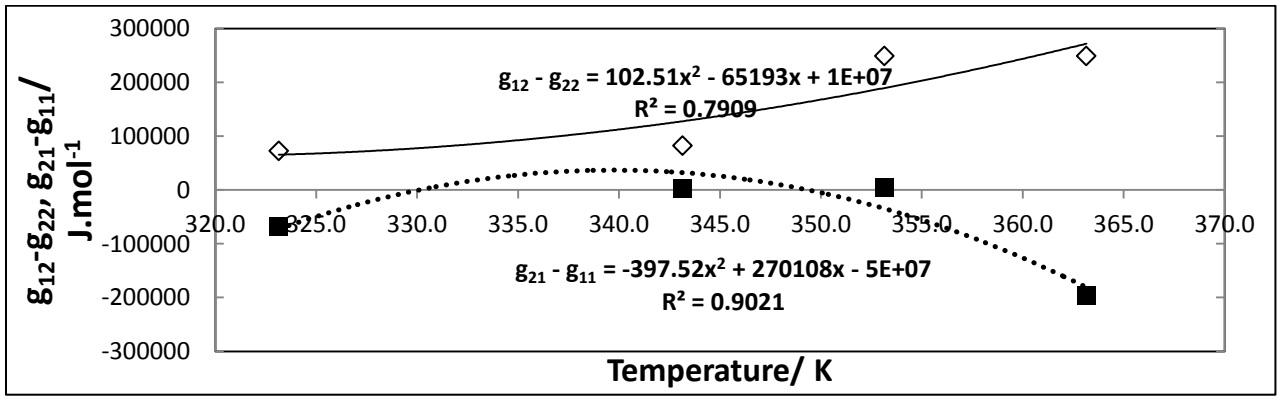

Figure G-1: Temperature dependence of the NRTL-PR model parameters for the system 1-hexene (1) + NMP (2). ◊ Te_{12}-g_{22}; ■, $g_{21} - g_{11}$; ▬, fit for g_{12}-g_{22}; ⋯, fit for $g_{21} - g_{11}$.

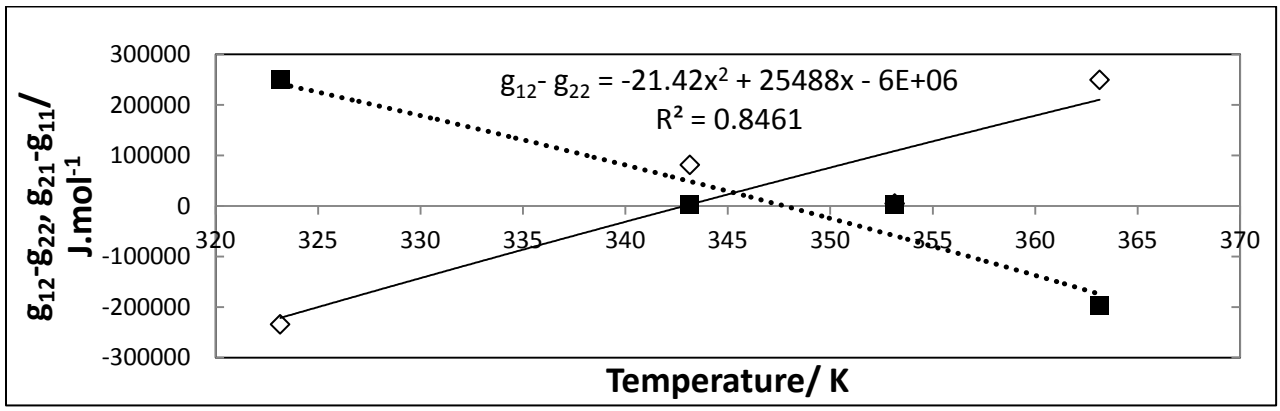

Figure G-2: Temperature dependence of the NRTL-SRK model parameters for the system 1-hexene (1) + NMP (2). ◊, g_{12}-g_{22}; ■, $g_{21} - g_{11}$; ▬, fit for g_{12}-g_{22}; ⋯⋯; fit for $g_{21} - g_{11}$.

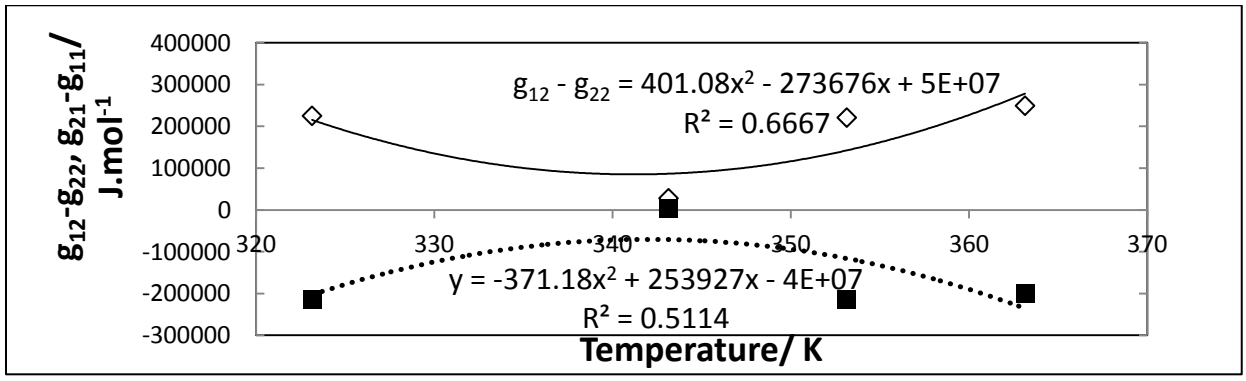

Figure G-3: Temperature dependence of the NRTL-PR-WS model parameters for the system 1-hexene (1) + NMP (2).◊, g_{12}-g_{22}; ■, $g_{21} - g_{11}$; ▬, fit for g_{12}-g_{22}; ⋯⋯; fit for $g_{21} - g_{11}$.

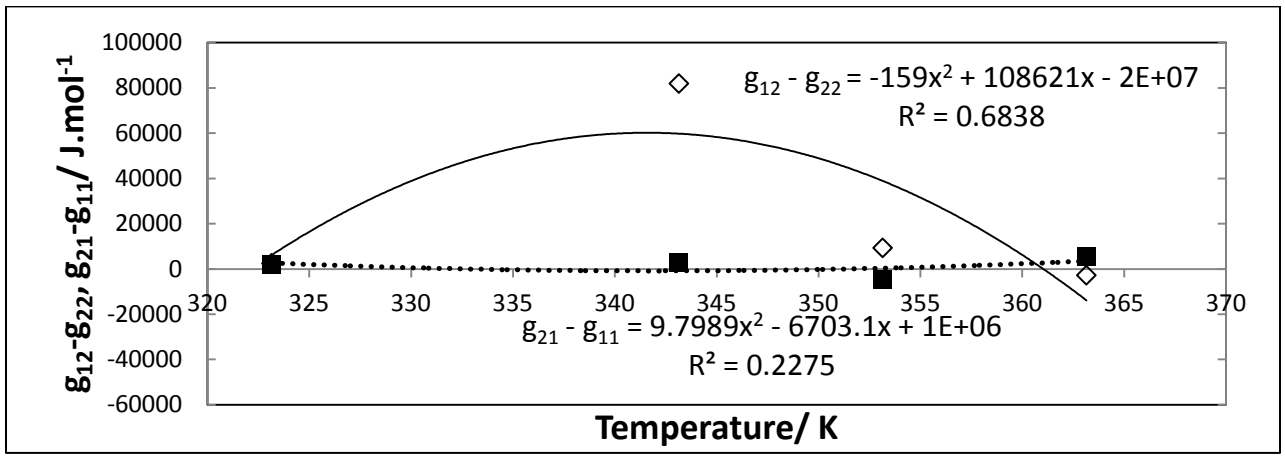

Figure G-4: Temperature dependence of the NRTL-SRK-WS model parameters for the system 1-hexene (1) + NMP (2). ◊ Te_{12}-g_{22}; ■, $g_{21} - g_{11}$; ▬, fit for g_{12}-g_{22}; ·····; fit for $g_{21} - g_{11}$.

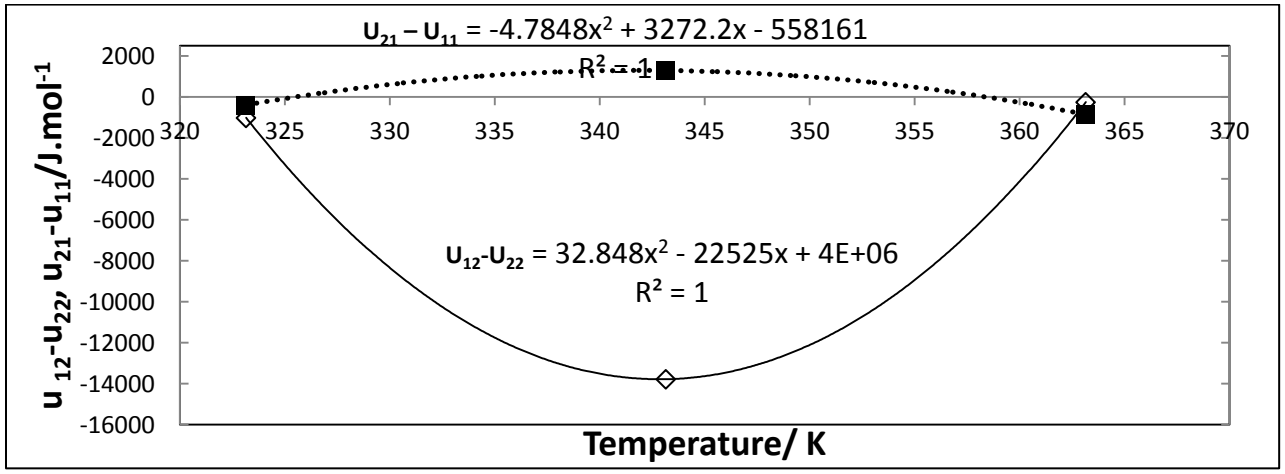

Figure G-5: Temperature dependence of the UNIQUAC-HOC model parameters for the system 1-hexene (1) + NMP (2). ◊, U_{12}-U_{22}; ■, $U_{21} - U_{11}$; ▬, fit for U_{12}-U_{22}; ·····; fit for $U_{21} - U_{11}$.

G.3: Plots of Binary Interaction Parameters for the System: n-Hexane (1) + NMP (2)

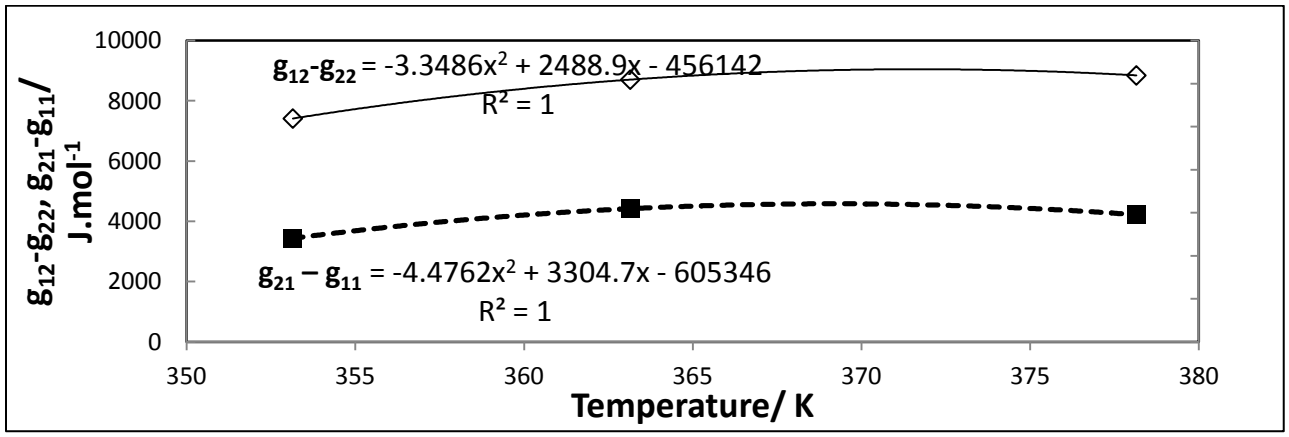

Figure G-6: Temperature dependence of the NRTL-PR model parameters for the system n-hexane (1) + NMP (2). ◊ Te_{12}-g_{22}; ■, $g_{21} - g_{11}$; ▬, fit for g_{12}-g_{22}; ·····; fit for $g_{21} - g_{11}$.

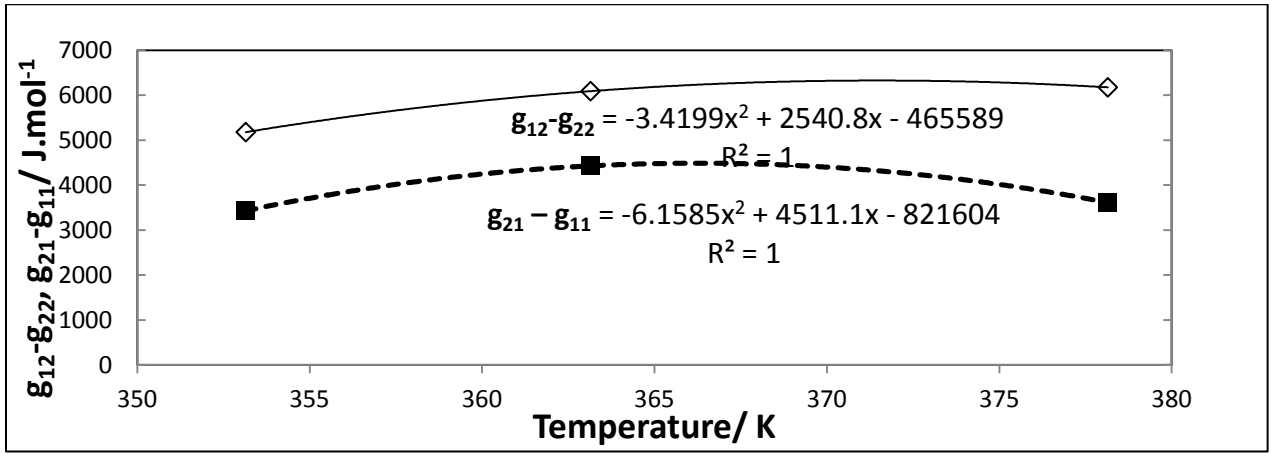

Figure G-7: Temperature dependence of the NRTL-SRK model parameters for the system n-hexane (1) + NMP (2). ◊the$_{12}$-g_{22}; ■, $g_{21} - g_{11}$; ▬, fit for g_{12}-g_{22}; ·····; fit for $g_{21} - g_{11}$.

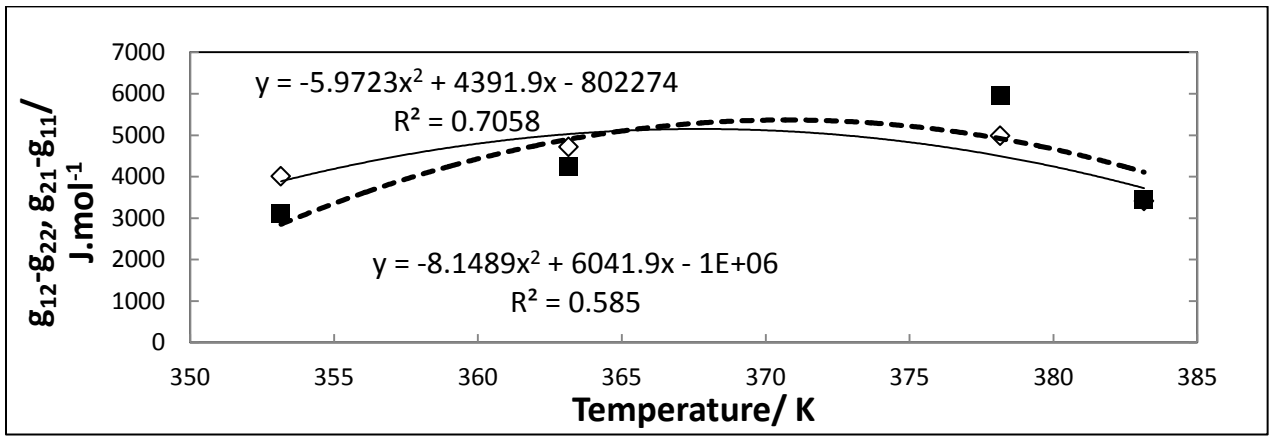

Figure G-8: Temperature dependence of the NRTL-PR-WS model parameters for the system n-hexane (1) + NMP (2). ◊, g_{12}-g_{22}; ■, $g_{21} - g_{11}$; ▬, fit for g_{12}-g_{22}; ·····; fit for $g_{21} - g_{11}$.

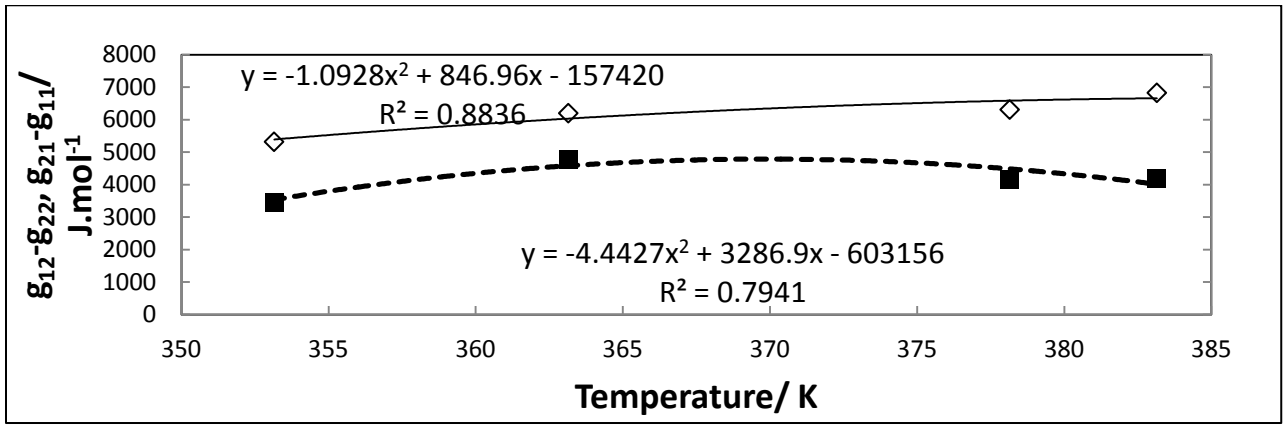

Figure G-9: Temperature dependence of the NRTL-SRK-WS model parameters for the system n-hexane (1) + NMP (2). ◊, g_{12}-g_{22}; ■, $g_{21} - g_{11}$; ▬, fit for g_{12}-g_{22}; ·····; fit for $g_{21} - g_{11}$.

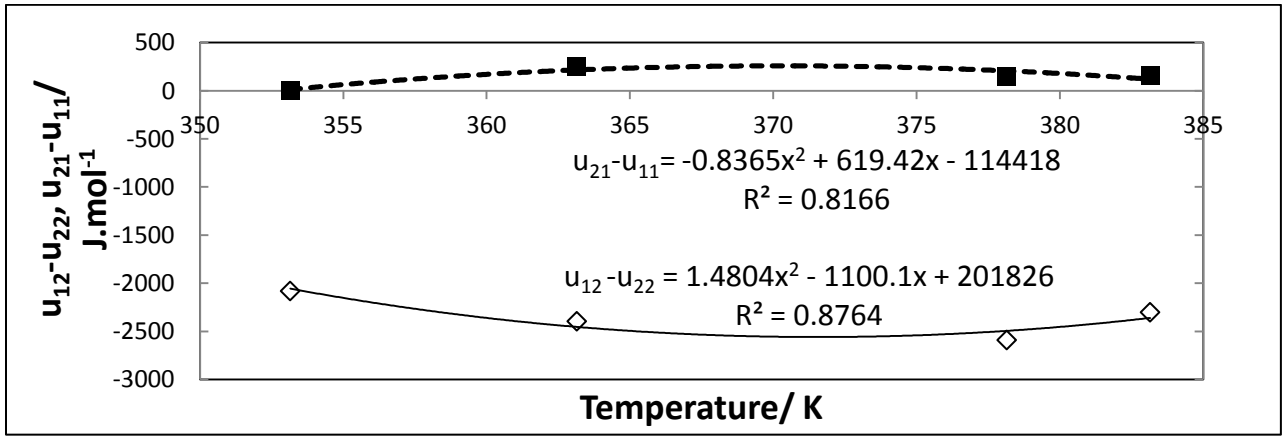

Figure G-10: Temperature dependence of the UNIQUAC-HOC model parameters for the system n-hexane (1) + NMP (2). ◊, U_{12}-U_{22}; ■, $U_{21} - U_{11}$; ▬, fit for U_{12}-U_{22}; ·····; fit for $U_{21} - U_{11}$.

G.4: Plots of Binary Interaction Parameters for the System: 1-Hexene(1) + n-Hexane(2)

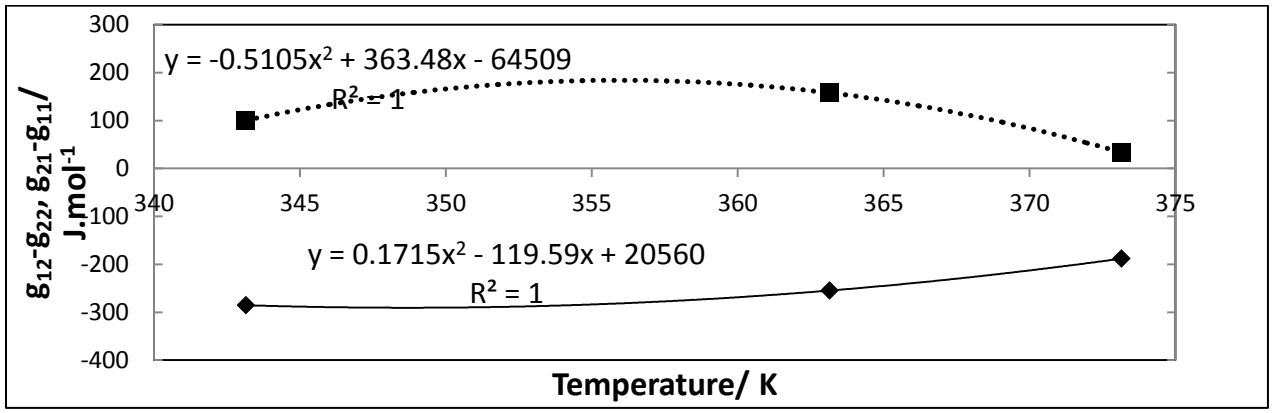

Figure G-11: Temperature dependence of the NRTL-RKS-WS model parameters for the system 1-hexene (1) + n-hexane (2). ◊, g_{12}-g_{22}; □, $g_{21} - g_{11}$; ▬, fit for g_{12}-g_{22}; ·····; fit for $g_{21} - g_{11}$.

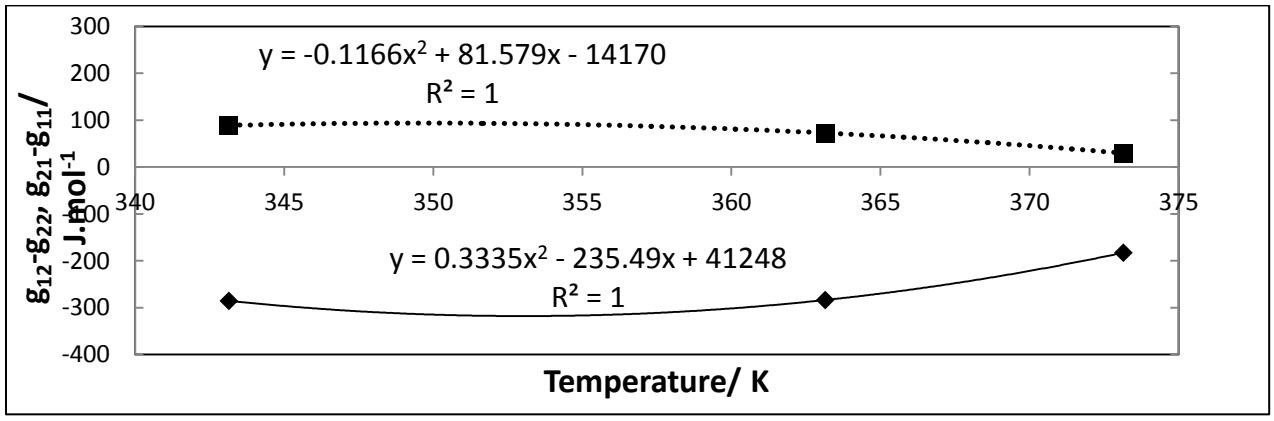

Figure G-12: Temperature dependence of the NRTL-PR-WS model parameters for the system 1-hexene (1) + n-hexane (2). ◊, g_{12}-g_{22}; □, $g_{21} - g_{11}$; ▬, fit for g_{12}-g_{22}; ·····; fit for $g_{21} - g_{11}$.

Appendix H: Relative Volatility Plots

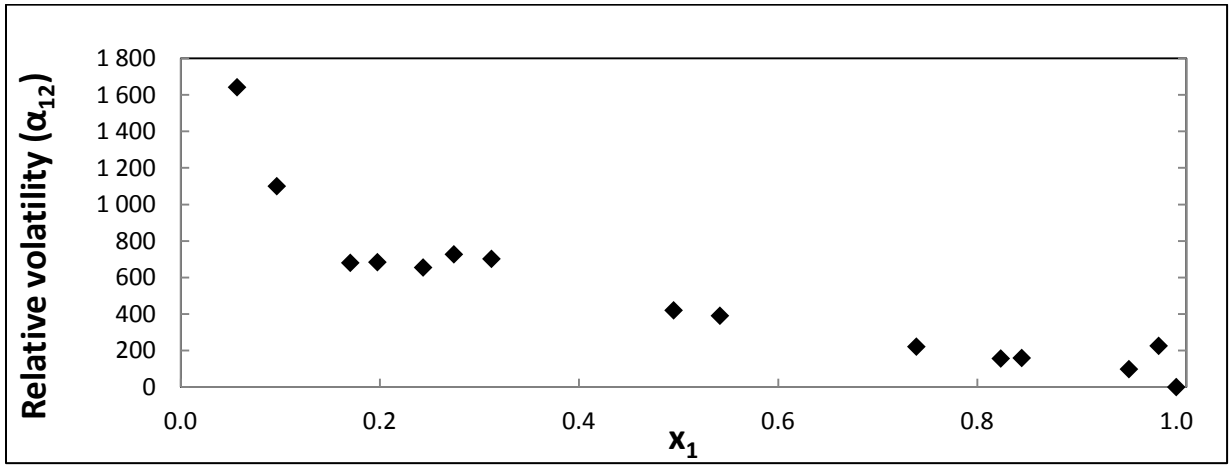

Figure H-1: Plot of relative volatility for the 1-hexene (1) + NMP (2) system at 323.15 K.

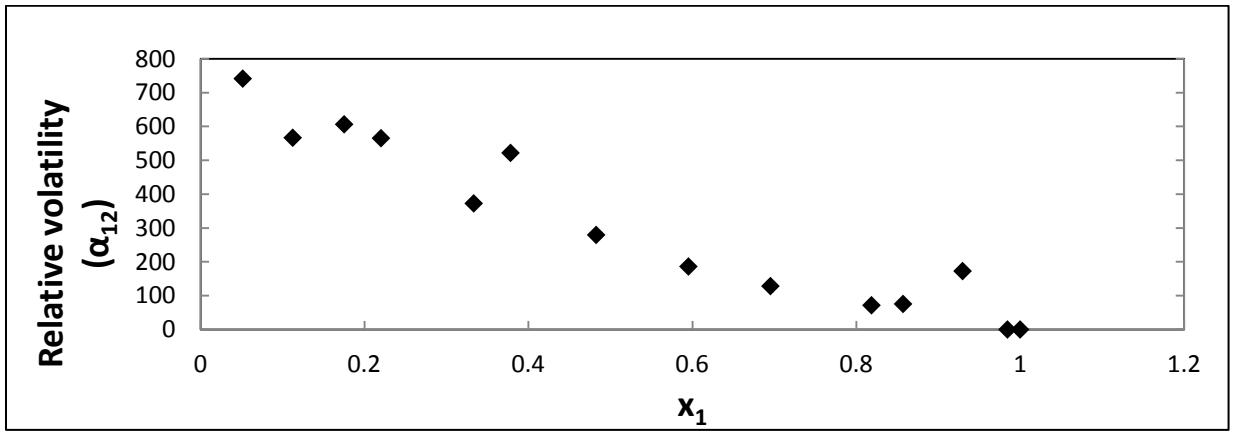

Figure H-2: Plot of relative volatility for the 1-hexene (1) + NMP (2) system at 343.15 K.

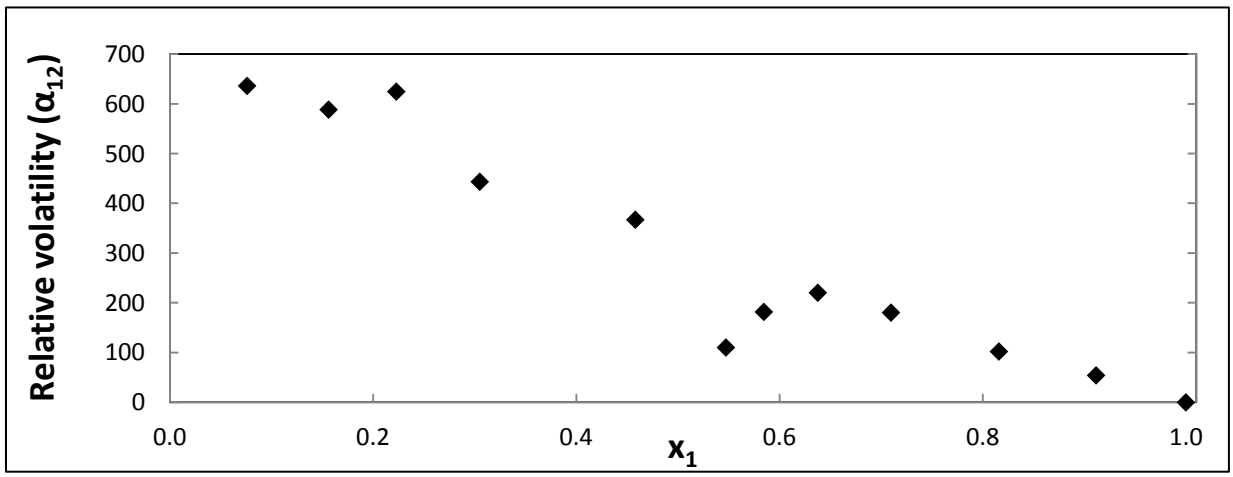

Figure H-3: Plot of relative volatility for the 1-hexene (1) + NMP (2) system at 353.15 K.

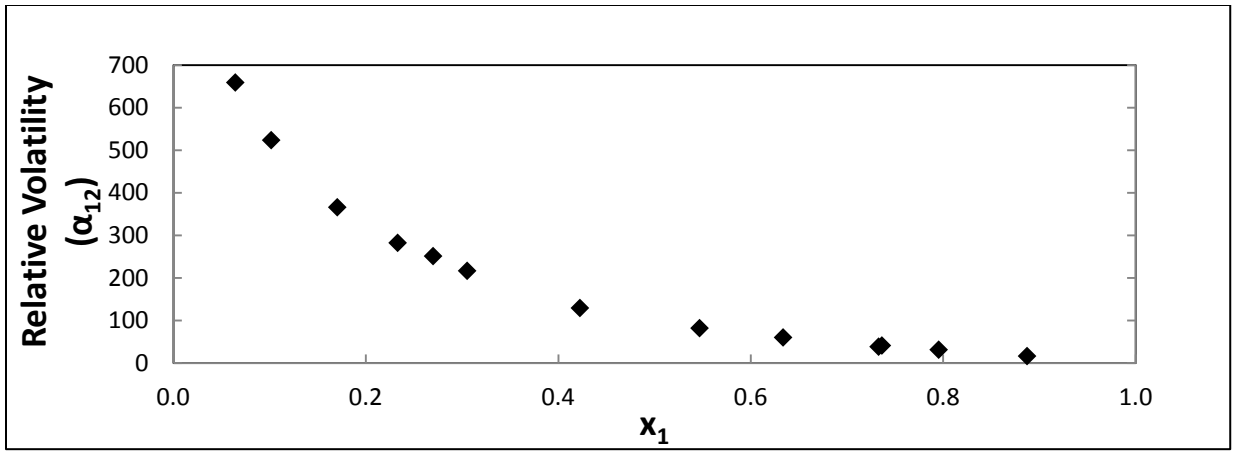

Figure H-4: Plot of relative volatility for the n-hexane (1) + NMP (2) system at 353.15 K.

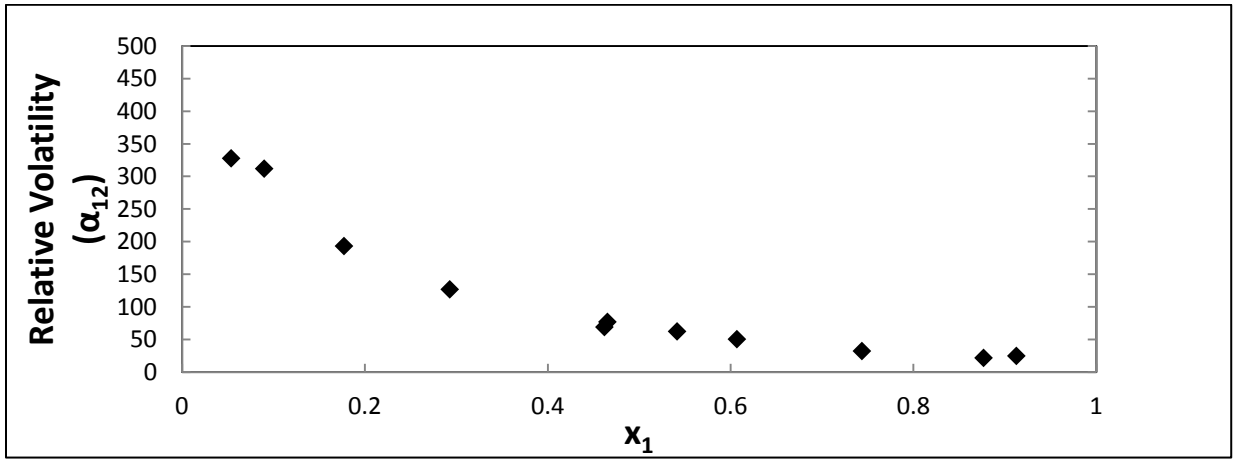

Figure H-5: Plot of relative volatility for the n-hexane (1) + NMP (2) system at 378.15 K.

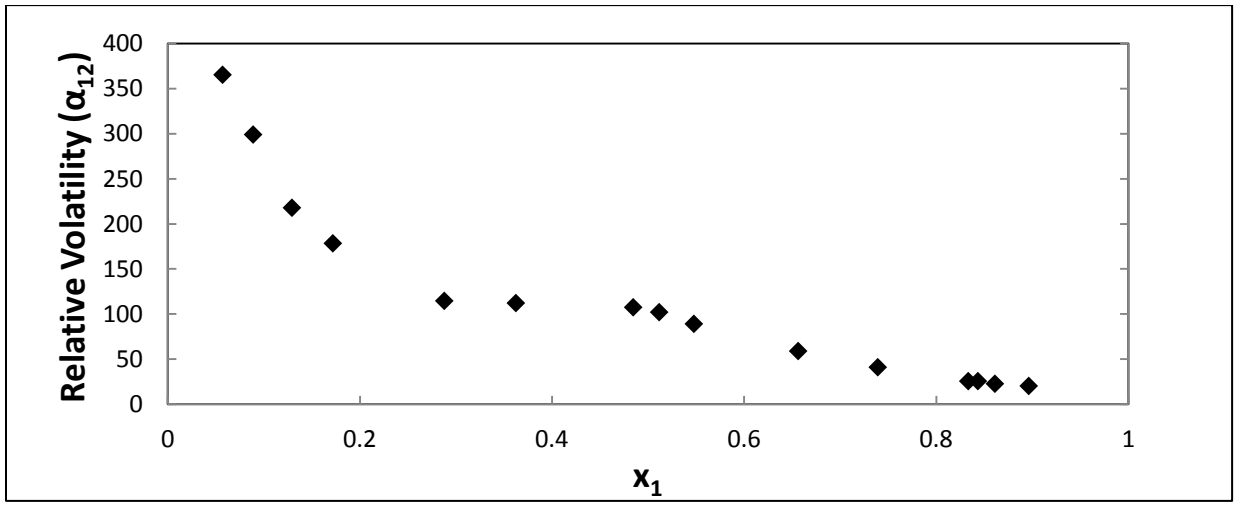

Figure H-6: Plot of relative volatility for the n-hexane (1) + NMP (2) system at 383.15 K.

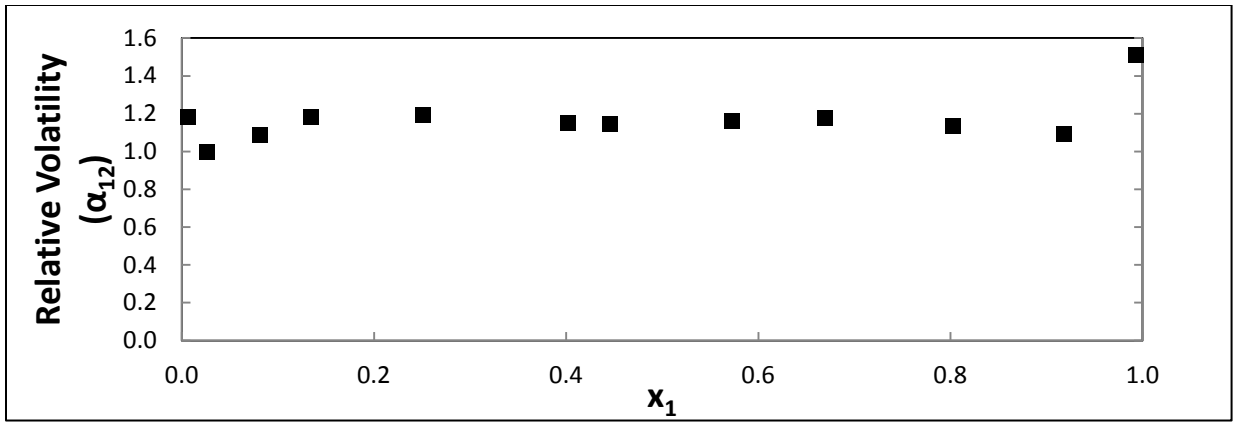

Figure H-7: Plot of relative volatility for the n-hexane (1) + 1-hexene (2) system at 343.15 K.

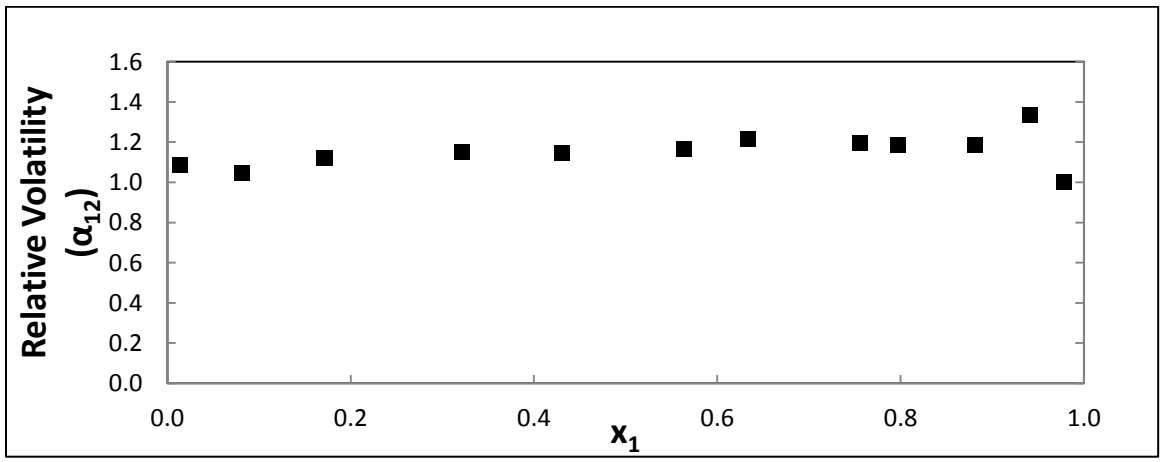

Figure H-8: Plot of relative volatility for the n-hexane (1) + 1-hexene (2) system at 383.15 K.